Inaugural dissertation

for

obtaining the doctoral degree

of the

Combined Faculty of Mathematics, Engineering and Natural Sciences of the

Ruprecht - Karls - University

Heidelberg

Presented by

M.Sc. M.Sc. Malin Schmidt, born in Karlsruhe

Oral examination: 19.04.2023

The psychedelic psilocin fosters neuroplasticity in iPSC-derived human cortical neurons

Referees:

Prof. Dr. Rainer Spanagel

Prof. Dr. med. Philipp Koch

Zu wissen was war
Ist zu wissen weswegen
Ist zu wissen wofür
Ist zu wissen wogegen

Fabian Leonhard

Table of Content I

LIST OF FIGURES II

LIST OF TABLES III

LIST OF ABBREVIATIONS IV

ABSTRACT 1

ZUSAMMENFASSUNG 3

1 INTRODUCTION 5

1.1 THE DEVELOPMENT OF THE HUMAN BRAIN 5
1.2 IPSC TECHNOLOGY AND ITS POTENTIAL IN DRUG INVESTIGATION AND DISEASE MODELLING 7
1.2.1 Differentiation of iPSCs into forebrain progenitors *8*
1.3 PSYCHEDELICS 9
1.3.1 Psilocybin *13*
1.3.2 Brief overview of psychedelic history *13*
1.3.3 Crisis of classical psychopharmacotherapy *14*
1.3.4 Psychedelics as drugs in the treatment and research of psychiatric disorders *15*
1.4 MENTAL DISORDERS 17
1.4.1 Cognitive and neuronal dysfunction in psychiatric disorders *17*
1.5 PSYCHEDELICS AND NEURONAL PLASTICITY 18
1.5.1 Psychedelics as mediators of global brain activity and neuronal excitability *18*
1.5.2 Psychedelic induce molecular and cellular changes *19*
1.6 PATHWAYS ASSOCIATED WITH THE PSYCHEDELIC MODE OF ACTION 20
1.6.1 The serotonergic 5-HT2A receptor plays a key role in psychedelic-mediated neuroplasticity *20*
1.6.2 The brain-derived neurotrophic factor is a key factor in psychedelic-mediated neuroplasticity and psychiatric disorder pathophysiology *24*
1.7 THE LEADING ROLE OF THE ANNEXIN A2 – S100A10 COMPLEX IN THE CLEAVAGE OF PRO-BDNF INTO M-BDNF 26
1.7.1 Key players of the annexin A2 – S100A10 complex, their role in fibrinolysis, synaptic plasticity and link to psychiatric disorders *28*
1.8 AIMS OF THE STUDY 33

2 MATERIALS 35

2.1 CELL CULTURE 35
2.1.1 Cell culture media, solutions, additives, kits and buffers *35*
2.1.2 Cell lines *40*
2.2 MOLECULAR BIOLOGY 41
2.2.1 Molecular biology reagents, kits, enzymes and buffers *41*
2.2.2 Primers *42*
2.2.3 RT-PCR compositions and cycling programs *44*
2.2.4 Plasmid *46*
2.3 BACTERIA 46
2.4 VIRUS 47
2.5 BIOCHEMISTRY 47
2.5.1 Biochemistry: commercials, kits, self-made buffers and solutions *47*
2.5.2 Primary and secondary antibodies for immunocytochemistry and western blotting *48*
2.5.3 Buffers and solution chemicals and reagents *51*
2.6 COMMON CONSUMABLES AND EQUIPMENT 52
2.6.1 Cell culture, molecular biology and biochemistry consumables *52*
2.7 SOFTWARE 54

3 METHODS 55

3.1 HUMAN MATERIAL AND GENERATION OF FIBROBLAST-DERIVED HUMAN IPSCS 55
3.2 CELL CULTURE 55
3.2.1 Coating for iPS cultures and progenitors *55*

3.2.2 Maintenance of iPS cultures ... 56
3.2.3 Passaging of iPS cells ... 56
3.2.4 Freezing and thawing of iPS cells ... 56
3.2.5 Differentiation of iPS cells into neuronal progenitors ... 56
3.2.6 Passaging of neuronal progenitors ... 57
3.2.7 Freezing and thawing of neural progenitors ... 57
3.2.8 Coating for neuronal cultures ... 57
3.2.9 In vitro differentiation of neural progenitors into human cortical neurons ... 58
3.2.10 Splitting of phase 1 neurons ... 59
3.2.11 Freezing and thawing of neurons ... 59
3.2.12 Co-culture of human cortical neurons with mouse astrocytes ... 59
3.3 Molecular biology ... 60
3.3.1 Isolation of gDNA ... 60
3.3.2 SNP analysis ... 61
3.3.3 Ribonucleic acid isolation ... 61
3.3.4 Synthesis of complementary DNA ... 61
3.3.5 Agarose gel electrophoresis ... 62
3.3.6 Determination of cDNA, gDNA and RNA concentration ... 62
3.3.7 RNA bulk sequencing ... 62
3.4 Transformation of bacteria and isolation of plasmid DNA ... 63
3.5 Transfection with lipofectamine ... 63
3.6 Transduction with Adeno-associated virus tagged to mCherry ... 63
3.7 Biochemistry ... 64
3.7.1 ICC ... 64
3.7.2 Protein isolation and measurement of protein concentration ... 64
3.7.3 SDS-polyacrylamide gel electrophoresis and western immunoblotting ... 64
3.7.3.1 Special WB case: cleavage of recombinant pro-BDNF into m-BDNF ... 65
3.7.3.2 Special WB case: cleavage of recombinant pro-BDNF-Alexa-680 into m-BDNF-Alexa-680 ... 65
3.8 Cell viability assay ... 66
3.9 Electrophysiology ... 66
3.10 Neuroplasticity and 5-HT2A-R experiments in cortical neurons ... 67
3.10.1 Treatment of cortical neurons with psilocin ... 67
3.10.2 Treatment of cortical neurons with ketanserin ... 67
3.10.3 Treatment of cortical neurons with chelerythrine ... 68
3.10.4 Treatment of cortical neurons with dynasore ... 68
3.11 Imaging ... 68
3.12 Analysis of IF ... 68
3.12.1 Pixel per length neurite ... 68
3.12.2 Density (particle per length neurite) ... 69
3.12.3 Intensity per area ... 69
3.12.4 Sholl analysis ... 69
3.12.5 Analysis of axon initial segment length and distance to the soma ... 70
3.13 Statistical analysis ... 70
3.14 Appendix information ... 70

4 RESULTS ... 71

4.1 Generation of dorsal forebrain neurons from human iPSC ... 71
4.2 Effect of psilocin administration on 5-HT2A-R localization ... 73
4.3 Effects of psilocin on neuroplasticity in iPSC-derived human cortical neurons ... 75
4.3.1 Psilocin alters neuroplasticity marker AIS and reduces cortical excitability in short-term ... 76
... 78
4.3.2 Influence of psilocin on pre-and postsynaptic proteins and synaptogenesis ... 80
4.4. Influence of psilocin on neurotrophic factor BDNF ... 84
4.5 Psilocin-induced activation of m-BDNF/phospho-TrkB associated downstream pathways ... 87
4.5.1 Psilocin activated the pro-survival AKT pathway ... 87
4.5.2 Psilocin induced increase in neurite arborization ... 87
4.5.3 Psilocin induced increase in immediate early genes ... 90
4.6 Deciphering the psilocin-mediated increase in BDNF ... 91

4.6.1 Psilocin-induced BDNF increase was PKC- and endocytosis-mediated 91
4.6.2 Psilocin-induced BDNF increase was 5-HT2A-R-mediated 93
4.7 BDNF BASE LEVEL DIFFERENCES IN BD AND AUD PATIENT-DERIVED CORTICAL NEURONS AND INFLUENCE OF PSILOCIN TREATMENT 94
4.8 PSILOCIN TARGETED THE FIBRINOLYTIC ANNEXIN A2 – S100A10 COMPLEX 94
4.8.1 Psilocin-induced expression of a gene set involved in plasmin generation 97
4.8.2 Psilocin increased annexin A2 and p11 protein level and complex formation 98
4.9 PSILOCIN INDUCED INCREASE IN P11-BDNF AND P11-PRO-BDNF CO-LOCALIZATION 100
4.10 PSILOCIN FOSTERS PLASMIN-MEDIATED CLEAVAGE OF PRO-BDNF INTO M-BDNF 102

5 DISCUSSION 105

5.1 PROLOGUE 106
5.2 PSILOCIN PROVOKES ACUTE EFFECTS ON THE RECEPTOR PRESENTATION AND A SUBACUTE DOWNREGULATION OF THE 5-HT2A-R 106
5.3 PSILOCIN FOSTERS NEUROPLASTICITY IN HUMAN CORTICAL NEURONS 109
5.4 PSILOCIN INDUCES INCREASE IN BDNF LEVEL AND ACTIVATION OF PROSURVIVAL AND NEUROPLASTICITY ASSOCIATED BDNF DOWNSTREAM CASCADES 112
5.5 BDNF LEVELS ARE ALTERED IN CELL LINES DERIVED FROM SELECTED PSYCHIATRIC DISORDER PATIENTS 115
5.6 PSILOCIN MEDIATES NEUROPLASTICITY BY TARGETING THE ANNEXIN A2 – S100A10 COMPLEX AND ASSOCIATES 117
5.7 THE ANNEXIN A2 – S100A10 COMPLEX AS NOVEL ANTIDEPRESSANT TARGET 120
5.8 SUMMARY 123

6 APPENDIX 125

7 REFERENCES 166

CONTRIBUTIONS 189

ACKNOWLEDGEMENTS 191

List of Figures

Figure 1. Corticogenesis. 6
Figure 2. iPSC technology: reprogramming, disease modelling and personalized medicine. 8
Figure 3. Chemical structure of psychedelic compounds of serotonin analogues. 12
Figure 4. Schematic (and incomplete) presentation of signal transduction pathways hypothesized to be involved in psychedelic-mediated neuroplasticity in the cortex. 21
Figure 5. Biased agonism of the 5-HT2A-R. 23
Figure 6. m-BDNF/phospho-TrkB complex associated downstream pathways. 26
Figure 7. Extracellular plasmin generation by the annexin A2 – S100A10 complex. 28
Figure 8. Coagulation and fibrinolysis. 29
Figure 9. Antidepressant actions of the annexin A2 – S100A10 complex. 31
Figure 10. Timeline for the *in vitro* differentiation of iPSCs into cortical neurons. 60
Figure 11. Validation of iPSC-derived neural progenitors and cortical neurons. 73
Figure 12. Validation of 5-HT2A-R expression and effect of psilocin on receptor presentation. 75
Figure 13. Psilocin-induced increase in differentially expressed genes associated with neuroplasticity GO terms. 77
Figure 14. Psilocin modulated length and distance to the soma of neuroplasticity indicator AIS. 78
Figure 15. Psilocin and TCB-2 reduced excitability in cortical neurons in short-term. 79
Figure 16. Effect of psilocin on neuritic presynaptic SV2A, synaptophysin and postsynaptic PSD-95. 81
Figure 17. Psilocin promotes dendritic synaptogenesis. 83
Figure 18. Psilocin-induced increase in sEPSC amplitude in long-term. 84
Figure 19. Influence of different psilocin concentrations and treatment conditions on BDNF level. 85
Figure 20. Psilocin induced increase in BDNF level. 87
Figure 21. Psilocin induced activation of prosurvival AKT downstream cascade. 88
Figure 22. Psilocin induced increase in neurite complexity. 89
Figure 23. Psilocin induced increase in immediate early genes. 91
Figure 24. Psilocin induced increase in BDNF level was PKC- and endocytosis-mediated. 92
Figure 25. Psilocin induced increase in BDNF level was 5-HT2A-R-mediated. 93
Figure 26. BDNF base level differences and psilocin effect in BD and AUD patients. 95
Figure 27. Psilocin induced enrichment of pathways associated with fibrinolysis. 96
Figure 28. Upregulation of genes of the annexin A2 – S100A10 complex and associates by psilocin 98
Figure 29. Psilocin induced upregulation of core proteins of the annexin A2 – S100A10 complex. 100
Figure 30. Psilocin induced increase in p11, BDNF and pro-BDNF and their co-localization. 101
Figure 31. Psilocin increased plasmin-mediated cleavage of pro-BDNF into m-BDNF. 103
Figure 32. Psilocin modulates neuronal plasticity in iPSC-derived human cortical neurons. 105
Figure 33. Psilocin provokes acute effects on receptor presentation and a subacute downregulation of the 5-HT2A-R. 109
Figure 34. The annexin A2 – S100A10 complex as novel antidepressant drug target. 122
Figure 35. The psychedelic psilocin fosters neuroplasticity in iPSC-derived human cortical neurons. 123
Figure 36. Appendix 12 of Figure 12I. Effect of psilocin on 5-HT2A-R presentation. 125
Figure 37. Appendix 14 of Figure 14C-D. Psilocin-induced AIS length increase and AIS shift to the soma. 128
Figure 38. Appendix 15 of Figure 15A, C, E. Psilocin and TCB-2 reduced excitability in short-term. 130
Figure 39. Appendix 16A of Figure 16C. Effect of psilocin on neuritic presynaptic SV2A. 131
Figure 40. Appendix 16B of Figure 16D. Effect of psilocin on neuritic postsynaptic PSD-95. 132
Figure 41. Appendix 16C of Figure 16G. Effect of psilocin on neuritic presynaptic synaptophysin. 134
Figure 42. Appendix 17A of Figure 17C-D. Long-term effect of psilocin on neuritic presynaptic synapsin. 135
Figure 43. Tbc. Appendix 17A of Figure 17E-F. Long-term effect of psilocin on neuritic postsynaptic PSD-95. 136

Figure 44. Tbc. Appendix 17A of Figure 17G. Long-term effect of psilocin on neuritic synapsin and PSD-95 co-localization. 137
Figure 45. Appendix 17B of Figure 17J-N. Long-term effect of psilocin on dendritic synapsin and PSD-95 co-localization. 139
Figure 46. Appendix 18 of Figure 18A, C. Psilocin induced electrophysiological changes in synaptic properties over time. 140
Figure 47. Appendix 19A of Figure 19B. Influence of different psilocin concentrations on BDNF level. 141
Figure 48. Appendix 19B of Figure 19C. Influence of psilocin concentrations on cell viability. 142
Figure 49. Appendix 19C of Figure 19E. Influence of artificial (10 min 10 μM) psilocin trigger versus physiological (6 hrs 100 nM) psilocin stimulation on BDNF level. 143
Figure 50. Appendix 20A of Figure 20C. Psilocin induced BDNF level increase. 145
Figure 51. Appendix 20B of Figure 20E-F. Psilocin-induced BDNF level increase for different treatment conditions. 147
Figure 52. Appendix 21 of Figure 21E. Psilocin induced activation of prosurvival AKT downstream cascade. 148
Figure 53. Appendix 22 of Figure 22B. Psilocin induced increase in neurite complexity. 150
Figure 54. Appendix 23 of Figure 23B, E. Psilocin induced increase in immediate early genes. 151
Figure 55. Appendix 24 of Figure 24B, D. Influence of chelerythrine and dynasore co-treatment on BDNF level. 153
Figure 56. Appendix 25 of Figure 25B. Influence of ketanserin treatment on BDNF level. 155
Figure 57. Appendix 26A of Figure 26A, B. BDNF base level differences in BD and AUD patients. 156
Figure 58. Appendix 26B of Figure 26D. Effect of psilocin on BDNF level of neurons derived from BD patients. 158
Figure 59. Appendix 26C of Figure 26E. Effect of psilocin on BDNF level of neurons derived from AUD patients. 159
Figure 60. Appendix 29 of Figure 29C. Psilocin induced p11 level increase. 160
Figure 61. Tbc. Appendix 29 of Figure 29E. Influence of psilocin on annexin A2 and p11 – annexin A2 co-localization. 161
Figure 62. Tbc. Appendix 29 of Figure 29H. Psilocin induced upregulation of core proteins of the AIIt complex. 162
Figure 63. Appendix 30A of Figure 30C.Psilocin-induced p11 and BDNF increase and their co-localization. 163
Figure 64. Appendix 30B of Figure 30D. Psilocin induced p11 and pro-BDNF increase and their co-localization. 164
Figure 65. Appendix 31 of Figure 31C-E. Psilocin increases plasmin mediated cleavage of pro-BDNF into m-BDNF. 165

List of Tables

Table 1. Cell culture base media. 35
Table 2. Commercial cell culture stock solutions and additives. 35
Table 3. Small molecules, growth factors, drugs and solutions for cell culture. 36
Table 4. Commercial kits for cell culture. 37
Table 5. Self-made buffer for cell culture. 38
Table 6. Composition of self-made 100x N2-supplement. 38
Table 7. Composition of ready-to-use cell culture media and solutions. 38
Table 8. Healthy control cell lines. 40
Table 9. BD cell lines. 40
Table 10. AUD cell lines. 40
Table 11. Molecular biology: commercial reagents. 41
Table 12. Molecular biology: commercial kits. 41
Table 13. Enzymes. 41
Table 14. Molecular biology: self-made buffers. 42
Table 15. Primers for real-time (RT)- polymerase chain reaction (PCR) and RT quantitative PCR (RT-qPCR) 42
Table 16. Composition of standard RT-PCR reaction. 44
Table 17. Standard RT-PCR cycling program. 44
Table 18. RT-PCR cycling program for mycoplasma quality control. 44
Table 19. RT-PCR cycling program for fingerprint quality control. 44
Table 20. Composition of RT-qPCR master mix. 45
Table 21. Composition of standard RT-qPCR reaction. 45
Table 22. Standard RT-qPCR cycling program. 45
Table 23. Composition of standard cDNA synthesis reaction. 45
Table 24. Standard cycling program for cDNA synthesis. 45
Table 25. Commercial bacteria stock solutions. 46
Table 26. Media and solutions used for cultivation of bacteria. 46
Table 27. Self-made media for cultivation of bacteria. 46
Table 28. Biochemistry: commercials. 47
Table 29. Biochemistry: commercial kits. 47
Table 30. Biochemistry: self-made buffers and solutions. 47
Table 31. Primary antibodies used for immunocytochemistry (ICC). 48
Table 32. Secondary antibodies used for ICC. 49
Table 33. Fluorescent probes. 50
Table 34. Primary antibodies used for Western blotting (WB). 50
Table 35. IR-dye conjugated secondary antibodies used for WB. 50
Table 36. Biochemistry: chemicals and reagents. 51
Table 37. Common consumables. 52
Table 38. Notable laboratory equipment. 53
Table 39. Computer software and other digital resources. 54
Table 40. Pre-defined particle size of proteins measured with ComDet. 69

List of Abbreviations

Abbreviation	Full name	Abbreviation	Full name
(v/v)	volume percent	CDK	Cyclin dependent kinase 4
(w/v)	weight percent	cDNA	complementary DNA
%	percent	CME	clathrin-mediated endocytosis
°C	degree celsius	CNS	central nervous system
1X	single concentrated	CP	cortical plate
5-HT	5-hydroxytryptamine, serotonin	CRE	Ca^{2+} response element
5-HT2A-R	5-hydroxytryptamine receptor 2A	CREB	cyclic AMP response element-binding protein
5-HTR	serotonergic receptors	CRISPR	clustered regulatory interspaced palindromic repeats
5-MeO-DMT	5-methoxy-dimethyltryptamine	Ct	threshold cycle
AA	arachidonic acid	Ctrl	control
AAV	adeno-associated virus	DAG	diacylglycerol
ACSF	artificial cerebrospinal fluid	DALY	disability adjusted life years
AIS	Axon initial segment	DAPI	4,6-diamidino-2-phenylindole
AKT	Protein kinase B	DAPT	N-[N-(3,5.Difluorophenacetyl)-L-alanyl]-S-phenylglycine t-butyl ester
ALK	Type-I activin receptor-like kinases	ddH_2O	double-distilled water
AMPA	α-amino-3-hydroxy-5-methyl-4-isoxazolepropionic acid	DEPC	diethyl pyrocarbonate
AP	action potential	DMN	default-mode network
APS	ammonium persulfate	DMSO	dimethyl sulfoxide
ASCL1	Achaete-scute family bHLH transcription factor 1	DMT	*N,N*-Dimethyltryptamine
ATP	adenosine triphosphate	DNA	deoxyribonucleic acid
AUD	Alcohol use disorder	dNTPs	deoxynucleoside triphosphates
BCA	bicinchoninic acid	DOI	2,5-dimethoxy-4-iodoamphetamine
BD	Bipolar disorder	DSM	Diagnostic and Statistical Manual of Mental Disorders
BDNF	brain-derived neurotrophic factor	E	embryonic day
BMP	bone morphogenic protein	E. coli	Escherichia coli
BOLD	blood-oxygen-level-dependent	e.g.	*exempli gratia* (for example)
bp	base pair	E8	Essential 8 medium
BP	biological process	ECT	electroconvulsive therapy
BSA	bovine serum albumin	EDTA	ethylenediaminetetraacetic acid
BtMG	Betäubungsmittelgesetz	EEA-1	Early endosomal antigen-1
$CaCl_2$	calcium chloride	EGF	epidermal growth factor
CaMK	Ca^{2+}/calmodulin-dependent protein kinase	EGR	Early growth response protein
Cas9	CRISPR associated protein 9	EGTA	Ethylene glycol tetraacetic acid
CBF	cerebral flood flow	ER	endoplasmic reticulum
CC	cellular compartment	ERK	Extracellular-signal regulated kinases

ESC	embryonic stem cell	KLF4	Kruppel-like factor 4
et al.	*et alia* (and others)	KO	knock out
FBS	fetal bovine serum	KOSR	KnockOut serum replacement
FDA	Food and Drug Administration	l	litre
FDP	fibrin degradation products	L-type VGCC	L-type voltage-gated calcium channels
FGF	fibroblast growth factor	LAAP	L-ascorbic acid 2-phosphate
Fig	Figure	LB	lysogeny broth
fMRI	functional magnetic resonance imaging	LSD	Lysergic acid diethylamide
FOX	forkhead box	m	milli-
g	gram	M	molar
GABA	γ-aminobutyric acid	m-BDNF	mature BDNF
GAD	glutamate decarboxylase	MAP2	Microtubule-associated protein 2
GAP-43	growth-associated protein 43	MAPK	Mitogen-activated protein kinase
gDNA	genomic DNA	MDD	Major depressive disorder
GE	ganglionic eminence	MDMA	3,4-Methylenedioxymethamphetamine
GFAP	glial fibrillary protein	mEPSCs	miniature excitatory postsynaptic currents
GO	gene ontology	MF	molecular function
GPCR	G protein-coupled receptor	mFC	Medial frontal cortex
GRIA	glutamate ionotropic receptor AMPA type subunit 1	mGluR	metabotropic glutamate receptor
GRIN	glutamate ionotropic receptor NMDA type subunit 1	min	minute
GTPases	guanosine triphosphate hydrolases	MMP	metalloproteinases
HCL	hydrochloric acid	mPFC	medial prefrontal cortex
HEK	human embryonic kidney	mRNA	messenger RNA
HPPD	Hallucinogen Persisting Perception Disorder	mTOR	mammalian target of rapamycin
hr	hour	MW	molecular weight
hrs	hours	MYTL1	Myelin transcription factor 1 like
Hz	hertz	MZ	marginal zone
ICC	immunocytochemistry	n	nano-
ICD	International Statistical Classification of Diseases and Related Health Problems	n.s.	not significant
IEGs	immediate-early genes	Na^+	Sodium
IF	immunofluorescence	NaCl	Sodium chloride
IL-6	Interleukin-6	NEAA	non-essential amino acid
iN	induced neurons	NEC	neuroepithelial cells
IP	intermediate progenitor	NeuN	neuronal nuclei
IP3	inositol-1,4,5 trisphosphate	NEUROD	neuronal differentiation
iPSC	induced pluripotent stem cell	NGN2	Neurogenin 2
IZ	intermediate zone	NMDA	N-methyl-D-aspartate
JAK/STAT	Janus kinase/signal transducers and activators of transcription	NPC	neural progenitor cell
K^+	Potassium	Ø	diameter
KEGG	Kyoto Encyclopedia of Genes and Genomes	OCD	Obsessive-compulsive disorder

OCT	Octamer-binding transcription factor	SD	standard deviation
p	significance level	SDS	sodium dodecyl sulphate
PAGE	polyacrylamid gel electrophoresis	sec	second
PAI-1	Plasminogen activator inhibitor-1	sEPSCs	spontaneous excitatory postsynaptic currents
PAP	psychedelic-assisted psychotherapy	seq	sequencing
PAX	Paired box	SMAD	Small mothers against decapentaplegic
PBS	phosphate buffered saline	SMARCA3	SWI/SNF-related, matrix-associated actin-dependent regulator of chromatin, subfamily A, member 3
PCF	prefrontal cortex	SNARE	Soluble N-ethylmaleimide-sensitive-factor attachment receptor
PCR	polymerase chain reaction	SNP	single nucleotide polymorphism
PEI	polyethylenimine	SOX2	Sex determining region Y-box2
Pen/Strep	Penicillin/Streptomycin	SP	subplate
PET	positron emission tomography	SSRI	Selective serotine reuptake inhibitors
PFA	paraformaldehyde	STED	Stedycon
pH	potential of hydrogen	SUD	Substance use disorder
PI	phosphatidyl inositol	SV2A	Synaptic vesicle glycoprotein 2A
PI3K	phosphatidylinositol 3-kinase	SVZ	subventricular zone
PIP2	phosphatidylinsositol-4,5-biphosphate	TBR1	T-box brain protein 1
PKC	protein kinase C	TBS-T	tris-buffered saline with Tween®20
PLA	phospholipase A2	TEMED	*N,N,N',N'*-tetramethylethylenediamine
PLC	phospholipase C	TF	transcription factor
PMA	phorbol 12-myristate 13-acetate	TGF	transforming growth factor B
PP	preplate	TLR	Toll like receptor
pro-BDNF	proneurotrophin BDNF	TNF-a	Tumor necrosis factor-a
PSD-95	postsynaptic density 95	tPA	tissue plasminogen activator
Psilocybin	4-phosphoryloxy-*N,N*-dimethyltryptamine	TRD	Treatment resistant depression
PtdIns(4,5)P2	phosphatidylinositol 4,5-bisphosphate	TrkB	Tropomyosin-related kinase B
PTSD	posttraumatic stress disorder	TTX	Tetrodotoxin
qPCR	quantitative PCR	TUBB3	Beta-III-tubulin
RA	retinoic acid	uPA	urokinase-type plasminogen activator
RAB	Ras-associated binding	uPAR	urokinase-type plasminogen activator receptor
RBFOX	RNA-binding protein FOX	vGLUT	vesicular glutamate transporter
RGC	radial glia cell	VZ	ventricular zone
RIN	RNA integrity number	WB	Western blot
RMP	Resting membrane potential	WNT	Wingless/integrated
RNA	ribonucleic acid	x g	times gravity
ROCK inhibitor	Rho-associated protein kinase inhibitor	YLD	years lived with disability
ROI	region of interest	µ	micro
RT	room temperature		
RT-PCR	real-time PCR		
RT-qPCR	real-time quantitative PCR		

Abstract

Psychedelics have the fascinating potential to induce altered states of consciousness. First promising research for their therapeutical application stopped in the early 70's when psychedelics were criminalized. Since the 90's psychedelic research is regaining revival. On the one hand new psychopharmacological entities are urgently needed because the number of patients suffering from psychiatric disorders is constantly increasing and novel drug release is declining. Justified one the other hand by the broad therapeutical potential in psychiatric disorders and the rapid and long-lasting effects, often described after just a single administration. Psychedelics might act here as "*psychoplastogens*[1]", which means that they have neuroplasticity-promoting effects. They might restore synaptic and neuronal dysfunctions, associated with psychiatric disorders, by generating a plastic cellular state in which remodulations and "*brain network resetting*[2]" are likely. Support for that theory comes until now from animal research. One key candidate amongst the class of serotonergic psychedelics, named because they target the 5-HT2A serotonin receptor, is psilocybin. Psilocybin, the compound of hallucinogenic fungi, often referred as "magic mushrooms", is intensively investigated in the treatment of depression, anxiety, obsessive-compulsive disorder and substance abuse disorder.

In this doctoral thesis I first employed human induced pluripotent stem cell-derived cortical neurons for deciphering the effects and therapeutic mode of action of psilocybin. I can show that psilocin (the active metabolite of psilocybin) leads to neuroplastic, morphological and functional changes that start shortly after administration and become manifested in time, such as synaptogenesis. As one of many findings, I can first show a subacute downregulation of the 5-HT2A receptor after psilocin administration, a mechanism well-known to prevent an overshooting of the serotonergic signaling. A normalization provides an explanation for the antidepressant mode of action in depression, where an increased 5-HT2A receptor density is described. Remarkably, psilocin further directly targets main components and associates of the plasmin-generating annexin A2 – S100A10 complex which are on their own key candidates in antidepressant drug response. Not only the core proteins of the complex annexin A2 and p11 as docking station for plasminogen, the precursor of plasmin but also plasminogen-cleaving enzymes were upregulated. But moreover, this complex mediates the cleavage of precursor (pro)-BDNF into mature (m)-BDNF in the brain. In line with that I can first replicate that psilocin increases neurotrophic key factor BDNF and its associated downstream pathways which are linked to neuronal survival and plasticity in a human *in vitro* system. Second, I can first show that psilocin leads to an elevated cleavage of pro-BDNF in m-BDNF. That finding is of paramount importance because recent studies show that actually an imbalance of the pro-BDNF into m-BDNF cleavage, resulting in reduced m-BDNF levels might be more important in depression pathophysiology than total BDNF level reductions.

My doctoral thesis suggests that exposure of human neurons to psilocin provokes a dynamic cascade which induces a state of enhanced neuronal plasticity. That neuroplasticity booster alone could explain why psilocin is effective in the treatment of neuropsychiatric disorders. But moreover, I can directly provide a novel explanation for the antidepressant mode of action of psilocybin. I first describe with the annexin A2 – S100A10 complex a new highly potent drug target for the treatment of psychiatric disorders that paves the way for the development of new antidepressant entities.

Zusammenfassung

Psychedelika haben das faszinierende Potential veränderte Bewusstseinszustände hervorzurufen. Erste vielversprechende Forschung zu ihrer therapeutischen Nutzbarkeit wurde in den frühen 70er Jahren eingestellt als Psychedelika kriminalisiert wurden. Seit den 90er Jahren erlangt die psychedelische Forschung eine Renaissance. Einerseits werden neue psychopharmakologische Wirkstoffe dringend benötigt, da die Zahl der Menschen mit psychiatrischen Erkrankungen ständig zunimmt und die Zahl der neu zugelassenen Medikamente abnimmt. Anderseits ist das breite therapeutische Potential bei psychiatrischen Erkrankungen und die schnelle und langanhaltende Wirkung, die oft schon nach einmaliger Verabreichung beschrieben wird, ein Grund dafür. Psychedelika könnten hier als „*Psychoplastogene*[1]“ wirken, was bedeutet, dass sie neuroplastizitätsfördernde Wirkung haben. Sie können synaptische und neuronale Dysfunktionalität, die mit psychiatrischen Störungen in Verbindung gebracht werden, wiederherstellen, indem sie einen plastischen Zellzustand erzeugen, in dem Umstrukturierungen und eine „*Neuordnung des Gehirns*[1]“ wahrscheinlich sind. Die Theorie wird bisher von der Tierforschung unterstützt. Ein Schlüsselkandidat aus der Klasse der serotonergen Psychedelika, die so heißen, weil sie auf den serotonergen 5-HT2A Rezeptor abzielen, ist Psilocybin. Psilocybin, der Wirkstoff halluzinogener Pilze, die auch als „Zauberpilze“ bezeichnet werden, wird intensiv bei der Behandlung der Depression, der Angststörung, der Zwangsstörung und bei Drogenmissbrauch erforscht.

In dieser Doktorarbeit habe ich als Erstes kortikalen Neurone verwendet, welche aus humanen induziert pluripotenten Stammzellen generiert wurden, um die Effekte und die therapeutische Wirkungsweise von Psilocybin zu entschlüsseln. Ich kann zeigen, dass Psilocin (das aktive Metabolit von Psilocybin) zu neuroplastischen, morphologischen und funktionellen Veränderungen führt, die kurz nach der Verabreichung beginnen und sich mit der Zeit manifestieren, wie der Synaptogenese. Als eine von vielen Erkenntnissen kann ich zunächst eine subakute Herabregulation des 5-HT2A Rezeptors nach der Verabreichung von Psilocin zeigen, ein Mechanismus, von dem bekannt ist, dass er ein Überschießen der serotonergen Signalgebung verhindert. Eine Normalisierung liefert eine Erklärung für die antidepressive Wirkungsweise bei Depressionen, wo eine erhöhte 5-HT2A Rezeptordichte beschrieben wird. Bemerkenswerterweise zielt Psilocin darüber hinaus direkt auf Hauptkomponenten und assoziierte Partner des Plasmin generierenden Annexin A2 – S100A10 Komplexes ab, die für sich genommen Schlüsselkandidaten für das Ansprechen auf antidepressive Medikamente sind. Nicht nur die Kernproteine des Annexin A2 – S100A10 Komplexes als Andockstelle für Plasminogen, den Vorläufer von Plasmin, sondern auch Plasminogen spaltende Enzyme werden hochreguliert. Aber darüber hinaus vermittelt dieser Komplex die Prozessierung des Vorläufers pro-BDNF in das reife m-BDNF im Gehirn. Im Einklang damit kann ich erstmals in einem humanen *in vitro* System nachweisen, dass Psilocin den neurotrophen Schlüsselfaktor BDNF und die damit verbundenen nachgeschalteten Signalwege, die mit dem neuronalen Überleben und der Plastizität verbunden sind, erhöht. Zweitens kann ich zeigen, dass Psilocin zu einer erhöhten Prozessierung von pro-BDNF in m-BDNF führt. Diese Erkenntnis ist von größter Bedeutung, da neuere Studien zeigen, dass ein Ungleichgewicht bei der Spaltung von pro-BDNF in m-BDNF, das zu einer Verringerung des m-BDNF-Spiegels führt, für die Pathophysiologie der Depression wichtiger sein könnte als eine Verringerung des Gesamt-BDNF-Spiegels. Meine Doktorarbeit legt nahe, dass die Exposition von humanen Neuronen mit Psilocin eine dynamische Kaskade auslöst, die einen Zustand erhöhter neuronaler Plastizität hervorruft. Allein diese Verstärkung der Neuroplastizität könnte erklären, warum Psilocin bei der Behandlung neuropsychiatrischer Störungen effizient ist. Mit dem Annexin A2 – S100A10 Komplex beschreibe ich als Erstes ein neues hochwirksames Ziel für die Behandlung psychiatrischer Störungen, das den Weg für die Entwicklung neuer Antidepressiva ebnet.

1 Introduction

1.1 The development of the human brain

The adult human brain is a fascinating organ with about 19 - 23 billion neurons and 60 trillion estimated neuronal connections[3,4]. Brain development starts in the first trimester after gestation and is discussed to be a life spanning process. Maturation and differentiation of glial cells continues during childhood. During development there is a massive overload of neuronal production that is reduced prenatally by programmed cell death by about 50%. An excess of neuronal connections is further eliminated by synaptic exuberance and pruning mostly occurring postnatally. Although neurogenesis is mostly a prenatal process, adult neurogenesis has been described so far in two brain regions, the hippocampal subgranular zone of the dentate gyrus and the subventricular zone (SVZ) of the lateral ventricles[5]. The development of the human brain starts with the invagination of the neural plate leading to the formation of the neural tube at the third week of gestation (embryonic day E20 - E27; E20, meaning 20 days after conception). At the anterior end of the closing neural tube the three primary brain vesicles develop. The embryonic vertebrate brain is divided into the prosencephalon (the most anterior brain vesicle), the mesencephalon and the rhombencephalon. The embryonic prosencephalon develops into the adult telencephalon, the largest part of the brain, and the diencephalon. The rhombencephalon divides into the metencephalon and the myelencephalon, whereas the mesencephalon does not undergo further division. This spatial orientation along the rostral-caudal axis is the first organization process of the developing nervous system. The dorsal region of the telencephalon becomes the adult cerebral cortex. The two hemispheres of the telencephalon enclose the fluid-filled space, the lateral ventricles. The development of the glutamatergic neurons of the cerebral cortex starts with a layer that surrounds the lateral ventricles, called the ventricular zone (VZ). In this region the neural progenitors are located. For review see[4,6]. By mid-gestation the number of neurons is considerably increased by the factor billion[7,8]. This is realized by several rounds of symmetric cell division of mitotic progenitors, the neuro-epithelial cells (NECs), into two identical neural progenitors in order to increase the number of proliferating cells in the VZ. This process starts with gastrulation until E42 and is hypothesized to be significantly involved in increasing the neural progenitor pool[9]. NE cells convert (also morphologically) into radial glial cell (RGC) progenitors. Subsequently, cortical neurogenesis starts with E42 and is completed by E108[10–12]. RG progenitors undergo asymmetrical cell division, marked by the generation either of one RGC progenitor and one post mitotic neuron or of one so-called intermediate progenitor (IP) daughter cell. These cells are transiently amplifying before they give rise to differentiated neurons. The rising number of IPs enables the development of the SVZ. Interestingly, while at early stages the neural progenitors can dived in any kind of neuron in later stages there is fate restriction in the type of neuron, they can form. The newly formed neurons generated by RGC or IP cells leave the proliferative zone and migrate to build up the 6-layered structure of neocortex[13]. For review see[4,14]. The first formed structure resulting from neuronal migration out of the proliferating zone is the preplate (PP). The subsequent migration from neurons into this structure leads to a separation of the PP into an upper

marginal zone (MZ) and a deeper subplate (SP) layer and forms a layer in between, the cortical plate (CP). The six-layered cortex (differing in the composition and type of neurons) of the mature brain is assembled by an inside-out migration process which means that the deepest layer 6 is formed initially by the first wave of migrating neurons. Subsequent migration of neurons forms more superficial layers. When reaching their final destination in the cortex the neurons are integrated in their neural networks by building neuronal processes. The adult cerebral cortex contains about 70-80% excitatory, glutamatergic cortical projection neurons (also known as pyramidal cells) and about 20-30% inhibitory γ-aminobutyric acid (GABA)ergic interneurons[15,16]. While glutamatergic neurons develop at the VZ and SVZ of the developing cortex, GABAergic interneurons derive from the medial and caudal ganglionic eminence (GE) of the ventral telencephalon. Glutamatergic neurons migrate radially and assemble inside-out. In contrast, GABAergic interneurons migrate first tangentially and then radially[16–20]. The single steps of corticogenesis are depicted in **Figure 1.** For review see[4,14].

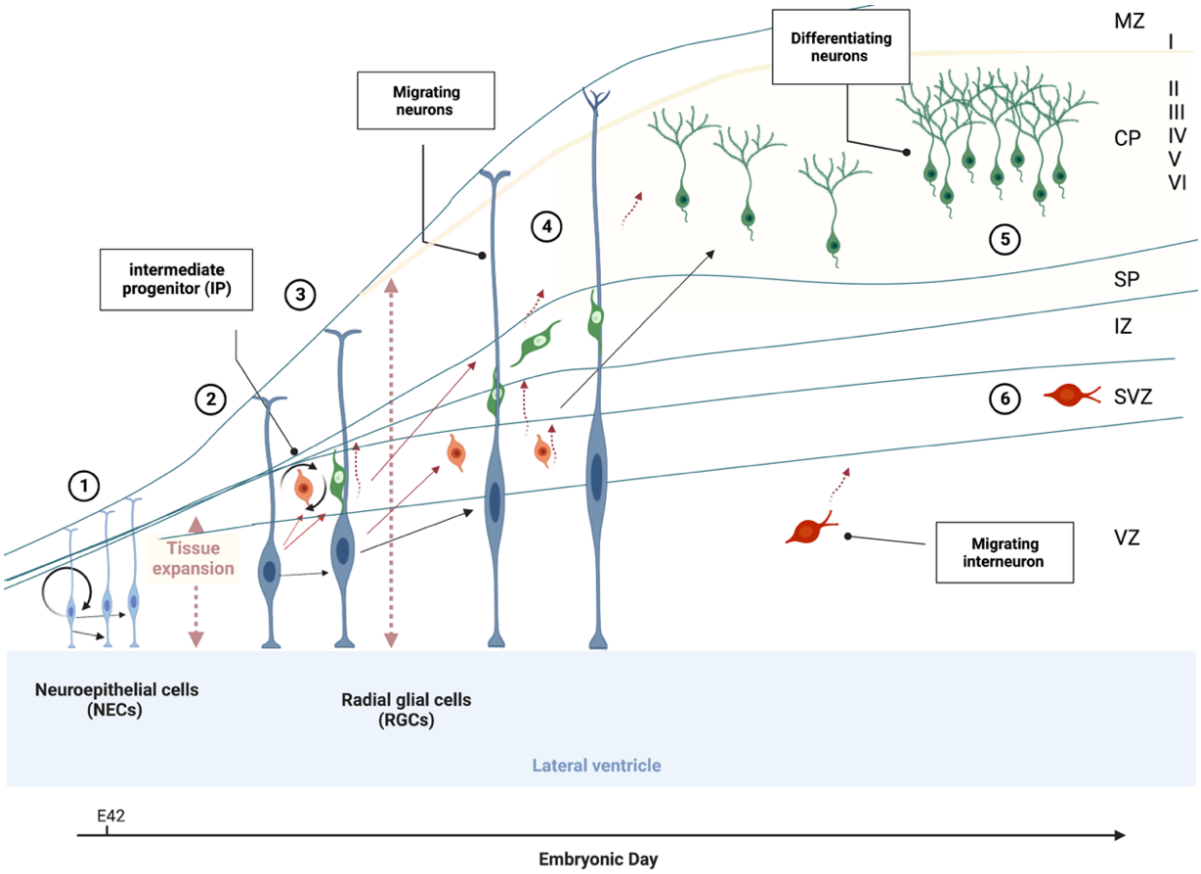

Figure 1. Corticogenesis.
1. NE undergo several rounds of symmetric cell division into two identical neural progenitors to increase the neural progenitor pool. 2. NE cells convert into RG cells which undergo asymmetrical cell division. 3. RGCs generate one RGC progenitor and one post mitotic neuron or one IP that amplifies transiently and give rise to a differentiated neuron, located in the SV. 4. Newly formed neurons generated by RGC or IP cells migrate in the PP (not shown) that is separated into an upper MZ and a deeper SP. Further migration forms a layer in between, the CP. 5. The six-layered cortex assembles by an inside-out migration process which means that the deepest layer 6 is formed first. 6. GABAergic interneurons derive from the medial and caudal GE of the ventral telencephalon. Image based on[14] and created with *Biorender.com.* CP, cortical plate; GE, ganglionic eminence; IP, intermediate progenitor; IZ, intermediate zone; MZ, marginal zone; NE, Neuro-epithelial; NEC, neuroepithelial cells; SP, subplate; SVZ, subventricular zone; RGC, radial glial cell; VZ, ventricular zone.

1.2 iPSC technology and its potential in drug investigation and disease modelling

Adult somatic cells (like fibroblast or peripheral blood cells) can be reprogrammed into induced pluripotent stem cells (iPSCs), thereby regaining all of the pluripotent differentiation potency of an embryonic stem cell (ESC) and show a similar stem cell gene expression profile. iPSCs can be differentiated in all cell types of the three germ layers. Following the seminal Yamanaka protocol, the four transcription factors (TFs) octamer-binding transcription factor 4 (OCT4), sex determining region Y 2 (SOX2), c-MYC and kruppel-like factor 4 (KLF4) are transduced via a viral vector into adult cells[21–23].

It is a powerful tool to generate neurons and neuronal circuitries, model brain disorders and to identify the molecular mechanisms of drug interventions. Further it allows high throughput drug screening (including drug toxicity and drug efficacy testing) and thus paves the way for the development of new psychopharmacological entities. Notably, the reprogramming of somatic cells of patient-derived human origin and the following differentiation into any cell type desired that is disease causing or involved in the aetiology of the disease can be used for disease modelling ("disease in a dish" approach) or for developing personalized medicine. Further, direct conversion or also called transdifferentiation provides the opportunity to directly differentiate somatic cells in the target cell by skipping the reprogramming step in between[24]. Gene editing additionally enables genetical modification for example to generate isogenic controls.

With iPSCs there are no ethical concerns and judicial limitations such as for the work with human ESCs and animal research. And moreover, drugs that are efficiently tested in psychiatric animal models might not be necessarily transferable to the human system[25]. This technology therefore provides a bridge between biological differences of humans and animals. Furthermore, there is no restriction in the accessibility (e.g., the access to human cortical neurons is limited and was based so far on post mortem tissue) and expendability of those cells because of the unlimited expansion potential of iPSCs.

Moreover, stem cell-based therapies have ground-breaking potential particularly as regenerative medicine in neurodegenerative disorders, like Parkinson's and Huntington's disease. Exemplarily in the cell replacement therapy autologous iPSC-derived patient cells can be transplanted and replace damaged cells by healthy ones and thereby eliminating the risk of immune reactions.

The organoid technology, *in vitro* derived three-dimensional cell aggregates that do have an organ-like structure, further refined stem cell technology. With organoids it became possible to reconstruct self-organization of tissue, cell interaction and architecture in a more *in vivo* like environment and thereby mimic organ developmental processes. **Figure 2** summerizes selected possibilities of iPSC technology applications (for review see:[26–29]).

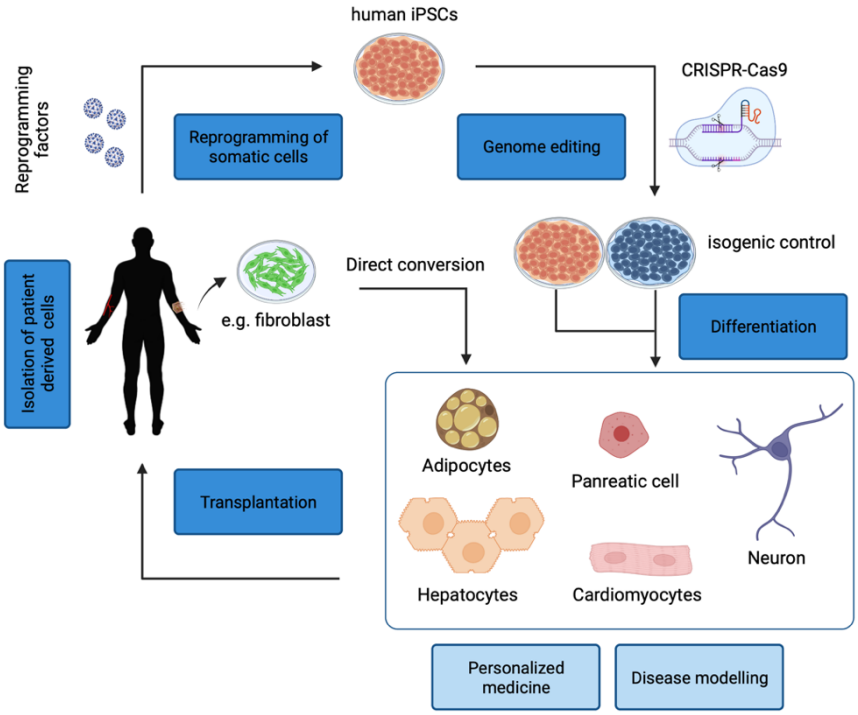

Figure 2. iPSC technology: reprogramming, disease modelling and personalized medicine.
Patient-derived adult somatic cells can be reprogrammed into iPS cells by viral transduction of the TFs OCT4, SOX2, cMYC and KLF4. Genome editing enables the generation of isogenic controls. iPSCs can be differentiated into the desired cell type and used for disease modelling but also for personalized medicine. Genetic modified cells can be transplanted back into the patient. Direct conversion skips the reprogramming step and directly differentiates adult somatic cells in the required cell type. Illustration based on[28] and was generated with *Biorender.com*. Cas9, CRISPR associated protein 9; CRISPR, clustered regulatory interspaced palindromic repeats; iPSC, induced pluripotent stem cell; TF, transcription factor.

1.2.1 Differentiation of iPSCs into forebrain progenitors

Notably, it is possible to generate region-specific NE cells that tend to differentiate into distinct neuronal subtypes. Neural progenitor cells (NPCs) of the forebrain can be gained from iPSCs by dual small mothers against decapentaplegic (SMAD) inhibition of the bone morphogenic protein (BMP) and transforming growth factor B (TGF)-β signaling plus inhibition of the wingless/integrated (WNT) pathway by adding small inhibitor molecules[30–32]. TGF-β pathway inhibition is achieved by the small molecule SB-431542 that blocks the phosphorylation of type-I activin receptor-like kinases (ALKs) ALK4, ALK5 and ALK7 and thereby inhibit SMAD2/3. BMP pathway inhibition is accomplished by small molecule LDN-193189 that blocks BMP type-I-receptors type-I ALK2 and ALK3 and thereby prevent activation of SMAD1, SMAD5 and SMAD8. Both inhibitory processes prevent the TF SMAD from translocating into the nucleus. Whereby, XAV939 is used as a WNT pathway inhibitor. As a consequence, stem cells become NP cells with forebrain identity by default. Functional human induced neurons (iN) can be also gained through direct conversion of fibroblasts by overexpressing the three

neurogenic TFs achaete-scute family bHLH transcription factor 1 (ASCL1), BRN2, myelin transcription factor 1 like (MYTL1) in the mouse[33] or by adding neuronal differentiation (NEUROD)1[34], respectively ASCL1 and neurogenin 2 (NGN2)[35,36]. While epigenetic and genomic traces of aging are removed in iPS cells, direct conversion can conserve it.

1.3 Psychedelics

Psychedelics are mind-altering substances that have the fascinating "*capacity [reliably] to induce states of altered perception, thought, and feeling that are not experienced otherwise except in dreams or at times of religious exaltation*"[37]. Manifold and broad symptoms are described which include changes in perception (visual, auditory or somatosensory) and in mood and memory, spiritual and mystical experiences but also states of depersonalization and derealization[38,39].

The intra- (within one subject) and interpersonal (between subjects) heterogeneity of the perceived symptoms towards those drugs depends also on the so-called "set and setting"[40]. Meaning that the current mental expectation, the beliefs and thoughts about those drugs and their expected effects ("set") but also the present situation in which the drug is administered, the environmental surrounding ("setting"), influence the users' response to the drug. For example, non-pharmacological factors like personality traits, the emotional state before drug intake and the experience of psychological problems are associated with mystical and pleasant experience[41]. But still the concentration of the drug dose is the best predictor for the acute drug effects[42,43]. For example, mystical-type experience augmented with increasing psilocybin doses as well as positive ratings about attitudes, mood and behavior[44,45]. For review see[46,47].

The psychedelic experience has long-term effects on personal well-being but also can lead to changes in personality traits. For example, even 14-month after a session with a high psilocybin dose 58% of healthy participants state this trip as *"among the five most personally meaningful"* experiences of their lives[48]. And 67% of the participants described it as amongst the "*five most spiritual significant experiences*" of their lives[48]. That is in line with a finding from Studerus and colleagues that still 8 to 16-month after psilocybin administration this experience is described as very enriching[49].

Even if personality traits are considered to be relatively stable over the adult life span Griffith and colleagues could show that a high-dose of psilocybin can in fact change the openness personality domain as one of the big fives of personality traits measured be the NEO Personality Inventory[50]. Those effects indeed remained even stable for one year if a mystical experience was reported[50]. A metanalysis could show that around 40% of the interviewed 110 participants reported long-lasting changes in their so-called "aesthetic experiences" and the connection to the environment and the nature after psilocybin intake[49]. That is in line with a previous study showing that lysergic acid diethylamide (LSD) administration led to subjective perceived changes. Participants reported themselves as less anxious,

less egocentric, less materialistic and aggressive. On the contrary, the stated themselves as more understanding towards self and others, more tolerant and more appreciative of music and art[51]. Studerus argues that psychedelic administration therefore has the "*potential of increasing life satisfaction*"[49] (for review see:[47]).

Long lasting illegalization and stigmatization of psychedelics led to safety concerns in public and politics. Particularly, histories about the so-called "horror-trips" or "bad-trips" (meaning aversive emotions or feelings during a psychedelic trip) or "flashback" (delayed, intermittent recurrence of symptoms[52]) are apparently inerasable anchored in several people's minds. Although, psychedelics do not provoke addiction or dependency[53] in Germany most psychedelics are listed as "Betäubungsmittel" in the „Betäubungsmittelgesetz" (BtMG) under annex I and are illegal. An exception can only be requested for research purposes.

In a meta-analysis investigating the acute and long-term effects of psilocybin administration most of the 110 participants of the study experience the session as "*pleasurable*", "*enriching*" and "*non-threating*"[49]. Nevertheless, in a comparable study 39% of interviewed participants describe the consumption of psilocybin as top 5 of the most challenging experience of their lifetime and even 11% admitted that they put self or others at risk of physiological harm[54]. But the likelihood of risk for adverse effects was dependent on drug dose, duration of the experience and absence of social support[54]. Psychological adverse drug reactions like dysphoria, panic or anxiety can be found in a small proportion of subjects especially after application of high doses but were manageable by social support[49]. The authors argue that there is an acceptable level of risk by applying moderate drug doses to well-prepared and screened subjects under monitored setting[49].

Another often mentioned adverse reaction, nonspecifically defined as "flashbacks" (meaning the sudden and unexpected reoccurrence of all or certain aspects of hallucinogenic aspects later after drug intake) was first described by Sandison and Cooper[55]. "Flashbacks" can be diagnostically covered by the Hallucinogen Persisting Perception Disorder (HPPD) in the Diagnostic and Statistical Manual of Mental Disorders (DSM)-V or by the International Statistical Classification of Diseases and Related Health Problems (ICD-10) diagnosis under the F16 code "Mental and behavioral disorders due to use of hallucinogens"[56,57]. HPPD can be persisting for month or years and causing substantial morbidity but is less common in research or treatment settings than for illicit use[58]. Interestingly the prevalence of HPPD is unknown[59].

But those risks are of psychological and not of physiological nature since there is low physiological toxicity and organic brain damage[52,60,61]. Although hallucinogens are the substances with the least toxicity risk[62] (for example psilocybin has the least risk for dependency amongst the substances analyzed[63]) as physical side effects nausea, mydriasis and an increase in blood pressure and pulse are described[60,64]. A metanalysis of studies where neurophysiological test were carried out on LSD or other hallucinogenic users found few long-term neurophysiological deficits attributable to hallucinogen use but also points out that confounding variables like premorbid cognitive and personality function and

prior substance abuse complicated interpretation[65]. Another metanalysis shows that the administration of psilocybin is safe and tolerable and does not cause acute or long-lasting negative effects[49]. There was no evidence for subsequent drug abuse, persisting perception disorders, psychosis or long-term impairments[49] and non-significant risk for changes in personality and attitudes[52]. For review see[60].

There are numerous termini (also interchangeable used) for substances that have mind-altering properties such as hallucinogens, psychedelics, entheogens (ancient Greek: "god within"), psychotomimetics (means that they introduce a mental state that fosters psychosis[66]), emphatogens (terminus by Metzner, 1985 which means that they induce feelings of empathy, today also known as entactogens meaning "touching within"[67]). The wording is often demonstration of the political or theoretical background of the person using it[40,68]. In this doctoral thesis I will follow the overall tendency to choose the term "psychedelics*"* instead of the also popular wording "hallucinogen*"*, which is often used to include a broader category of psychoactive substances. The main reason for my decision is that not all of those substances provoke hallucinations and if they do so, hallucinations are only one effect of the drugs, often experienced in non-ordinary high doses[60]. The term "psychedelic" was created by Humphrey Osmond because of the "mind manifesting capability" of those psychoactive drugs[69]. For review see[46,47].

There is the categorization into classical and non-classical psychedelics. Classic psychedelics are for example LSD, psilocybin, ayahuasca/*N*,*N*-dimethyltryptamine (DMT), 5-methoxy-*N*,*N*-dimethyltryptamine (5-MeO-DMT), ibogaine and mescalin. Those drugs do have an indole molecular structure, which non-classic psychedelics do not contain[70]. Non-classic psychedelics are for example the dissociative anesthetic ketamine and the entactogen 3,4 Methylenedioxymethamphetamine (MDMA). Classical psychedelics can be further grouped by their alkaloid groups in the tryptamine group, such as psilocybin, LSD and DMT. The second is the phenethylamine group, with the well-known representant mescaline.

The structural similarity of serotonin, that was detected 1953 in the human brain[71], with the tryptamine of LSD (discovered previously by Hofmann in 1943[72]) led to the conclusion that mental changes caused by LSD arise from an "*interference with serotonin in the human brain"*[73]. And in fact, serotonergic hallucinogens unfold their mechanistic action as agonists or partial agonists of the brains' serotonin 5-hydroxytryptamine receptor 2A (5-HT2A-R)[74,75]. Those agonists do have structural similarity to the neurotransmitter serotonin (5-hydroxytryptamine, 5-HT).

Non-classical psychedelics unfold their action by different biological mechanisms. **Figure 3** lists the chemical structure of psychedelic compounds and their origin in nature. For review see[46,47,60].

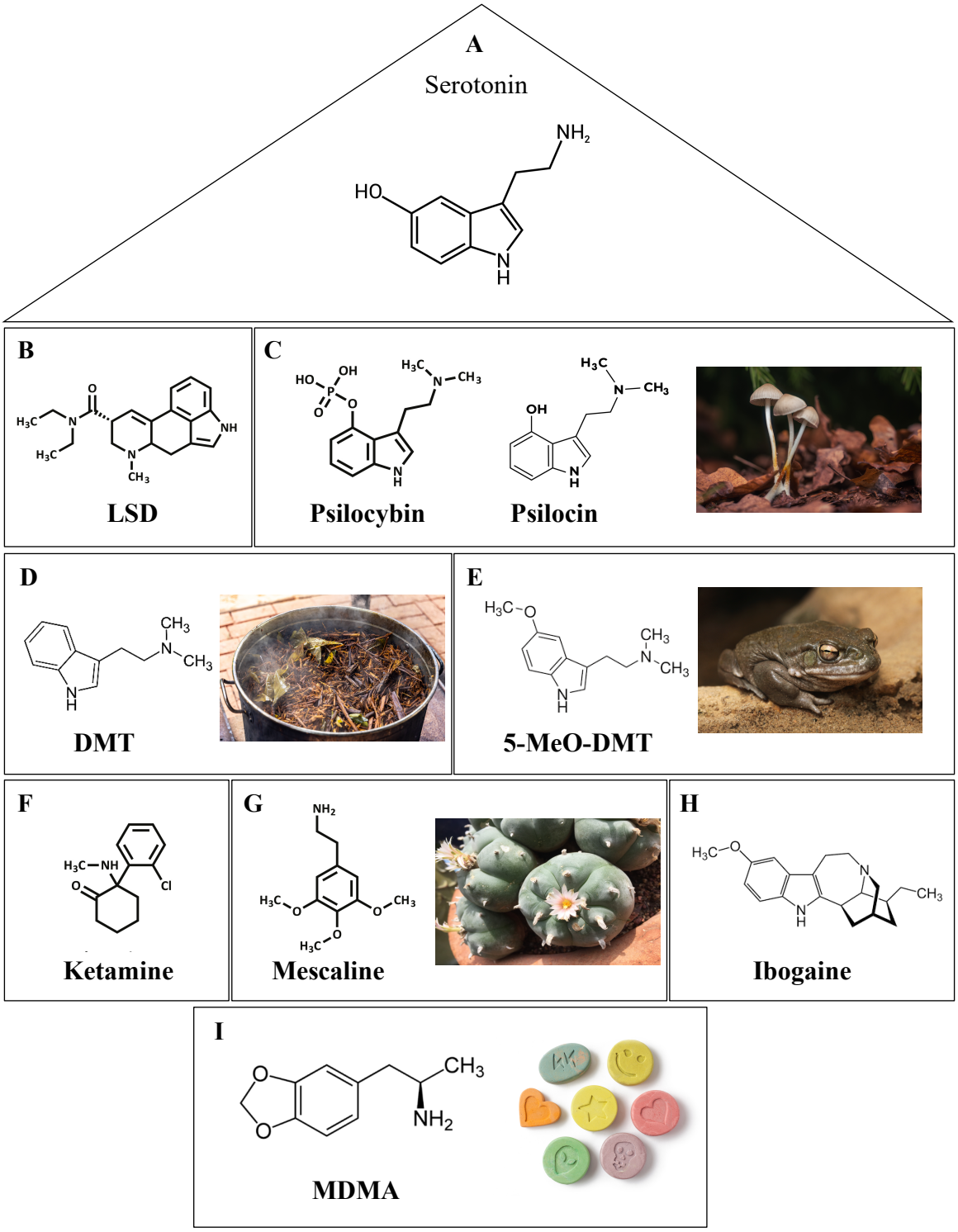

Figure 3. Chemical structure of psychedelic compounds of serotonin analogues.
(A) Serotonin. **(B)** Semi-synthetic d-lysergic acid diethlyamide (LSD). **(C)** Mushrooms of genius *Psilocybe*, so-called „magic mushrooms“ contain pro-drug psilocybin and its active principle psilocin. **(D)** Psychoactive Ayahuasca „tea": *Psychotria viridis* leaves (plant containing *N,N*-Dimethyltryptamine (DMT)) is brewed with the bark of *Banisteriopsis caapi* (monoamine-oxidase inhibitor preventing break down of DMT). **(E)** Colorado River Toad (*Incilius alvarius)* secretes 5-methoxy-dimethyltryptamine (5-MeO-DMT) for its defense. **(F)** Dissociative ketamine. **(G)** Peyote cactus (*Lophophora williamsii*) containing mescaline. **(H)** Ibogaine and **(I)** entactogen 3,4-Methylenedioxymethamphetamine (MDMA) containing Ecstasy pills. Image sources purchased from *Adobe Stock (stock.adobe.com).* Chemical structures are derived from PubChem (*https://pubchem.ncbi.nlm.nih.gov).*

1.3.1 Psilocybin

Psilocybin (4-phosphoryloxy-*N,N*-dimethyltryptamine) is the psychedelic compound, of so-called "magic mushrooms" hallucinogenic fungi which mostly belong to the genus *Psilocybe*, isolated first 1958 by Albert Hofmann[76–78]. Psilocybin is quickly converted in the intestine to psilocin after ingestion, the active principle of psilocybin that can cross the blood brain barrier[79]. The intake of 12 - 20 mg of psilocybin, which is considered to be a moderate dose, leads to psychedelic effects that starts 10 - 40 minutes (min) after ingestion, last for 3 to 6 hours (hrs) with a peak after around 80 min[80]. From a chemically perspective psilocybin is an indolamine that is structurally similar to the neurotransmitter serotonin. Psilocin is therefore an agonist of the 5-HT2A receptor (5-HT2A-R) but it also non-selectively binds to other serotonin such as 5-HT1A/B/D/E, 5-HT2B, 5-HT5, 5-HT6 and 5-HT7 receptors. For review see[47,79,81] .

1.3.2 Brief overview of psychedelic history

Descriptions and drawings of indigenous cultures indicating the ancient use of hallucinogenic and psychoactive natural occurring plants can be found all over the world[82,83]. Both naturally occurring plant-hallucinogens and newly chemically synthesized hallucinogenic substances (like LSD) are used in spiritual and ritual ceremonies as wells as for hedonic reasons. First experimental trials to make use of psychedelics started in the 50's by the US army and the CIA who tested those secretly as incapacitating or interrogation agents, often and without the ethical consideration of informed consent. Since the 50's and 60's the effects of psychedelics were first investigated for therapeutical application in psychiatric disorders. During that early time frame already hundreds of papers were published. Early psychedelic research focused mainly on terminally illness (e.g., cancer) for improving the acceptance and anticipation of upcoming death[84–86]. Another big research pillar was the induction of psychosis- or schizophrenia-like states by psychedelics to get insides of the development of schizophrenia because of the relative similarity of the psychedelics effects with those described during psychosis[87–91]. Focus was also set on research on the treatment of substance dependency[92–96]. A myriad of those studies showed promising outcome but have nowadays to be interpreted with care because of their methodological weakness compared to modern empirical research standards. For example, non-inclusion of control groups or anectodical descriptions complicated reproducibility and study comparability. A high variation of methods and lacking of standardization led to inconsistent results. Moreover, often those studies ignored (or were not aware of the importance) of the concept of "set and setting". The application of high doses of the drugs to not well-prepared and informed participants made some of the studies ethical critical from modern perspective. But also approaches of implementing psychedelic administration in psychotherapy developed over time, elaborating the importance the concept of "set and setting"[97–104].

Simultaneously, the consumption of psychedelic drugs moved into the publicity and became one of the hallmarks of the "flower power movement", with its origin in the United States and considerably shaped the mental spirit of a whole epoque. The open consumption of drugs like LSD and marijuana of the "love and peace movement", mostly carried by college students and "hippies" revolting against war and authorities and for sexual openness provoked consternation in broad civil society groups and politics. Drugs were seen as causative for rejection of mainstream and public order by the youth. Horror stories about side effects causing health damage were circulating and are still present today. At the same time honest research trials became apparently discredited by colorful characters like the prominent Harvard University professor Timothy Leary, who openly animated to the consumption of drugs. As a result, already in the 60's and early 70's restrictive prohibition and criminalization of psychedelics, originating in the United States, terminated promising research for about three decades. It was not until the 90's psychedelic that psychedelic research reveals revival and psychedelics are nowadays discussed as game changer in the psychopharmacology of psychiatric disorders. For review see[60]

1.3.3 Crisis of classical psychopharmacotherapy

More and more studies were recently published that criticize classical drugs in terms of their effect dependency on environmental factors, responsiveness, side effects and modifications of the brain architecture following drug administration. For example, Alboni and colleagues performed a study in order to explain the inconsistent and incomplete effects of selective serotine reuptake inhibitors (SSRIs) in the treatment of depression[105]. They exposed mice to chronic stress to induce a depression-like phenotype and then treated them with the SSRI fluoxetine. They figured out that those mice that where in the following exposed to an enriched environment improved their depression-like phenotype compared to a control condition while those mice that were exposed to a stressful condition showed a worsening. They argued that not the drug itself "*determines*" the effect on the depression-like phenotype but the drug "*induces*" it[105]. Concluding that depending on the environment in which the patients live SSRI intake might provoke an antidepressant outcome or not. Gueorguieva and colleagues classified the response trajectory of patients who received SSRI and those who received a placebo. The majority of patients which were treated with SSRI showed an improvement compared to a placebo group (called "trajectory responders") but some of them developed even worse (so-called "trajectory non-responders"). Interestingly, that implies that the mean response of trajectory SSRI non-responders was significantly lower than the mean response of placebo takers, underlining the inconsistency of treatment effects[106]. Also, the time delayed onset of drug actions as well as the risk of recurrency of symptoms is problematic. It is well- known that it takes weeks to months for classic antidepressants to reach their full effects[107]. Remarkably, the recurrency risk for new episode of mania or bipolar depression, depression,

panic disorder or schizophrenia is much shorter after discontinuing abruptly lithium, antipsychotics, antidepressants or psychotropic medication than after gradual discontinuation[108–110]. Both phenomena increase the risk for patient morbidity. Another point that has to be considered in the long-term use of antidepressants is that they are less efficient in recurrent depression and in prevention of relapse[111,112]. Moreover, it has been described that they could worsen long-term outcome and cause paradoxical effects[111]. Ironically, the chronic administration of antidepressants diminishes subsequent pharmacological response and reduces remission phases and increases thereby vulnerability for depression and relapse[111,112]. The "oppositional model of tolerance" explains that the continued treatment leads to drug tolerance because it stimulates processes that oppose the initial acute effects of a drug[113]. Shockingly, patients suffering from such a antidepressants tolerance, called tachyphylaxis, showed an initial good response to the drug[114]. The recurrence of depressive symptoms despite ongoing treatment is not rare[115]. Also, side effects that are developed during ongoing antidepressant treatment, such as tardive dysphoria, a chronic depressive state, are well described[116]. As a result, there is growing concern about classical psychopharmacological treatment and at the same time the development and the approval of new psychopharmacological drugs is declining[117]. Particularly, in consideration of the massive social and socio-economic burden caused by a dramatically high number of patients suffering from psychiatric disorders, unpredictably rising, there is a huge need for the development of new medications[118,119]. For review see[2,47,60].

1.3.4 Psychedelics as drugs in the treatment and research of psychiatric disorders

Since the 90's psychedelics have become again the subject of an intriguing stream of clinical research in psychiatric disorders[2,120]. New hints for therapeutic benefit came from the dissociative ketamine, an *N*-methyl-d-aspartate (NMDA) receptor antagonist and anesthetic. Ketamine is well described for its rapid and robust antidepressant effect in treatment resistant depression (TRD) or bipolar depression also in comorbidity with persisting suicidal thoughts[121–127]. Double-blinded clinical studies with single doses and/ or repeated doses of ketamine show a significant decrease in depressive symptoms, suicidal ideation within hrs after acute treatment as well up to 3-month follow ups[121–127]. Moreover, symptoms of patients with chronic posttraumatic stress disorder (PTSD) with comorbid depression are significantly reduced[128]. Ketamine also shows remarkable effects in substance use disorder (SUD), like alcohol, cocaine and opioid dependency. Abstinence rates are significantly increased and use rates and craving are decreased[129–135]. The therapeutical potential and additional benefit of ketamine compared to the classical antidepressants like SSRIs is mostly seen in its therapeutical velocity. Meaning that compared to classical drugs the broad therapeutical effect of this psychedelics is rapid, robust and described after a single administration[136]. That insight opens the

research field in searching more fast-acting substances that do have ketamine-like effects in the spectrum of psychedelic substances.

Serotonergic psychedelics like MDMA, DMT and psilocybin again came in the spotlight of research. And in fact, modern clinical research supports a role for serotonergic psychedelics in the effective treatment of various psychiatric disorders. Exemplarily, the administration of MDMA in two 8-hrs drug-assisted psychotherapy sessions to treatment-resistant chronic PTSD patients lead to a fast and long-lasting (up to 45 month) significantly reduce in PTBS symptoms[137,138]. This finding could be replicated in a randomized, double-blind, active-placebo controlled study[139.] Further, in an open-label study with recurrent depressive patients, treatment with ayahuasca, with its psychoactive component DMT, lead to a significant decrease in depressive symptoms only hrs after drug intake that was stable within 21 days[140,141].

Psilocybin is discussed as fast-acting and long-lasting antidepressant in anxiety as well as in depression, TRD populations, obsessive-compulsive disorder (OCD), addiction and life-threatening cancer[142–152]. For example, it has been shown in open-label trials in a cohort of TRD that two oral doses of psilocybin led to reduction in depressive symptoms within 5 weeks post-treatment, persistent up to 6 months[143,152]. A moderate dose of psilocybin led to a significant reduction in anxiety, and mood improvement up to 6 months post treatment studied in a double-blind, placebo-controlled study of patients with advanced-stage cancer and anxiety[145]. Not surprisingly psilocybin is stated as "breakthrough therapy" by the United States Food and Drug Administration (FDA) in the treatment of depression since 2019. Moreover, alcohol dependence and craving significantly decreased following psilocybin administration within 4 weeks, stable in a 36-weeks follow up in in patients with alcohol dependency[149,150], supporting the role of psilocybin in treatment of SUDs. Heavy drinking days where significantly reduced 32 weeks following psilocybin administration in alcohol use disorder (AUD) patients that receive the drug and psychotherapy compared to a control group that receives only psychotherapy and an active placebo[153]. Furthermore, psilocybin shows beneficial effect in treatment of tobacco addiction[154–156]. Aside from that, the former idea of using psilocybin and ketamine as a model (or covering at least some aspects) for psychosis as one symptom of schizophrenia regains revival[157–161]. For example, the activation of 5-HT2 receptors by psilocybin is similar to metabolic findings in acute psychosis in schizophrenia in positron emission tomography (PET)[158].

Finally, it should be mentioned that in psychedelic-assisted psychotherapy (PAP) psychedelics are applied for therapeutical purpose by trained psychotherapists[60,118]. In Germany already ketamine-assisted psychotherapy is offered. Numerous phase II studies, mostly with psilocybin, are running recently in order to further investigate the effect of psychedelics in psychiatric disorders and to contribute to their legalization and usage as medication.

1.4 Mental disorders

Mental disorders are a global burden which count estimated for 14.3% of deaths worldwide, which are notably 8 million deaths per year also because there is an increased risk for committing suicide[162,163]. Moreover, mental disorders accounted for 7.4% of disability-adjusted life years (DALY) worldwide and are the leading cause of years lived with disability (YLD)[164]. Direct (e.g., for medication) and indirect costs (e.g., because of income loss) make them to a global public health problem[165]. Among those Major depressive disorder (MDD) count for 40.5 % of DALYs caused by mental disorders[164]. It is a severe and highly prevalent (affects one in six adults in their lifetime, mostly female) psychiatric disorder[166,167]. The symptoms range from loss of pleasure and interests, impaired cognition and memory, disruptions in sleeping, eating and sexual activity[167]. Alarming is the constantly increasing number of patients (increased incidence among quarantined people during COVID pandemic[168]) which can be indirectly detected by augmentation of antidepressants prescriptions in adolescents and adults[168]. AUD count for 9.6 % of DALYs caused by mental disorders and is therefore among the most prevalent illness which accounts to the world's largest risk factors for premature mortality (reduction of life expectancy of more than 20 years), disability and loss of health[164,169]. Diagnosis criteria include heavy alcohol use and loss of control over alcohol intake, craving, unsuccessful effort to stop drinking despite social, interpersonal, biological and psychological problems caused by alcohol consumption[170]. Bipolar disorder (BD) belongs to the affective disorders with a lifetime prevalence of 2.4%[171] and is characterized by recurrent manic (diagnosed in DSM-V as BD 1) or hypomanic (diagnosed in DSM-V as BD 2) episodes that can alternate with depressive episodes. Symptoms within a manic episode might include feelings of grandiosity, disinhibition, distractibility, elevated mood, decreased need for sleep, engagement in risky behaviors and can also include psychotic symptoms. Hypomania is accompanied by milder manic symptoms. However, depression is the most common BD symptom which is often described as first episode. Depressive episodes last longer than manic or hypomanic episodes during the course of the disease[172]. BD count for 7.0 % of DALY caused by mental disorders and is one of the leading causes for disability with a tremendous suicide risk (20 - 30 % greater than in general population)[164,172–174].

1.4.1 Cognitive and neuronal dysfunction in psychiatric disorders

Promising research results lead to the question about the potential therapeutical mechanisms of psychedelics in psychiatric disorders patients. It is widely accepted from functional magnetic resonance imaging (fMRI), post-mortem and cellular studies that patients and animal models of neuropsychiatric disorders and stress show alterations in prefrontal brain structure and functionality. Cognitive impairments such as cognitive inflexibility, rigidity and executive dysfunction are for example known in depression and addiction[175–180]. A meta-analysis that includes MRI images of about 16,000 patients

with psychiatric disorders like schizophrenia, BD, MDD, addiction, OCD and anxiety disorders showed that those heterogeneous disorders shared a common grey-matter loss in brain areas that are involved in executive functions[181]. Notably, it is discussed that neuropsychiatric disorders are (or at least partially) caused by synaptic dysfunction because many synaptic proteins are linked to psychiatric disorders and synaptic dysfunction has been described. The theory is so well known that the term "*synaptopathy*" has been coined[182]. Also, disruption in spine density, spine morphology and retraction of dendrites and spines as well as neuronal atrophy, loss of synapses and decreased brain size indicates a disruption in neuroplasticity[1,181–188]. Recent studies further suggest a reduction in immediate early genes (IEGs) in psychiatric disorders and stress. IEGs are molecular markers for plastic brain changes that contribute to long-term neuronal plasticity related to learning and memory that are often affected in psychiatric disorders[189–191].

1.5 Psychedelics and neuronal plasticity

Nichols and colleagues provide a cognitive theory for the reason of the therapeutical effects of psychedelics. Psychedelics may act by "*destabilizing local brain network hubs and global network connectivity"* that enables "*brain network resetting*"[2]. Particularly for psychiatric disorders, the administration of psychedelics may generate a plastic cellular state where remodulations of the neuronal network are likely.

1.5.1 Psychedelics as mediators of global brain activity and neuronal excitability

Hint for that theory on a global brain level came from fMRI studies. Daws and colleagues found a decrease in in fMRI network modularity, arguing that antidepressant effect of psilocybin is based on a global increase in brain network integration[192]. Further they found that 5-HT2A rich higher-order networks are more functionally interconnected after drug administration[192]. Overall insights of animal and human fMRI studies indicate that psychedelics reduce brain activity, although opposing opinions are also represented because the 5-HT2A-R is expressed on excitatory pyramidal glutamatergic neurons and on inhibitory GABAergic interneurons[193–198]. Acting on glutamatergic neurons the resulting glutamate release would lead to an increase excitability while activating GABAergic interneurons and the subsequent GABA release would decrease excitability[198]. Lee and colleagues argue that *the actions of psilocybin might be due to a mixture of actions on both excitatory and inhibitory neuronal circuits*[199]. Most likely the excitability outcome might be therefore an interplay between activating excitatory and inhibitory neurons, as psilocin does not exclusively target one type of neuron.

For example, DOI reduces low-frequency oscillations and disorganizes prefrontal network activity, which is reversed by antipsychotic drugs, and decreases activity of pyramidal neurons in the prefrontal cortex (PFC)[200,201]. And serotonin itself reduces rat prefrontal gamma oscillations[202]. In human fMRI studies psilocybin reduces brain activity (e.g., cerebral flood flow (CBF) and blood-oxygen-level-dependent (BOLD) signal and oscillations) and connectivity[203–205], hypothesized as reflecting a state of unconstrained cognition and increasing brain network entropy[203,204]. Moreover, the oscillatory power was reduced in posterior and frontal association cortices and the default-mode network (DMN, "task negative" network present at a default or baseline state, given up during goal-directed tasks[206,207]), suggesting a desynchronization of oscillatory rhythms after psilocybin intake[208]. Interestingly, reduction in CBF and in the amygdala could be correlated with reduced depressive symptoms following psilocybin administration in TRD[148]. Psilocybin and ketamine treatment increase the cognitive flexibly, in case of psilocybin up to 4-weeks post treatment in MDD patients[176,209]. Contrary, psilocybin increases PFC glucose metabolism in a PET study[158].

Two studies shows that psilocybin and DOI increase excitatory glutamatergic neurotransmission *in vitro*. The frequency and amplitude of miniature excitatory postsynaptic currents (mEPSCs) and spontaneous excitatory postsynaptic currents (sEPSCs) after psilocybin or DMT treatment was significantly increased in rodent brain slices of medial frontal cortex (mFC), respectively medial prefrontal cortex (mPFC) neurons, suggesting increased excitatory neurotransmission[1,210]. Also, here the data situation is inconsistent. Because another study could clearly show that activation of 5-HT2A/2C receptors by agonists reduced neuronal excitability[211]. In order to administer the effect of DOI they performed whole-cell-patch clamp recording *in vitro* of cultured cortical neurons. Bath-applied DOI (just as serotonin) depressed spontaneous action potentials (APs) and decreased current-evoked-firing[211].

1.5.2 Psychedelic induce molecular and cellular changes

Interestingly, despite promising clinical studies, the molecular and cellular changes induced in the patients' brains – on a single cell or network level after psychedelic drug administration are barley understood and come mostly from animal studies. But many papers show striking evidence for a clear association of psychedelics administration and the promotion of synaptic plasticity. For example, a guiding study by Olson and colleagues in 2018 showed that the treatment with serotonergic psychedelics promote the growth of dendritic spines, increase the synthesis of synaptic proteins, strengthen synaptic responses and promote neuritogenesis[1]. They coined the expression "*psychoplastoge*n'', originating from the Greece words: *psych* (mind), - *plast* (molded), - *gen* (producing) which underline the plasticity promoting effects of those serotonergic substances tested[1]. In detail they examined psychedelics and entactogens (like DMT, psilocin, 2,5-dimethoxy-4-iodoamphetamine (DOI), MDMA and LSD). Those substances increased (most potently by LSD) dendritic arbor complexity (reflected by total length and

number of branches) in embryonic rat cortical neurons *in vitro*[1], already replicated for 5-MeO-DMT administration in mice dentate gyrus *in vivo*[212].

Olson and colleagues further showed that 24 hrs treatment with DOI, DMT, and LSD promote spinogenesis and synaptogenesis in mature rat cortical cultures, demonstrated by a shift in spine morphology, supporting immature (thin and filopodium) over more mature (mushroom) spine types and increased co-localization of pre- and postsynaptic marker vesicular glutamate transporter (vGLUT) and postsynaptic density 95 (PSD-95) protein. Ketanserin (a 5-HT2A-R antagonist) blocked the effect on dendritic spines, suggesting a 5-HT2A-R mediation[1]. Dakic and colleagues confirmed an upregulation of proteins involved in formation of dendritic spines and cytoskeletal reorganization after 5-MeO-DMT administration in human cerebral organoids[213].

Additionally, psychedelics can stimulate proliferation, adult neurogenesis and cell survival. Exemplarily, the non-psychedelic alkaloid harmine, one major component of ayahuasca, can efficiently increase proliferation in human NPCs and increase adult mice neurogenesis *in vitro*[214]. One *in vivo* study confirmed adult neurogenesis after a single injection of 5-MeO-DMT in adult mice in dentate gyrus[212]. And DMT increases survival of iPSC-derived human cortical neurons under hypoxic stress, suggesting an important neuroprotective function in ameliorating the adverse effects of hypoxic or ischemic brain insult[215].

Moreover, psychedelics lead to an increase in IEGs, like cFOS, early growth response protein (EGR)1 and EGR2 [216–224]. While *EGR1* and *EGR2* genes are specifically upregulated by psychedelics, *cFOS* upregulation also occurred after non-hallucinogenic drug administration[221,224]. This expression of IEGs is explainable by mitogen-activated protein kinase (MAPK) pathway activation, already shown for LSD[225].

1.6 Pathways associated with the psychedelic mode of action

In the following the psychedelic associated 5-HT2A-R and the m-BDNF associated downstream pathways are discussed in detail and illustrated in **Figure 4.**

1.6.1 The serotonergic 5-HT2A receptor plays a key role in psychedelic-mediated neuroplasticity

There are 14 classes of serotonergic receptors. All are G protein-coupled receptors (GPCR), except 5-HT3, which is a ligand gated ion channel[226–229]. The 5-HT2 receptor superfamily consists of the 5-HT2A, 5-HT2B and 5-HT2C receptors[230]. The 5-HT2A-R is widely expressed in the brain[231] such as in the frontal cortex with highest level in layer 5 pyramidal neurons[194–197,231–234]. 5-HT2A-R activation plays a leading role in psychedelic-mediated response (please refer to **Fig. 4**).

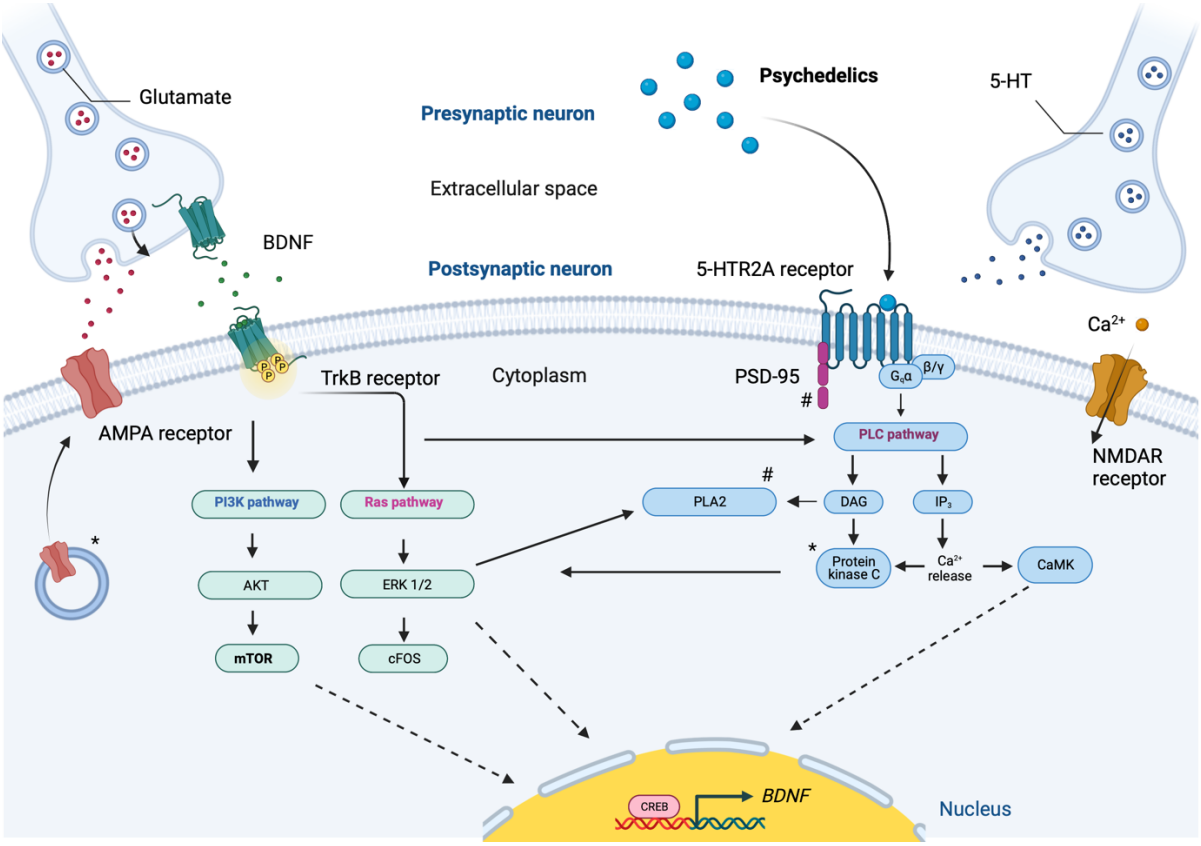

Figure 4. Schematic (and incomplete) presentation of signal transduction pathways hypothesized to be involved in psychedelic-mediated neuroplasticity in the cortex.
Serotonergic psychedelics bind to the 5-HT2A-R and activate via G-protein amongst others PLC and PLA pathways. Similar to m-BDNF-TrkB complex activation this leads to an increase in intracellular Ca^{2+} and PKC activation. BDNF binds to the TrkB receptor and activates mTOR signaling and NMDAR-mediated synaptic plasticity over the PI3K/AKT pathway. Hallucinogen induced glutamate release provoked mTOR activation and BDNF release which is AMPAR-mediated. 5-HT2A-R activation stimulates glutamate release, thus AMPAR upregulation and trafficking and increases glutamatergic signaling and BDNF release. Further, m-BDNF-TrkB complex and 5-HT2A-R activation stimulate the expression of IEGs, like cFOS. 5-HT2A interacts and co-localizes with PSD-95. The PI3K and ERK 1/2 signaling cascades and CaMK activate CREB that mediates BDNF gene transcription. Image generated with *Biorender.com* and based on[81]. 5-HT, Serotonin; 5-HT2A-R, serotonergic 2A receptor; AKT, protein kinase B; AMPAR, α-amino-3-hydroxy-5-methyl-4-isozalopropionic acid receptor; BDNF, brain-derived neurotrophic factor; CaMK2, Ca^{2+}/calmodulin-dependent protein kinase; CREB, cyclic AMP-responsive element-binding protein; DAG, diacylglycerol; ERK 1/2, extracellular regulated kinase 1/2; IP3, inositol triphosphate; IEGs, immediate early genes; MAPK, mitogen-activated protein kinase; mTOR, mammalian target of rapamycin; NFκβ-α, nuclear factor kappa B protein complex alpha; NMDAR, N-methyl-D-asparate receptor; PI3K, phosphatidylinositol-4, 5-bisphosphate 3-kinase; PSD-95, postsynaptic density 95 protein; PKC, protein kinase C; PLA2, phospholipase A2; PLC, phospholipase C; TrkB, tropomyosin receptor kinase B.

Serotonergic psychedelics mainly (but not exclusively) target this receptor that is responsible for the mind-altering effects, known because selective inhibition leads to an abrogation of the psychedelic induced neurophysiological and neuroplasticity effects[43,47,75,158,159,218,235–239]. 5-HT2A-R activation triggers manifold downstream cascades[226–230]. Best investigated is the phosphatidyl inositol (PI) pathway. In this pathway the binding of an agonist to its corresponding membrane-spanning GPCR recruits the Gq/11 protein that activates the membrane-associated phospholipase C (PLC).

PLC cleaves the membranous phospholipid phosphatidylinsositol-4,5-biphosphate (PIP2) into inositol-1,4,5 trisphosphate (IP3) and diacylglycerol (DAG) which is anchored in the membrane. The second messenger IP3, binds to the IP3 receptor and induces the release of Ca^{2+} from intracellular Ca^{2+} stores of the endoplasmatic reticulum (ER), increasing the cytosolic Ca^{2+} concentration. If the Ca^{2+} concentration is increased, cytosolic protein kinase C (PKC) is anchored via DAG to the membrane. Once activated, PKC can phosphorylate different substrates[227,228,230,240–243]. However, it is not clear whether this pathway is directly involved in the psychedelic action. While the head-twitch behaviour (typical behavioural response of rodents after psychedelic administration) is completely absent in 5-HT2A knockout (KO) mice, it is still present but decreased in Gqα subunit KO mice[244], suggesting a partial role of this protein in drug effects[218,245]. Further, the replicable finding of DOI induced *FOS* gene expression was abolished in Gqα KO mice[245].

Additionally, the Janus kinase/signal transducers and activators of transcription (JAK/STAT) and the MEK- extracellular-signal regulated kinases (ERK) 1/2 5-HT2A downstream signaling pathways seems to be activated by hallucinogenic agonists of the 5-HT2A-R[230,246]. The activation of the 5-HT2A-R is further coupled to the phospholipase A2 (PLA) pathway, mediating arachidonic acid (AA) release[247–249] and additional activates Src, involved in LSD induced psychological effects[218]. Moreover, the activation of the 5-HT2A-R could explain psychedelic induced IEG activation[250]. For example, LSD induced *cFOS* expression in the prefrontal cortex is blocked by a 5-HT2A-R antagonist[250].

Besides, 5-HT2 interacts and co-localize with PSD-95 protein[230,251,252]. Interestingly, head-twitch behavior and *cFOS* and *EGR1* gene expression is affected in PSD-95 KO mice suggesting that PSD-95 modulates 5-HT2A-R function and is essential for hallucinogenic actions[253]. Additionally, 5-HT2A-R stimulation leads to the activation of α-amino-3-hydroxy-5-methyl-4-isoxazolepropionic acid (AMPA) receptors which is correlated with augmented glutamate concentrations[254], also, shown in fMRI and animal studies after psilocybin, respectively ketamine and DOI administration[81,255–258]. PSD-95 seems to be involved in this process by anchoring activity dependent AMPA-type glutamate receptor in the membrane[259,260].

Interestingly, some agonists (and antagonists) have a higher binding affinity for distinct conformational states of receptors. Binding itself lead to the stabilization of distinct active conformational states. Depending on those the probability of stimulating one (or more) distinct transduction pathways instead of activating another is increased. Also, the subcellular location of the receptor, where it is translocated after ligand-binding and the time spent in this compartment can prime the signal cascade that is activated due to different interacting partners[232]. This phenomenon which enables an individual agonist-specific signal response is known as “functional selectivity”, “agonist-directed trafficking” or “biased agonism”[230,232,261–263] (illustrated in **Fig. 5**). In fact, the 5-HT2A-R belongs to the first receptors known to be functional selective[247,264,265]. That could explain why some high affinity agonists of the 5-HT2A-R do have hallucinogenic properties and others do not (e.g., serotonin)[230,248,266–268].

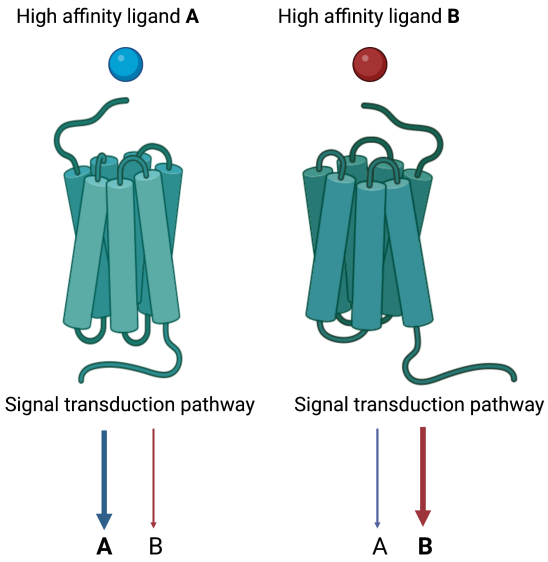

Figure 5. Biased agonism of the 5-HT2A-R.
The 5-HT2A-R is functional selective which enables an individual agonist-specific response. A mechanism also known as "agonist-directed trafficking" or "biased agonism". Selective agonists have a higher binding affinity for distinct conformational states of a receptor and thereby stabilize distinct active conformational states. Depending on those the probability of stimulating for example the transduction pathway A by ligand A is increased instead of activating transduction pathway B. Image is based on[230] and created with *Biorender.com.*

The 5-HT2A-R uses a multiplicity of mechanism that self-regulate it's signaling. One regulating mechanism is receptor downregulation (meaning a reduced receptor surface density) and desensitization. Downregulation and desensitization occur after chronic and acute stimulation with agonists[232,269–271], should avoid overstimulation and are hypothesized to contribute to the therapeutical action of drugs that target the serotonergic system[271–276]. Downregulation and desensitization are regulated by receptor internalization[272,277]. It is known that the binding of agonists and antagonists to the 5-HT2A-R could provoke a 5-HT2A-R internalization *in vivo* and *in vitro*[265,272,277–280]. The agonist induced internalization takes place via a dynamin-dependent and clathrin-mediated endocytosis (CME) mechanism and (in case of 5-HT as an agonist) is PKC-activation mediated[277,281]. Another described common self-regulation mechanism of the receptor is recycling which allow multiple rounds of ligand binding and modifies activation and inhibition of signaling[282]. For example, the agonist induced internalized 5-HT2A-R is guided to the endosome and recycled within 2.5 hrs after internalization to the surface[265,277].

Moreover, receptor oligomerization that crosslinks different pathways is discussed for 5-HT2A signaling. 5-HT2 receptors can form homo-and heterodimers with serotonergic receptors *in vitro*[283,284]. Interestingly, also heteromeric complexes formation for example with metabotropic glutamate receptor 2 (mGluR2) occur[285,286]. This complex formation plays a role in hallucinogenic induced

neuropsychological responses[221]. Remarkably, in a rat model of alcohol dependency mGluR2 is down-regulated and can be restored after psilocybin administration[188].

1.6.2 The brain-derived neurotrophic factor is a key factor in psychedelic-mediated neuroplasticity and psychiatric disorder pathophysiology

One key candidate in explaining the mechanism by which neuroplasticity is induced by psychedelics is the brain-derived neurotrophic factor (BDNF). BDNF is a neurotrophic and neuroplastic factor that belongs to the neurotrophin protein family. BDNF is widely expressed in the adult mouse brain such as in the hippocampus and in the cerebral cortex[287,288].

BDNF is synthetized by neurons as a precursor protein, proneurotrophin BDNF (pro-BDNF, 32 kDa) and is converted into its mature BDNF form (m-BDNF, 13.2 - 15.9 kDa) by proteolytical cleavage of the pro-domain. Both pro-BDNF and m-BDNF play an important role in neurodevelopment, brain maintenance, synaptic plasticity, cognition, learning, memory and mood related behaviors[289]. Pro-BDNF is cleaved intracellularly in the trans-Golgi network by furin or in secretory vesicles by convertases. Extracellularly pro-BDNF is cleaved by metalloproteinases 2 (MMP) and 9[290]. In the brain also the serine protease plasmin mediates the extracellular cleavage of pro-BDNF in m-BDNF by the enzyme tissue plasminogen activator (tPA)[291].

Mature and pro-BDNF are transported in secretory vesicles to axonal terminals where they are released constitutive or activity depended in the presynaptic cleft[292,293]. m-BDNF is suggested to be release in an activity dependent manner from pre- and postsynaptic sides[294]. For example, in neuronal cells membrane depolarization leads to release of pro-BDNF and m-BDNF[292,293,295,296].

m-BDNF and pro-BDNF bind to different receptors, activate different intracellular pathways and have therefore opposing biological roles. While m-BDNF binds to the high affinity tropomyosin-related kinase B (TrkB) receptor that is associated with synaptic plasticity, pro-BDNF binding to the p75 receptor is linked to apoptosis[293,297–299]. Binding of m-BDNF leads to a dimerization and autophosphorylation of the TrkB receptor. The m-BDNF/phospho-TrkB complex activation stimulates a myriad of prosurvival and synaptic plasticity associated downstream cascades associated with neuroplasticity. Main BDNF associated pathways are illustrated in **Figure 6.** For review see[289,293,300–304].

For example, activation of the prosurvival and antiapoptotic phosphatidylinositol 3-kinase (PI3K)/protein kinase B (AKT) pathway modulates NMDA-mediated synaptic plasticity, dendritic growth and branching, protein transport and translation via mammalian target of rapamycin (mTOR)[289,302,304–308]. mTOR activation itself seems to play a key role in psychedelic-mediated response. For example, glutamate release triggered by hallucinogens provoked prefrontal and hippocampal mTOR activation and BDNF release which is AMPAR-mediated[81,255–258,309–313]. And mTOR dependent synapse formation could explain the antidepressant effect of NDMA antagonists[314]. Inhibition of mTOR and

TrkB receptor prevents psychedelic induced neuroplasticity, suggesting a TrkB and mTOR-mediated pathway[1].

Further, the complex activates MAPK that is involved in neuronal protein synthesis, dendritic growth and branching and expression of IEGs, like *cFOS* (which are increased after psychedelics administration[216–220,223])[302,315,316]. Additionally, BDNF activates PLC-γ, that leads to the activation of PKC through its role in increasing intracellular Ca^{2+}-signaling concentration and thereby rapidly modulates ion channels and enhances synaptic plasticity. By activation of guanosine triphosphate hydrolases (GTPases) BDNF provokes the growth of neuronal fibers[289,299,302,317].

The PI3K and MAPK signaling cascades are associated with long-lasting BDNF induced transcriptional changes also by the phosphorylation of transcription factor cyclic AMP response element-binding protein (CREB), binding to the critical Ca^{2+} response element (CRE) within the BDNF gene that activates *BDNF* gene transcription[289,318,319]. In cortical neurons BDNF transcription is further regulated by Ca^{2+} influx and Ca^{2+}/calmodulin-dependent protein kinase (CaMK) activation[320,321].

Interestingly, serotonin, serotonergic antidepressants and agonist of serotonergic receptors efficiently increase BDNF levels[322–326]. Incubation with serotonin increase *BDNF* messenger RNA (mRNA) gene expression by a calcium and PKC dependent pathway, inhibited by 5-HT2A-R antagonist ketanserin[326].

The remarkable role of BDNF in synaptic plasticity underlines its importance in the etiology and in the therapy of psychiatric disorders. Particularly because alterations in BDNF levels and an impairment of the BDNF signaling in patients or in animal models of psychiatric disorders are associated with pathophysiology[300,327]. BDNF serum and/ or plasma and TrkB levels have been described to be reduced in psychiatric disorder patients for example during depressive and manic episodes in BD, MDD, in PTSD, in suicide victims and in alcohol dependent individuals[328–338]. And the environmental factor stress (e.g., early life time trauma or acute stressors) which increases the vulnerability for developing a psychiatric disorder (based on the “diathesis-stress model”) has been shown to reduce BDNF levels in rodents and humans[339].

Well-established treatment methods such as electroconvulsive therapy (ECT) treatment, antidepressant or lithium treatment augment BDNF levels, influenced by environmental factors[105,332,338,340–345]. Interestingly, psychedelics can increase levels of neurotrophic factors, like BDNF, and prevent stress induced BDNF decrease[1,43,222,294,346–353]. Double blind, randomized, placebo-controlled studies mostly found an increase in circulating (plasma or serum) BDNF level in healthy controls and TRD patients after acute (within 24 hrs), subacute or chronic (24 hrs up to one week) administration of ayahuasca or LSD[43,348,353]. In a mouse model ketamine and NMDAR antagonists provoke antidepressant-like effects that are BDNF-synthesis dependent[354]. And the inhibition of BDNF associated pathways prevents psychedelic induced neuroplasticity[1].

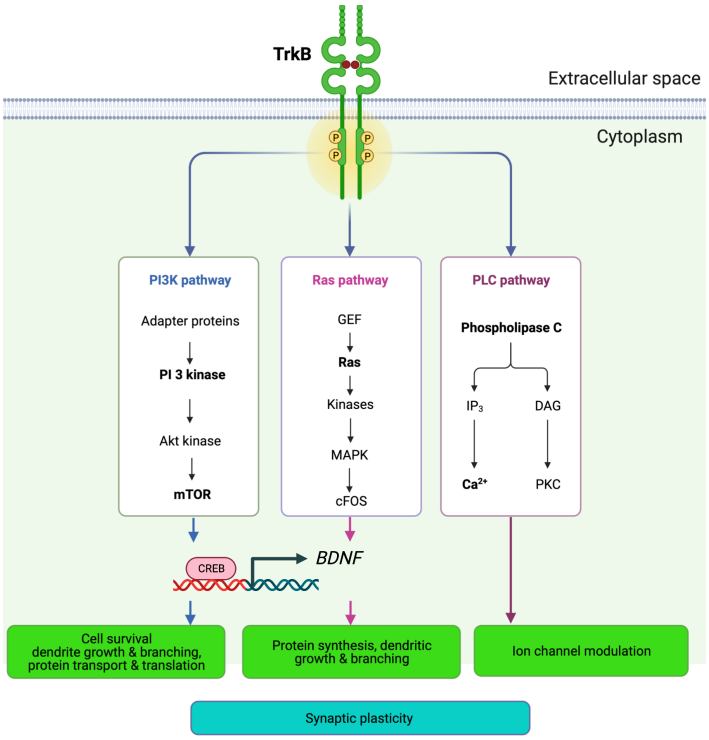

Figure 6. m-BDNF/phospho-TrkB complex associated downstream pathways.
The m-BDNF/phospho-TrkB complex activates the PI3K/AKT, the MAPK and the PLC-γ pathway which are associated with neuroplasticity and survival. The PI3K and MAPK signaling cascades activate CREB that mediates *BDNF* gene transcription. Image generated with *Biorender.com*. AKT, protein kinase B; BDNF, brain-derived neurotrophic factor; CREB, cyclic AMP response element-binding protein; mTOR, mammalian target of rapamycin; IP3, inositol-1,4,5 trisphosphate; DAG, diacylglycerol; MAPK, mitogen-activated protein kinase; PKC, protein kinase C; PLC, phospholipase C; PI3K, phosphatidylinositol 3-kinase.

1.7 The leading role of the annexin A2 – S100A10 complex in the cleavage of pro-BDNF into m-BDNF

In the brain the annexin A2 – S100A10 complex is responsible for the plasmin-mediated extracellular cleavage of pro-BDNF in m-BDNF by tPA[291]. This heterotetrameric cell surface complex, also known as AIIt complex, is built up by two annexin A2 proteins and one S100A10 dimer. The binding of tPA and the zymogen plasminogen to the complex promotes the tPA-mediated cleavage of the inactive precursor plasminogen into active plasmin (illustrated in **Fig. 7**).

Annexins are calcium dependent phospholipid membrane binding proteins, described first for their ability to "annex" (Greek for to aggregate) membranes[355]. They are multicompartmental and involved in manifold membrane associated processes like endocytosis, exocytosis, restructuring and the repair of membranes and vesicular trafficking. The annexin protein family is ubiquitously expressed in vertebrates and invertebrates but also in fungi, protozoa and plants. The N-terminal domain of the protein is the side for post-translational modification, ligand binding and protein interaction. This side

is highly variable amongst the annexin proteins. The carboxyl domain is conserved and contains the calcium binding motif. There are 12 annexin isoforms in humans. One of the best researched annexin isoforms is the vertebrate annexin A2, a 36-kDa size protein coded by the *ANXA2* gene that is located on chromosome 15 (15q21). For review see[356–359].

S100 proteins are vertebrate specific dimeric, acidic, calcium EF hand-type Ca^{2+} binding proteins named by their solubility in 100% saturated ammonium sulfate[360]. S100 proteins are regulators of cell survival, proliferation, Ca^{2+} homeostasis, membrane-cytoskeletal interactions. They are modulators of ion channels. Moreover, they are involved in learning and memory. S100 proteins act intra-or extracellularly and are secreted constitutively, stimulus induced or after injury. One of the best studied family members is the S100A10 protein that is calcium insensitive as the calcium binding side is inactive due to a mutation. S100A10 is therefore permanently in a Ca^{2+} insensitive on-state. S100A10, also known as p11, is a 11-kDa size protein coded by the *S100A10* gene that is located on chromosome 1 (1q21.3). In the following I will refer to S100A10 as p11, besides it is mentioned together with annexin A2 as part of the annexin A2 – S100A10 complex. For review see[361–364].

After assembly the complex is shuttled to the plasma membrane. The shuttling to the membrane is achieved by invagination into multivesicular endosomes and release as exosomes, by *s*oluble *N*-ethylmaleimide-sensitive-factor attachment receptor (SNARE)-mediated fusion or by building up a transmembrane spanning channel in association with phosphatidylinositol 4,5-bisphosphate (PtdIns(4,5)P2) formation.

Annexin A2 serves as an extracellular p11 receptor that transports and anchors p11 to the plasma membrane. Initiation of complex formation and translocation to the cell surface is based on external signals like heat stress, hypoxia or thrombin stimulation[358,365].

P11 and annexin A2 are binding partners that regulate each other's function, availability and stability. Exemplarily, the binding of p11 to annexin A2 facilitates the membrane binding process by reducing the calcium dependency and thereby needing less intracellular calcium for activation. In an annexin A2 KO tumor cell line p11 protein level and *p11* mRNA expression were significantly lower[366]. And p11 protein is only detectable in cells that do express both, p11 and annexin A2 mRNA. Also, in annexin A2 overexpressing cells p11 protein level is up-regulated[367]. Binding of p11 to annexin A2 prevents ubiquitin-mediated degradation of p11[368]. The stability of S100A10 on the cell surface increases the more annexin A2 – S100A10 complexes are available.

Plasmin generation leads to the extracellular cleavage of surface annexin A2 that binds to Toll like receptor (TLR) 4 and initiates PKC activation. PKC phosphorylation dissociates the intracellular annexin A2 – S100A10 complex and prevents translocation to the outer cell membrane and further plasmin generation[358,368].

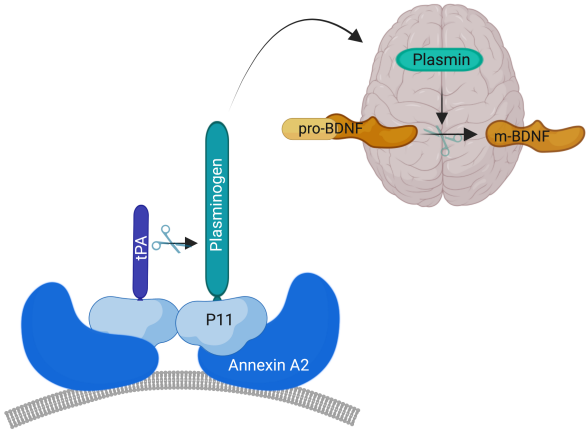

Figure 7. Extracellular plasmin generation by the annexin A2 – S100A10 complex.
The annexin A2 – S100A10 (aka AIIt) complex consists of two annexin A2 proteins and a p11 (aka S100A10) dimer. It binds tPA and plasminogen, that is cleaved into plasmin. In the brain plasmin cleaves extracellularly pro-BDNF into m-BDNF, mediated by tPA. tPA, tissue plasminogen activator. Image generated with *Biorender.com*.

1.7.1 Key players of the annexin A2 – S100A10 complex, their role in fibrinolysis, synaptic plasticity and link to psychiatric disorders

Interestingly, the plasmin-generating annexin A2 – S100A10 complex was longtime mainly known for its role in fibrinolysis. After a vascular injury endothelial cells induce coagulation to stimulate hemostasis by the expression of coagulation factors. That results in the activation of thrombin which cleaves fibrinogen in fibrin. The polymerization of fibrin monomers results in the formation of fibrin clots which terminates hemorrhage. Fibrinolysis is needed for tissue healing as it is the biological mechanism that negatively regulates prolonged blood coagulation and accumulation of fibrin clots. The key enzyme of breaking down fibrin clots into fibrin degradation products (FDP) is plasmin (illustrated in **Fig. 8**). Besides this important function the complex also plays an important role in oncogenesis and inflammation. Tumor cells, macrophages or neutrophils use plasmin to proteolytically cleave the extracellular matrix for invasion and metastasis, respectively to cross tissue barriers to reach spots of inflammation or tumor sites. For review see[365,369–371].

That neuroinflammation is linked to depression pathophysiology is already well known as the concentration of inflammatory markers (e.g., Interleukin (IL)-6 and tumor necrosis factor-α (TNF-α)) is increased in depression and in suicide victims[372,373] and inhibition of proinflammatory cytokines can improve depressed mood[371,374–376]. But that fibrinolysis might be involved in depression pathophysiology as-well is relatively new. Interestingly, a hypothetical paper describes a connection between a disruption of the fibrinolytic system and the etiology of depression[376].

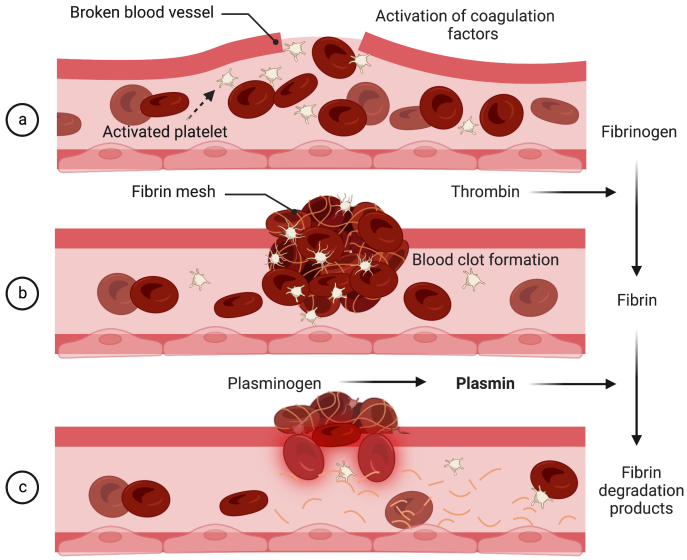

Figure 8. Coagulation and fibrinolysis.
a) In vascular injury (e.g., broken blood vessel) coagulation factors are activated. b) Thrombin cleaves fibrinogen into fibrin. In the following a blood clot is formed by the polymerization of fibrin and thereby prevents hemorrhage. c) In fibrinolysis fibrin is cleaved by plasmin in FDP, to prevent further growth of blood clots. FDP, fibrin degradation products. Image generated with *Biorender.com*.

First, studies underline the proinflammatory role of the coagulation key player fibrinogen[371], its involvement in microglia activation and inhibition of plasticity associated neurite outgrowth[377,378]. Second, upregulation of fibrinolytic key players is associated with synaptic plasticity and antidepressant effects[376].

One of those fibrinolytic players associated with the annexin A2 – S100A10 complex and synaptic plasticity is the extracellular serine protease tPA, the enzyme that cleaves plasminogen in plasmin[291]. tPA is widely expressed by neurons and microglia in the human brain, in the neocortex and the limbic system[379]. The neuromodulator tPA is an IEG downstream target of CREB-1, induced by neuronal activity, which is involved in activity-dependent neuroplasticity and synaptic growth[380–384]. tPA regulates synaptic restructuring by activating metalloproteases that degrade the extracellular matrix[385–387]. It also modulates glutamatergic and dopaminergic neurotransmission[388]. tPA knockdown in mice and significantly reduced tPA levels are associated with depression-like-phenotype and MDD[389]. Injection of a tPA overexpressing vector, SSRI, electroconvulsive seizure treatment or physical exercise can increase tPA[341,376,389–394]. Upregulation of endogenous tPA levels might be therefore an interesting target in the treatment of depression[376].

Moreover, the annexin A2 – S100A10 complex player plasminogen activator urokinase-type plasminogen activator (uPA) is a marker for suicidality and depression[395]. uPA binds to the urokinase-

type plasminogen activator receptor (uPAR). P11 co-localizes plasminogen with the uPA/uPAR complex[396]. Also, uPA cleaves p11-bound plasminogen into the protease plasmin. For review see[369]. uPAR knockdown mice show a depressive-like-phenotype and cognitive impairments[397,398]. And mice lacking the *uPA* and *uPAR* gene are associated with neuroinflammation[399].

The annexin A2 – S100A10 complex itself interacts with proteins that are associated with psychiatric disorders and antidepressant effects. For example, the Ahnak protein which builds a multimeric complex with annexin A2 – S100A10 in the brain, regulates L-type voltage-gated calcium channels (L-type VGCC)[400–402] is associated with psychiatric disorders and KO mice display depressive-like-phenotype[403,404].

Remarkably, the annexin A2 – S100A10 complex is even involved in transcriptional elongation and epigenetic modifications (on histone 3) as it as interacts with SWI/SNF-related, matrix-associated actin-dependent regulator of chromatin, subfamily A, member 3 (SMARCA3)[400,405–407]. Also, chronic SSRI administration increases p11/Anxa2/SMARCA3 complex levels[400].

p11, the prominent core player of the annexin A2 – S100A10 complex is associated with depression and suicide and is considered to be a target for antidepressants[408–410]. First, *p11* gene expression and protein level is downregulated in MDD patients and in genetic animal models of depression[409,410]. Also, *p11* KO mice show a depressive-like phenotype and respond worse to antidepressant treatment and cannot profit from antidepressant actions of BDNF[325,411,412]. Second, *p11* mRNA levels are increased in rodent cortex after ECT or antidepressant therapy and mice that overexpress *p11* behaved similar to those receiving antidepressant treatment[105,393,401,408]. Interestingly, p11 interacts with serotonin receptors, regulates their cell surface localization and modulates ion channels and BDNF levels [325,408,410,411,413].

Finally, and most importantly, plasmin, generated by the annexin A2 – S100A10 complex, mediates the extracellular cleavage of pro-BDNF in m-BDNF by the enzyme tPA *in vitro* in the brain[291]. A constantly increasing number studies, choose a more sophisticated approach by not only investigating total BDNF level differences in the pathophysiology of psychiatric disorders but separately consider differences of pro-BDNF and m-BDNF levels. They found that pro-BDNF levels are elevated in patients with MDD and in rodents that show depressive-like behaviors, while levels of m-BDNF are reduced, suggesting a deficient cleavage or an insufficient transformation of pro-BDNF into m-BDNF that might be correlated with pathophysiology[389,393,414–419]. Interestingly, SSRI treatment can reverse elevated serum levels of pro-BDNF in MDD patients[389]. Absolutely justifiable, drugs that counterbalance the imbalance of the m-BDNF-to-pro-BDNF level are discussed in depression therapy. For review see[300,415].

Figure 9 illustrates the antidepressant actions associated with the annexin A2 – S100A10 complex.

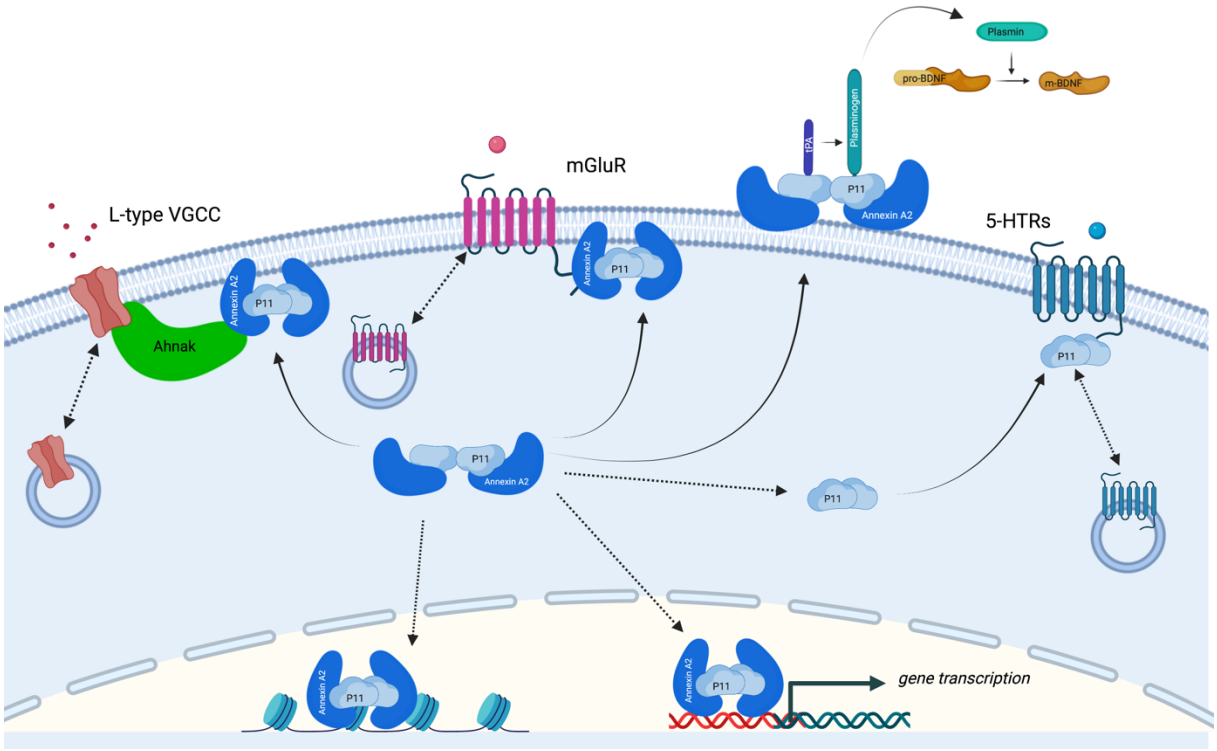

Figure 9. Antidepressant actions of the annexin A2 – S100A10 complex.
S100A10, aka p11 interacts with serotonin receptors, modulates their surface localization and thus regulates serotonergic signaling (upregulation of 5-HTRs is associated with increased serotonergic signaling and antidepressant effects, facilitated by increased SSRI-mediated *p11* gene expression) and plays a role in receptor trafficking. The annexin A2 – S100A10 complex interact with the Ahnak protein which regulates L-type VGCC and mGluR5 surface localization. mGluR2, 5-HTR and L-type VGCC play a role antidepressant action, respectively are associated with psychiatric disorders. The annexin A2 – S100A10 complex is involved in epigenetic modifications and gene transcription. Plasmin generation of the annexin A2 – S100A10 cleaves extracellularly pro-BDNF into m-BDNF. Image was based on[420] and was created with *Biorender.com*. 5-HTRs, serotonergic receptors; L-type VGCC, L-type voltage-gated calcium channels; mGluR, metabotropic glutamate receptor; tPA, tissue-type plasminogen activator.

1.8 Aims of the study

The serotonergic psychedelic psilocybin is discussed as fast-acting and long-lasting antidepressant especially in the therapy of depression and addiction[2,120,143,144,146,148–156,254]. Animal studies suggest that psilocybin (and other) psychedelics act as *psychoplastogens*[1] because they promote neuroplasticity and thereby might restore neuronal dysfunction and synaptopathies, which are associated with psychiatric disorder pathophysiology[1,181–188].

The precondition of this doctoral thesis was first the question whether iPSC-derived human cortical neurons can be used as an *in vitro* model system to investigate the effects of psilocin, the active principle of psilocybin. Of importance was hereby the confirmation of the expression of the cellular machinery that is required to transmit, process and translate psilocin-induced signaling (e.g., the 5-HT2A-R expression).

Further, a major aim was the replication of the so far only in the animal system described molecular, cellular and functional effects of psychedelics in the human system, based on the belief that psilocin might act through an evolutionally conserved mechanism: namely (amongst others) downregulation of the 5-HT2A-R[250,276], modulation of neurotransmission[1,210,211], upregulation of IEGs[216–223] and neurotrophin expression and their associated downstream pathways[1,43,222,294,346–353] and synaptogenesis [1]. Moreover, a 5-HT2A-R mediation of those effects should be investigated, as serotonergic psychedelics mainly target this receptor that is responsible for psychedelic induced neurophysiological and neuroplasticity effects[43,47,75,158,159,218,235–239].

Finally, a superior aim was the identification of a novel mechanism of psilocybin-mediated antidepressant response with the objective to detect a new therapeutic drug target for the treatment of psychiatric disorders, mainly depression. The implication of such a mechanism would be a tremendous success, considering the constantly increasing number of patients that suffer from depression. The identification of such a mechanism also provides the basis for the development of novel antidepressant substances.

2 Materials

2.1 Cell culture

2.1.1 Cell culture media, solutions, additives, kits and buffers

All cell culture reagents were prepared under sterile conditions or sterile-filtered after preparation. Cell culture media were stored at 4°C.

Table 1. Cell culture base media.

Medium	Manufacturer	Catalogue number	Registered office
Advanced DMEM	Thermo Fisher Scientific	12491-023	Waltham, USA
Advanced MEM	Thermo Fisher Scientific	12492-013	Waltham, USA
DMEM/F-12 with glutamine	Thermo Fisher Scientific	11320-074	Waltham, USA
DMEM/F-12 with glutamine and HEPES	Thermo Fisher Scientific	11330-057	Waltham, USA
DMEM with GlutaMAX™	Thermo Fisher Scientific	61965-059	Waltham, USA
Neurobasal™	Thermo Fisher Scientific	21103049	Waltham, USA

Table 2. Commercial cell culture stock solutions and additives.

Compound	Concentration	Manufacturer	Catalogue number	Registered office
B-27™ supplement	50x	Thermo Fisher Scientific	17504-044	Waltham, USA
Ethylenediaminetetraacetic acid (EDTA) 0.5M, pH 8.0 UltraPure™	0.5 M	Thermo Fisher Scientific	15575020	Waltham, USA
Geltrex™, hESC-qualified	15 mg/ml	Thermo Fisher Scientific	A1413302	Waltham, USA
GlutaMAX™ supplement	100x	Thermo Fisher Scientific	35050038	Waltham, USA
KnockOut™ Serum Replacement		Thermo Fisher Scientific	10828028	Waltham, USA
MEM Non-Essential Amino Acids Solution (NEAA)	100x	Thermo Fisher Scientific	11140035	Waltham, USA
Phosphate buffered saline (DPBS)	1x	Thermo Fisher Scientific	14190144	Waltham, USA
Penicillin/Streptomycin (10.000 U/ml)	100x	Thermo Fisher Scientific	15140122	Waltham, USA
TrypLE™ Express	1x	Thermo Fisher Scientific	12605-028	Waltham, USA

Table 3. Small molecules, growth factors, drugs and solutions for cell culture.

Compound	Concentration	Solvent	Final concentration	Manufacturer	Catalogue number	Registered office
BMP-4	20 µg/ml	0.1% BSA in double-distilled water (ddH_2O)	10 ng/µl	Miltenyi Biotec	130-111-165	Bergisch Gladbach, Germany
Borate buffer, pH 8.4	25 mM	ddH_2O	25 mM	Thermo Fisher Scientific	15583	Waltham, USA
Bryostatin 1	27 µM	Ethanol	0.27 nM	Merck Millipore	203811-10UG	Burlington, USA
Calcium chloride ($CaCl_2$)	60 mM	ddH_2O	1.8 mM	Sigma-Aldrich	31307-1KG	St. Louis, USA
CHIR99021	10 mM	Dimethyl sulfoxide (DMSO)	3 µM	Cell Guidance Systems	SM13-50	Cambridge, UK
Chelerythrine	1 mM	DMSO	1 µM	Cayman Chemical	11314	Ann Arbor, USA
Cyclopamine	5 mM	Ethanol	5 µM	Cayman Chemical	Cay11321-10	Ann Arbor, USA
N-[N-(3,5.difluorophenacetyl)-L-alanyl]-S-phenylglycine t-butyl ester (DAPT)	25 mM	DMSO	5 µM	Cell Guidance Systems	SM15-50	Cambridge, UK
DMSO	N/A	N/A	N/A	Sigma-Aldrich	D5879	St. Louis, USA
DNase I	10 mg/ml	ddH_2O	10 µg/µl	Roche	43813000	Basel, Switzerland
Dynasore	100 mM	DSMO	50 µM	Cayman Chemical	Cay14062-5	Ann Arbor, USA
EGF	100 µg/µl	ddH_2O	100 ng/µl	Cell Guidance Systems	GFH26	Cambridge, UK
Ethanol	N/A	N/A	N/A	Sigma-Aldrich	32205	St. Louis, USA
FGF-2 (147)	10 µg/ml	ddH_2O	10 ng/ml	Cell Guidance Systems	32205	Cambridge, UK
FGF-2 (154)	200 µg/ml	0.1% BSA in ddH_2O	200 ng/ml	Cell Guidance Systems	GFH146-1000	Cambridge, UK
Forskolin	25 mM	DMSO	10 µM	Cell Guidance Systems,	SM18-100	Cambridge, UK
GABA	100 mM	ddH_2O	300 µM	Sigma-Aldrich	A5835-33710G	St. Louis, USA
D(+)-Glucose	400 mg/ml	ddH_2O	1.6 mg/ml	Carl Roth	HN06.2	Karlsruhe, Germany
Insulin	5 mg/ml	10 mM NaOH	500 µg/ml	Sigma-Aldrich	91077C	St. Louis, USA
Ketanserin	75 mM	DMSO	75 µM	ApexBio	APE-B2248	Houston, USA
L-Ascorbic acid	500 mM	ddH_2O	200 µM	Sigma-Aldrich	A8960-5G	St. Louis, USA
L-Ascorbic acid 2-	64 mg/ml	ddH_2O	64 µg/ml	Sigma-Aldrich	A8960-5G	St. Louis, USA

phosphate (LAAP)						
Laminin, murine	1-2 mg/ml	PBS	3.75 µg/ml	Sigma-Aldrich	L2020	St. Louis, USA
LDN-193189 hydrochloride	10 mM	DMSO	1 µM	Stemcell Technologies	72147	Vancouver, Canada
LM22A	1 mM	DMSO	1 µM	Sigma-Aldrich	SML0848-25MG	St. Louis, USA
LM22B	10 mM	DMSO	1 µM	Tocris Bioscience	6037	Bristol, UK
Palbociclib (PD-0332991)	2 mM	DMSO	2 µM	Selleckchem	S1116	Houston, USA
Progesterone	50 µg/ml	Ethanol	630 ng/ml	Sigma-Aldrich	P8783	St. Louis, USA
Pro-BDNF	100 µg/ml	PBS	100 ng/ml	Sigma Aldrich	SRP6053-10UG	St. Louis, USA
Pro-BDNF	1 µg/µl	ddH_2O	20 - 80 ng/µl	Alomone Labs	B-257	Jerusalem, Israel
Psilocin	10 mM	DMSO	10 µM	THC-Pharm	520536	Frankfurt am Main, Germany
Putrescine	80.6 mg/ml	ddH_2O	1.611 mg/ml	Sigma-Aldrich	51799	St. Louis, USA
Plasmin	10 U/mg	ddH_2O	5 U/mg	Merck Millipore	527621-10U	Burlington, USA
Plasminogen	10 ng/ µl; 1 µg/ml	25 mM Tris and 150 mM NaCl, pH 8.0	2.5 ng/µl	R&D Systems	1939-SE-200	Minneapolis, USA
ROCK inhibitor (Y-27632)	5 mM	ddH_2O	5 or 10 µM	Cell Guidance Systems	Y-27632	Cambridge, UK
Polyethylenimine (PEI)	1%	ddH_2O	1:2000	Sigma Aldrich	P3143	Darmstadt, Germany
SB-431542	100 mM	DMSO	10 µM	Cell Guidance Systems	SM33-50	Cambridge, UK
Sodium selenite	70 µg/ml	ddH_2O	14 ng/ml; 529 ng/ml	Sigma-Aldrich	214485	St. Louis, USA
TGF-β1	20 µg/ml	ddH_2O	2 ng/ml	Cell Guidance Systems	GFH109	Cambridge, UK
TCB-2	25 mM	ddH_2O	10 µM	Tocris Bioscience	2592	Bristol, UK
Transferrin	50 mg/ml	ddH_2O	11 µg/ml	Sigma-Aldrich	T3705-5G	St. Louis, USA
XAV939	10 mM	DMSO	2 µM	Cell Guidance Systems	SM38-50	Cambridge, UK

Table 4. Commercial kits for cell culture.

Kit	**Manufacturer**	**Catalogue number**	**Registered office**
Orangu™ cell counting solution	Cell Guidance Systems	OR01-500	Cambridge, UK
Lipofectamine 2000	Thermo Fisher Scientific	11668030	Waltham, USA

Table 5. Self-made buffer for cell culture.

Buffer / Solution	Component	Concentration
Borate buffer	Boric acid adjust pH to 8.4 with NaOH	25 mM

Table 6. Composition of self-made 100x N2-supplement.

2.5 ml of N2-supplement were used for 500 ml of DMEM/F-12 with glutamine (1:200).

Component	Volume	Final concentration
DMEM/F-12 with glutamine	3.5 ml	70% (v/v)
Pen/Strep	50 µl	1% (v/v)
Insulin (5 mg/ml)	500 µl	0.5 mg/ml
Progesterone (50 µg/ml)	63 µl	630 ng/ml
Putrescine (80.6 mg/ml)	100 µl	1.611 mg/ml
Sodium selenite (70 µg/ml)	37 µl	520 ng/ml
Transferrin (50 mg/ml)	1.0 ml	10 mg/ml
Total	**5 ml**	

Table 7. Composition of ready-to-use cell culture media and solutions.

Medium (base)	Additive / component	Final concentration
ACSF	NaCl $MgCl_2$ $CaCl_2$ KCl Glucose	125 mM 1 mM 2 mM 2.5 mM 10 mM
Astrocyte base medium (DMEM/F-12 with glutamine)	Pen/Strep Glucose N2	1% (v/v) 1.6 mg/ml 0.5% (v/v)
Astrocyte standard medium (Astrocyte base medium)	N2 Glucose B-27 EGF FGF-2 (147)	0.5% (v/v) 1.6 mg/ml 0.1% (v/v) 100 ng/µl 10 ng/ml
Astrocyte differentiation medium (Astrocyte base medium)	BMP-4 N2 Glucose	10 ng/µl 0.5% (v/v) 1.6 mg/ml
Cytobuffer	Myo-Inositol Polyvinylalcohol PBS	240 mM 5 mg/ml (v/v) 0.2x
Freezing medium	KnockOut™ Serum Replacement Cytobuffer DMSO Freshly added ROCK inhibitor	70% (v/v) 20% (v/v) 10% (v/v) 5 - 10 µM
Essential 8 (E8) (DMEM/F-12 with glutamine and HEPES)	Pen/Strep L-ascorbic acid 2-phosphate Sodium selenite FGF-2 (154) Insulin TGF-β1 Transferrin	1% (v/v) 64 µg/ml 14 ng/ml 200 ng/ml 20 µg/ml 2 ng/ml 11 µg/ml
hiPSC freezing medium	KnockOut™ Serum Replacement E8 medium DMSO Freshly added ROCK inhibitor	50% (v/v) 40% (v/v) 10% (v/v) 5 - 10 µM
Intracellular solution	K-gluconate	115 mM

	KCl Na-phosphocreatine Mg- adenosine triphosphate (ATP) GTP EGTA HEPES Adjust pH to 7.3 osmolarity 300 mOsm	20 mM 10 mM 4 mM 0.3 mM 0.2 mM 10 mM
Neural base medium 1 (DMEM/F-12 with glutamine)	GlutaMAX™ $CaCl_2$ Pen/Strep B-27-supplement with RA N2 NEAA Glucose	0.1% (v/v) 1.8 mM 1% (v/v) 1% (v/v) 0.5% (v/v) 1% (v/v) 1.6 mg/ml
Neural base medium 2 (Neurobasal)	Pen/Strep GlutaMAX™ B-27-supplement with RA Glucose	1 % (v/v) 0.1 % (v/v) 1 % (v/v) 1.6 mg/ml
Neural base medium 3 (Advanced MEM)	Pen/Strep GlutaMAX™ B-27-supplement with RA Glucose	1% (v/v) 0.1% (v/v) 1% (v/v) 1.6 mg/ml
Neural progenitor induction medium phase 1 (Advanced DMEM/F-12 with glutamine)	Pen/Strep GlutaMAX™ B-27-supplement with RA SB-431542 Cyclopamine LDN-193189 XAV939	1% (v/v) 1% (2 mM) 1% (v/v) 10 µM 5 µM 1 µM 2 µM
Neural progenitor induction medium phase 2 (Advanced DMEM/F-12 with glutamine)	Pen/Strep GlutaMAX™ B-27-supplement with RA LDN-193189	1% (v/v) 1% (2 mM) (v/v) 1% (v/v) 200 nM
Neural progenitor induction medium phase 3 (Advanced DMEM/F-12 with glutamine)	Pen/Strep GlutaMAX™ B-27-supplement with RA FGF-2 (147)	1% (v/v) 1% (2 mM) (v/v) 1% (v/v) 20 ng/ml
Neuronal differentiation, phase 1 (Neural base medium 1)	Ascorbic acid LM22A LM22B PD-0332991 DAPT	200 µM 1 µM 1 µM 2 µM 5 µM
Neuronal differentiation, phase 2 (Neural Base medium 2)	As for phase 1 with the addition of CHIR99021 Forskolin GABA	 3 µM 10 µM 300 µM
Neuronal differentiation, phase 3 (Neural base medium 2)	Ascorbic acid LM22A LM22B PD-0332991 CHIR99021	200 µM 1 µM 1 µM 2 µM 3 µM
Neuronal differentiation, phase 4 (Neural base medium 2)	As for phase 3 but without CHIR99021	
Neuronal differentiation, phase 5 (Neural base medium 3)	Ascorbic acid LM22A LM22B PD-0332991 Bryostatin 1	200 µM 1 µM 1 µM 2 µM 0.27 nM
Wash medium (DMEM with GlutaMAX™)	Pen/Strep	1% (v/v)

2.1.2 Cell lines

The cell lines listed were reprogrammed and characterized in our group. Their generation was not part of this doctoral thesis.

Table 8. Healthy control cell lines.

Cell line	Clone	Name	Gender/ age	Origin
28	#1	Ctrl 1	female/ 44 years	Dermal fibroblasts reprogrammed using sendai virus
68	#3	Ctrl 2	female/ 25 years	as above
69	#2	Ctrl 3	female/ 23 years	as above
112	#3	Ctrl 4	male/ 19 years	as above
35	#2	Ctrl 5	male/ 23 years	as above

Table 9. BD cell lines.

Cell line	Clone	Name	Gender/ age	Diagnosis (DSM-V)	Age at first episode/ diagnosis	Family history of BD	Origin
BD4	#9	BD1 1	male/ 24 years	BD 1	-/ 22 years	yes	Dermal fibroblasts reprogrammed using sendai virus
BD3	#4	BD1 2	male/ > 55 years	BD 1	50/ 55 years	no	as above
BD1	#3	BD1 3	male/ 36 years	BD 1	19/ 19 years	yes	as above
BD2	#2	BD2 1	male/ 48 years	BD 2	17/ 21 years	yes	as above

Table 10. AUD cell lines.

Cell line	Clone	Name	Gender / age	Diagnosis	Origin
04	#11	AUD1	male/ 57 years	AUD	Dermal fibroblasts reprogrammed using sendai virus
02	#1	AUD2	male/ 68 years	AUD	as above

2.2 Molecular biology

2.2.1 Molecular biology reagents, kits, enzymes and buffers

Table 11. Molecular biology: commercial reagents.

Compound	Manufacturer	Catalogue number	Registered office
1 kb marker, Quick-Load®	New England Biolabs	N0468S	Ipswich, USA
100 bp marker, Quick-Load®	New England Biolabs	N0467S	Ipswich, USA
Adult brain total RNA, human	BioCat	R1234035-50-BC	Heidelberg, Germany
DNA polymerase buffer (10x)	Biozym	311611	Hessisch Oldendorf, Germany
Deoxynucleotide triphosphates (dNTPs)	Steinbrenner Laborsysteme	SL-Set-L-dNTPs	Wiesenbach, Germany
Fetal brain total RNA, human	Tebu Bio	1F01-50	Le-Perray-en-Yvelines, France
peqGREEN DNA/RNA binding dye	VWR	peql37-5010	Radnor, USA
Protein marker PS10 plus	GeneON Bioscience	310004	Ludwigshafen, Germany
RNAse AWAY	Thermo Fisher Scientific	10666421	Waltham, USA
ROX	GENAXXON	A351513	Ulm, Germany
Syber® Green I	Sigma-Aldrich	S9430	St. Louis, USA
TriFast™, peqGOLD	VWR	30-2010	Radnor, USA
qPCR reaction buffer	Promega	M890A	Madison, USA

Table 12. Molecular biology: commercial kits.

Kit	Manufacturer	Catalogue number	Registered office
ExtractMe Genomic DNA	blirt	EM13-050	Gdansk, Poland
iScript™ cDNA synthesis kit	Bio-Rad Laboratories	17088991BUN	Hercules, USA
Plasmid midiprep kit, PureLink™ HiPure	Thermo Fisher Scientific	K210015	Waltham, USA
RNA 6000 Nano kit	Agilent Technologies	5067-1511	Santa Clara, USA

Table 13. Enzymes.

Enzyme	Manufacturer	Catalogue number	Registered office
DNAse I, amplification grade	Sigma-Aldrich	AMPD1-1KT	St. Louis, USA
DNAse I, cell culture	Sigma-Aldrich	10104159001	St. Louis, USA
Proteinase K (20 mg/ml)	GeneON Bioscience	405-001	Ludwigshafen, Germany
Go® Taq G2 Flexi DNA Polymerase	Promega	M7808	Madison, USA
Taq DNA polymerase	Biozym	331610	Hessisch Oldendorf, Germany

Table 14. Molecular biology: self-made buffers.

Buffer / solution	Component	Concentration
DNA sample buffer (10x)	Tris-HCl, pH 7.6 Bromphenol blue Glycerol	50 mM 0.25% (w/v) 60%
gDNA isolation lysis buffer	Tris-HCl, pH 8.5 EDTA SDS NaCl Proteinase K	100 mM 5 mM 0.2% (w/v) 200 mM 133 ng/µl

2.2.2 Primers

All primers were ordered from Integrated DNA Technologies Inc. (Coralville, USA) and reconstituted at 100 µM in nuclease-free H_2O for 30 min at 37°C and 400 rpm in a thermomixer.

Table 15. Primers for real-time (RT)- polymerase chain reaction (PCR) and RT quantitative PCR (RT-qPCR)

Primer name	Sequence (5'->3')	Size base pair (bp)
HTR2A-For	TTGGGCTACAGGACGATT	383
HTR2A-Rev	GAAGAAAGGGCACCACATC	
18s rRNA-For	AAACGGCTACCACATCCAAG	143
18s rRNA-Rev	CCTCCAATGGATCCTCGTTA	
ANK3-For	TGGAATGATTGAACGGAGTACAGG	142
ANK3-Rev	AGTGAAGCCTGACTTGGCTG	
ARC-For	TCAGCTCCAGTGATTCACGC	163
ARC-Rev	GGGAACCTTGAGACCTGTTGT	
BDNF-For	TTTGGTTGCATGAAGGCTGC	199
BDNF-Rev	TGAGGACCAGAAAGTTCGGC	
BCL11B-For	CAACCCGCAGCACTTGTC	80
BCL11B-Rev	CCTCGTCTTCTTCGAGGATGG	
DLG4-For	AGCCCCAGGATATGAGTTGC	90
DLG4-Rev	CCCAGACCTGAGTTACCCCT	
EGR2-For	ACTGGGAGGCCCCTTTGACCA	119
EGR2-Rev	AGACGGGAGCAAAGCTGCTGG	
FOS-For	CAAGCGGAGACAGACCAACT	177

FOS-Rev	AGTCAGATCAAGGGAAGCCA	
GAD1-For	ATCCTGGTTGACTGCAGAGAC	80
GAD1-Rev	CCAGTGGAGAGCTGGTTGAA	
GRIA2-For	GGATCCTCATTAAGAACCCCAGT	148
GRIA2-Rev	TGAGGGCACTGGTCTTTTCC	
GRIA4-For	AGGTGAATGTGGACCCAAGG	177
GRIA4-Rev	AAGGTCAGCTTCATTCTCTTCG	
GRIN1-For	GGCAACACCAACATCTGGAA	71
GRIN1-Rev	CCATCCGCATACTTGGAAGAC	
GRIN2B-For	CTCACCCCCTTTCCGCTTT	156
GRIN2B-Rev	AAGGCATCCAGTTTCCCTGTT	
NEUROD6-For	ACTCAGCCTGAAAAGATTTGG	89
NEUROD6-Rev	TGGTTCTCTAATCTTAAATTACCTT	
NPAS4-For	AACACTACCGCCTGTTGGC	133
NPAS4-Rev	GCAGTAATGGGTCCCTCTGG	
NRXN1-For	GTGTTTTGCCGGTGCTGTTA	133
NRXN1-Rev	CTTTTACCTTGGTCGCCCATC	
RBFOX3-For	GCGCTGAGCCCGTTGAAAT	104
RBFOX3-Rev	CTCCTTCTGGACCGTCCTTG	
Mycoplasma-For	GGGAGCAAACAGGATTAGATACCCT	> 200
Mycoplasma-Rev	TGCACCATCTGTCACTCTGTTAACCTC	
SLC17A7-For	AGCTGGGATCCAGAGACTGT	116
SLC17A7-Rev	CCGAAAACTCTGTTGGCTGC	
SLC17A6-For	TCAGATTCCGGGAGGCTACA	175
SLC17A6-Rev	TGGGTAGGTCACACCCTCAA	
SV2A-For	AACCTAGACCAGGCACTCAT	99
SV2A-Rev	ACCCCTCCCCACAGTTACTTA	
SYN1-For	CAGCTCAACAAATCCCAGTCTC	99
SYN-1Rev	GGTCTCAGCTTTCACCTCGT	
TBR1-For	ACGAACAACAAAGGAGCTTCA	68

TBR1-Rev	TGGTACTTGTGCAAGGACTGTA	
TUBB3-For	GAGCGGATCAGCGTCTACTA	77
TUBB3-Rev	GGTTCCAGGTCCACCAGAA	

2.2.3 RT-PCR compositions and cycling programs

Table 16. Composition of standard RT-PCR reaction.

Component	**Volume [µl]**	**Final concentration**
10x Taq reaction buffer	2.5	1x
10 mM dNTP mix	0.25	each 200 µM
10 µM primer mix	2.0	each 400 nM
Taq DNA polymerase (5 U/µl)	0.125	0.625 U
Template DNA	variable	0.4 - 10 ng
ddH_2O	variable	
Total	**25**	

Table 17. Standard RT-PCR cycling program.

Step	**Temperature [°C]**	**Duration**	
Initial Denaturation	95	1 min	
Denaturation	95	15 s	35 cycles
Annealing	60	15 s	
Elongation	72	10 s	
Final elongation	72	5 min	
Short-term storage	4	hold	

Table 18. RT-PCR cycling program for mycoplasma quality control.

Step	**Temperature [°C]**	**Duration**	
Initial denaturation	95	2 min	
Denaturation	95	15 s	35 cycles
Annealing	58	15 s	
Elongation	72	15 s	
Final elongation	72	10 min	
Short-term storage	4	hold	

Table 19. RT-PCR cycling program for fingerprint quality control.

Step	**Temperature [°C]**	**Duration**	
Initial denaturation	95	2 min	
Denaturation	95	20 s	30 cycles
Annealing	58	25 s	
Elongation	72	40 s	
Final elongation	72	10 min	
Short-term storage	4	hold	

Table 20. Composition of RT-qPCR master mix.

Component	**Volume [µl]**	**Final concentration**
5x reaction buffer	2000	1x
$MgCl_2$	1	2.5 mM
10 mM dNTP mix	20 each	each 200 µM
DMSO	400	4% (v/v)
Syber® Green I	7.5	1 x
ROX	1.25	25 nM
ddH_2O	1511.25	
Total	**4000**	

Table 21. Composition of standard RT-qPCR reaction.

Component	**Volume [µl]**	**Final concentration**
RT-qPCR Master Mix	12.5	1x
10 µM primer mix	1	each 100 nM
GoTaq® DNA polymerase	0.15	0.75 U
Template DNA	variable	10 ng
ddH_2O	variable	
Total	**25**	

Table 22. Standard RT-qPCR cycling program.

Step	**Temperature [°C]**	**Duration**	
	50	2 min	
Initial Denaturation	95	10 min	
Denaturation	95	20 s	40 cycles
Annealing	60	20 s	
Elongation	72	20 s	
	95	15 s	
Final elongation	60	1 min	
	95	0.05°C/ sec	
Short-term storage	4	hold	

Table 23. Composition of standard cDNA synthesis reaction.

Component	**Volume [µl]**
5x iScript™ reaction mix	4
iScript™ reverse transcriptase	1
RNA template (500 ng – 1 µg)	variable
Nuclease-free H_2O	variable
Total	**20**

Table 24. Standard cycling program for cDNA synthesis.

Step	**Temperature [°C]**	**Duration [min]**
Priming	25	5
Reverse transcription	46	20
Enzyme inactivation	95	1
Short-term storage	4	hold

2.2.4 Plasmid

Plasmid used for live cell imaging of the 5-HT2A-R (cMyc-5-HT2A-mCherry) was friendly provided by the group of Gonzáles-Maeso (Department of Physiology and Biophysics, School of Medicine, Virginia Commonwealth University, USA) described in[421].

2.3 Bacteria

Commercial bacteria stock solutions, supplements and media. Amplification of plasmid DNA was performed in Escherichia coli (E. coli) DH5a.

Table 25. Commercial bacteria stock solutions.

Compound	Manufacturer	Catalogue number	Registered office
Ampicillin	Sigma-Aldrich	A9518	St. Louis, USA
Bacto-Agar	BD Biosciences	214010	Franklin Lakes, USA
Bacto-Tryptone	BD Biosciences	211705	Franklin Lakes, USA
Glucose	Carl Roth	HN06.2	Karlsruhe, Germany
LB medium powder	Carl Roth	X968.4	Karlsruhe, Germany
$MgCl_2$	Merck Millipore	105833	Burlington, USA
$MgSO_4$	Merck Millipore	105886	Burlington, USA
NaCl	Sigma-Aldrich	31434	St. Louis, USA
Yeast Extract	BD Biosciences	212750	Franklin Lakes, USA

Table 26. Media and solutions used for cultivation of bacteria.

Medium / Solution	Concentration	Solvent	Final concentration
Ampicillin stock solution	100 mg/ml	ddH_2O	100 µg/ml
LB (Luria/Miller)	25 g/L	ddH_2O	25 g/L
LB agar	15 g/L	ddH_2O	15 g/L

Table 27. Self-made media for cultivation of bacteria.

Medium (base)	Additive / component	Final concentration
LB medium	LB medium powder Ampicillin	20% (w/v) 100 µg/ml
LB agar	LB medium powder Bacto-Agar Ampicillin	20% (w/v) 15% (w/v) 100 µg/ml
SOC medium	Bacto-Tryptone Yeast extract NaCl KCl $MgCl_2$ $MgSO_4$ Glucose	2% (w/v) 0.5% (w/v) 10 mM 2.5 mM 10 mM 10 mM 200 mM

2.4 Virus

AAV_CamKIIa p-hCHR2(134a)-mCherry (friendly provided by AG Grinevich, Central Institute of Mental Health, Mannheim, Germany).

2.5 Biochemistry

2.5.1 Biochemistry: commercials, kits, self-made buffers and solutions

Table 28. Biochemistry: commercials.

Gel	Manufacturer	Catalogue number	Registered office
16.5% Mini-PROTEAN® Tris-Tricine Gel	Bio-Rad Laboratories	4563063	Hercules, USA
Tris-Tricine-SDS buffer (10x)	Sigma-Aldrich	T1165-500ML	St. Louis, USA
Zeba™ Dye and Biotin Removal Spin Columns and Filter Plates, 0.5-10 ml	Thermo Fisher Scientific	A44296S	Waltham, USA

Table 29. Biochemistry: commercial kits.

Kit	Manufacturer	Catalogue number	Registered office
Alexa Fluor™ 680 Antibody Labeling Kit	Thermo Fisher Scientific	A20188	Waltham, USA
BCA Protein Assay	Thermo Fisher Scientific	23228	Waltham, USA

Table 30. Biochemistry: self-made buffers and solutions.

Buffer / solution	Component	Concentration
Anode buffer (1x), SDS-PAGE	Tris-HCl, pH 8.8	200 mM
Ammonium persulfate (APS) stock solution	APS	10% (w/v) in ddH_2O
DAPI staining solution	DAPI	300 nM in PBS
Glucose stock solution	D(+)-Glucose 0.2 µm sterile-filtered	400 mg/ml
Gel buffer for polyacrylamide gels, SDS-PAGE	Tris-HCl, pH 8.5 SDS	3 M 0.3% (w/v)
Mounting solution	Tris-HCl, pH 8.5 Glycerol Mowiol DABCO®	100 mM 25% 10% 0.6%
PBS	NaCl KCl Na_2HPO_4 KH_2HPO_4	137 mM 2.7 mM 10.0 mM 1.8 mM
Protein lysis buffer	Tris-HCl, pH 7.4 NaCl SDS EDTA Phosphatase inhibitor tablet Protease inhibitor tablet	50 mM 150 mM 1% (w/v) 25 mM 1 tablet/ 10 ml 1 tablet/ 10 ml

Sample buffer (6x), SDS-PAGE	Tris-HCl, pH 6.8 SDS Glycerol 2-Mercaptoethanol Bromophenol blue	93.75 mM 6% 6% 9% 0.25%
SDS stock solution	SDS	10% (w/v) in ddH_2O
SDS-Polyacrylamide, stacking gel, western blotting	Gel buffer, SDS-PAGE Bis/ acrylamide APS TEMED	24.8% (v/v) 3.84% (v/v) 0.00672% (w/v) 0.224%
SDS-Polyacrylamide, separating gel, western blotting	Gel buffer, SDS-PAGE Bis/ acrylamide glycerol APS TEMED	33.3% (v/v) 10% (v/v) 10% (v/v) 0.028% (w/v) 0.09% (v/v)
TAE (1x), agarose gel buffer	Tris, pH 8.0 EDTA acetic acid	200 mM 1 mM 0.114%
1x TAE	Tris Acetic acid EDTA	40 mM 20 mM 1 mM
TBS (10x)	Tris-HCl, pH 7.4 NaCl KCl	248 mM 1.37 M 26.8 mM
TBS-T (1x)	TBS (10x) Tween® 20	10% (v/v) 0.1% (v/v)
Transfer buffer, SDS-PAGE	Tris-glycine buffer (10x) Methanol SDS	10% (v/v) 20% (v/v) 0.08% (v/v)
Tris-glycine buffer (10x)	Tris-HCl, pH 8.8 Glycine	250 mM 1.92 M
Tris-HCl/SDS for polyacrylamide gels	Tris-HCl, pH 8.45 SDS	3 M 0.3% (w/v)
Triton X-100 stock solution	Triton X-100	10% (v/v) in PBS

2.5.2 Primary and secondary antibodies for immunocytochemistry and western blotting

The antibody was of polyclonal origin if no clone number is mentioned.

Table 31. Primary antibodies used for immunocytochemistry (ICC).

Antibody (clone)	**Host species**	**Dilution**	**Blocking Solution in 10% Fetal bovine serum (FBS)**	**Manufacturer**	**Catalogue number**	**Registered office**
Annexin A2 (D11G2)	rabbit	1:200	0.1% Saponin	Cell Signaling Technologies	8235S	Danvers, USA
Ankyrin G (N106/36)	mouse	1:100	0.1% Saponin	NeuroMap	75-147	Davis, USA
BDNF	rabbit	1:300	0.1% Saponin	Elabscience	E-AB-18244.200	Houston, USA
B-III-Tubulin	guinea-pig	1:1000	0.1% Saponin/ 0.1% - 0.3% Triton X	Synaptic Systems	302304	Göttingen, Germany
B-III-Tubulin (TUJ1)	mouse	1:2000	0.1% Saponin/ 0.1% - 0.3% Triton X	BioLegend	801202	San Diego, USA

CTIP-2 (25B6)	rat	1:500	0.3% Triton X	Abcam	ab18465	Cambridge, UK
cFOS (9F6)	rabbit	1:500	0.3% Triton X	Cell Signaling Technologies	2250	Danvers, USA
FOXA2	goat	1:500	0.3% Triton X	R&D Systems	AF2400	Minneapolis, USA
OCT3/4 (A-9)	mouse	1:500	0.3% Triton X	Santa Cruz	Sc-365509	Santa Cruz, USA
GFAP	mouse	1:500	0.1% Triton X	Synaptic Systems	173011	Göttingen, Germany
Extracellular 5-HT2AR	rabbit	1:100	Blocking solution	Alomone Labs	ASR-033	Jerusalem, Israel
Ki67 (D3B5)	rabbit	1:500	0.3% Triton X	Cell Signaling Technologies	9129S	Danvers, USA
MAP2	chicken	1:7000	0.1% Saponin/ 0.1% - 0.3% Triton X	BioLegend	822501	San Diego, USA
mCherry	rabbit	1:1000	0.3% Triton X	Cell Signaling Technologies	43590S	Danvers, USA
NESTIN 196908	mouse	1:600	0.3% Triton X	R&D Systems	MAB-1259	Minneapolis, USA
NeuN (D4G4O)	rabbit	1:200	0.3% Triton X	Cell Signaling Technologies	24307S	Danvers, USA
PAX6 (Poly19013)	rabbit	1:500	0.3% Triton X	Biolegend	901301	San Diego, USA
Pro-BDNF	rabbit	1:400	0.1% Triton X	Alomone Labs	ANT-006	Jerusalem, Israel
PSD-95	rabbit	1:250	0.1% Saponin	Cell Signaling Technologies	2507S	Danvers, USA
S100A10 (p11) (4E7E10)	mouse	1:400	0.1% Saponin	Cell Signaling Technologies	5529	Danvers, USA
SOX2 (D6D9)	rabbit	1:500	0.3% Triton X	Cell Signaling Technologies	3579S	Danvers, USA
SV2A	guinea-pig	1:500	0.1% Saponin	Synaptic Systems	119004	Göttingen, Germany
Synapsin I/II/III (A17080A)	mouse	1:500	0.1% Saponin	BioLegend	853701	San Diego, USA
Synaptophysin (SP17)	mouse	1:500	0.1% Saponin	BioLegend	837104	San Diego, USA
TAU	guinea-pig	1:700	0.1% Saponin/ 0.1% - 0.3% Triton X	Synaptic Systems	314004	Göttingen, Germany
TBR1	rabbit	1:500	0.3% Triton X	Abcam	ab31940	Cambridge, UK
vGLUT2	guinea-pig	1:200	0.1% Triton X	Synaptic Systems	135304	Göttingen, Germany

Table 32. Secondary antibodies used for ICC.

Secondary antibodies were diluted 1:1000.

Antibody	**Host species**	**Manufacturer**	**Catalogue number**	**Registered office**
anti-chicken IgG Alexa Fluor-488	goat	Thermo Fisher Scientific	A11039	Waltham, USA
anti-guinea-pig IgG Alexa Fluor-488	goat	Thermo Fisher Scientific	A11073	Waltham, USA

anti-guinea-pig IgG Alexa Fluor-568	goat	Thermo Fisher Scientific	A11075	Waltham, USA
anti-mouse IgG Alexa Fluor-488	goat	Thermo Fisher Scientific	A11001	Waltham, USA
anti-mouse IgG Alexa Fluor-568	goat	Thermo Fisher Scientific	A11004	Waltham, USA
anti-rabbit IgG Alexa Fluor-488	goat	Thermo Fisher Scientific	A11008	Waltham, USA
anti-rabbit IgG Alexa Fluor-555	goat	Thermo Fisher Scientific	A21428	Waltham, USA
anti-rabbit IgG Alexa Fluor-647	goat	Thermo Fisher Scientific	A21244	Waltham, USA
anti-rat IgG Alexa Fluor-555	goat	Thermo Fisher Scientific	A21434	Waltham, USA

Table 33. Fluorescent probes.

Antibody (clone)	Dilution	Manufacturer	Catalogue number	Registered office
4,6-diamidino-2-phenylindole (DAPI)	300 nM	Biolegend	422801	San Diego, USA

Table 34. Primary antibodies used for Western blotting (WB).

Antibody (clone)	Host species	Dilution	Manufacturer	Catalogue number	Registered office
Actin (8H10D10)	mouse	1:20,000	Cell Signaling Technologies	3700S	Danvers, USA
Actin (13E5)	rabbit	1:20,000	Cell Signaling Technologies	4970S	Danvers, USA
AKT (pan) (C67E7)	rabbit	1:2500	Cell Signaling Technologies	4691S	Danvers, USA
Annexin A2 (D11G2)	rabbit	1:2000	Cell Signaling Technologies	8235S	Danvers, USA
BDNF	rabbit	1:500	Elabscience	18244.200	Houston, USA
pAKT (S473) D9E XP®	rabbit	1:2500	Cell Signaling Technologies	4060S	Danvers, USA
Pro-BDNF	mouse	1:100	Santa Cruz	sc-65513	Santa Cruz, USA
S100A10 (p11) (4E7E10)	mouse	1:400	Cell Signaling Technologies	5529S	Danvers, USA
pTrkB	mouse	1:500	Santa Cruz	SC-8058	Santa Cruz, USA

Table 35. IR-dye conjugated secondary antibodies used for WB.

Secondary antibodies were diluted 1:15,000.

Antibody (clone)	Host species	Manufacturer	Catalogue number	Registered office
Anti-mouse DyLight™ 680	goat	Cell Signaling Technologies	5470S	Danvers, USA

Anti-mouse DyLight™ 800	goat	Cell Signaling Technologies	5257S	Danvers, USA
Anti-rabbit DyLight™ 680	goat	Cell Signaling Technologies	5366S	Danvers, USA
Anti-rabbit DyLight™ 800	goat	Cell Signaling Technologies	5151S	Danvers, USA

2.5.3 Buffers and solution chemicals and reagents

Table 36. Biochemistry: chemicals and reagents.

Chemical	Manufacturer	Catalogue number	Registered office
2-Mercaptoethanol	Merck Millipore	805740	Burlington, USA
2-Propanol (isopropanol)	Th. Geyer	1157-5L	Renningen, Germany
30% Bis/acrylamide	Carl Roth	3029.1	Karlsruhe, Germany
Agarose	Sigma-Aldrich	A9539-500G	St. Louis, USA
Ammonium persulfate (APS)	Sigma-Aldrich	A3678-25G	St. Louis, USA
Bovine serum albumin (BSA)	Sigma-Aldrich	A3294-50G	St. Louis, USA
Bromophenol blue	Sigma-Aldrich	B8026-5G	St. Louis, USA
Chloroform	Sigma-Aldrich	32211-1L	St. Louis, USA
DAPCO®	Carl Roth	0718.2	Karlsruhe, Germany
DMSO	Sigma-Aldrich	D5879-2.5L-M	St. Louis, USA
Diethyl pyrocarbonate (DEPC)	Carl Roth	K028.1	Karlsruhe, Germany
EDTA	Acros Organics	147850010	Fair Lawn, USA
EGTA	Sigma-Aldrich	E3889-10G	St. Louis, USA
Ethanol	Th. Geyer	2246.1000	Renningen, Germany
Fetal bovine serum (FBS)	Thermo Fisher Scientific	10270-106	Waltham, USA
Glycerol	Sigma-Aldrich	15523-1L-M	St. Louis, USA
Glycine	Thermo Fisher Scientific	10070150	Waltham, USA
HEPES	Carl Roth	9105.4	Karlsruhe, Germany
Hydrochloric acid (HCL)	Th. Geyer	836.1000	Renningen, Germany
KCl	Th. Geyer	1632	Renningen, Germany
Methanol	Carl Roth	0082.1	Karlsruhe, Germany
$MgCl_2$	Promega	A351b	Madison, USA
Mowiol®4-88	Carl Roth	0713.1	Karlsruhe, Germany
Myo-Inositol	Sigma-Aldrich	I5125	St. Louis, USA
Paraformaldehyde (PFA)	Sigma-Aldrich	16005	St. Louis, USA
Polyethylenimine (PEI)	Sigma Aldrich	P3143	St. Louis, USA
Polyvinylalcohol	Sigma-Aldrich	P8136	St. Louis, USA
Phosphatase inhibitor mini tablets	Thermo Fisher Scientific	A32957	Waltham, USA
Protease inhibitor mini tablets, EDTA-free	Thermo Fisher Scientific	A32955	Waltham, USA
Saponin	Fluka	84510	
Sodium chloride (NaCl)	Sigma-Aldrich	S5886-1KG	St. Louis, USA
SDS, pellets	Carl Roth	CN30.1	Karlsruhe, Germany
Sodium hydroxide, pellets	Carl Roth	6771.2	Karlsruhe, Germany
N,N,N,N'-tetramethylethylenediamine (TEMED)	Sigma-Aldrich	T9281-50ML	St. Louis, USA
TRIS	Carl Roth	4855.2	Karlsruhe, Germany
Triton X-100	Merck Millipore	1.08603.1000	Darmstadt, Germany
Trypan blue	Lonza	17-942E	Basel, Switzerland
Tween® 20	Sigma-Aldrich	P2287-100ML	St. Louis, USA

2.6 Common consumables and equipment

2.6.1 Cell culture, molecular biology and biochemistry consumables

Table 37. Common consumables.

Consumable	Manufacturer	Catalogue number	Registered office
3.5 cm Ø TC dish, standard F	Sarstedt	83.3900	Nümbrecht, Germany
3.5 cm Ø Ibidi, high	Ibidi	81156	Gräfelfing, Germany
10 cm Ø TC dish, Cell+	Sarstedt	83.3902.300	Nümbrecht, Germany
6-well plate, TC standard F	Sarstedt	833.920.005	Nümbrecht, Germany
12-well plate, TC Cell+	Sarstedt	833.921.300	Nümbrecht, Germany
24-well plate, TC Cell+	Sarstedt	833.922.300	Nümbrecht, Germany
48-well plate, TC Cell+	Sarstedt	83.3923.300	Nümbrecht, Germany
96-well plate, TC standard F	Sarstedt	83.3924.005	Nümbrecht, Germany
Bottle top filter, 500 ml	Thermo Fisher Scientific	15983307	Waltham, USA
Bottle top filter, 1000 ml	Thermo Fisher Scientific	15993307	Waltham, USA
Cell lifter (UltraCruz)	Santa Cruz	sc-395251	Santa Cruz, USA
Coverslip, 12 mm	VWR	631-1577	Radnor, USA
Cryotubes, conical bottom, 1 ml	Greiner Bio-One	123280	Frickenhausen, Germany
Microscope slides, glass	Carl Roth	H868.1	Karlsruhe, Germany
Nitrocellulose membrane Amersham Protran, 0.45 µm	Sigma-Aldrich	GE10600001	St. Louis, USA
Pasteur pipette, glass	Th. Geyer	7691061	Renningen, Germany
RT-PCR strip tubes, 0.2 ml	Biozym	710971	Hessisch Oldendorf, Germany
Petri dish, 10 cm Ø	Greiner Bio-One	633180	Frickenhausen, Germany
Pipette tip, 10 µl	Sarstedt	70.1130	Nümbrecht, Germany
Pipette tip, 200 µl	Sarstedt	70.760.002	Nümbrecht, Germany
Pipette tip, 1250 µl	Sarstedt	701.186	Nümbrecht, Germany
Pipetting reservoir, 25 ml	Cole-Parmer GmbH	B3125-50	Wertheim, Germany
RT-qPCR plate, 96-well	Steinbrenner Laborsysteme	4ti-0910/C	Wiesenbach, Germany
RT-qPCR plate seal	Steinbrenner Laborsysteme	4ti-0500	Wiesenbach, Germany
Reaction tube, 0.2 ml	Sarstedt	72.737.002	Nümbrecht, Germany
Reaction tube, 0.5 ml	Sarstedt	72.699	Nümbrecht, Germany
Reaction tube, 1.5 ml	Sarstedt	72.690.001	Nümbrecht, Germany
Reaction tube, 2.0 ml	Sarstedt	72.695.200	Nümbrecht, Germany
Serological pipettes, 5 ml	Sarstedt	861.253.001	Nümbrecht, Germany
Screw cap tube, 15 ml	Sarstedt	62.554.502	Nümbrecht, Germany
Screw cap tube, 50 ml	Sarstedt	62.547.254	Nümbrecht, Germany
Serological pipettes, 5 ml	Sarstedt	861.253.001	Nümbrecht, Germany
Serological pipettes, 10 ml	Sarstedt	861.254.001	Nümbrecht, Germany
Serological pipettes, 25 ml	Sarstedt	861.685.001	Nümbrecht, Germany
Serological pipettes, 50 ml	Th. Geyer	7695555	Renningen, Germany
Western blot filter tissue	VWR	115-2166	Radnor, USA

Table 38. Notable laboratory equipment.

Appliance	Name	Manufacturer	Registered office
Agarose gel electrophoresis chamber	EasyPhor Midi	Biozym	Hessisch Oldendorf, Germany
Agarose gel imaging system	GeneFlash	Syngene	Bangalore, India
Autoclave	Laboclav	SHP Steriltechnik AG	Detzel Schloss, Germany
Balance	BL610	Sartorius	Göttingen, Germany
Balance	BP121S	Sartorius	Göttingen, Germany
Block heater	Thermomixer comfort	Eppendorf	Hamburg, Germany
Centrifuge	Labofuge 400R	Thermo Fisher Scientific	Waltham, USA
Centrifuge	5415 D	Eppendorf	Hamburg, Germany
Centrifuge, coolable	Z216MK	Hermle	Gosheim, Germany
Centrifuge, plates	5810	Eppendorf	Hamburg, Germany
CO_2 Incubator	C170 E3	Binder	Tuttlingen, Germany
Electrophoresis RNA quality control	Bioanalyzer 2100	Agilent Technologies	Santa Clara, USA
Extraction hood	mc6® das Laborsystem	Waldner GmbH & Co	Wangen, Germany
Freezer -80°C	Hera freeze	Thermo Fisher Scientific	Waltham, USA
Freezer -150°C	VIP plus	Panasonic	Kadoma, Japan
Freezing container	Mr. Frosty™	Thermo Fisher Scientific	Waltham, USA
Flow hood, sterile laminar	Scanlaf Mars	Labogene	Lillerød, Denmark
Gel electrophoresis power supply	PowerPac™ Basic Power Supply EPS 301	Bio-Rad Laboratories	Hercules, USA
Gel electrophoresis chamber	Mini-PROTEAN 2-D electrophoresis cell chamber	Bio-Rad Laboratories	Hercules, USA
RT-PCR cycler	Biometra TAdvanced	Analytik Jena	Jena, Germany
pH meter	ProfiLab WTW pH597	Xylem Inc.	Washington, USA
Liquid nitrogen store	Cryotech	Thermo King	Minneapolis, USA
Microplate reader	Wallac Victor2 1420	Perkin Elmer	Waltham, USA
Microplate reader	PowerWave™ XS	BioTek	Winooski, USA
Microscope	Celldiscoverer 7	Carl Zeiss	Oberkochen, Germany
Microscope	DM6 B	Leica	Wetzlar, Germany
Microscope, brightfield	Inverted DMIL LED	Leica	Wetzlar, Germany
Microscope, confocal	TCS SP5 II	Leica	Wetzlar, Germany
Pipette-boy	Pipet Filler S1	Thermo Fisher Scientific	Waltham, USA
RT-qPCR cycler	QuantStudio 7 Flex	Thermo Fisher Scientific	Waltham, USA
Quantification RNA, DNA	Qubit 4.0 Fluorometer	Thermo Fisher Scientific	Waltham, USA
Roll Mixer	Sunlab SU 1400	Neolab	Heidelberg, Germany
Sonication device	Branson Ultrasonics™ Sonifier 250	Thermo Fisher Scientific	Waltham, USA
Spectrophotometer	NanoDrop™ 1000	Thermo Fisher Scientific	Waltham, USA
Table centrifuge	C1301-230V	Corning	Corning, USA
Thermomixer	Thermomixer comfort 5355	Eppendorf	Hamburg, Germany
Vacuum pump	FTA-1	Thermo Fisher Scientific	Waltham, USA
Vortex	Bio Vortex V1	VWR	Radnor, USA
Warm water bath	ED-17	JULABO Labortechnik	Seelbach, Germany
Warm water bath for cell culture		Köttermann GmbH	Uetze, Germany
Water purifier	Milli-Q® Integral 5	Merck Millipore	Burlington, Massachusetts, USA
Western blot imager	Odyssey IR imaging system	LI-COR Biosciences	Lincoln, USA
Western blot transfer system	Trans-Blot® Turbo™	Bio-Rad Laboratories	Hercules, USA

2.7 Software

Table 39. Computer software and other digital resources.

Computer program	**Supplier**
Biorender.com	BioRender
Excel 2019	Microsoft
ImageJ (FIJI), version v.0.5.3	National Institutes of Health (NIH), open source
Image studio v. 2.0	LI-COR
Mendeley reference manager	Mendeley Ltd.
PowerPoint 2019	Microsoft
Quant Studio 7 Flex RT-qPCR software	Thermo Fisher Scientific
R Studio, version 1.4.1106© 2009 for macOS	RStudio PBC, open source
Word 2019	Microsoft

3 Methods

3.1 Human material and generation of fibroblast-derived human iPSCs

iPS cells were generated from dermal fibroblasts of healthy and patient adult donors (**see Table 8 - 10**). Reprogramming was not part of this doctoral thesis. The study was approved by the local ethics committee. All experiments with human material were in accordance with the Declaration of Helsinki. All participants gave written informed consent. Control cell lines (Ctrl): Ctrl 1 female, age at timepoint of biopsy: 44; Ctrl 2 female, age at timepoint of biopsy: 25; Ctrl 3 female, age at timepoint of biopsy: 23; Ctrl 4 male, age at timepoint of biopsy 19; Ctrl 5 male, age at timepoint of biopsy: 23. Three BD1 patient cell lines: BD1 1 male, age at timepoint of biopsy: 24; BD1 2 male, age at timepoint of biopsy: > 55; BD1 3 male, age at timepoint of biopsy: 36. One BD2 patient cell line: BD2 1 age at timepoint of biopsy: 48 and two AUD patient cell lines: AUD1 male, age at timepoint of biopsy: 57; AUD2 male, age at timepoint of biopsy: 68. Reprogramming was done using CytoTune®-iPS 2.1 Sendai Reprogramming Kit (Thermo Fisher Scientific, A16517). Control iPS and AUD patient cells were obtained from Dr. Sandra Horschitz (Hector Institute for Translational Brain Research, Central Institute of Mental Health, Mannheim, Germany). iPS cells from BD patients were obtained from Prof. Dr. Philipp Koch (Hector Institute for Translational Brain Research, Central Institute of Mental Health, Mannheim, Germany). Chromosomal alterations were excluded by genome-wide single nucleotide polymorphism (SNP) analysis. iPSCs were screened for their stem cell properties by the capability of *in vitro* differentiation into the three embryonic germ layers, ectoderm, mesoderm and endoderm (characterization in in our group, data not shown) and for pluripotent stem cells markers *in vitro*.

3.2 Cell culture

Cells were cultured at 37°C, ambient O_2 and 5% CO_2 concentration under sterile conditions in an incubator. Applications with the cells were carried out in a sterile flow hood by using sterile and autoclaved instruments and medium.

3.2.1 Coating for iPS cultures and progenitors

Cultivation of iPS cells and neuronal progenitors was carried out on Geltrex™-coated plates or dishes. Cell culture plates were coated over night at 4°C or 1h at 37°C with 5% (v/v) Geltrex™ diluted 1:50 in DMEM with GlutaMAX™ containing 1% (v/v) penicillin/streptomycin (Pen/Strep) (wash medium). Geltrex™ solution and coated plates and dishes were stored at 4°C. Solution was re-used up to three times.

3.2.2 Maintenance of iPS cultures

Fibroblast-derived iPS cells were kept as colonies under feeder free-conditions in stem cell state on 5% (v/v) Geltrex™-coated plates in Essential 8 (E8) medium (DMEM/F12 with L-glutamine and HEPES supplemented with 1% (v/v) Pen/Strep (v/v), 64 µg/ml LAAP, 14 ng/ml sodium selenite, 200 ng/ml fibroblast growth factor (FGF)-2 (154), 2 ng/ml TGF-β1, 20 µg/ml insulin, 11 µg/ml transferrin) that was changed daily. All iPS cells used in the present study were verified as free from mycoplasma contamination and in regular intervals for their genetic "fingerprint" identity by RT-PCR.

3.2.3 Passaging of iPS cells

Colonies were passaged when they reached a confluency of more than 80%. For passaging confluent iPS colonies were washed twice with phosphate buffered saline (DPBS) and then incubated with 0.5 mM ethylenediaminetetraacetic acid (EDTA) for 5 - 10 min at RT until the colonies started to detach. After aspirating the EDTA solution the fractured colonies were gently resuspended in E8 medium containing 5 µM Rho-associated protein kinase (ROCK) inhibitor. Depending on confluency and experimental purpose, cells were split and seeded on new plates.

3.2.4 Freezing and thawing of iPS cells

For freezing confluent iPS colonies were washed twice with DPBS and then incubated with 0.5 mM EDTA for 5 - 10 min at RT until the colonies start to detach. After removing the EDTA solution the fractured colonies were gently taken up in wash medium. Cells were transferred to a 15 ml tube and centrifuged at 1000 g for 4 min. The pellet was gently resuspended in 500 µl hiPSC freezing medium (50% (v/v) KnockOut™ serum replacement (KOSR), 40% (v/v) E8 medium, 10% (v/v) DMSO) supplemented with freshly added 10 µM ROCK inhibitor transferred to a cryotube and slowly frozen in a Mr. Frosty™. Storage of samples was done first at - 80 °C, then transferred to -150 °C and for long-term storage in liquid nitrogen at -196°C. For fast thawing cryotubes were placed in a water bath at 37°C. 500 µl was resuspended in 5 - 10 ml wash medium, transferred to a 15 ml tube and centrifuged for 4 min at 800 g. The pellet was gently resuspended in E8 medium supplemented with 5 µM ROCK inhibitor and seeded and seeded on 5% (v/v) Geltrex™-coated plates (amount depending on the size of the pellet).

3.2.5 Differentiation of iPS cells into neuronal progenitors

The transition of human iPS cells into neuronal progenitors was based on the induction of neuroectoderm by inhibiting mesoderm or endoderm formation by dual SMAD inhibition of BMP and TGF-β signaling[30–32]. For *in vitro* differentiation of fibroblast-derived iPSCs into neural progenitors E8 medium was replaced by neural progenitor induction medium phase 1 (advanced DMEM/F-12 medium with

glutamine, with 1% (v/v) Pen/Strep (v/v), 2 mM GlutaMAX™, 1% (v/v) B-27 supplement with retinoic acid (RA), 10 µM SB-431542, 1 µM LDN-193189, 2 µM XAV939 and 5 µM cyclopamine) when iPS cells reached 70-80% confluency. At day 4, cells were dissociated 1:2 to a monolayer, continue using aforementioned medium. Upon day 8 cells were dissociated 1:2 and medium was changed to neural progenitor induction medium phase 2 (advanced DMEM/F-12 medium with glutamine with 1% (v/v) Pen/Strep, 2 mM GlutaMAX™, 1% (v/v) B-27 supplement with RA, 200 nM LDN-193189) for 8 more days. In the last step medium was changed to neural progenitor induction medium phase 3 (advanced DMEM/F-12 medium with glutamine with 1% (v/v) Pen/Strep, 2 mM GlutaMAX™, 1% (v/v) B-27 supplement with RA, 20 ng/ml FGF-2 (157). In this step cells could be passaged up to three times until first neurons become visible. Neural progenitor induction media (media composition in **Table 7**) was changed daily and cells were cultivated on 5% (v/v) Geltrex™-coated dishes.

3.2.6 Passaging of neuronal progenitors

Dissociation into single cells and plating into monolayer was done using TrypLE™ for 5 - 15 min at 37 °C until the cells start to detach. Cells were then transferred with wash medium to a 15 ml tube and centrifuged for 4 min at 1000 g. The pellet was gently resuspended in corresponding neural progenitor induction medium supplemented with 5 µM ROCK inhibitor.

3.2.7 Freezing and thawing of neural progenitors

Neural progenitors could be frozen and thawed in all three phases of neural induction. For freezing cells were dissociated using TrypLE™ for 5 - 15 min at 37 °C until the cells start to detach. Cells were then transferred to a 15 ml tube and centrifuged at 1000 g for 4 min. The pellet was gently resuspended in 500 µl freezing medium (70% (v/v) KOSR, 20% (v/v) cytobuffer, 10% (v/v) DMSO) supplemented with freshly added 10 µM ROCK inhibitor, transferred to a cryotube and slowly frozen in a Mr. Frosty™. Storage of samples occurred first at - 80 °C and were then transferred to - 150°C. For fast thawing cryotubes were put in a water bath at 37°C. 500 µl of sample was resuspended in wash medium, transferred to a 15 ml tube and centrifuged for 4 min at 800 g. The pellet was gently resuspended in that neural induction media in which the cells have been cultivated before freezing and seeded on 5% (v/v) Geltrex™-coated plates (amount depending on the size of the pellet). Neural induction was proceeded as described in **3.2.5**.

3.2.8 Coating for neuronal cultures

Coverslips for immunostainings were pretreated with 37% hydrochloric (HCl) acid for 1h at RT, following three washing steps with dH_2O and one washing step with 70% ethanol prior to autoclaving. For the long-term neuronal cultivation of plates and dishes (containing pre-treated coverslips) were coated with 1:2000 of 1% polyethylenimine (PEI) in 25 mM boric acid (pH 8.4) for 10 min. The plates

were washed three times with autoclaved ddH_2O and coated with 3.75 µg/ml laminin in DPBS overnight at 4°C. PEI/Laminin coated plates and dishes were stored at 4°C and quickly used-up or were frozen for longer storage at - 20°C.

3.2.9 *In vitro* differentiation of neural progenitors into human cortical neurons

For *in vitro* differentiation of neural progenitors into a homogeneous culture of human cortical neurons a highly standardized protocol based on the work by Kemp and Telezhkin and colleagues[422,423], which was further developed and modified by our working group at the Hector Institute for Translational Brain Research (headed by Prof. Dr. Philipp Koch), was used. Mature cortical neurons expressed neuronal and synapse associated proteins and cortical layer markers and were screened by their electrophysiological properties. (**Fig. 11**). The differentiation states were separated into five maturation phases, marked by different media compositions (media composition in **Table 7,** illustrated in **Fig. 10**). B-27 supplement in combination with N2 supplement ensured the synchronized growth of neurons of the central nervous system (CNS) *in vitro*. In phase 1 and 2 the Ca^{2+} concentration was elevated, Notch signalling was inhibited and cell-cycle exit was forced in the neuronal progenitors. DAPT which forced neural cells to commit neuronal differentiation and cyclin dependent kinase (CDK) 4 inhibitor PD-0332991 prevented further proliferation. In phase 2 GABA was supplemented to simulate the effect of GABAergic interneurons. Forskolin, a cAMP pathway activator and CHIR99021 which activates the WNT pathway was added. During the whole differentiation BDNF associated TrkB pathways were activated by administration of LM22A and LM22B. In neuronal differentiation phase 5 Bryostatin 1, as a PKCε activator, was added. TrkB and WNT signalling are pathways associated with neuronal plasticity to promote synapse formation and neuronal network formation. *In vitro* differentiation of neural progenitors into human cortical neurons was launched by the change from neural progenitor induction medium phase 3 to neural differentiation medium phase 1, defined as day 0 of differentiation. Neural differentiation phase 1 medium consisted of neural base medium 1 (DMEM/F-12 medium with glutamine, 0.1% (v/v) GlutaMAX™, 1.8 mM $CaCl_2$, 1% (v/v) Pen/Strep, 1% (v/v) B-27, 0.5% (v/v) N2 supplement (prepared in the laboratory as follows: DMEM/F-12 with glutamine, 500 µg/ml insulin, 10 mg/ml transferrin, 520 ng/ml sodium selenite, 1.611 mg/ml putrescine and 630 ng/ml progesterone), 1% (v/v) NEAA, 1.6 mg/ml glucose) supplemented with 200 µM ascorbic acid, 1 µM LM22A, 1 µM LM22B, 2 µM PD-0332991, 5 µM DAPT and was applied until day 3 of differentiation. The cells were split on the final plate format into phase 2 medium. After splitting the medium was changed half the other day to remove death cells and cell debris. Neural differentiation medium phase 2 - 4 media consisted of neural base medium 2 with Neurobasal™ (plus1.6 mg/ml glucose, 1% (v/v) Pen/Strep, 0.1% (v/v) GlutaMAX™ and 1% (v/v) B-27) and was supplemented additionally to phase 1 medium with 3 µM CHIR99021, 10 µM forskolin and 300 µM GABA. At day 10 of differentiation medium was changed to neural differentiation medium phase 3 containing 3 µM CHIR99021. From day 17 on, CHIR99021 was removed in phase 4. At day 24 medium was changed to neural differentiation phase 5

medium in neural base medium 3 (advanced MEM, 1.6 mg/ml glucose, 1% (v/v) Pen/Strep, 0.1% (v/v) GlutaMAX, 1% (v/v) B-27) and 0.27 nM Bryostatin 1 for the next 14 days. Medium was changed every 3-4 days half.

3.2.10 Splitting of phase 1 neurons

Dissociation of phase 1 neurons into single cells was done using TrypLE™ for about 5 - 15 min at 37 °C until the cells start to detach. Cells were then transferred to a 15 ml tube and centrifuged at 1000 g for 4 min. In case of a genomic deoxyribonucleic acid (gDNA) contamination 10 µg/µl DNAse I was added before centrifugation and the cell solution was incubated for 10 min at 37°C in a water bath by flicking the tube from time to time. The pellet was gently resuspended into corresponding media supplemented with 5 µM ROCK inhibitor and seeded on PEI/Laminin coated (for staining plus coverslips) plates.

3.2.11 Freezing and thawing of neurons

Neurons could be frozen up to day 3 of differentiation. For freezing cells of 2 - 3 wells of a 6-well plate were dissociated using TrypLE™ for 5 min at 37 °C until the cells start to detach. Neurons were then transferred to a 15 ml tube and centrifuged at 1000 g for 4 min. The pellet was gently resuspended in 500 µl freezing medium (70% (v/v) KOSR, 20% (v/v) cytobuffer, 10% (v/v) DMSO) supplemented with freshly added 10 µM ROCK inhibitor, transferred to a cryotube and slowly frozen in a Mr. Frosty™. Storage of samples occurred first at - 80 °C and were then transferred to - 150°C. For thawing cryotubes were placed in a water bath at 37°C. 500 µl of sample was resuspended in 5 - 10 ml wash medium, transferred to a 15 ml tube and centrifuged for 4 min at 800 g. The pellet was gently resuspended in that media in which cells have been cultivated before freezing and seeded on PEI/laminin coated plates (amount depending on the size of the pellet).

3.2.12 Co-culture of human cortical neurons with mouse astrocytes

For electrophysiological experiments mouse astrocytes were plated in a density of around 30,000 cells/well on PEI/laminin coated coverslips on 24-well plates. Mouse astrocytes were cultured in astrocyte standard medium, consisting of astrocyte base medium (1% (v/v) Pen/Strep, 0.5% (v/v) N2, 1.6 mg/ml glucose) supplemented with 0.5% (v/v) N2, 1.6 mg/ml glucose, 0.1% B-27, 100 ng/µl epidermal growth factor (EGF), 10 ng/ml FGF-2 (147) until they reached 80 - 90% density. Medium was changed every other day. 3 days before the phase 1 neurons were split in a density of 200,000 cells onto the astrocytes the medium was changed to astrocyte differentiation medium, consisting of astrocyte base medium and 0.5% (v/v) N2, 1.6 mg/ml glucose and 10 ng/µl BMP-4. Medium was changed daily. Since the moment the cortical neurons were plated on the astrocytes the medium was changed to neural differentiation medium and differentiated was continued as described **3.2.9.**

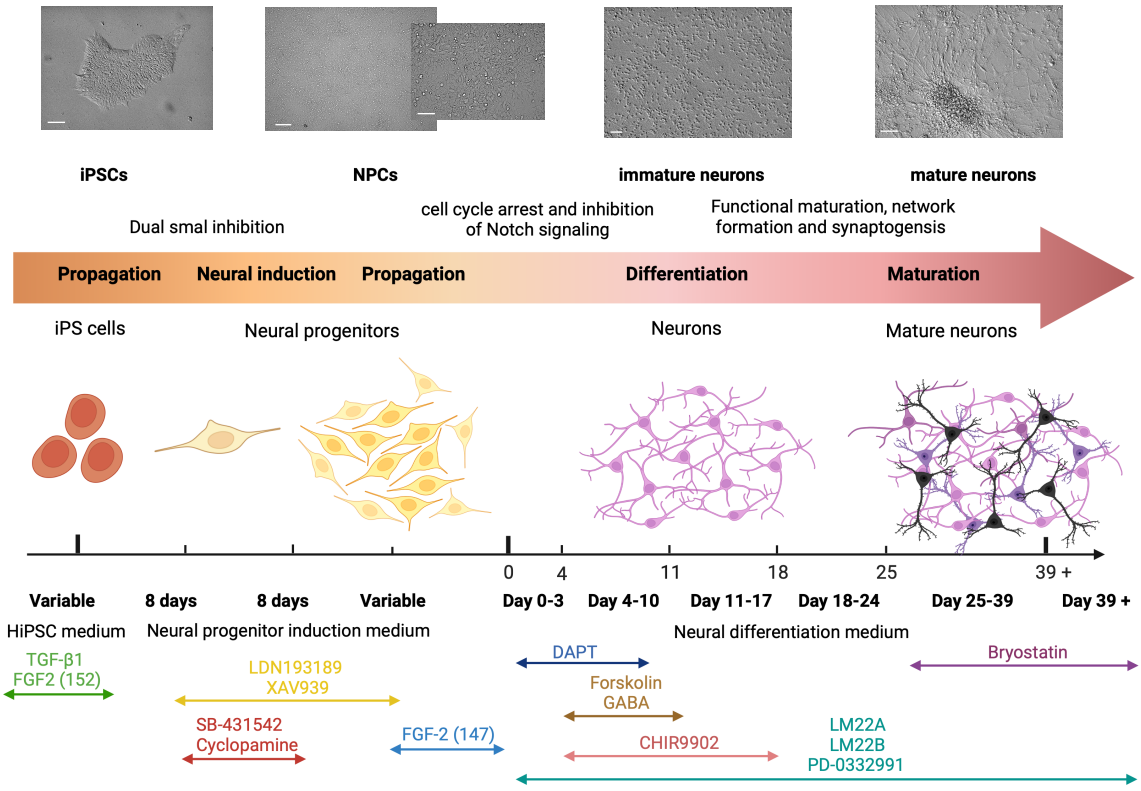

Figure 10. Timeline for the *in vitro* differentiation of iPSCs into cortical neurons.
The *in vitro* differentiation of human iPSCs over a neural progenitor step by dual SMAD into cortical neurons, including maturation and network formation processes is based on highly standardized protocol. The different media compositions and time phases of their administration are described in **Table 7** and in subchapter **3.2.9**. The start of the neural differentiation is marked as day 0. Scale bar iPSCs, close-up NPC and neurons: 50 µm; NPC scale bar: 150 µm.

3.3 Molecular biology

3.3.1 Isolation of gDNA

Cells of one well of a 6 well plate were washed with ice cold PBS. Cells were harvested by using a cell lifter and were transferred into a 1.5 ml tube and kept on ice. In the following the cells were centrifuged for 5 min at 5000 g at 4 °C. The supernatant was removed and the cells were gently resuspended in 150 µl lysis buffer (100 mM Tris-HCl (pH 8.5), 5 mM EDTA, 0.2% (w/v) sodium dodecyl sulphate (SDS), 200 mM sodium chloride (NaCl) supplemented with 133 ng/µl proteinase K) and incubated at 37°C and 500 rpm for 1 h. Inactivation of proteinase K was done at 95°C for 10 min. Precipitation of gDNA was achieved by adding 105 µl isopropanol, incubation at RT for 30 min (solution was vortexed every 10 min) and further centrifuged at 12,000 g for 10 min at RT. The pellet was washed twice with 70% ethanol and in the following centrifuged at RT 12,000 g for 10 min. After the last washing step all ethanol had to evaporate by letting air-dry the pellet for about 30 min, then resuspended in 100 µl ddH_2O and was further incubated for 30 min at 37°C and 400 rpm on a heating block. Storage of gDNA was done at - 20°C.

3.3.2 SNP analysis

To identify chromosomal alterations and karyotypic abnormalities gDNA from an early passage of iPSCs was extracted with the ExtractMe Genomic DNA kit according to the manufacturer's instructions. SNP analysis with 900 ng of gDNA was performed by the Life&Brain Genomics (Bonn, Germany) using an Infinium® Global Screening Array-24 BeadChip (Illumina; San Diego, USA) and further processed by Josef Frank (Department of Genetic Epidemiology in Psychiatry, Central Institute of Mental Health, Mannheim, Germany).

3.3.3 Ribonucleic acid isolation

Cells of 1 well of a 6 well plate were washed with in ice cold PBS. Cells were harvested by using a cells lifter and were transferred into a 1.5 ml tube and kept on ice. In the following the cells were centrifuged for 5 min at 5000 g at 4 °C. The supernatant was removed and the cells were gently resuspended in 500 µl peqGold Trifast™ and incubated for 10 min at room temperature. 100 µl of chloroform was added to the lysate. After gently mixing by inverting the tubes the Trifast and chloroform containing lysates were incubated for 10 min at room temperature. Tubes were then centrifuged for 5 min at 12,000 g at 4°C. Two phases were occurring. The upper clear, aqueous nucleic acid phase was transferred into a new tube. The lower pink protein phase was discarded. 250 µl of isopropanol was added to each sample. For the ribonucleic acid (RNA) precipitation tubes were kept for 2 - 3 hrs on ice or overnight at - 20°C. Tubes were centrifuged for 15 min at 4°C of 12,000 g and supernatant was discarded. The pellet was washed two times with 75% ethanol in DEPC water and centrifuged for 10 min at 4 °C at 12,000 g. After the last washing step all ethanol had to evaporate by first discarding the ethanol and afterwards letting air-dry the pellet for about 30 min. The pellet was resuspended in 20 µl DEPC-treated H_2O and shook at 400 rpm at 37 °C. To prevent DNA contamination the DNAase I Amplification grade kit was used. Samples were incubated for 15 min with a mixture of each 2.5 µl of DNAse I and reaction buffer. After incubation 2.5 µl of stop solution was added. Samples were incubated for 10 min at 70°C on a heating block. Long-term storage of RNA was performed at - 80°C. RNA isolation was performed in a sterile chemical fume hood.

3.3.4 Synthesis of complementary DNA

Complementary DNA (cDNA) was synthesized via the iScript™ cDNA synthesis kit according to manufacturer's instructions. 500 ng - 1 µg cDNA was used to reversely transcribe RNA into cDNA. The resulting cDNA was diluted 1:5 in nuclease-free H_2O. Primers were designed for each gene using `Primer-BLAST` database (https://www.ncbi.nlm.nih.gov/tools/primer-blast/) or design was based on literature research.

3.3.5 Agarose gel electrophoresis

Samples were mixed with 10 x DNA sample buffer. DNA fragments were separated in a 1 - 2% (w/v) agarose gel in 1x TAE buffer, containing 1: 15,000 peqGreen for staining of DNA. A reference DNA marker (100 bp or 1 kbp) was included to determine the size of the amplicons. Gels run for 50 min at 100 V and were imaged on a GeneFlash imaging system.

3.3.6 Determination of cDNA, gDNA and RNA concentration

The determination of the DNA, RNA and cDNA concentration was carried out with the NanoDrop™ 1000 system.

3.3.7 RNA bulk sequencing

RNA isolation was performed as described in **3.3.3**. RNA concentration was measured with the Qubit 4.0. For quality control RNA integrity number (RIN) measurement was done with RNA 6000 Nano Kit according to the manufacturer's instructions on the Bioanalyzer 2100 (Department of Genetic Epidemiology, Central Institute of Mental Health, Mannheim, Germany). For each sample, 30 µl of RNA solution (60 ng/µl) in ddH_2O was sent to the High Throughput Sequencing (seq) Unit of the Genomics & Proteomics Core Facility at the DKFZ (Heidelberg, Germany) to be processed. Samples were run through in-house quality control and only samples with an RNA integrity number (RIN) ≥ 6.0 were used for cDNA library preparation according to the TruSeq Stranded protocol (Illumina) (average RIN of the own samples = 8,7). Libraries were sequenced to 50 bp single reads on one lane on the Illumina HiSeq 4K platform. The DKFZ Omics IT and Data Management Core Facility performed the RNAseq processing workflow. Total counts per feature were imported to R[424] and analyzed using DESeq2[425]. All features without any counts were removed, for differential testing with DESeq2 the formula "~timepoint" was used. Euclidean distance between samples was calculated from rlog transformed counts using the stats package[424.] The sample distance plot was generated using the pheatmap package[426] with the viridis plasma color scale[427]. Principal component analysis was performed on rlog transformed counts with the top 500 variable features using prcomp[424]. For clustering, the cmeans algorithm was used with k = 12. Features from specific gene clusters were used to perform gene ontology (GO) enrichment analysis using enrichGO from the clusterProfiler package[428]. The organism database used for this analysis was org.Hs.eg.db[429]. Heatmaps for RNAseq expression data show z-scaled DESeq2 normalized counts. GO circle plots were created using the GOplot package[430]. RNA bulk seq data analysis was performed in collaboration with Dr. Anne Hoffrichter (Hector Institute for Translational Brain Research, Central Institute of Mental Health, Mannheim, Germany). RNA bulk seq analysis was performed to figure out which genes are differentially expressed after psilocin administration. Neuronal cultures were analyzed at day 42. Biological batch replicates of each samples ensured intra-cell lines stability of results. In detail gene expression profile one and three days after a

single 10 min administration of 10 µM psilocin cortical neurons in biological duplicates was analyzed in control cell lines. In a condition that should simulate the physiological effect of psilocin in the brain the gene expression profile 72 hrs after a 6 hrs administration of 100 nM psilocin was explored. To examine a possible 5-HT2A-R involvement the cells were co-treated with a 7.5-fold excess with the selective 5-HT2A-R antagonist ketanserin in an additional setup that was included for each experimental condition. Multiple comparisons between the different treatment conditions and between DMSO control condition were performed. Top-down-based approach was explorative data-driven and blind to hypothesis.

3.4 Transformation of bacteria and isolation of plasmid DNA

Chemically competent E. coli DH5α bacteria (50 µl) were thawed on ice for 10 min. 500 ng of plasmid DNA was added and gently mixed by flicking the bottom of the tube with a finger. The bacteria-plasmid solution was incubated for 15 min on ice. Plasmid DNA was introduced by heat shock at 42°C for 42 sec. Cells were further incubated on ice for 5 min. After addition of 300 µl of SOC medium (lysogeny broth (LB) medium without antibiotics) the bacteria grew for 1 h at 37°C at 600 rpm. Finally, bacteria were plated on LB agar plates, containing ampicillin (100 µg/ml) for selection at 37°C overnight. Plasmid DNA was isolated with the PureLink™ HiPure midiprep kit according to the manufacturer's instructions and eluted in 100 - 200 µl ddH_2O.

3.5 Transfection with lipofectamine

For live cell imaging around 200,000 cells/well were plated onto 3.5 cm Ibidi dish. An artificial human 5-HT2A-R C-terminally tagged with mCherry (friendly provided by the working group of Gonzáles-Maeso, Department of Physiology and Biophysics, School of Medicine, Virginia Commonwealth University, USA) was transfected with Lipofectamine 2000 according to manufacturer's instruction. Life cell imaging was performed 2 and 3 days after transfection. To visualize the acute effects cell prior and after psilocin administration a video of the same single cell was made. For the treatment condition the video was stopped and psilocin diluted in advanced MEM media was gently added to the dish, then video recording was continued.

3.6 Transduction with Adeno-associated virus tagged to mCherry

For Sholl analysis around 50,000 cells/well were cultured on 24 well PEI/laminin coated coverslips. Cells were transduced 2 weeks before treatment with adeno-associated virus AAV_CamKIIa p-hCHR2(134a)-mCherry (friendly provided by AG Grinevich, Central Institute of Mental Health, Mannheim, Germany). Treatment of neurons with psilocin was carried out when mCherry expression was visible by microscope.

3.7 Biochemistry

3.7.1 ICC

After a first washing with PBS, cells were fixed in 4% paraformaldehyde (PFA), washed three times with PBS and blocked and/or permeabilized in blocking solution containing 10% FBS in PBS. For permeabilization 0.1% (v/v) saponin or 0.1 % - 0.3% (v/v) Triton X-100 (depending on the cell localization of the protein of interest) was added for one hr. Dilution of primary and secondary antibodies were performed in same blocking solution as used for blocking. For dilution of primary antibodies, the recommendation of the manufacturer was followed. Primary antibodies were incubated over night at 4°C. Samples were washed three times with corresponding blocking solution. Secondary antibodies, conjugated to Alexa Fluor 488, 568, 555 or 647, were diluted 1:1000 and were applied for 1 hr at room temperature. Samples were then washed once in PBS to remove unbound antibodies. Counterstaining of cell nuclei (intercalation in gDNA) was carried out by using 300 nM DAPI (in DPBS) staining solution, incubated for 5 min at room temperature and washed three times in PBS and once with ddH_2O. For primary and secondary antibody dilution see **Table 31 - 33**. Slides were mounted with mounting solution on glass coverslip and air-dried overnight. Long-time storage of slides was performed at 4°C. Analysis and quantification was performed with ImageJ.

3.7.2 Protein isolation and measurement of protein concentration

Cells were washed with ice cold DPBS, harvested by using a cell lifter and were transferred into a 1.5 ml tube on ice. In the following the cells were centrifuged for 5 min at 5000 g at 4 °C. The supernatant was removed and the sample was stored at - 20°C. For protein isolation, cells were resuspended (depending on the size of the pellet) in 150 - 300 µl of protein lysis buffer (50 mM Tris-HCL (pH 7.4), 150 mM NaCl, 25 mM EDTA, 1% (v/v) SDS with one protease and one phosphatase inhibitor mini tablet per 10 ml of protein solution) and incubated for 10 min at room temperature and then incubated 1 hr on ice. To shear gDNA and reduce viscosity samples were sonicated (20% duty cycles, 50% output, five pulses) from a Branson Ultrasonics™ sonifier 250. Samples were centrifuged for 5 min for 5000 g at 4°C. Supernatant was transferred to a new tube. Protein concentration was measured with the bicinchoninic acid (BCA) protein assay following the manufacturer's instructions. Samples were diluted 1:5 in ddH_2O and the absorption at 562 nm was measured in a PowerWave™ XS microplate reader. The protein concentration of samples was calculated based on the included BSA standard dilution series.

3.7.3 SDS-polyacrylamide gel electrophoresis and western immunoblotting

15 - 30 µg of protein was mixed with 6x denaturing protein sample buffer and boiled for 5 min at 95 °C. For the separation of proteins an SDS-polyacrylamide gel electrophoresis (SDS-PAGE) with the Bio-Rad technique was performed in a Mini-PROTEAN 2-D electrophoresis cell chamber and with the PowerPac™ Basic Power Supply which enables the separation of samples according to their molecular

weight (MW). First, the polyacrylamide gel runs for about 30 min with 30 V for stacking of proteins and then for about 1.5 - 2 hrs at 110 V. A semi-dry blotting was performed using the Trans-Blot Turbo™ transfer system performed with 20 V and 1 A for 30 - 60 min (depending on the size of proteins). For blotting 0.45 µm pore size nitrocellulose blotting membrane was used. The membrane was surrounded from both sides by 6 layers of WB filter tissue. Filter tissue and membrane were wetted in transfer buffer. Membranes were blocked for 60 min in 5% BSA in tris-buffered saline with Tween®20 (TBS-T) in a 50 ml tube. Primary antibodies were diluted in 5% BSA in TBS-T and were incubated over night at 4°C or for 1 h at room temperature on a rolling mixer. The membrane was washed three times in TBS-T for 10 min at room temperature on the next day. Infrared DyLight™ IR-conjugated secondary antibodies in TBS-T (dilution 1: 15,000) were applied for 1 hr at room temperature. Washing in TBS-T was carried out three times and once in TBS for 10 min at room temperature. Visualisation of tagged proteins was carried out with Odyssey IR WB imaging system from Li-COR. For primary and secondary antibody dilution see **Table 34 - 35**. Signals were normalized by β-actin levels (unless indicated differently) and for quantification region of interests (ROIs) were set around lanes and intensity was measured with the densitometry analysis in ImageJ.

3.7.3.1 Special WB case: cleavage of recombinant pro-BDNF into m-BDNF

The supernatant of mature cortical neurons of a control condition and cells that were previously treated for 72 hrs permanently with 10 µM psilocin was taken and enriched with recombinant 100 ng/µl pro-BDNF (Sigma Aldrich) and recombinant 1 µg/µl plasminogen, pipetted back on the cells. Cells were treated for 1h at 37°C in an incubator. Cells plus supernatant were taken, centrifuged for 10 min at 1500 g. In the following the supernatant and pellet was separated. The latter was lysed as depicted in **3.6.2** with protein lysis buffer. 25 µg of protein was loaded for WB. 16.5% Mini-PROTEAN® Tris-Tricine Gel were used for separation of proteins (**Fig. 31B-C**).

3.7.3.2 Special WB case: cleavage of recombinant pro-BDNF-Alexa-680 into m-BDNF-Alexa-680

100 µg of recombinant pro-BDNF (Alomone Labs) was labelled with Alexa-Fluor 680 with the Alexa Fluor™ 680 Labeling Kit according to the manufacturer's instructions. Instead of the provided columns of the Kit, the Zeba™ Dye and Biotin Removal Spin Columns were used. Mature cortical neurons of a control condition and cells, that were previously treated for 72 hrs permanently with 10 µM psilocin or TCB-2, were incubated with recombinant 10 ng/µl plasminogen for 1h at 37°C in an incubator. The supernatant was taken and treated with recombinant 40 ng/µl pro-BDNF-Alexa-680 for 5h at 37°C (**Fig. 31D**) or with 20 ng/µl pro-BDNF-Alexa-680 for 1h (**Fig. 31E**) or with or with 80 ng/µl pro-BDNF-Alexa-680 for 6h (**Fig. 31F**) or with 36 ng/µl pro-BDNF-Alexa-680 for 9h at 37°C (**Fig. 31G**) in a RT-PCR cycler. The supernatant was mixed with 6x denaturing protein sample buffer. 16.5% Mini-

PROTEAN® Tris-Tricine Gel were used for separation of proteins. The SDS-PAGE runs for about 30 min with 30 V for stacking of proteins and then for about 30 min at 110 V. The gel was directly visualized with the Odyssey IR WB imaging system from Li-COR (for Alexa-Fluor 680).

3.8 Cell viability assay

Cell viability assay to determine the number of viable cells was performed with the Orangu™ according to the manufacturer's instruction in a 96 well plate. 5 µl per well of dye solution was added 2 hrs prior to measurement to 50 µl of medium and incubated at 37°C in an incubator. The absorbance was measured at 450 nm in a Power Wave™ microplate reader (Department of Genetic Epidemiology, Central Institute of Mental Health, Mannheim, Germany). After a first measurement, defined as control, cells were triggered for 10 min with 10 µM psilocin. After each measurement dye-containing medium was replaced by fresh medium. Measurement was repeated 24 hrs up to 72 hrs after psilocin treatment.

3.9 Electrophysiology

Whole-cell patch-clamp recordings from iPSC-derived cortical neurons on PEI/laminin-coated coverslips cultured on mouse astrocyte cells were made using an EPC9 amplifier and PatchMaster (HEKA Elektronik GmbH). The neurons were identified with a Zeiss Axioskop using infrared differential interference contrast video microscopy in the recording chamber. Neurons were perfused at 2 ml/min (peristaltic pump; Ismatec GmbH) with carbogen (95% O_2; 5% CO_2)-saturated artificial cerebrospinal fluid (ACSF) containing 125 mM NaCl, 1 mM $MgCl_2$, 2 mM $CaCl_2$, 2.5 mM KCl, 10 mM D-glucose, 25 mM $NaHCO_3$, 1.25 mM NaH_2PO_4 (pH 7.3, osmolarity 300 mOsm). Pipettes were pulled from borosilicate glass capillaries (GB150F-8P, 1.5 mm o.d., 0.86 i.d.; Science Products GmbH) with a P-97 micropipette puller (Sutter Instrument). Pipettes had resistances between 4–6 MΩ when filled with intracellular solution containing 115 mM K-gluconate, 20 mM KCl, 10 mM Na-phosphocreatine, 4 mM Mg-ATP, 0.3 mM GTP, 0.2 mM ethylene glycol tetraacetic acid (EGTA) and 10 mM HEPES (pH 7.3, osmolarity 300 mOsm). In voltage-clamp, input resistance was determined at -70 mV based on currents evoked by small voltage steps (-3 mV; 300 ms), whereas with increasing depolarizing steps (10 mV; 300 ms) inward and outward currents were evoked. In current-clamp, the resting membrane potential (RMP) was determined and APs were evoked with increasing current injections (10 pA; 300 ms). The amplitude of the first evoked AP was analyzed, and the number of all APs evoked by 10 depolarizing steps was summed up. sEPSCs were recorded at -70 mV. Recordings were made at room temperature and were sampled at 20 kHz. Offline analysis was done with FitMaster (HEKA Elektronik GmbH). Spontaneous synaptic activity was analyzed using MiniAnalysis (Synaptosoft). Recording was done by Dr. Mahnaz Davoudi (Hector Institute for Translational Brain Research, Central Institute of Mental Health, Mannheim, Germany) in cooperation with PD Dr. Georg Köhr (Department of

Neurophysiology, Mannheim Center for Translational Neuroscience, University of Heidelberg/Medical Faculty Mannheim, Germany).

3.10 Neuroplasticity and 5-HT2A-R experiments in cortical neurons

For immunostainings around 200,000 cells/well (50,000 for Sholl analysis) were plated onto coverslips in 24-well plates. For WB, DNA- and RNA-based experiments around 2 - 6 million cells/well were plate on 6 well plate dishes or 10 cm dishes. Treatment of cortical neurons started at day 42 of differentiation. 3 days prior to experiments, for drug dissolving and during course of the experiment culture medium was replaced with neural base medium 3 containing 1% (v/v) Pen/Strep, 1.6 mg/ml glucose, 0,1% (v/v) GlutMAX™, 0,1% (v/v) B-27 and 200 µM ascorbic acid to avoid distorting effects of small molecules on cellular signal transduction pathways.

3.10.1 Treatment of cortical neurons with psilocin

10 mM DMSO stock solution of light sensitive psilocin was diluted 1:1000 (final DMSO concentration = 0,001%) to a final concentration of 10 µM psilocin. For the short trigger mature cortical neurons were treated for 10 min with psilocin, washed once with advanced MEM containing 1% (v/v) Pen/Strep and were further cultured and then fixed or harvested after indicated time points post treatment. For the permanent treatment, condition cells were treated for 24 (96) hrs permanently with 10 µM psilocin. For the 96 hrs plus 6 days washout condition cells were treated for 96 hrs permanently with 10 µM psilocin, washed once and were further cultured in neural differentiation phase 5. For RNA bulk seq a "physiological treatment" condition was included where cells were additionally treated for 6 hrs with 100 nM psilocin, washed once with advanced MEM containing 1% (v/v) Pen/Strep and were further cultured and then fixed or harvested after the indicated time points. For analyzing psilocin induced effects on 5-HT2A-R presentation cortical neurons were treated for 10 min with 10 µM Psilocin, fixed immediately (acute stimulation condition) or respectively after 24 hrs.

3.10.2 Treatment of cortical neurons with ketanserin

To determine whether psilocin induced neuroplasticity effects were 5-HT2A-R dependent 75 mM DMSO stock solution of ketanserin was diluted 1:1000 to a final concentration of 75 µM ketanserin (final DMSO concentration = 0,001%). Cells were pretreated with 75 µM ketanserin for 10 min to block the 5-HT2A-R, then treated for another 10 min with psilocin and ketanserin (final psilocin concentration = 10 µM, final ketanserin concentration = 75 μM, final DMSO concentration = 0,002%), washed once with advanced MEM containing 1% (v/v) Pen/Strep and further cultured for 24 hrs post treatment.

3.10.3 Treatment of cortical neurons with chelerythrine

To investigate whether psilocin induced neuroplasticity effects were PKC-mediated 1 mM DMSO stock solution of chelerythrine was diluted 1:1000 to a final concentration of 1 µM chelerythrine (final DMSO concentration = 0,001%). Cells were treated for 10 min with psilocin and chelerythrine (final psilocin concentration = 10 μM, final chelerythrine concentration = 1 μM, final DMSO concentration = 0,002%), washed once with advanced MEM containing 1% (v/v) Pen/Strep and were further cultured and then fixed after 24 h post treatment.

3.10.4 Treatment of cortical neurons with dynasore

To determine whether psilocin induced neuroplasticity effects were endocytosis-mediated 100 mM DMSO stock solution of dynasore was diluted 1:2000 to a final concentration of 50 µM dynasore (final DMSO concentration = 0,0005%). Cells were pretreated with dynasore for 50 min to block endocytosis, then treated for another 10 min with psilocin (final psilocin concentration = 10 µM) and dynasore (final dynasore concentration = 50 µM; final DMSO concentration = 0,0015%), washed once with advanced MEM containing 1% (v/v) Pen/Strep and further cultured and then fixed after 24 h post treatment.

3.11 Imaging

Cells were observed with the Inverted Leica DMIL LED Microscope. Stem cell and neural progenitor properties were imaged with the Leica DM6 B microscope with Thunder imaging software. For neuroplasticity experiments and live cell imaging (in 37°C heated chambers) Leica confocal TCS SP5 II microscope was used. Brightfield images were made with Fluorescence Microscope Celldiscoverer 7 microscope from Zeiss. Stedycon (STED) imaging was performed with the FACILTIY LINE by Abberior Instruments.

3.12 Analysis of IF

To get a broad impression of drug induced neuroplasticity changes three dependent variables of the same image were analyzed. Unless otherwise stated density (particle per length neurite) was illustrated in the main figures of the results part. Graphic illustration of pixel per length neurite and intensity per area can be found in the appendix. Analysis was done for the initial experiments blinded to treatment conditions. ROIs were set blindly on the channel of the neuronal structure protein and then transferred to the channels of the protein of interest.

3.12.1 Pixel per length neurite

A straight-line ROI was chosen. The image of the protein of interest was converted to a binary black and white image (Process -> Binary -> Make binary), signals of the protein of interest were detectable as small black dots “pixels”. Number of pixels were manually calculated with the multi-point tool along

the line of the ROI. Pixel were counted if the lay directly on the line but also if they were in close proximity of the line. The length was measured in µm. The number of pixels was relativized by the length of the ROI reflecting protein of interest per length neurite in µm. Analysis was done with ImageJ.

3.12.2 Density (particle per length neurite)

A polygon selection of ROIs was chosen. The protein density and co-localization of particles was measured with the ComDet v.0.5.3 plug-in for ImageJ. A particle size (depending on experimenters' evaluation), constant for overall experiments and an intensity threshold (in SD), adjusted within each experiment, was defined. For co-localization analysis the channels of proteins that have to be co-localized were merged in advance. As maximal distance between co-localized spots 4.00 pixels were stated. The number of particles was divided by the total length of the neurite in µm measured with the straight-line tool spanning the polygonal ROI.

Table 40. Pre-defined particle size of proteins measured with ComDet.

Protein of interest	**ComDet pre-defined particle size**
5-HTR2A-R	1.00
Annexin A2	1.00
BDNF	1.00
pro-BDNF	2.00
PSD-95	1.00 -3.00
S100A10	1.00
Synapsin	3.00
Synaptophysin	3.00
SV2A	3.00

3.12.3 Intensity per area

A polygon selection of ROIs was chosen. Intensity per area was calculated with ImageJ (Analyze -> Tools -> Roi Manager -> Measure). Analysis was done with ImageJ.

3.12.4 Sholl analysis

Images were analyzed using the Sholl analysis plug-in of ImageJ (circle radii). Start radius: 25 µm, step size: 25 µm, end radius: 250 µm, set center from active ROI, preview). Crossings were calculated manually. For total number of crossings sum of all calculated crossings was calculated.

3.12.5 Analysis of axon initial segment length and distance to the soma

The axon initial segment (AIS) length in µm was measured by putting a straight-line tool on the structure that stained positive for ankyrin G. The distance to the soma of the AIS was defined as the distance in µm from the soma to the start of the structure that stained positive for ankyrin G. The straight-line tool for ImageJ was used for the length measurement.

3.13 Statistical analysis

Unless indicated otherwise, data for quantitative analysis was based on at least two genetically independent cell lines with two independent biological replicates. For statistical analysis the RStudio for macOS (Version 1.4.1106© 2009) was used. Graphs were generated with RStudio and show violin blots including single data points (scatterplot) with mean ± standard deviation (SD) and boxplot with median. The Kolmogorov-Smirnov test for equality of a probability distribution and the Levene test for homogeneity of variance were calculated prior statistical analysis. In case the data does not meet the assumption for parametric testing Kruskal-Wallis test for more than two group comparisons (post hoc Wilcoxon rank sum test, *p*-value adjustment Bonferroni correction), or for a two group comparison a Mann-Whitney-U-test for independent samples was calculated. Significance levels against the respective controls (unless indicated otherwise) were not significant (n.s) if $p > 0.05$, or significant * $p < 0.05$. Individual figure legends contain detailed information regarding the number of replicates, sample size and the applied statistical tests.

3.14 Appendix information

Complete and detailed statistics for each experiment are presented in the appendix. The appendix further contains graphs of additional calculations. In the main figures of the results part for ICC analysis mostly particle per length neurite (density) (see **3.12.2**) of distinct proteins was shown. In the appendix also the analyses of pixel per length neurite (see **3.12.1**) and intensity per area (see **3.12.3**), if those were calculated, were included. Further a table containing the descriptive statistics and corresponding post hoc *p*-values (if statistics were performed) were listed. Additionally, to increase transparency of the analysis, separate graphics illustrate the results for every single cell line included in the analysis.

4 Results

4.1 Generation of dorsal forebrain neurons from human iPSC

Since the cerebral cortex is a key region for psychedelic effects and associated with dysfunction in psychiatric disorders, the effect of psilocin on human cortical neurons was tested. Dermal fibroblasts of a subset of male, lithium-responsive BD patients with a strong family history of BD, a subset of male patients diagnosed with AUD and healthy control individuals were chosen for generating iPSCs via viral transduction of transcription factors c-MYC, SOX2, OCT3/4 and KLF4. Reprogramming of human fibroblast into iPSCs was not part of this thesis. Chromosomal alterations of iPSCs were excluded by genome-wide SNP analysis (**Fig. 11A**). iPSCs were further screened for their stem cell properties by the expression of pluripotent stem cells markers SOX2, OCT4 and proliferation marker Ki67 (**Fig. 11B**) by immunofluorescence (IF) microscopy. iPS cells were differentiated by a > 5-week lasting, highly standardized protocol over a neuronal progenitor step into cortical neurons (see **Fig. 10**). iPSCs were guided into the ectodermal neural progenitor lineage by preventing mesoderm and endoderm formation by dual inhibition of SMAD signalling[30]. Neuronal differentiation of NPCs was achieved by cell cycle arrest and inhibition of notch signalling by addition of small molecules[422,423]. Cortical NPCs expressed typical neural stem and progenitor cell markers such as NESTIN or SOX2 as well as the dorsal forebrain transcription factors paired box (PAX) 6 and they were negative for the midbrain marker forkhead box (FOX) A2 (**Fig. 11C**) validated by IF microscopy. In the following neuronal maturation process the embryonal development was mimicked by including phases of GABA, high calcium concentrations and PKC activation to achieve functional maturation and synaptogenesis[422,423,431]. Most > 5-week-old neurons differentiated from these progenitors stained positive for glutamatergic marker vGLUT 2 and express transcription factors T-box brain protein 1 (TBR1) and CTIP2, that are found in Layer 5/6 neurons of the human cortex[432,433], validated by IF microscopy. Mature neurons expressed neuronal antigen neuronal nuclei (NeuN), dendritic marker microtubule-associated protein 2 (MAP2) and axonal marker TAU. A low amount of glial fibrillary protein (GFAP) positive cells was found indicating presence of astrocytes in small density. Activity-dependent immediate early gene cFOS expression indicated neuronal activity (**Fig. 11D**). RT-PCR analysis of mature neurons revealed gene expression of neuronal subtype markers, neurotransmitter receptors, neuronal activity markers, neuronal markers and synapse-associated genes (**Fig. 11E**). The adult cerebral cortex contains mostly excitatory, glutamatergic neurons and am minority of inhibitory GABAergic interneurons[15,16]. The expression of glutamatergic and GABAergic markers, such as glutamate transporters and receptors (e.g., vGLUT1 (*SLC17A7* gene), vGLUT2 (*SLC17A6* gene), NMDA receptor subunits (e.g., glutamate ionotropic receptor AMPA type subunit 1 and 2 *GRIN1* gene, *GRIN2B* gene), AMPA receptor subunits (glutamate ionotropic receptor AMPA type *GRIA2* gene, *GIRA4* gene) and the glutamate decarboxylase (*GAD1* gene) was detected. Consistent with ICC data, neurons express cortical layer markers like CTIP2 (*BCL11B* gene) and *TBR1* (*TBR1* gene) which confirmed their forebrain identity. Further, mature neurons express neuronal markers like beta-III-tubulin (*TUBB3* gene), canonical marker NeuN (RNA-

binding protein FOX, *RBFOX3* gene), a marker for post mitotic neurons, maturity marker neuronal differentiation 6 (*NEUROD6* gene) and synaptic cell adhesion molecule neurexin-1 (*NRXN 1* gene). Maturity of neurons was characterized by the presence of pre- and postsynaptic proteins important for synapse formation but also proteins that enable the functionality of neurons. One of those structures is the AIS which is located at the proximal axon. It is the part of the axon where the AP is generated (for review see:[434]). The presence of the AIS was detected by the expression of ankyrin (*ANK*3 gene). Additionally, the expression of neural activity related immediate early genes (*NPAS4* gene, *ARC* gene, *FOS* gene) was detected. Mature neurons do express presynaptic synaptic markers synapsin (*SNY1* gene) and synaptic vesicle glucoprotein 2A (*SV2A* gene) which are involved in vesicle fusion. Further the postsynaptic density protein PSD-95 (*DLG4* gene), a scaffolding protein that link neurotransmitter receptors to the membrane, was expressed. Finally, cortical neurons expressed the neurotrophin BDNF (*BDNF* gene). Mature cortical neurons fired APs and showed network activity validated by electrophysiology using patch clamp recording **(Fig. 11F)**. Functional and mature neurons of dorsal forebrain identity and neuronal circuitries were thereby generated within >5 weeks in high purity.

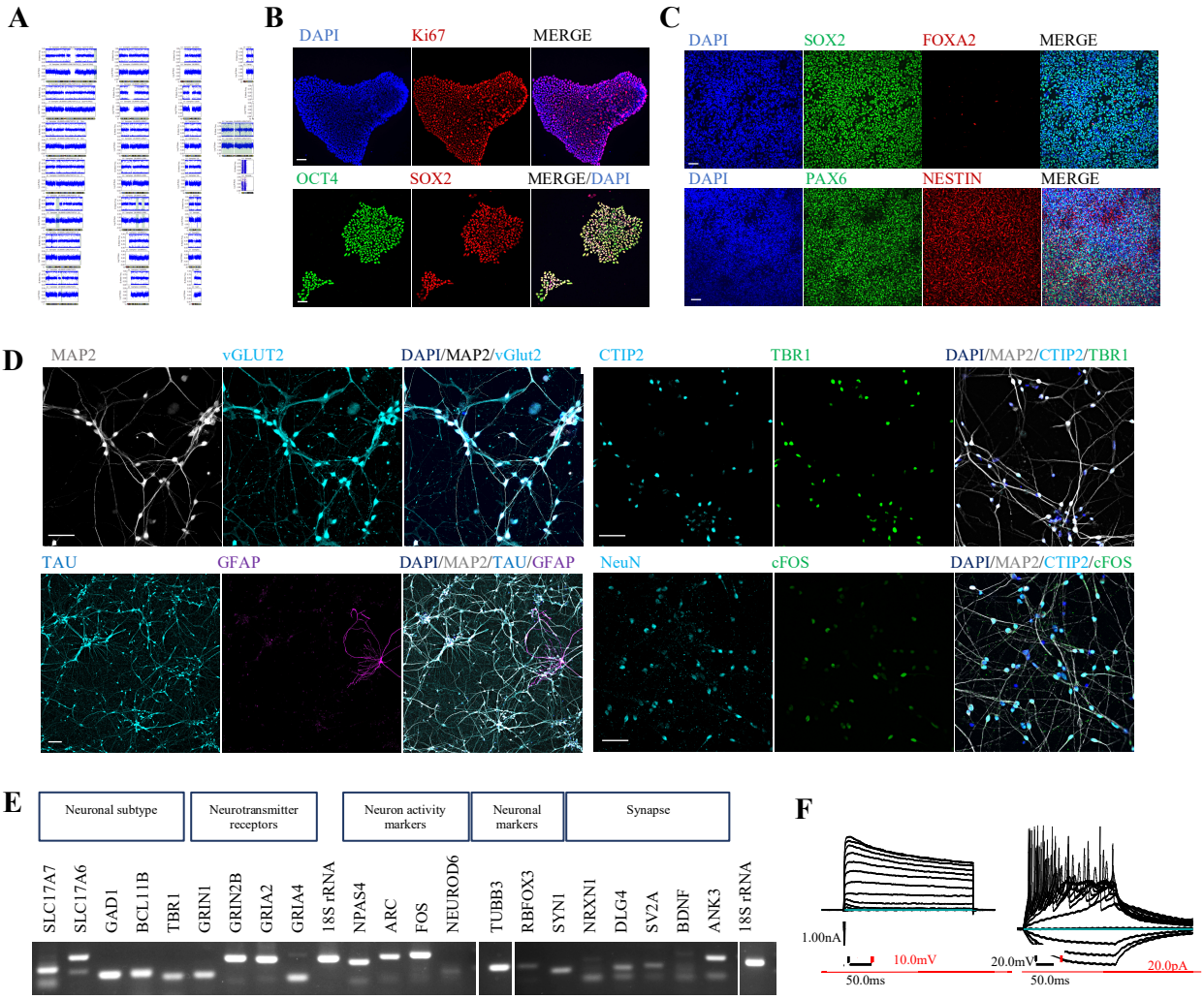

Figure 11. Validation of iPSC-derived neural progenitors and cortical neurons.
(A) iPSC clones were screened for chromosomal alterations by genome-wide SNP analysis. Exemplary full genome SNP of one Ctrl stem cell line. **(B)** iPS cells expressed pluripotent marker SOX2 and OCT4 and proliferation marker Ki67. **(C)** Neuronal progenitors expressed SOX2, PAX6 and NESTIN and were negative for FOXA2, as a midbrain marker. **(D)** Mature 40-day-old cortical neurons were glutamatergic (vGLUT2 expression) and expressed cortical layer transcription markers TBR1, CTIP2 and the neuronal markers NeuN, MAP2 and TAU. Immediate early gene cFOS expression was a sign for neuronal activity. GFAP expression indicated a low number of astrocytes. **(E)** RT-PCR analysis revealed expression of neuronal subtype markers, neurotransmitter receptors, neuronal activity markers, neuronal markers and synapse-associated genes. **(F)** Cortical neurons were electrophysiological active: representative trace of peak Na^+/ K^+ currents recorded in voltage clamp mode and representative recording of evoked AP pattern in current clamp mode during 300 ms of depolarization. Scale bar: 50 µm, for GFAP staining 100 µm. Electrophysical measurements were performed and representative traces were generated by Dr. Mahnaz Davoudi.

4.2 Effect of psilocin administration on 5-HT2A-R localization

Psilocin agonistically targets the serotonergic 5-HT2A-R[43,46,47,74,75,158,159,218,237,239,435,436], that is highly enriched in the prefrontal cortex[231–233,437,438]. Those receptors have a prominent role in psychedelic-mediated response (please refer to subchapter **1.6.1**). 5-HT2A-R expression in human iPSC-derived cortical neurons was therefore first assessed. RT-PCR confirmed that the 5-HT2A-R (*HTR2A* gene) was expressed in cortical neurons (**Fig. 12A).** By ICC targeting an extracellular epitope, I found the receptor to be present in the axonal and the somato-dendritic compartment of the neurons (**Fig. 12B**). Literature describes that the binding of agonists and antagonists to the 5-HT2A-R could provoke its internalization *in vivo* and *in vitro*[265,278–280,439,440]. Internalization has been shown to occur already 2 min after agonist activation and is completed within 10 min[439]. Down-regulation of serotonergic receptors has been described after chronic and acute administration with agonists[232,269–271] (please refer to subchapter **1.6.1**). I thus investigated the effect of acute, (10 min after exposure) and subacute (24 hrs following psilocin exposure) on TAU^+ axonal and $MAP2^+$ dendritic subcellular 5-HT2A-R presentation. For the following experiments I chose a concentration of 10 µM psilocin, the active principle of psilocybin. This psilocin concentration was, based on recent literature, investigating psilocin-induced neuroplasticity effects in rat cortical neurons[1]. For acute and subacute effects 5-HT2A-R density (particles per µm) was measured based on ICC staining. Interestingly, the acute exposure led to a significant decrease in axonal TAU^+ extracellular 5-HT2A-R, while $MAP2^+$ dendritic extracellular 5-HT2A-R level stayed unchanged (**Fig. 12C-D, I**). In a preliminary experiment the dynamin inhibitor dynasore abrogated CME, indicating that this acute downregulation was at least partially mediated by receptor internalization (**Fig. 12E**). I also detected axonal accumulation of 5-HT2A-R in extracellular aggregates, caused by dynasore treatment (**Fig. 12F**). Although, this speaks for an internalization process there was not a significant increase in co-localization of the receptor with early endosome markers Ras-associated binding (RAB) 5A and early endosomal antigen-1 (EEA1) protein after the expected psilocin induced internalization for different time points tested (data not shown). Live cell imaging data with an artificial human 5-HT2A-R C-terminally tagged with mCherry showed a clear

movement of the receptor from neurites to the soma after acutely adding psilocin indicated retrograde transport (**Fig. 12G**). After 24 hrs, both the TAU^{+} axonal (from $M_{Ctrl} = 0.35$, $SD = 0.28$ to $M_{10min} = 0.26$, $SD = 0.27$ to $M_{24hrs} = 0.12$, $SD = 0.15$) and MAP2^{+} dendritic (from $M_{Ctrl} = 0.57$, $SD = 0.42$ to $M_{10min} = 0.52$, $SD = 0.45$ to $M_{24hrs} = 0.21$, $SD = 0.2$) receptor density was significantly decreased, speaking for a subacute down-regulation of the receptor (**Fig. 12H-I, Appendix 12**). I thus found clear evidence that acute psilocin stimulation decreased axonal extracellular 5-HT2A-R level already 10 min after psilocin administration, stayed downregulated 24 hrs after treatment and even expanded to the dendritic compartment.

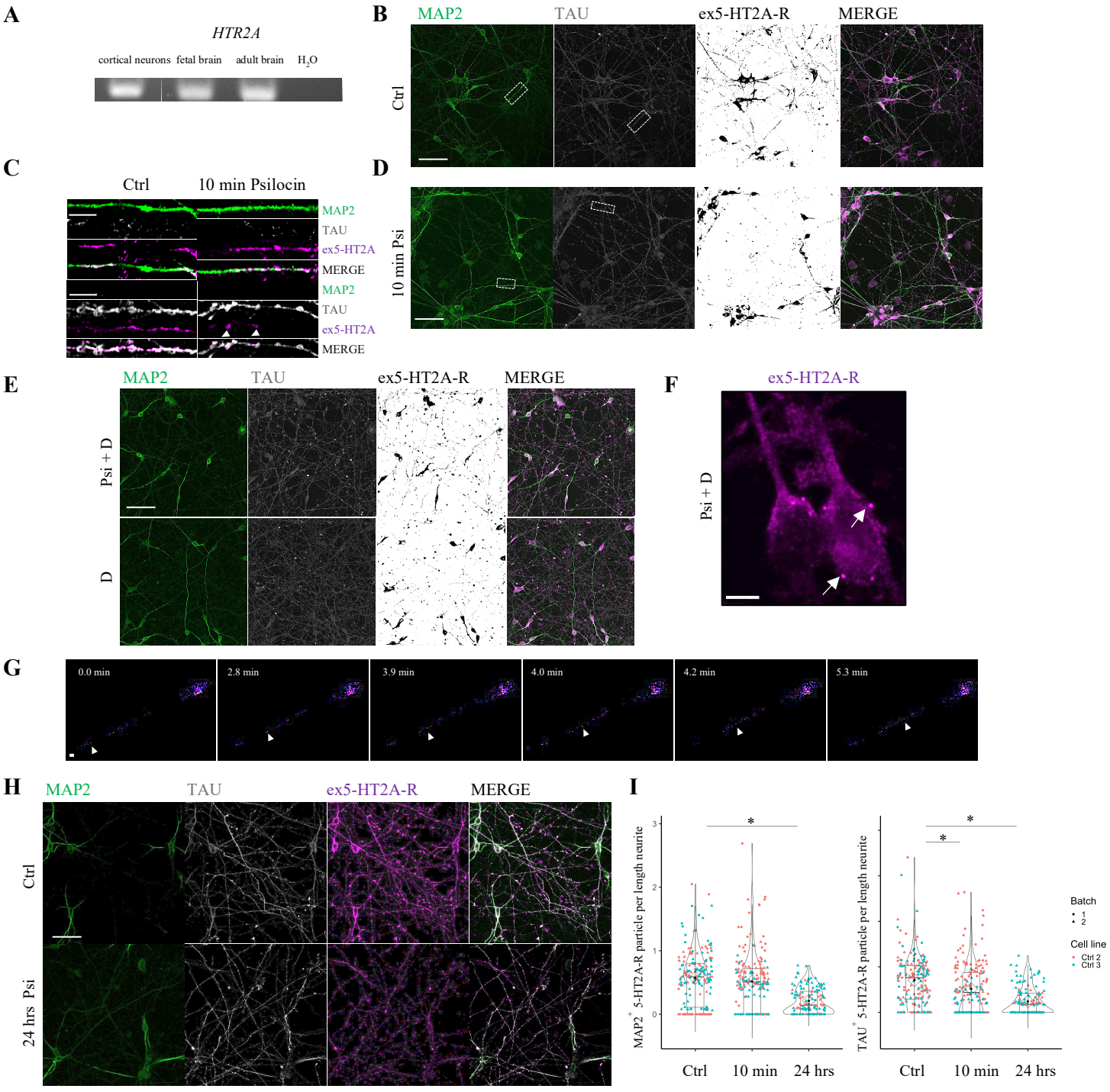

Figure 12. Validation of 5-HT2A-R expression and effect of psilocin on receptor presentation. **(A)** RT-PCR of the *HTR2A* gene (also expressed in commercialized samples of fetal and adult brain) confirmed expression of 5-HT2A-R. **(B)** Representative extracellular (ex)5-HT2A-R staining, scale bar: 50 µm. **(C-D)** Decrease in TAU^+ axonal receptor localization 10 min after 10 µM psilocin trigger (10 min Psi) compared to the untreated condition (Ctrl) may indicate receptor internalization, close up: scale bar: 10 µm **(D)** scale bar: 50 µm. **(E)** The decrease in ex5HT2A-R expression is prevented by inhibiting CME with dynasore co-treatment and monotreatment ("Psi + D" and "D") showing in the close-up **(F)** axonal 5-HTRA-R accumulation in extracellular aggregates, scale bar: 50 µm, close up-scale bar: 5 µm. **(G)** Live cell imaging with an artificial human 5-HT2A-R tagged to mCherry showed retrograde movement of the receptor from neurite to the soma after acutely adding psilocin. Scale bar: 5 µm. **(H)** After 24 hrs, both the axonal and dendritic receptor density was significantly decreased, speaking for a subacute down-regulation of the receptor. **(I)** The decrease in TAU^+ axonal receptor localization after acute psilocin administration was significant. There was a significant decrease in TAU^+ axonal and $MAP2^+$ dendritic extracellular receptor presentation 24 hrs later. For Ctrl $N = 180$ neurites, for 10 min $N = 180$ neurites, for 24 hrs $N = 135$ - 140 neurites were calculated. Two control cell lines each with two biological batches for $MAP2^+$ and TAU^+ 5-HT2A-R were included (except of 24 hrs for Ctrl 3 with one biological batch). Kruskal-Wallis-Test for independent samples was calculated. Post hoc Wilcoxon rank sum test. Bonferroni-correction, adjusted $p < .05$, mean ± SD. Significance levels against the respective control are $^*p < 0.05$.

4.3 Effects of psilocin on neuroplasticity in iPSC-derived human cortical neurons

In order to replicate plasticity promoting effects of psilocin described in literature in human cortical neurons and to find mechanisms that could explain those and thus its potential therapeutic mode of action RNA expression changes one day and three days following a single 10 min 10 µM psilocin administration was investigated with RNA bulk seq. A 5-HT2A-R involvement was addressed by including respectively a condition where the 5-HT2A-R was antagonistically inhibited with ketanserin. Biological batch replicates of each samples ensured intra-cell lines stability of results. Top-down-based approach was explorative data-driven and blind to hypothesis.

Already a comparison between the DMSO control and the 24 hrs after psilocin administration condition revealed hundreds of significant differentially expressed genes. GO terms as well as a Kyoto Encyclopedia of Genes and Genomes (KEGG) analysis gave first hints about a possible underlying mechanism in the action of psilocin. There was a significant enrichment in differentially expressed genes associated with manifold GO terms related to biological process (BP), molecular function (MF), cellular compartment (CC) as well as a KEGG involved in neuroplasticity already one day after psilocin administration in RNA bulk seq data (**Fig. 13A-B**). For example, in synaptic and vesicular organization (e.g., "synapse organization", "neuron to neuron synapse", "synaptic vesicle cycle"), synapse and axonal specialization (e.g., "postsynaptic specialization", "distal axon"), their regulation (e.g., "regulation of trans-synaptic signaling", "axon guidance") and axonogenesis. Interestingly, I found a significant 1.5-fold enrichment in differentially expressed genes associated with CC "neuron spine" and "growth cone", indicating a modulation of pathways involved in axon and spine formation. Also, differentially expressed genes associated with "glutamatergic synapse" GO term was significantly enriched by the factor 1.5, indicating a psilocin meditated targeting of the glutamatergic signaling.

3 days (in comparison to 1 day) after 10 min 10 µM psilocin administration this enrichment in differentially expressed genes associated with neuroplasticity GO terms (e.g., "neuron projection

guidance", "regulation of axonogenesis", "regulation of synapse organization") was persistent (**Fig. 13C-D**). There was even a stronger significant postsynaptic specialization (e.g., "postsynapse organization", "postsynaptic density membrane", "postsynaptic specialization membrane", "postsynaptic density"). Further, again a modulation of glutamatergic signaling was visible (e.g., "ionotropic glutamate receptor activity", "glutamate receptor activity", "glutamatergic synapse"). Those neuroplasticity-promoting GO terms were even complemented by GO terms associated with "learning" (factor: 2.2-fold enrichment), "learning or memory" (factor: 1.9-fold enrichment), "cognition" (1.8-fold enrichment) and addiction (e.g., "nicotine addiction", "cocaine addiction", "amphetamine addiction", around factor: 2-fold enrichment) This was interesting as it suggested a modulation of higher cognitive functions and behavior by psilocin. RNA bulk seq data confirmed expression of the *HTR2A* receptor gene expression (**Fig. 13E**) and a non-significant down-regulation of all serotonergic receptor genes one day after psilocin administration in line with ICC data (**Fig. 13F**).

In order to confirm this gene expression data and as psychedelics are discussed to restore neuronal dysfunction and synaptopathies (please refer to subchapter **1.4.1** and **1.5.2**) I sought to determine the short-term and long-term effects of psilocin on neuroplasticity markers, synaptic proteins and synaptogenesis on a cellular level.

4.3.1 Psilocin alters neuroplasticity marker AIS and reduces cortical excitability in short-term

I first investigated the subacute effect of psilocin administration on the morphology of the AIS, the part of the axon where the APs are generated. The AIS is considered to be an important modulator of the excitability of neurons as it can change its length and its distance to the soma in reaction to various stimuli (for review see:[434], **Fig. 14A**). I thus measured AIS length and distance to the soma in µm by using an antibody for the AIS scaffolding protein ankyrin G by ICC. In the 24 hrs condition I compared the 24 hrs post effect of a short-term trigger with 10 min psilocin treatment with its permanent administration. I further included a condition where I measured 48 hrs after a short-term trigger with 10 min psilocin. I found a significant increase in AIS length in µm (from M_{Ctrl} = 18.57, SD = 7.13 to M_{24hrs} = 24.56, SD = 10.05 and $M_{24hrs\ permanent}$ = 23.63, SD = 7.84) and a decrease in AIS distance to the soma (from M_{Ctrl} = 12.23, SD = 8.39 to M_{24hrs} = 9.71, SD = 6.34 and $M_{24hrs\ permanent}$ = 7.72, SD = 4.03) 24 hrs after psilocin administration. This effect was enduring 48 hrs after psilocin administration, significant for AIS length (from M_{Ctrl} = 18.57, SD = 7.13 to M_{48hrs} = 24.33, SD = 8.54) and non-significant for AIS distance to the soma (from M_{Ctrl} = 12.23, SD = 8.39 to M_{48hrs} = 9.85, SD = 4.98) (**Fig. 14B-D, Appendix 14**). The 24 hrs permanent condition did not differ considerably from the 24 hrs short term condition.

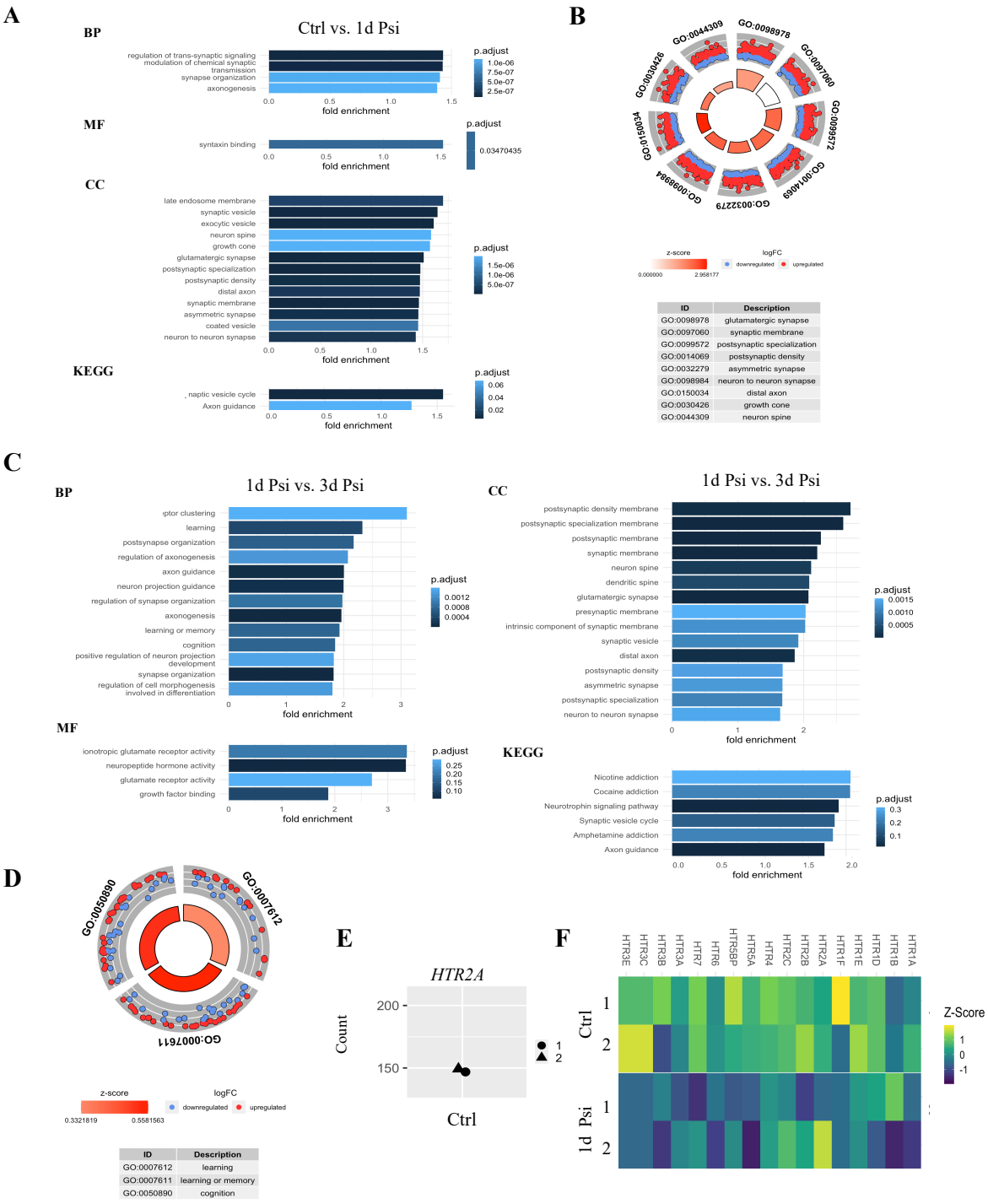

Figure 13. Psilocin-induced increase in differentially expressed genes associated with neuroplasticity GO terms.

(A) Enrichment in differentially expressed genes associated with (glutamatergic) synapse and axonal organization, specialization (e.g., neuron spine and growth cone) and regulation GO terms. **(B)** GO circle blot of selected GO terms one day after psilocin administration. **(C)** 3 days (in comparison to 1 day) after psilocin administration additionally enrichment in differentially expressed genes associated with learning, cognition and addiction. **(D)** GO circle blot of selected GO terms. GO circle blot: Inner ring displays a bar plot where the height of the bar indicates the significance of the term (- log10, adjusted p-value), color corresponds to the z-score. Outer ring shows scatterplots of the expression levels (log FC) for the genes in each term. **(E)** TPM scaled RNA bulk seq data of the *HTR2A* gene confirmed its expression. **(F)** Heat map (z-scaled), performed in biological duplicates of untreated condition (Ctrl), one day after 10 min 10 µM psilocin administration (1d Psi) revealed a non-significant down-regulation of serotonergic genes. Significance levels against the respective control $*p < 0.05$. BP, biological process; MF, molecular function; CC, cellular compartment; KEGG, Kyoto Encyclopedia of Genes and Genomes. Illustration of RNA bulk seq GO data, GO circle blots and heatmap were generated by Dr. Anne Hoffrichter.

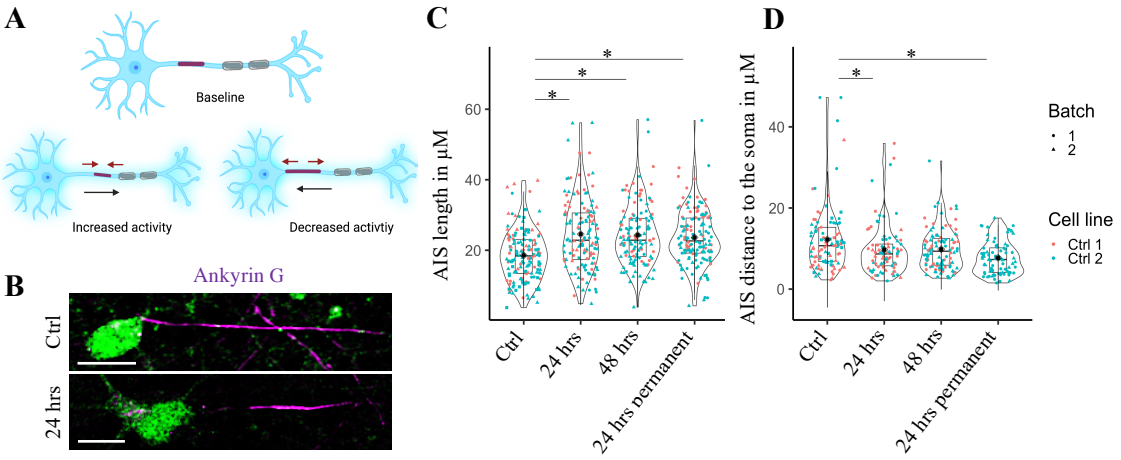

Figure 14. Psilocin modulated length and distance to the soma of neuroplasticity indicator AIS. **(A)** AIS elongation and shift to the soma is described to be a neuroplastic reaction of deprived neurons to become more excitable. Graphic illustration generated with *Biorender.com.* **(B)** Representative AIS image (ankyrin G staining) for the untreated control (Ctrl) and 24 hrs after 10 min 10 µM psilocin trigger (24 hrs) showed AIS elongation and a shift to the soma for the latter. Scale bar close up: 10 µm. **(C)** AIS length was significantly increased 24 hrs and 48 hrs after a 10 min 10 µM psilocin trigger (24 hrs, 48 hrs) and 24 hrs after permanent psilocin administration (24 hrs permanent). **(D)** AIS distance to the soma was significantly decreased 24 hrs after a 10 min 10 µM psilocin trigger and 24 hrs after permanent psilocin administration. Two Ctrl cell lines were included in the analysis each with two biological batches. AIS length: Ctrl with $N = 119$ neurites; 24 hrs with $N = 134$ neurites; 48 hrs with $N = 128$ neurites and 24 hrs permanent with $N = 145$. AIS distance to the soma: Ctrl with $N = 81$ neurites; 24 hrs with $N = 85$ neurites; 48 hrs with $N = 103$ neurites and 24 hrs permanent with $N = 80$. Kruskal-Wallis test for independent samples was calculated. Post hoc Wilcoxon rank sum test. Bonferroni-correction, adjusted $p < .05$, mean ± *SD*. Significance levels against the respective control are $*p < 0.05$.

In order to decipher how those modulations of the excitability marker AIS are reflected by functional changes I examined the influence of psilocin on the excitability of the cortical neurons *in vitro* as there is scientific disagreement whether psychedelics increase or decrease excitability in cortical neurons[1,210,211] (please refer to subchapter **1.5.1**). For measuring modulations of electrophysiological properties 24 hrs after psilocin administration whole-cell patch clamp recording on single cortical neurons cultured on mouse astrocytes was performed *in vitro*. In voltage-clamp mode input resistance, inward and outward currents were measured. In current-clamp mode RMP and APs were assessed. Further spontaneous synaptic activity was investigated by measuring sEPSCs. 24 hrs after psilocin administration there was a significant decrease in peak sodium (Na^+) current (from $M_{Ctrl} = - 1121.9$, $SD = 743.27$ to $M_{Psi} = - 632.82$, $SD = 630.53$), total number of APs (from $M_{Ctrl} = 30.36$, $SD = 18.25$ to $M_{Psi} = 8.64$, $SD = 7.63$), their amplitude (from $M_{Ctrl} = 95.91$, $SD = 19.22$ to $M_{Psi} = 81.54$, $SD = 18.09$) and of the RMP (from $M_{Ctrl} = - 50.18$, $SD = 14.29$ to $M_{Psi} = - 39.90$, $SD = 15.13$). No differences for peak potassium (K^+) current were found (**Fig. 15A-B**, **Appendix 15**). In line with that the frequency of sEPSCs significantly decreased (from $M_{Ctrl} = 1.76$, $SD = 2.68$ to $M_{Psi} = 0.51$, $SD = 0.47$). The amplitude of the sEPSCs did not significantly change. (**Fig. 15C-D**, **Appendix 15**). Further, an experiment was performed where the specific 5-HT2A receptor agonist TCB-2 was included to validate the functional specificity of psilocin in reducing cortical excitability. An in fact, a reduced excitability was also confirmed 24 hrs after dosing with TCB-2 in a first experiment (**Fig. 15E**, **Appendix 15**).

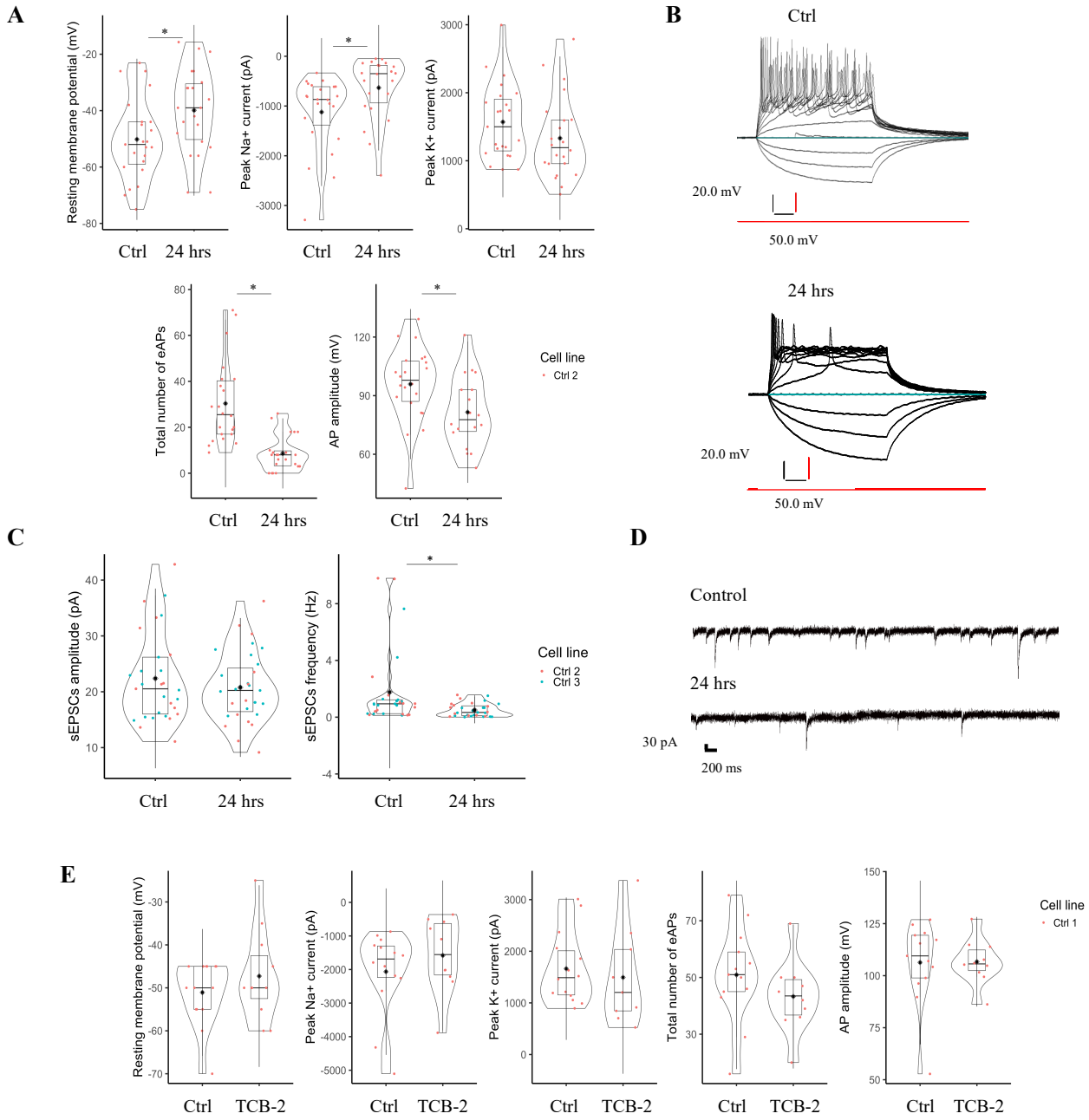

Figure 15. Psilocin and TCB-2 reduced excitability in cortical neurons in short-term.
(A-B) Effect of psilocin on intrinsic properties. **(A)** Significant decrease in RMP and peak Na^+ current, total AP number and APs amplitude 24 hrs after 10 min exposure to 10 µM psilocin (24 hrs), confirmed reduced excitability. No effect on peak K^+ current. For Ctrl N = 22 - 23 neurites, for 24 hrs N = 18 - 22 cells were measured. **(B)** Representative trace of peak Na^+ / K^+ currents recorded in voltage-clamp mode for control (Ctrl) and psilocin condition 24 hrs (24 hrs) after psilocin administration. **(C-D)** Short-term effect of psilocin on synaptic properties. **(C)** Significant decrease in sEPSCs frequency, with unchanged amplitude 24 hrs after permanent 10 µM psilocin administration (24 hrs). **(D)** Representative trace for control and psilocin condition 24 hrs after permanent 10 µM psilocin administration. Two Ctrl cell lines were included in the analysis. Ctrl with N = 29 cells, 24 hrs Psi with N = 31 cells. **(E)** 24 hrs permanent treatment with 5-HT2A-R agonist TCB-2 reduced total number of APs, peak Na^+ current and peak K^+ current. One Ctrl cell line was included in the analysis. Ctrl with N = 13 - 14 cells, 24 hrs TCB-2 with N = 9 - 11 cells. Mann-Whitney-U-test for independent samples was calculated, ± *SD*. Significance levels against the respective control are $*p < 0.05$. AP, action potential; eAP, evoked action potential; K^+, potassium; Na^+, sodium; RMP, resting membrane potential; sEPSC, spontaneous excitatory postsynaptic current. Electrophysical measurements were performed and representative traces were generated by Dr. Mahnaz Davoudi.

Taken together the results this thesis showed that subacute psilocin administration provoked a state of reduced functional excitability together with neuroplastic modulations of the AIS.

4.3.2 Influence of psilocin on pre-and postsynaptic proteins and synaptogenesis

Next, I analyzed the effect of psilocin administration on the density and intensity of the presynaptic marker SV2A and synaptophysin, as well as on the postsynaptic marker PSD-95 for different psilocin treatment durations by using ICC on neurites. I included a condition where I compared the 24 hrs post effect of a short-term 10 min psilocin trigger with 24 hrs permanent psilocin administration. I further included a condition where I measured 48 hrs after a short-term trigger with 10 min psilocin. I measured density (particles per µm) and intensity per area based on ICC staining.

I found a significant increase in SV2A intensity per area 24 hours after permanent psilocin administration (from M_{Ctrl} = 22.6, SD = 12.84 to $M_{24hrs\ permanent}$ = 37.42, SD = 24.57, **Fig. 16A-C, Appendix 16A**). There was no effect on SV2A density for the treatment conditions tested.

PSD-95 intensity was significantly increased 24 hours after permanent psilocin administration (from M_{Ctrl} = 20.75, SD = 13.03 to $M_{24hrs\ permanent}$ = 23.07, SD = 8.71). And PSD-95 density was significantly increased 48 hrs after psilocin administration (from M_{Ctrl} = 0.23, SD = 0.16 to M_{48hrs} = 0.29, SD = 0.17) (**Fig. 16A-B, D-F, Appendix 16B**).

For synaptophysin intensity per area was significantly increased for all conditions tested (from M_{Ctrl} = 16.31, SD = 8.73 to M_{24hrs} = 19.51, SD = 9.12, to M_{48hrs} = 20.76, SD = 6.03 to $M_{24hrs\ permanent}$ = 18.88, SD = 9.59, **Fig. 16E-G, Appendix 16C**).

In order to investigate long-term changes on synaptogenesis, density and intensity of the presynaptic protein synapsin and PSD-95 and their co-localization following 96 hrs permanent psilocin administration was investigated with ICC on TAU^+ neurites. There was a non-significant increasing trend in synapsin density (from M_{Ctrl} = 0.31, SD = 0.09 to M_{96hrs} = 0.35, SD = 0.2) and PSD-95 density (from M_{Ctrl} = 0.27, SD = 0.1 to M_{96hrs} = 0.31, SD = 0.17) and their co-localization (from M_{Ctrl} = 0.23, SD = 0.09 to M_{96hrs} = 0.25, SD = 0.15). Synapsin and PSD-95 intensity was significantly increased (synapsin intensity from M_{Ctrl} = 18.5, SD = 12.88 to M_{96hrs} = 24.16, SD = 15; PSD-95 intensity from M_{Ctrl} = 32.34, SD = 13.23 to M_{96hrs} = 47.16, SD = 18.27) (**Fig. 17A-G, Appendix 17A**).

I thus focused only on $MAP2^+$ dendritic synapsin and PSD-95 density and intensity by using ICC 96 hrs after permanent psilocin administration. I further included a condition 6 days after 96 hrs permanent psilocin administration to decipher long-lasting changes on synaptogenesis. And in fact, there was a significant increase in PSD-95 density (from M_{Ctrl} = 1.12, SD = 0.53 to M_{96hrs} = 1.39, SD = 0.57 to $M_{96hrs + 6\ days\ washout}$ = 1.27, SD = 0.5) and intensity (from M_{Ctrl} = 31.84, SD = 12,92 to M_{96hrs} = 36.81, SD = 15.35 to $M_{96hrs + 6\ days\ washout}$ = 37.95, SD = 16.4). Synapsin density non-significantly increased (from M_{Ctrl} = 0.25 SD = 0.21 to M_{96hrs} = 0.28, SD = 0.21 to $M_{96hrs + 6\ days\ washout}$ = 0.29, SD = 0.23). Interestingly, by focusing only on dendritic synapsin and PSD-95 co-localization there was a significant increase for both conditions tested (from M_{Ctrl} = 0.22, SD = 0.21 to M_{96hrs} = 0.27, SD = 0.2 to $M_{96hrs + 6\ days\ washout}$ = 0.28, SD = 0.22), indicating synaptogenesis promoting effects of psilocin (**Fig. 17H-N, Appendix 17B**).

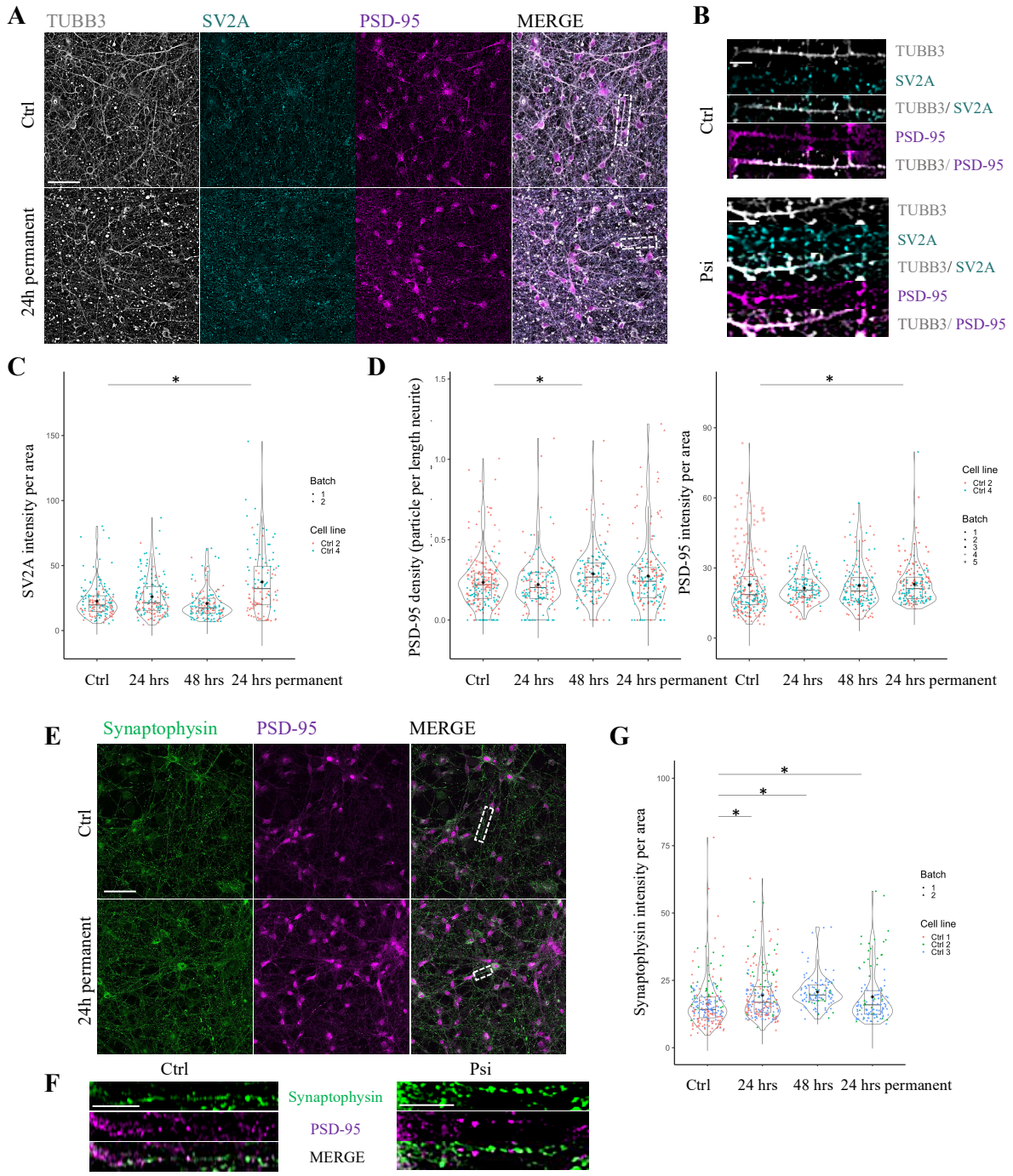

Figure 16. Effect of psilocin on neuritic presynaptic SV2A, synaptophysin and postsynaptic PSD-95.

(A) Representative image of a neuronal network for SV2A and PSD-95 for a pre-treatment condition (Ctrl) and 24 hrs after permanent psilocin administration (24 hrs permanent). Scale bar: 50 µm, **(B)** close up: 10 µm. **(C)** SV2A intensity per area was significantly increased 24 hrs after permanent psilocin administration. Ctrl with N = 150 neurites; 24 hrs with N = 150 neurites; 48 hrs with N = 150 neurites and 24 hrs permanent with N = 105 neurites. Two Ctrl cell lines were included in the analysis. **(D)** Significant increase in PSD-95 particle per length neurite 48 hrs after 10 min psilocin administration (48 hrs). Significant increase in PSD-95 intensity per area 24 hrs after permanent psilocin administration. For Ctrl N = 260 neurites, for 24 hours N = 155 neurites, for 48 hrs N = 150 neurites, for 24 hrs permanent N = 170 neurites were calculated. Two control cell lines were included. **(E)** Representative image for synaptophysin and PSD-95 of a neuronal network for a pre-treatment condition and 24 hrs after 24 hrs permanent psilocin administration. Scale bar: 50 µm, **(F)** close up: 10 µm. **(G)** Synaptophysin intensity per area was significantly increased 24 (24 hrs) and 48 hrs after a 10 min 10 µM psilocin trigger and 24 hrs after permanent psilocin administration. Three Ctrl cell lines were included in the analysis. Ctrl with N = 215 neurites; 24 hrs permanent with N = 215 neurites; 48 hrs with N = 105 neurites and 24 hrs permanent with N = 125 neurites. For all statistical analysis Kruskal-Wallis-Test for independent samples was calculated. Bonferroni-correction, adjusted $p < .05$, mean ± SD. Significance levels against the respective control are *$p < 0.05$.

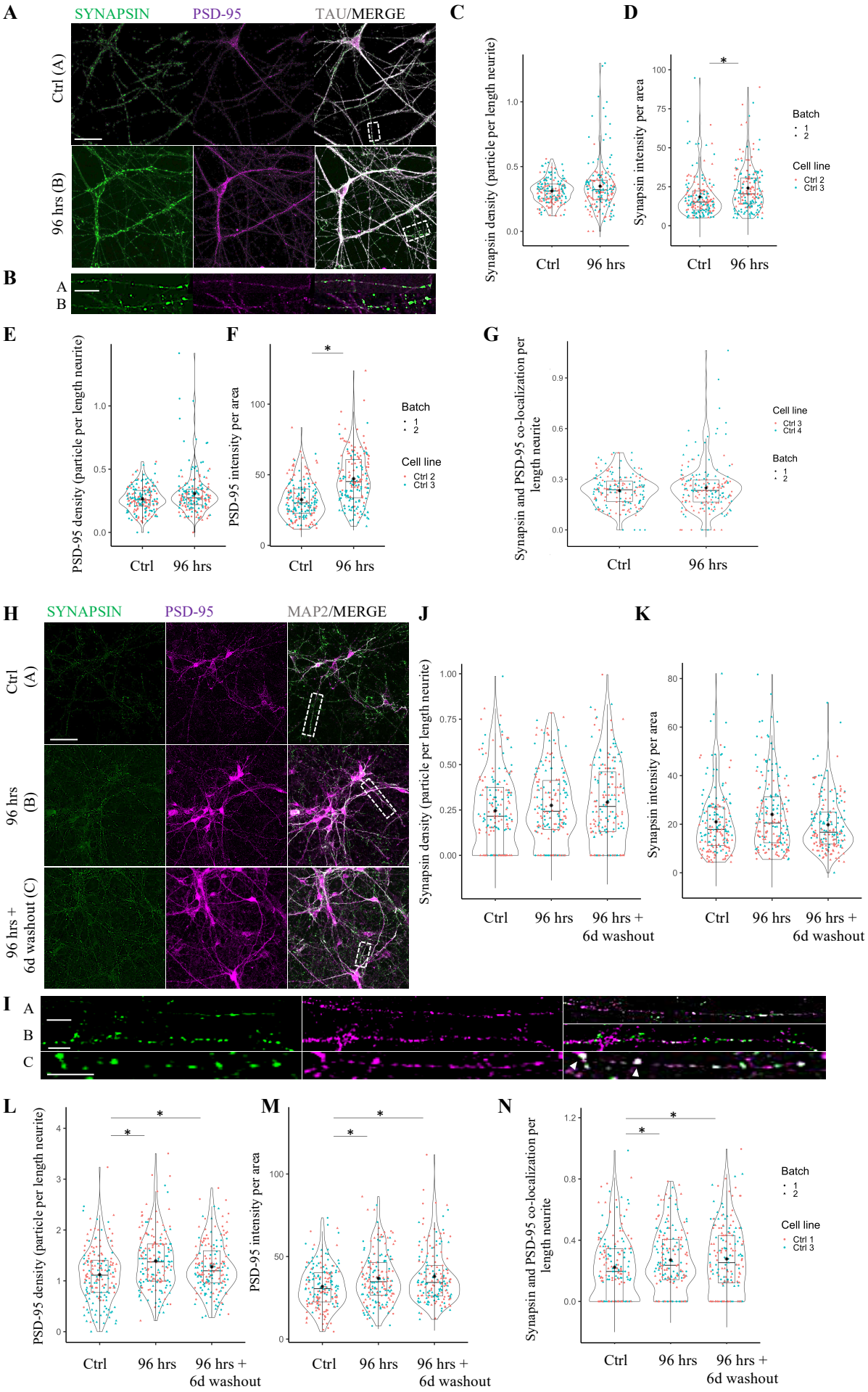
A
SYNAPSIN
PSD-95
TAU/MERGE
Ctrl (A)
96 hrs (B)
B
A
B
C
Synapsin density (particle per length neurite)
Ctrl
96 hrs
D
Synapsin intensity per area
Batch
1
2
Cell line
Ctrl 2
Ctrl 3
E
PSD-95 density (particle per length neurite)
F
PSD-95 intensity per area
G
Synapsin and PSD-95 co-localization per length neurite
Cell line
Ctrl 3
Ctrl 4
H
MAP2/MERGE
96 hrs + 6d washout (C)
J
K
96 hrs + 6d washout
I
L
M
N
Ctrl 1
Ctrl 3

Figure 17. Psilocin promotes dendritic synaptogenesis.
(A-B) Representative PSD-95 and synapsin staining for the untreated condition (Ctrl) and 96 hrs after permanent 10 µM psilocin administration (96 hrs) on TAU^{+} neurites. **(A)** Scale bar: 50 µm **(B)**, close-up: 10 µm. Non-significant increase in synapsin **(C)** density but significant increase in **(D)** intensity 96 hrs after permanent psilocin administration. Non-significant increase in PSD-95 **(E)** density but significant increase in **(F)** intensity 96 hrs after permanent psilocin administration (96 hrs). **(G)** Non-significant increase in PSD-95 and synapsin co-localization 96 hrs after permanent psilocin administration. For Ctrl N = 181 neurites, for 96 hrs N = 180 neurites were calculated. Two control cell lines each with two biological batches were included. **(H-I)** Representative MAP2^{+} dendritic PSD-95 and synapsin staining for the untreated condition (Ctrl), 96 hrs after permanent 10 µM psilocin administration (96 hrs) and 6 days after 96 hrs permanent 10 µM psilocin administration (96 hrs + 6d washout). **(H)** Scale bar: 50 µm **(I)**, close-up: 10 µm (white arrows: co-localization). Non-significant increase in synapsin **(J)** density and **(K)** intensity 96 hrs after permanent psilocin administration. **(L)** PSD-05 particle per length neurite and **(M)** intensity per area and **(N)** synapsin/ PSD-95 co-localization was significantly increased 96 hrs after permanent 10 µM psilocin treatment and 6 days after 96 hrs permanent psilocin treatment compared to an untreated control condition. Ctrl with N = 180 neurites; 96 hrs with N = 180 neurites, 96 hrs + 6d washout with N = 180 neurites. Two control cell lines each with two biological batches were included. For all analyses Kruskal-Wallis-Test for independent samples was calculated. Bonferroni-correction, adjusted $p < .05$, mean ± SD. Significance levels against the respective control are *$p < 0.05$.

Again, it was assessed whether those cellular changes are functionally reflected by measuring spontaneous EPSCs synaptic activity 96 hrs and 6 days after 96 hrs permanent psilocin administration. For measuring spontaneous synaptic properties whole-cell patch clamp recordings on single cortical neurons cultured on mouse astrocytes was performed *in vitro*. While sEPSC amplitude was significantly decreased after 96 hrs permanent psilocin administration (from M_{Ctrl} = 27.68, SD = 4.88 to M_{96hrs} = 21.66, SD = 9.87), the amplitude significantly increased after 96 hrs permanent psilocin administration plus 6 days of washout (from M_{Ctrl} = 20.5, SD = 6.63 to $M_{96hrs + 6d\ washout}$ = 29.43, SD = 7.32) compared to a control condition, confirming described cellular postsynaptic modulations. For both conditions sEPSC frequency not changed significantly. (**Fig. 18A-D, Appendix 18**).

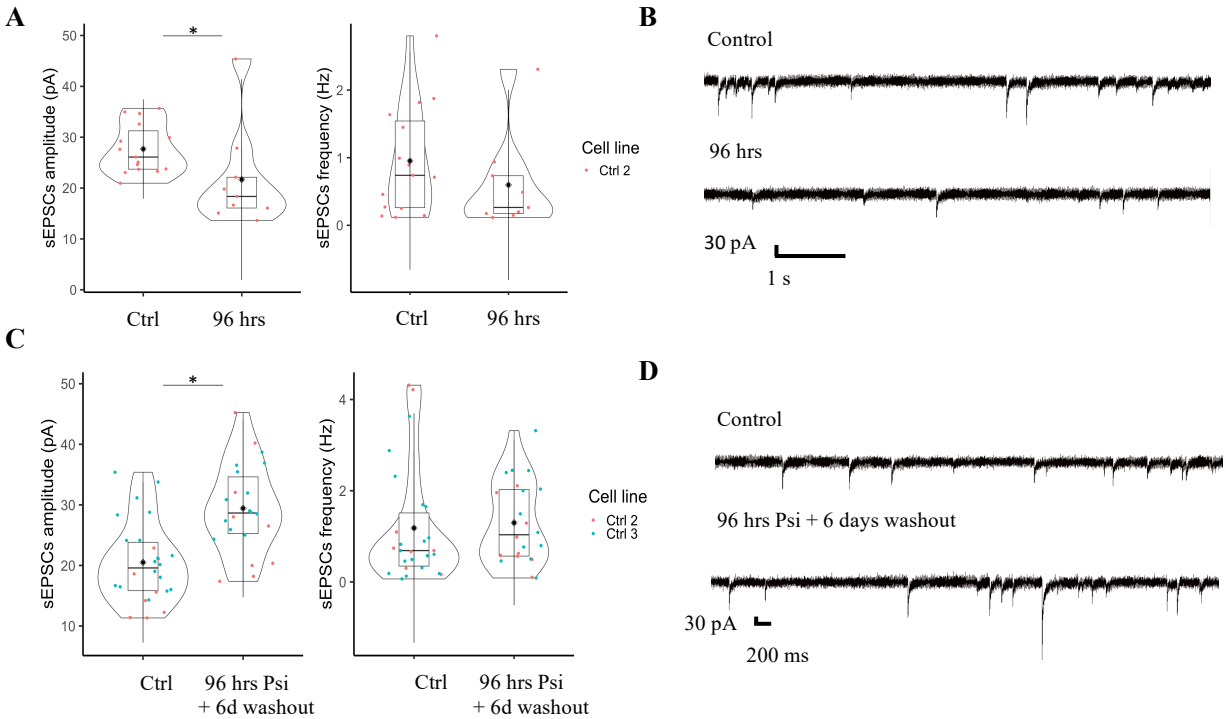

Figure 18. Psilocin-induced increase in sEPSC amplitude in long-term.
(A-B) Long-term effect of psilocin on synaptic properties. **(A)** Significant decrease in sEPSCs amplitude, with unchanged frequency after 96 hrs permanent 10 µM psilocin administration (96 hrs). **(B)** Representative trace for control and psilocin condition 96 hrs after permanent 10 µM psilocin administration. One Ctrl cell line was included in the analysis. Ctrl with $N = 15$ cells, 96 hrs Psi with $N = 9$ cells were measured. **(C–D)** Long-lasting effect of psilocin on synaptic properties. **(C)** Significant increase in sEPSCs amplitude, with unchanged frequency, 6 days washout after 96 hrs permanent 10 µM psilocin administration (96 hrs Psi + 6d washout) that speaks for postsynaptic modulations. **(D)** Representative trace for control and psilocin condition 6 days after 96 hrs permanent 10 µM psilocin administration. Two Ctrl cell lines were included in the analysis. Ctrl with $N = 26$ cells, 96 hrs Psi + 6d washout with $N = 22$ cells were measured. For all experiments Mann-Whitney-U-test for independent samples was calculated, ± *SD*. Significance levels against the respective control are *p < 0.05. Electrophysical measurements were performed and representative traces were generated by Dr. Mahnaz Davoudi.

4.4. Influence of psilocin on neurotrophic factor BDNF

Psychedelics have been shown to competently increase levels of neurotrophic factors, such as BDNF in humans and in animal models but so far not in iPSC-derived cortical neurons *in vitro*[1,43,222,294,346–353]. BDNF is a key factor involved in multiple pathways of neuroplasticity (please refer to subchapter **1.6.2**).

Evidently, a crucial question was to address whether psilocin increased BDNF density in iPSC-derived cortical neurons. In an initial experiment the most effective psilocin concentration and treatment duration (in terms of increasing BDNF particle per µm) was assessed with ICC. The strongest abundance in BDNF density was seen 24 hrs after a 10 min treatment with 10 µM psilocin in comparison to other psilocin concentrations (e.g., 10 nM, 100 nM, 1 µM) compared to a DMSO control condition (from $M_{DMSO} = 2.48$, $SD = 0.96$ to $M_{10\mu M} = 3.4$, $SD = 1.44$) (**Fig. 19A-B, Appendix 19A**).

Up to 72 hrs after 10 min 10 µM psilocin administration there was not a difference in cell viability, speaking for the non-toxicity of this psilocin concentration (from $M_{Ctrl} = 0.9$, $SD = 0.08$ to M_{24} hrs $= 0.84$, $SD = 0.06$ to $M_{48\ hrs} = 0.91$, SD = 0.03 to $M_{72\ hrs} = 0.99$, SD = 0.1). (**Fig. 19C, Appendix 19B)**.

As 10 µM psilocin is a rather strong concentration and 10 min treatment can be regarded as artificial treatment duration, one, considered to be more physiological, experimental condition was included. Here, 100 nM psilocin was applied for 6 hrs to the cells, comparable with the effective dose in the brain and the duration of a psilocybin induced trip in the human being. Although BDNF density was significantly increased for both conditions compared to a control condition, BDNF density was further significantly increased 24 hrs after the 10 min 10 µM psilocin condition compared to the 6 hrs 100 nM treatment condition (from $M_{Ctrl} = 1.77$, $SD = 0.83$ to $M_{10min\ 10\mu M} = 3.41$, $SD = 1.72$ to $M_{6h\ 100nM} = 2.3$, $SD = 1.24$). (**Fig. 19D-E, Appendix, 19C**).

Therefore, for most of the following experiments (if not stated differently) a treatment duration of 10 min and a 10 µM psilocin concentration was administered.

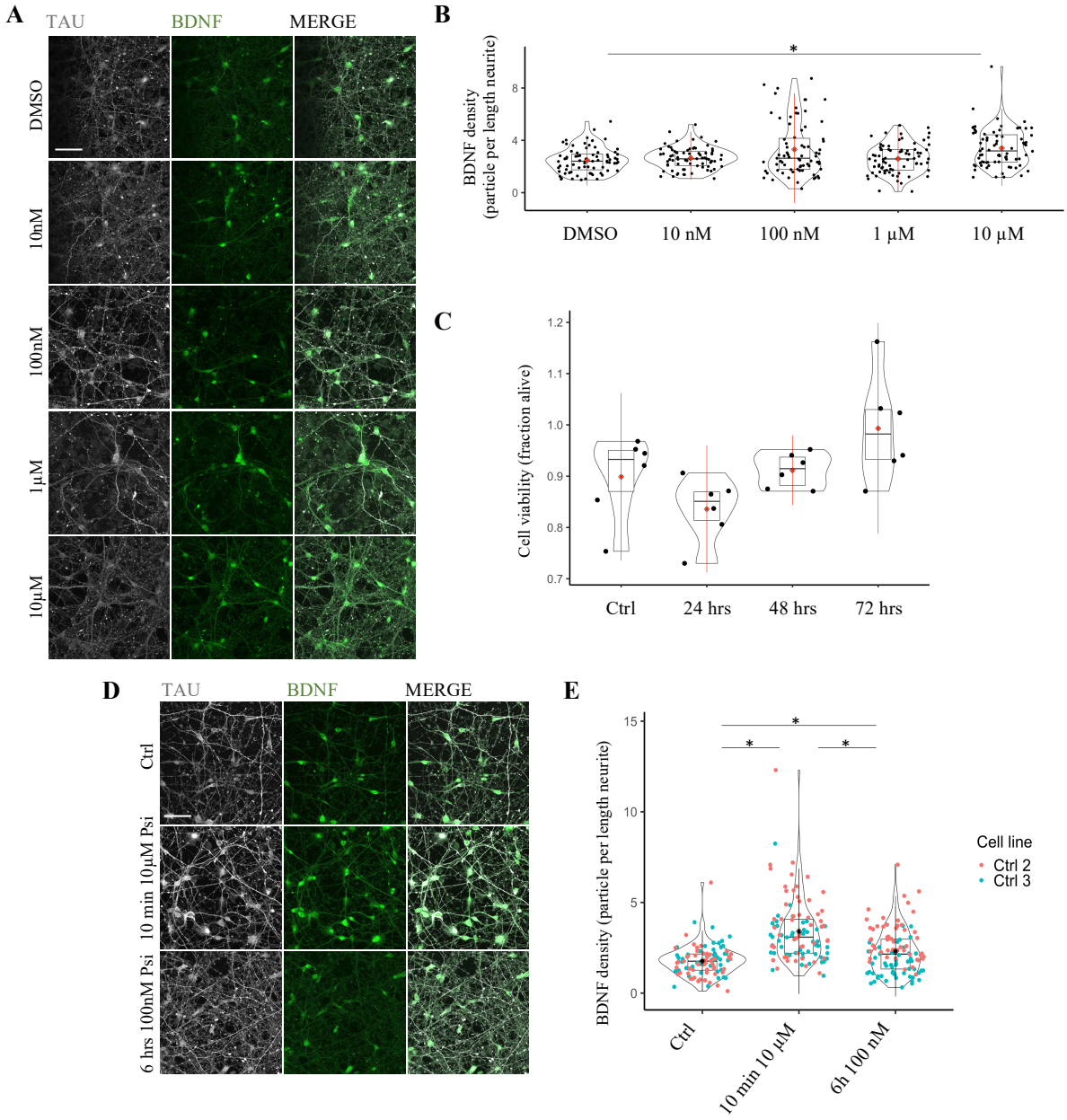

Figure 19. Influence of different psilocin concentrations and treatment conditions on BDNF level.

(A) Representative image of a neuronal network for pre-treatment condition (DMSO) and 24 hrs after a 10 min 10 nM, 100 nM, 1 µM or 10 µM trigger showed the strongest increase in BDNF signal for the 10 µM treatment condition. Scale bar: 50 µm. **(B)** BDNF density was exclusively significantly increased 24 hrs after 10 min 10 µM Psilocin trigger (10 µM). Ctrl cell line 1 was included in the analysis, with one biological batch. (Ctrl with $N = 76$ neurites; 24 hrs after a 10 min 10 nM ($N = 75$ neurites), respectively 100 nM ($N = 75$ neurites), respectively 1 µM ($N = 75$ neurites), respectively 10 µM ($N = 75$ neurites) psilocin trigger. **(C)** Cell viability assay demonstrated non-toxicity of psilocin up to 72 hrs post treatment. One Ctrl cell 3 line was included in the analysis. For each condition $N = 6$ technical replicates were included. **(D)** Representative image of a neuronal network 24 hrs after an "artificial" (10 min 10 µM Psi) and a "physiological" (6 hrs 100nM Psi) treatment condition. Scale bar: 50 µm. **(E)** BDNF density was significantly increased 24 hrs after a 10 min 10 µM psilocin trigger (10 min 10 µM) and 24 hrs after a 6 hrs 100 nM psilocin stimulation (6 hrs 100 nM). But BDNF density was also significantly increased for the" artificial" compared to the "physiological" stimulation. Two Ctrl cell lines were included in the analysis, each with one biological batch. (Ctrl with $N = 99$ neurites; 10 min 10 µM Psi with $N = 102$ neurites; 6 hrs100 nM Psi with $N = 102$ neurites). Kruskal-Wallis test for independent samples was calculated. Post hoc Wilcoxon rank sum test. Bonferroni-correction, adjusted $p < .05$, mean ± *SD*. Significance levels against the respective control are *$p < 0.05$.

24 hrs psilocin treatment led to a significant increase in BDNF density (particle per µm), stable reproducible in four biological independent control cell lines, validated by ICC (from M_{Ctrl} = 1.5, *SD* = 1.16 to M_{Psi} = 2.64, *SD* = 1.93) (**Fig. 20A-C, Appendix 20A**).

As the antibody that was used for ICC recognizes both variants of BDNF (pro-BDNF and m-BDNF) a WB was performed to distinguish between both. In first experiments I found an increase of pro-BDNF and the m-BDNF protein level (**Fig. 20D**). That was especially interesting for the m-BDNF variant which was repetitively not detectable under standard experimental conditions. Only after dosing with psilocin (and after plasminogen treatment, which will be illustrated later, see **Fig. 31**) and under optimized detection conditions m-BDNF reached the WB detection level. Also, the protein level of phosphorylated, activated TrkB receptor was increased which could speak for an increased binding of BDNF to its receptor (**Fig. 20D**).

Interestingly, the ICC effect was also significant after 24 hrs permanent psilocin administration and endured for 48 hrs (from M_{Ctrl} = 1.53, *SD* = 1.21 to M_{24hrs} = 2.26, *SD* = 2 to M_{48hrs} = 1.58, *SD* = 0.66 to $M_{24hrs\ permanent}$ = 1.58, *SD* = 0.52) (**Fig. 20E, Appendix 20B**). This result was confirmed by RT-qPCR for the experimental conditions tested (**Fig. 20F, Appendix 20B**) (fold change of *BDNF* gene expression from M_{Ctrl} = 1, *SD* = 0 to M_{Psi} = 2.24, *SD* = 0.81; to $M_{48\ hrs}$ = 7.61, *SD* = 1.45, to $M_{24\ hrs\ permanent}$ = 6.41, *SD* = 0.79).

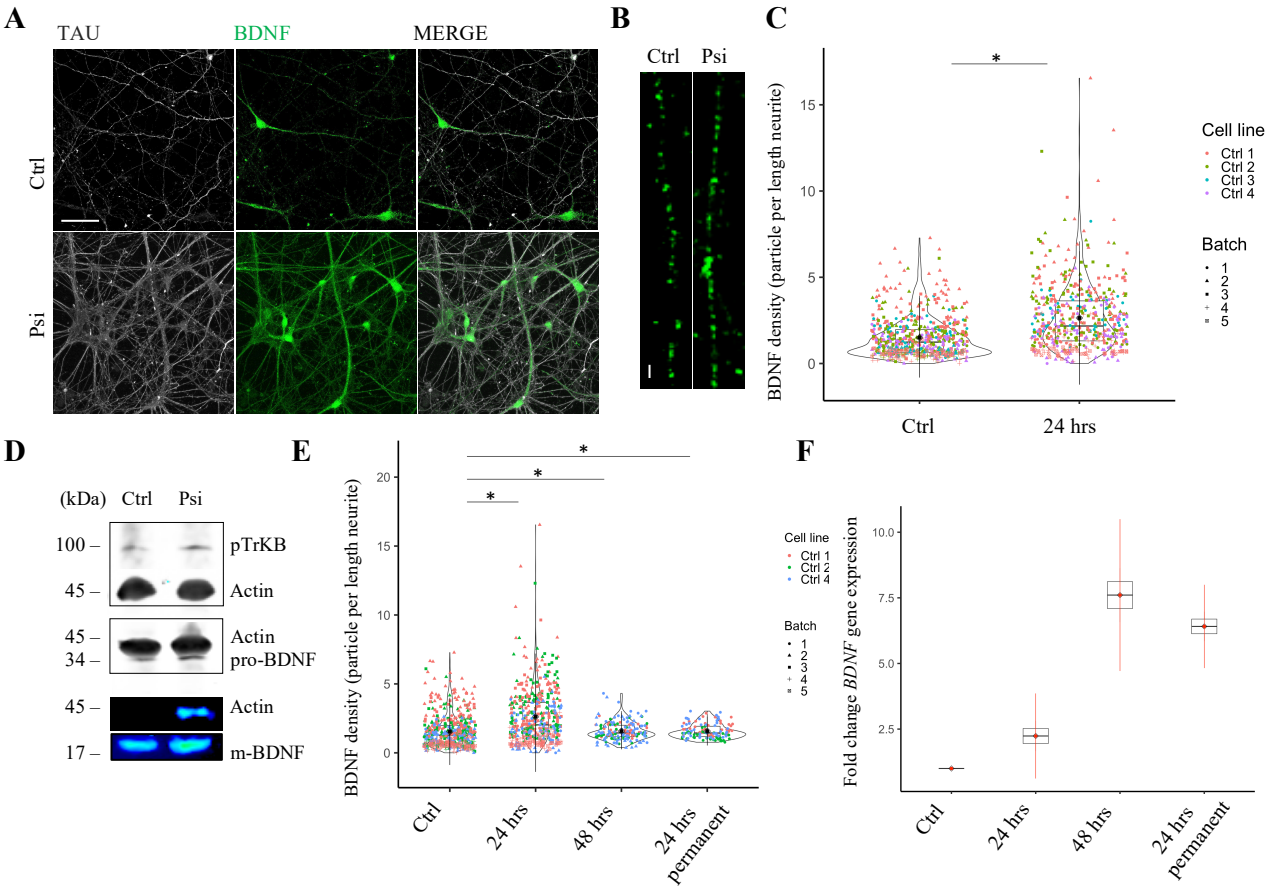

Figure 20. Psilocin induced increase in BDNF level.
(A) Representative image of a neuronal network for pre-treatment condition (Ctrl) and 24 hrs after a 10 min short psilocin trigger (Psi). Scale bar: 50 µm, **(B)** close up: 2 µm. **(C)** BDNF density was significantly increased 24 hrs after a 10 min 10 µM psilocin trigger (24 hrs). Four Ctrl cell lines were included in the analysis (Ctrl with $N = 613$ neurites; 24 hrs with $N = 529$ neurites). **(D)** Endogenous phosphorylated (activated) TrkB (pTrkB) receptor, pro-BDNF and m-BDNF protein level increased 24 hrs after psilocin (Psi) administration. **(E)** BDNF density was significantly increased 24 and still 48 hrs (24 hrs; 48 hrs) after a 10 min 10 µM psilocin trigger and after permanent psilocin administration (24 hrs permanent). Three Ctrl cell lines were included in the analysis (Ctrl with $N = 520$ neurites; 24 hrs with $N = 478$ neurites; 48 hrs with $N = 170$ neurites; 24 hrs permanent with $N = 125$ neurites). For all analysis Kruskal-Wallis test for independent samples was calculated. Post hoc Wilcoxon rank sum test. Bonferroni-correction, adjusted $p < .05$, mean ± *SD*. Significance levels against the respective control are $*p < 0.05$. **(F)** RT-qPCR revealed increase in *BDNF* gene expression 24 and still 48 hrs after a 10 min 10 µM psilocin trigger and after permanent psilocin administration. One BD1 3 cell line was included (Ctrl with $N = 2$ technical replicates; 24 hrs with $N = 2$ technical replicates; 48 hrs with $N = 2$ technical replicates, 24 hrs permanent with $N = 2$ technical replicates), no statistics were calculated.

4.5 Psilocin-induced activation of m-BDNF/phospho-TrkB associated downstream pathways

In order to decipher an activation of the m-BDNF/phospho-TrkB complex by psilocin I next focused on associated downstream pathways.

4.5.1 Psilocin activated the pro-survival AKT pathway

I first assessed the m-BDNF/phospho-TrkB downstream pro-survival AKT pathway (**Fig. 21A**) activation by calculating the ratio of phosphorylated Serin 473 pAKT-to-AKT protein level by WB. Phosphorylation of the AKT protein strongly increased 1 day after psilocin administration (**Fig. 21B**). That was accompanied by RNA bulk seq data that showed a non-significant enrichment in differentially expressed genes associated with PI3K-AKT KEGG term (**Fig. 21C**). pAKT-to-AKT ratio strongly increased 3 days after psilocin exposure reversed by 5-HT2A-R agonist ketanserin co-treatment, validated by WB (**Fig. 21D-E, Appendix 21)** (from $M_{Ctrl} = 0.82$, $SD = 0.2$ to $M_{Psi} = 1.27$ $SD = 0.19$ to $M_{Psi+Ket} = 0.85$, $SD = 0.19$), suggesting an involvement of the 5-HT2A-R.

4.5.2 Psilocin induced increase in neurite arborization

m-BDNF/phosphor-TrkB activated downstream pathways play a central role in dendritic branching (please refer to subchapter **1.6.2**). Dendritic complexity and neuritogenesis has been shown to be increased after administration with serotonergic psychedelics in rodents[1,212]. In order to replicate this effect, human cortical neurons were next transduced with AAV_CamKIIa p-hCHR2(134a)-mCherry. I performed Sholl analysis on mCherry-expressing neurons 24 and 48 hrs after a short psilocin trigger and 24 hrs after permanent psilocin administration in comparison to an untreated control condition (**Fig. 22A-C, Appendix 22**).

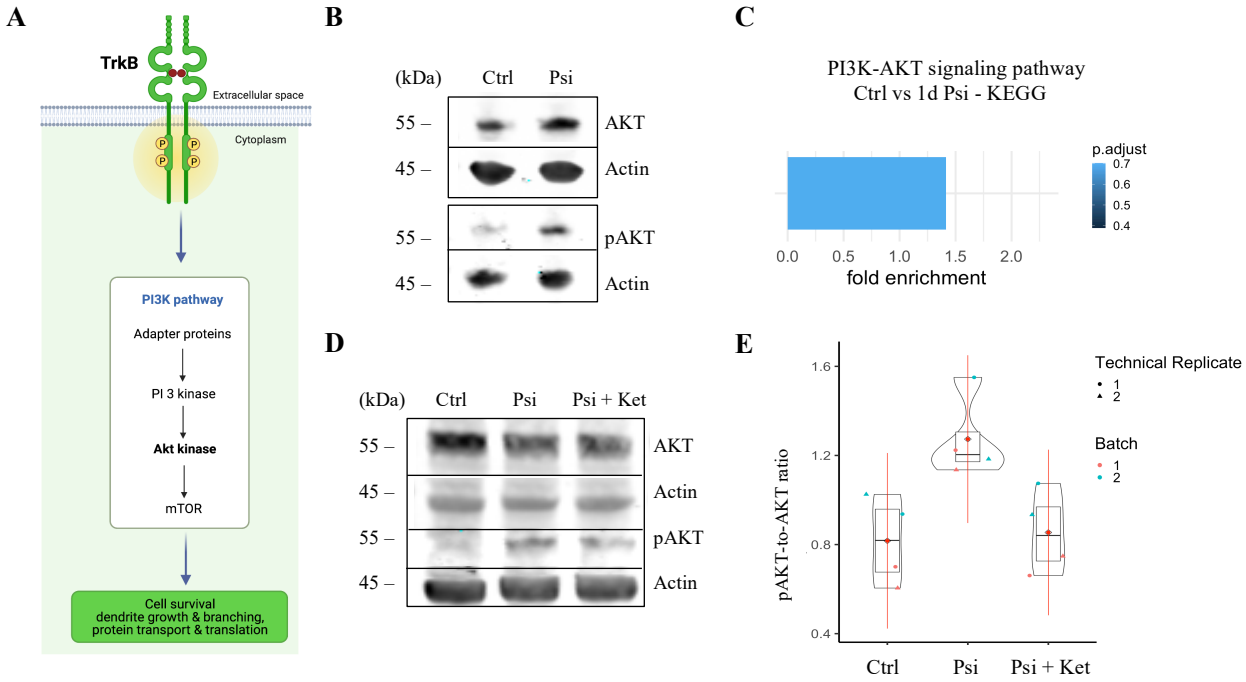

Figure 21. Psilocin induced activation of prosurvival AKT downstream cascade.
(A) m-BDNF/phospho-TrkB complex activates the prosurvival and antiapoptotic PI3K/AKT pathway via activation of mTOR. Graphic illustration generated with *Biorender.com.* **(B)** pAKT protein level, indicating an activation of pro survival AKT pathway, was increased after 24 hrs psilocin (Psi) exposure. Significance levels against the respective control $*p < 0.05$. **(C)** RNA bulk seq data showed a non-significant 1.4-fold enrichment in differentially expressed genes associated with PI3K/AKT KEGG term 24 hrs after psilocin administration. **(D)** pAKT protein level was still increased 72 hrs after psilocin exposure, reversed by selective 5-HT2A-R antagonist ketanserin co-treatment (Psi + Ket), **(E)** both effects were not significant. Ctrl cell line 3 was included in the analysis (Ctrl with $N = 4$ data points, Psi with $N = 4$ data points; Psi + Ket with $N = 4$ data points), each with two biological batches. For analysis Kruskal-Wallis test for independent samples was calculated. Post hoc Wilcoxon rank sum test. Bonferroni-correction, adjusted $p < .05$, mean ± *SD*. Significance levels against the respective control are $*p < 0.05$. pAKT, phosphorylated AKT; KEGG, Kyoto Encyclopedia of Genes and Genomes. Illustration of RNA bulk seq KEGG data was generated by Dr. Anne Hoffrichter.

The number of total neurite crossings significantly increased in neurons treated with psilocin (from $M_{Ctrl} = 10.9$, $SD = 5.71$ to $M_{24hrs} = 15.33$, $SD = 8.4$ and $M_{24hrs\ permanent} = 15.83$, $SD = 6.83$ to $M_{48hrs} = 14.11$, $SD = 6.5$). This increase in neuronal branching originated from an increase of primary crossings (non-significant at 48 hrs and a non-significant trend at 24 hrs after a short trigger, but significant for the 24 hrs permanent condition ($M_{Ctrl} = 4.1$, $SD = 2.12$ to $M_{24hrs} = 5.42$, $SD = 3.72$ and $M_{24hrs\ permanent} = 5.83$, $SD = 2.88$ to $M_{48hrs} = 5.49$, $SD = 2.42$) and in particular secondary crossings (significantly increased at 24 and 48h post treatment from $M_{Ctrl} = 2.74$, $SD = 1.37$ to $M_{24hrs} = 3.96$, $SD = 2.28$ and to $M_{24hrs\ permanent} = 4.17$, $SD = 1.96$ to $M_{48hrs} = 3.91$, $SD = 1.83$) but not tertiary crossings (except of a significant increase for the 24 hrs permanent psilocin condition $M_{Ctrl} = 2.23$, $SD = 1.21$ to $M_{24hrs\ permanent} = 3.02$, $SD = 1.44$). There was not a recognizable difference between short and permanent administration of psilocin within the 24 hrs group. Consistent with that finding, the neurite and axon outgrowth modulator growth-associated protein 43 (GAP-43)[441,442] was significantly upregulated 1 day (factor 0.8, log2 fold change) and still non-significantly 3 days after psilocin administration, prevented by ketanserin co-treatment suggesting a 5-HT2A-R-mediated effect in RNA bulk seq experiment (**Fig. 22D**).

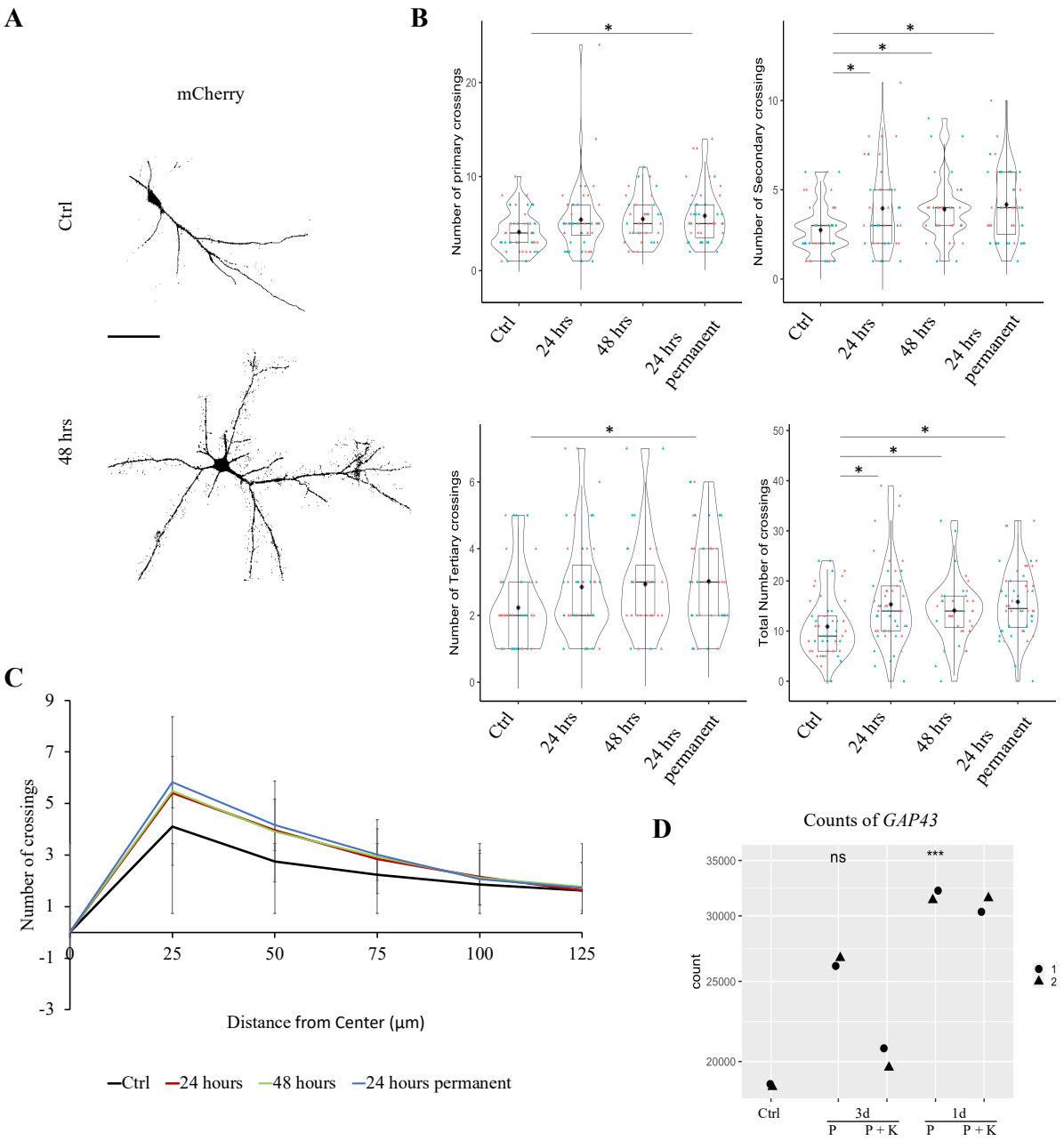

Figure 22. Psilocin induced increase in neurite complexity.
(A-C) Cells were transduced with AAV_CamKIIa p-hCHR2(134a)-mCherry. **(A)** Representative image for pre-treatment condition (Ctrl) and 48 hrs after a 10 min short psilocin trigger (48 hrs) for mCherry staining showed an increase in neurite crossings for the latter. **(B)** Singular analysis: 24 hrs after permanent psilocin administration (24 hrs permanent) the number of primary (25 µm distance from soma) and tertiary (75 µM distance to the soma) crossings significantly increased compared to the untreated control condition (Ctrl). The number of secondary crossings (50 µm distance from soma) and the total number of neurite crossings significantly increased 24 (short and permanent) and 48 hrs after a 10 min 10 µM psilocin trigger. Two Control cell lines with two biological batches (Ctrl with N = 43 - 48 neurites; 24 hrs with N = 47 - 48 neurites; 48 hrs with N = 31 - 35 and 24 hrs permanent with N = 46 - 47 neurites were included. For all statistical analysis Kruskal-Wallis test for independent samples was calculated. Bonferroni-correction, adjusted p< .05, mean ± SD. Significance levels against the respective control are *$p < 0.05$. **(C)** Sholl analysis summary for results shown in figure **(B)**. **(D)** TPM scaled RNA bulk seq data, performed in biological duplicates, showed an increase in neurite and axon outgrowth modulator *GAP43* expression. Significant one day (1d P) and non-significant three days (3d P) after psilocin administration, non-significantly prevented by ketanserin co-treatment (1d P + K; 3d P + K). Significance levels against the respective control ***$p < 0.001$.

4.5.3 Psilocin induced increase in immediate early genes

Research clearly demonstrates that IEG gene expression is increased after psychedelic administration[216–223,443]. The expression of IEG cFOS is an important BDNF downstream associate as the m-BDNF/phospho-TrkB complex stimulates its expression via the MAPK pathways (please refer to subchapter **1.6.2**). RNA bulk seq data that showed a non-significant 1.2-fold enrichment in differentially expressed genes associated with MAP KEGG term which was still 1,5-fold enriched three days after psilocin administration compared to the 1-day condition (**Fig. 23A)**. cFOS expression is evaluated as a sign of an induction of neuronal activity and/ or Ca^{2+} influx. That was confirmed by a strong up-regulation of *cFOS* gene expression validated by RT-qPCR 24 hrs after permanent psilocin administration (fold change of *cFOS* gene expression from $M_{Ctrl} = 1$, $SD = 0$ to $M_{24hrs} = 7.75$, $SD = 2.14$) (**Fig. 23B, Appendix 23**).

This data was in line with RNA bulk seq gene expression data where I found a significant upregulation of the FOS family member genes *FOSL1*, *FOSL2* (paralogous transcription factors) and a non-significant upregulation for *FOS* gene 24 hrs following psilocin administration (*FOS*: factor 2.2, log2 fold change, *FOSL1*: factor 1.8, log2 fold change, *FOSL2*: factor 0.8, log2 fold change). Expression of the three mentioned genes was non-significantly prevented by co-treatment with 5-HT2A-R antagonist ketanserin, indicating and involvement of the 5-HT2A-R (**Fig. 23C-D**).

Consistently, I found a significant upregulation of the psychedelic-specific *EGR2* gene[218,444] in RT-qPCR data 24 hrs after permanent psilocin administration (fold change of *EGR2* gene expression from $M_{Ctrl} = 1$, $SD = 0$ to $M_{24hrs} = 1.96$, $SD = 0{,}2$). (**Fig. 23E, Appendix 23**) and an upregulation of the major mediator and regulator of synaptic plasticity and early neuronal activity marker[445] *EGR1* gene 3 days after psilocin treatment by RNAseq gene expression data, not prevented by ketanserin co-treatment (factor 2.2, log2 fold change) (**Fig. 23F**).

I conclude that psilocin-induced activation of m-BDNF/phospho-TrkB associated downstream pathways.

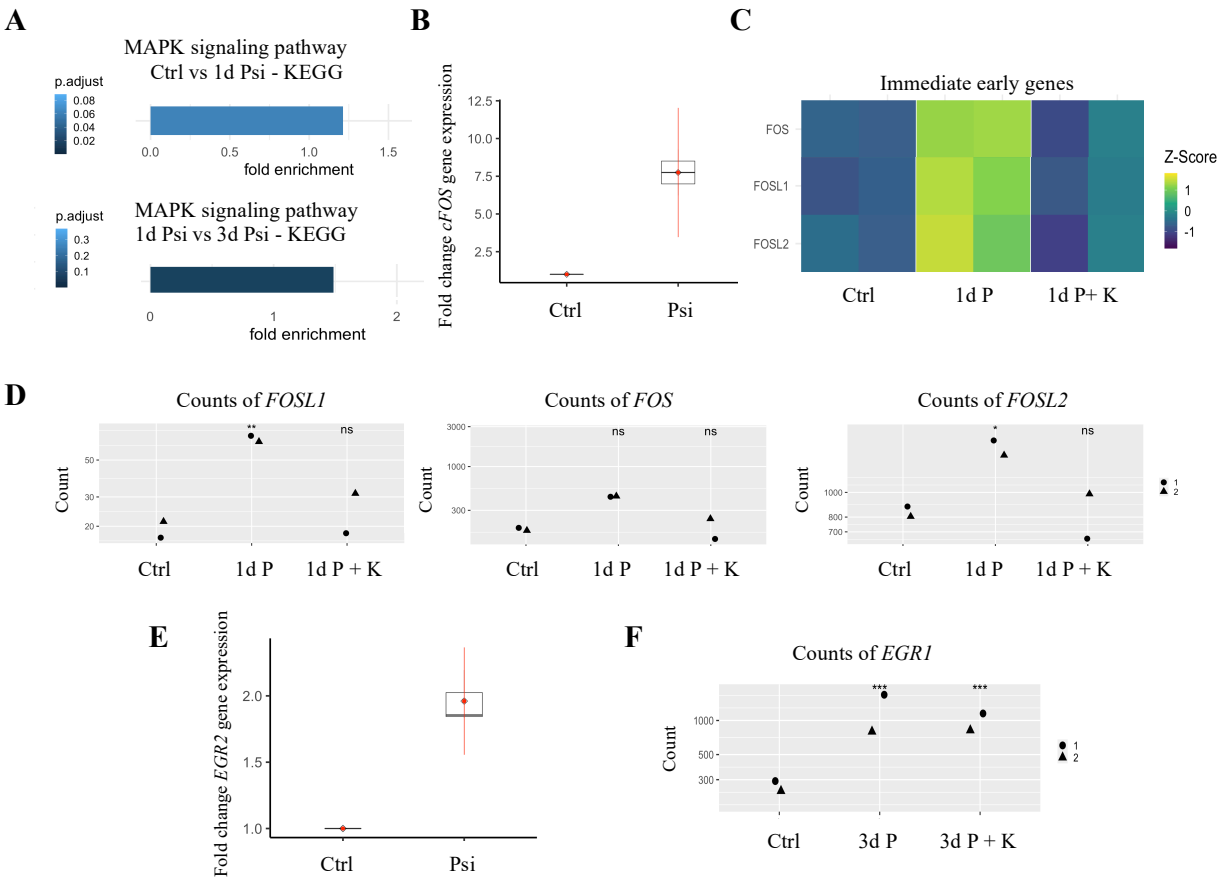

Figure 23. Psilocin induced increase in immediate early genes.
(A) RNA bulk seq data showed a non-significant 1.2-fold enrichment in differentially expressed genes associated with MAP KEGG, still 1.5-fold enriched three days after psilocin administration. Significance levels against the respective control $*p < 0.05$. **(B)** *cFOS* gene expression 24 hrs after permanent 10 µM psilocin administration was increased, validated by RT-qPCR. One control cell line was included (Ctrl with $N = 3$ technical replicates; Psi with $N = 2$ technical replicates), no statistics were calculated. **(C)** Heat map (z-scaled) and **(D)** TPM scaled and RNA bulk seq data showed a significant up-regulation of the *FOSL1* and *FOSL2* and a non-significant up-regulation of the immediate early *FOS* gene one day after psilocin administration (1d P), non-significantly prevented by ketanserin co-treatment (1d P + K). Significance levels against the respective control $*p < 0.05$, $**p < 0.01$. **(E)** RT-qPCR revealed an increase in *EGR2* gene expression 24 after permanent 10 µM psilocin administration. One control cell line was included (Ctrl with $N = 3$ technical replicates; Psi with $N = 3$ technical replicates), no statistics were calculated. **(F)** TPM scaled RNA bulk seq data revealed a significant increase of *EGR1* gene 3 days after 6 hrs 100 nM stimulation with psilocin (3d Psi), not reversed by ketanserin co-treatment (3d P + K). Significance levels against the respective control $***p < 0.001$. Heat map (z-scaled) and KEGG illustrations of RNA bulk seq data were generated by Dr. Anne Hoffrichter.

4.6 Deciphering the psilocin-mediated increase in BDNF

The next step was to decipher potential biological mechanisms that were involved in the psilocin-induced BDNF increase.

4.6.1 Psilocin-induced BDNF increase was PKC- and endocytosis-mediated

First, it is already described that an agonist-induced 5-HT2A-R internalization takes place via the endosomal pathway, in detail via a CME mechanism[446]. Second, PKC, (also downstream of the 5-

HT2A-R and the m-BDNF/pTrkB complex) activation is sufficient and necessary for the serotonin-induced internalization process[439] (please refer to subchapter **1.6.1**). Therefore, I started with inhibiting those two mechanisms in presence of psilocin and again assessed BDNF density (particle per µm) 24 hrs after administration with ICC. PKC (phosphorylation and translocation) was selectively and potently inhibited with chelerythrine[447,448]. Dynamin activity that is essential for CME was inhibited with dynasore (**Fig. 24A**)[449]. Interestingly, the prior described increase in BDNF density was abrogated if the cells were co-treated with chelerythrine or dynasore (from $M_{Ctrl} = 3.13$, $SD = 1.48$ to $M_{Psi} = 4.6$, $SD = 2.37$ to $M_{Psi + Chel} = 2.97$, $SD = 1.74$ to $M_{Psi + D} = 3.36$, $SD = 1.01$), speaking for an endocytosis and PKC-mediated process (**Fig. 24B-C, Appendix 24**). Also, psilocin-induced *BDNF* gene increase, validated with RT-qPCR, could be abrogated by co-treatment with chelerythrine (**Fig. 24D, Appendix 24**) (from $M_{Ctrl} = 1$, $SD = 0$ to $M_{Psi} = 2.24$, $SD = 0.81$; to $M_{Psi + Chel} = 1.17$, $SD = 0.41$). I conclude that psilocin-induced BDNF increase in human cortical neurons is PKC- and endocytosis-mediated.

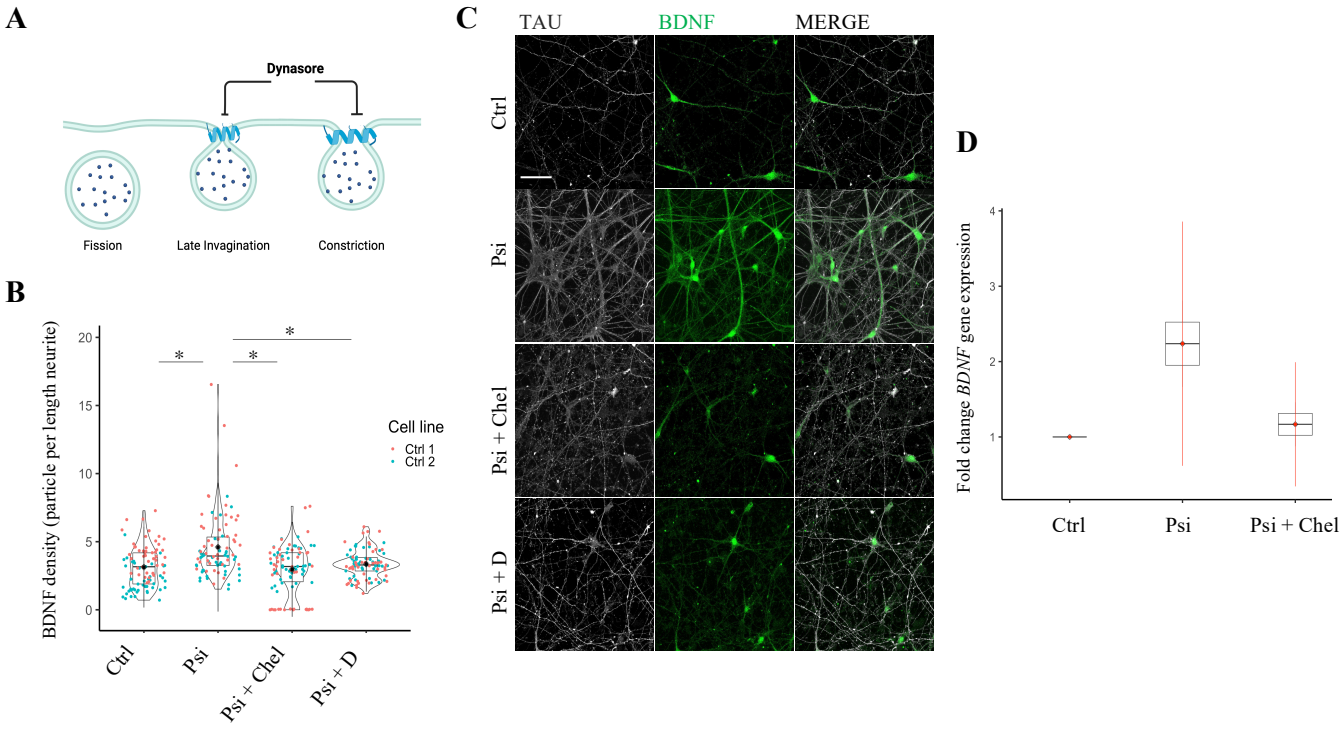

Figure 24. Psilocin induced increase in BDNF level was PKC- and endocytosis-mediated
(A) Dynasore, a dynamin inhibitor, inhibits late invagination and constriction of vesicle formation and thereby endocytosis. Figure adapted by[457] and generated with *Biorender.com*. **(B)** Chelerythrine (Psi + Chel, selective PKC inhibitor) or dynasore (Psi + D, inhibition of clathrin-coated vesicle invagination) co-treatment significantly reduced BDNF density compared to the psilocin monotreatment condition (Psi). Two Ctrl cell lines were included in the analysis, each with one biological batch. (Ctrl with $N = 90$ neurites; Psi with $N = 90$ neurites; Psi + Chel with $N = 90$; Psi + D with $N = 90$ neurites). Kruskal-Wallis test for independent samples was calculated. Post hoc Wilcoxon rank sum test. Bonferroni-correction, adjusted $p < .05$, mean ± *SD*. Significance levels against the respective control and for multiple group comparisons are $*p < 0.05$. **(C)** Representative image 24 hrs after the simultaneous treatment of 10 µm psilocin with chelerythrine or dynasore, scale bar: 50 µm. **(D)** RT-qPCR revealed increase in *BDNF* gene expression, reversed by chelerythrine co-treatment. One BD1 3 cell line was included (Ctrl with $N = 2$ technical replicates; Psi with $N = 2$ technical replicates; Psi + Chel with $N = 2$ technical replicates), no statistics were calculated.

4.6.2 Psilocin-induced BDNF increase was 5-HT2A-R-mediated

Next, the role of 5-HT2A-R activation in the psilocin-promoting BDNF density augmentation was sought to determine as it is known that 5-HT2A-R activation plays an important role in psychedelic mediated response and the neuroplasticity effects (please refer to subchapter **1.6.1**). I therefore inhibited receptor activation with the 5-HT2A-R antagonist ketanserin and measured BDNF density (particle per µm) 24 hrs after administration with ICC. Based on literature I choose a 7.5-fold excess of ketanserin[1] compared to psilocin. Notably, ketanserin efficiently blocked psilocin-induced BDNF density increase (from $M_{Ctrl} = 2.49$, $SD = 1.44$ to $M_{Psi} = 4.03$, $SD = 2.3$; to $M_{Psi + Ket} = 2.11$, $SD = 1.44$). Monotreatment with ketanserin, provoked the same effect (to $M_{Ket} = 1.4$, $SD = 1.17$) (**Fig. 25A-B, Appendix 25**). That was confirmed by RNA bulk seq data which showed a non-significant increase in *BDNF* gene expression one day after psilocin administration that was non-significantly prevented by ketanserin co-treatment (from $M_{Ctrl} = 207.81$, $SD = 25.87$ to $M_{1dPsi} = 264.46$, $SD = 36.05$; to $M_{1dPsi + Ket} = 200.71$, $SD = 41.64$) (**Fig. 25C-D**). I conclude that psilocin-induced BDNF increase in human cortical neurons is 5-HT2A-R-mediated.

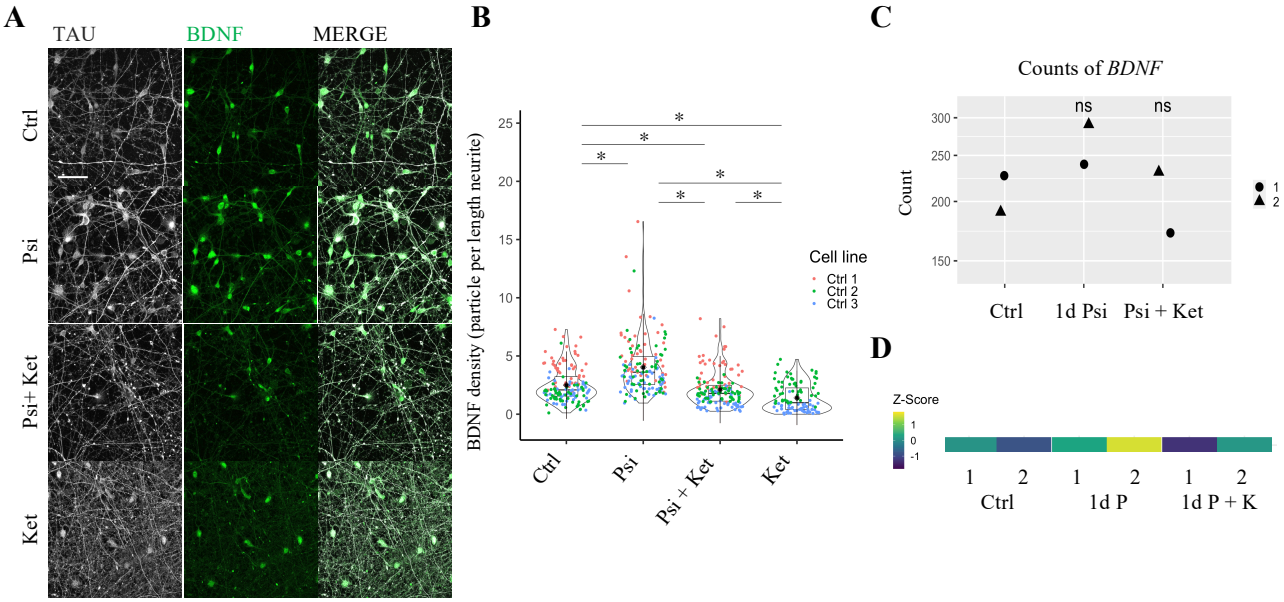

Figure 25. Psilocin induced increase in BDNF level was 5-HT2A-R-mediated.
(A) Representative image 24 hrs after the simultaneous treatment with ketanserin and psilocin (Psi + Ket) and single treatment with ketanserin (Ket), compared to a control condition (Ctrl) and 24 hrs after psilocin treatment (Psi), scale bar: 50 µm. **(B)** Ketanserin co-treatment and ketanserin monotreatment significantly reduced BDNF density compared to the 24 hrs monotreatment psilocin condition suggesting a 5-HT2A-mediated process. Ketanserin monotreatment provoked a significant reduction in in BDNF density compared to ketanserin co-treatment with psilocin. Three Ctrl cell lines were included in the analysis, each with one biological batch (Ctrl with $N = 144$ neurites; Psi with $N = 147$ neurites; Psi + Ket with $N = 147$ neurites; Ket with $N = 102$ neurites). For analysis Kruskal-Wallis test for independent samples was calculated. Post hoc Wilcoxon rank sum test. Bonferroni-correction, adjusted $p < .05$, mean ± *SD*. Significance levels against the respective control and for multiple group comparisons are $*p < 0.05$. **(C)** TPM scaled and **(D)** heat map (z-scaled) RNA bulk seq, performed in biological duplicates showed a non-significant increase in *BDNF* gene expression one day after psilocin administration (1d P), prevented by ketanserin co-treatment (1d P & K). Significance levels against the respective control $*p < 0.05$. Heat map (z-scaled) illustration of RNA bulk seq data was generated by Dr. Anne Hoffrichter.

4.7 BDNF base level differences in BD and AUD patient-derived cortical neurons and influence of psilocin treatment

BDNF serum and/ or plasma levels have been described to be reduced in psychiatric disorder patients, like BD, MDD, suicide victims and in alcohol dependence[328–334] (please refer to subchapter **1.6.2**). To test whether BDNF levels are decreased in neurons derived from patients diagnosed with BD and AUD, iPSCs of a subset of male, lithium-responsive BD patients with a strong family history of BD and a subset of iPSCs of male patients suffering from AUD were differentiated in into cortical neurons. For BD 1 three cell lines and for BD 2 one cell line were included in the analysis. For AUD two cell lines were included. BDNF base level density (particle per µm) of BD 1, BD 2 and AUD patients was investigated by ICC and compared to healthy controls (here four cell lines were included). Interestingly, BDNF density of BD 1 (M_{BD1} = 1.75, *SD* = 1.28) and BD 2 patients (M_{BD2} = 2.89, *SD* = 1.35) was significantly increased compared to healthy controls (M_{Ctrl} = 1.5, *SD* = 1.16). Notably, BDNF density was significantly decreased in AUD patients (M_{AUD} = 0.39, *SD* = 0.26) compared to healthy controls and BD patients (**Fig. 26A-C**, **Appendix 26A**).

Decreased BDNF levels can be augmented after psychopharmacological treatment, seizures but also due to psychedelics[1,43,222,294,346–353 105,332,338,340–345] (please refer to subchapter **1.6.2)**. An additional question was therefore whether psilocin treatment can increase BDNF levels in BD and AUD patients, like this was the case for the control cell lines (see **Fig. 20A-C**). I included a condition where I compared the 24 hrs post effect of a short-term 10 min psilocin trigger with 24 hrs permanent psilocin administration. I further included a condition where I measured 48 hrs after a short-term trigger with 10 min psilocin. I measured density (particles per µm) and intensity per area based on ICC staining. For both patient groups only BDNF intensity was significantly increased for all treatment conditions tested (BD patients: from M_{Ctrl} = 29.82, *SD* = 14.8 to M_{24hrs} = 43.76, *SD* = 17.64; to $M_{24hrs\ permanent}$ = 59.86, *SD* = 29.37 to M_{48hrs} = 43.54, *SD* = 18.39; AUD patients: from M_{Ctrl} = 19.08, *SD* = 7.43 to M_{24hrs} = 29.55, *SD* = 17.32; $M_{24hrs\ permanent}$ = 31.33, *SD* = 16.93 to M_{48hrs} = 26.45, *SD* = 10.15) (**Fig. 26D-E,** for further information please refer to **Appendix 26B-C).**

4.8 Psilocin targeted the fibrinolytic annexin A2 – S100A10 complex

Interestingly, I found a strong and significant enrichment in differentially expressed genes associated with "negative regulation of coagulation" and "negative regulation of blood coagulation" BP term, one day after psilocin administration (both around factor 5-fold enrichment, $p < 0.05$) in Bulk seq data. Exactly the opposite BP term ("regulation of coagulation" and "regulation of blood coagulation", both around factor 7.5-fold enrichment, $p < 0.05$), came up by ketanserin co-administration suggesting a 5-HT2A-R-mediated effect (**Fig. 27A**). The previous described psilocin mediated effect was true also 3 days after psilocin administration (both around factor 10-fold enrichment, *n.s.*).

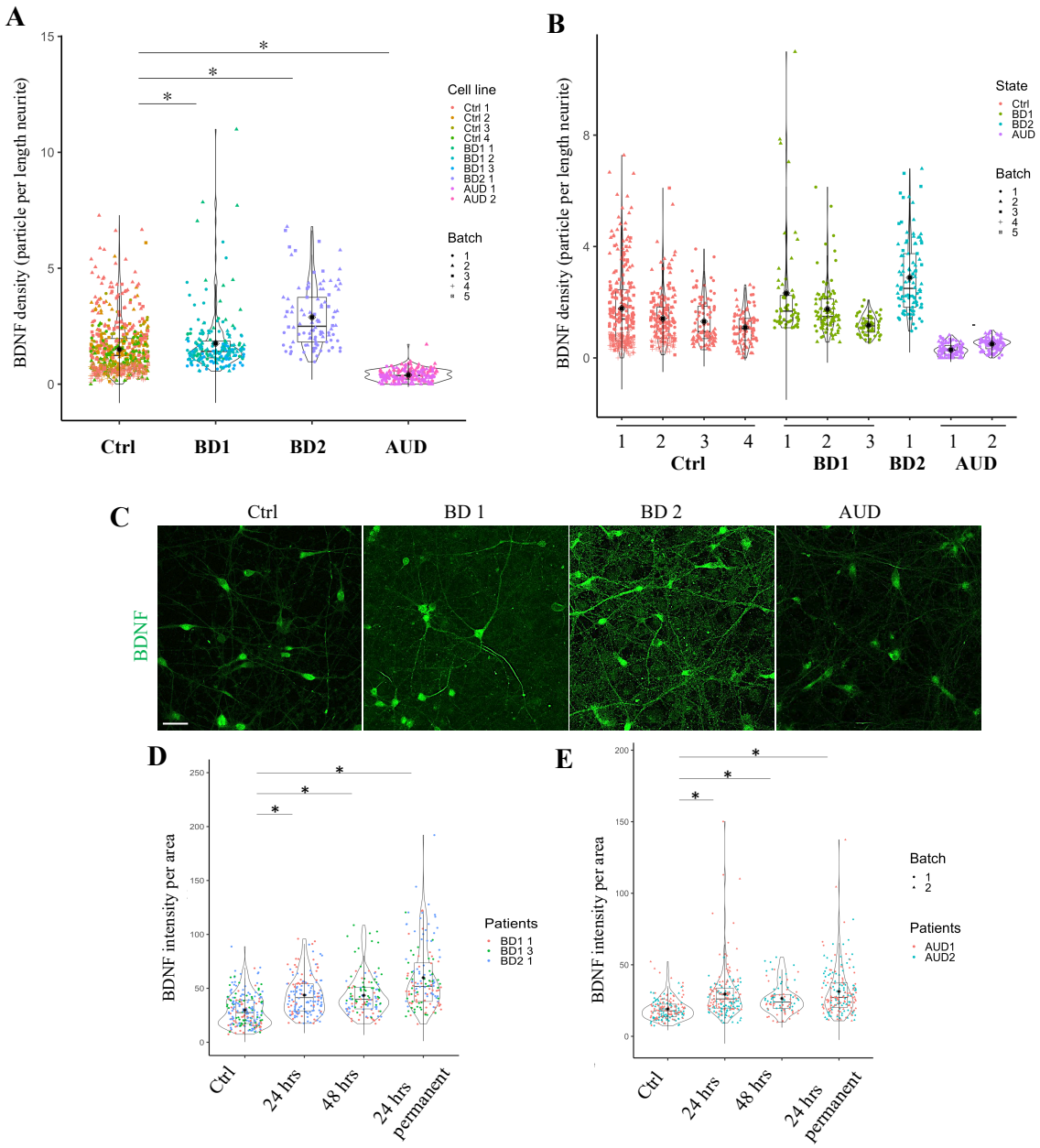

Figure 26. BDNF base level differences and psilocin effect in BD and AUD patients.
(A) Significantly increased BDNF density in BD 1 and BD 2 patients. AUD patients show a significantly reduced BDNF density compared to healthy controls. Ctrl with $N = 613$ neurites; BD 1, $N = 203$ neurites, BD 2 with $N = 100$ neurites, AUD with $N = 180$ neurites. **(B)** Four Ctrl cell lines were included (Ctrl 1 with $N = 249$ neurites and five biological batches; Ctrl 2 with $N = 181$ neurites and 4 biological batches; Ctrl 3 with $N = 93$ neurites with two biological batches and Ctrl 4 with $N = 90$ neurites with two biological batches). Three BD cell lines were included in the analysis (BD1 1 with $N = 57$ neurites and two biological batches. BD1 2 $N = 90$ neurites and two biological batches. BD1 3 with $N = 56$ neurites with and one biological batch. BD2 1: $N = 100$ neurites with three biological batches. For analysis two AUD cell line were included (AUD 1 with $N = 90$ neurites and 2 biological batches. AUD 2 with $N = 90$ neurites and two biological batches. **(C)** Representative BDNF staining for Ctrls, BD 1, BD 2 and AUDs, scale bar: 50 µm **(D)** BDNF intensity per area was significantly increased 24 and 48 hrs after a 10 min psilocin trigger (24 hrs; 48 hrs) and after 24 hours permanent psilocin administration (24 hrs permanent) in neurons derived from BD patients. Three BD cell lines were included in the analysis (Ctrl with $N = 213$ neurites; 24 hrs with $N = 155$ neurites; 48 hrs with $N = 128$ neurites; 24 hrs permanent with $N = 150$ neurites). **(E)** BDNF intensity per area was significantly increased 24 and 48 hrs after a 10 min psilocin trigger and after 24 hrs permanent psilocin administration in neurons derived from AUD patients. For analysis two AUD cell lines were included. Neurites counted: Ctrl with $N = 180$ neurites; 24 hrs with $N = 180$ neurites; 48 hrs with $N = 90$ neurites and 24 hrs permanent with $N = 180$ neurites. For all statistical analysis Kruskal-Wallis test for independent samples was calculated. Bonferroni-correction, adjusted $p < .05$, mean ± *SD*. Significance levels against the respective control are $*p < 0.05$.

Further, “plasminogen activation” and “fibrinolysis” were the first and third BPs that came up (both factors around 30-fold enrichment, *n.s.*) three days after psilocin administration (**Fig. 27B**). Additionally, a non-significant 5-fold enrichment in differentially expressed genes associated with the “complement and coagulation cascade” KEGG term 24 hrs after psilocin administration was found (**Fig. 27C**).

Taken together those results indicate that genes were differentially expressed that were involved in fibrinolysis, a process that prevents blot clot formation in the body during blood coagulation. Essential for this process is the formation of the annexin A2 – S100A10 heterotetrameric complex (please refer to subchapter **1.7**).

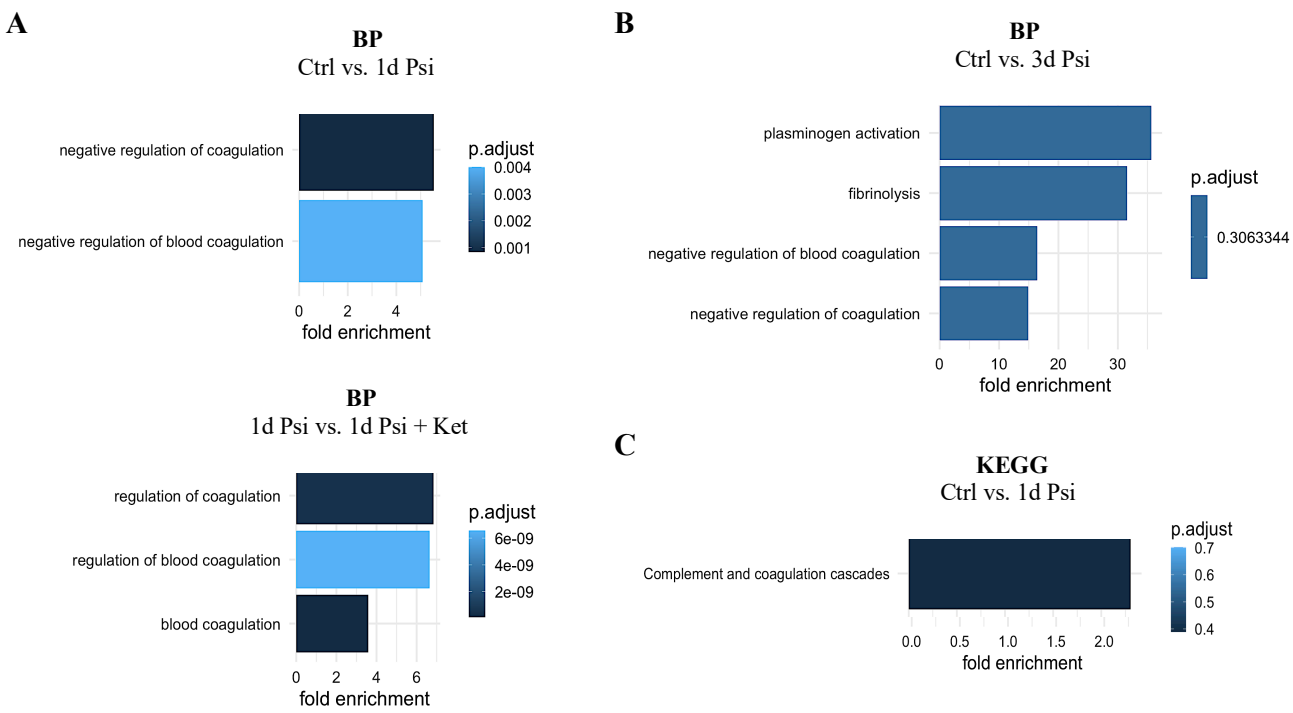

Figure 27. Psilocin induced enrichment of pathways associated with fibrinolysis.
(A) Enrichment in differentially expressed genes associated with “negative regulation of coagulation” and “negative regulation of blood coagulation“ BP term, prevented by ketanserin co-administration, 1 day after psilocin administration **(B)** 3 days after psilocin administration enrichment in differentially expressed genes associated with “negative regulation of coagulation” and “negative regulation of blood coagulation“ BP term. Further enrichment in differentially expressed genes associated with “fibrinolysis“ and “plasminogen activation“ BP term **C)** Enrichment in differentially expressed genes associated with “complement and coagulation cascades“ KEGG term. Significance levels against the respective control *$p < 0.05$. BP, biological process; KEGG, Kyoto Encyclopedia of Genes and Genomes. Illustration of RNA bulk seq GO data was generated by Dr. Anne Hoffrichter.

4.8.1 Psilocin-induced expression of a gene set involved in plasmin generation

A deeper lock on differentially expressed genes associated with the fibrinolytic GO term (**Fig. 28A-C**) revealed that 24 hrs after dosing for 10 min with 10 µM psilocin the *ANXA2* gene that codes for the annexin A2 protein and the *S100A10* gene that codes for the S100A10 protein (also known as p11) were significantly upregulated. *ANXA2* was up-regulated by the factor 1.5 and *S100A10* by the factor 1.9 (log2 fold change). Ketanserin co-treatment prevented the *ANXA2* and *S100A10* gene expression increase non-significantly. Still 3 days after psilocin administration there was a non-significant increase in both genes (data not shown).

Moreover, after psilocin treatment the enzymes that cleave plasminogen into plasmin, like uPA, coded by the *PLAU* gene (factor 2, log2 fold change) and tPA, coded by the *PLAT* gene (factor 0.9, log2 fold change) were significantly upregulated 1 day after psilocin administration. uPA was even significantly increased 3 days after psilocin stimulation (factor 1.3, log2 fold change, data not shown). Besides, the uPA receptor (*PLAUR* gene) was significantly increased (factor 1.4, log2 fold change) 1 day after psilocin administration. Again, ketanserin prevented increase in gene expression of the *PLAU*, the *PLAUR* and the *PLAT* gene. The most important binding partner of the annexin A2 – S100A10 complex in the brain Ahnak, coded by the *AHNAK* gene (factor 0.8, log2 fold change) and the plasminogen receptor, coded by the *PLGRKT* gene (factor 0.9, log2 fold change) were significantly increased 1 day after psilocin administration. This effect could be non-significantly reversed by the simultaneous treatment with ketanserin. Simultaneously, *F5* a gene that code for the coagulation factor 5 protein, an important protein involved in the coagulation process, was significantly downregulation after psilocin administration (factor -1, log2 fold change).

Further, some major inhibitors of plasmin generation were significantly differentially expressed 1 day after psilocin administration such as the plasminogen activator inhibitor (PAI)-1, encoded by the *SERPINE1* gene, that mainly inhibits tPA and uPA activity. An isoform with the same function is PAI-2, encoded by the *SERPINE2* gene that was significantly downregulated. Psilocin administration significantly decreased *SERPINF2* gene expression, that codes for alpha-2-antiplasmin that inhibits plasmin activity, suggesting to a reduced inhibition of plasmin activity. *ADAMTSL3* and *ADAMTS16* are genes that code for MMPs that are also involved in the fibrinolytic process and are described to be activated by plasmin, were significant differentially expressed 1 day after psilocin administration. Additional *ANXA* genes (such as *ANXA1*, *ANXA3*, *ANXA5*) and *S100* genes (such as *S100A2*, *S100A3*, *S100A4*, *S100A6*, *S100A11*, *S100A16*, *S100B*), coding for other isoform genes were significantly increased 1 day after psilocin administration. Particularly the so far not well described *ANXA3* gene was significantly increased 24 hrs and 3 days after psilocin treatment (24 hrs factor 2.3, log2 fold change; 3 days factor 1.6, log2 fold change). Ketanserin prevented increased its gene expression (**Fig. 28D**).

This thesis therefore first postulates that psilocin fast and directly targets the fibrinolytic annexin A2 – S100A10 complex and associated, as major gene protagonists of this plasmin generating complex are differentially expressed

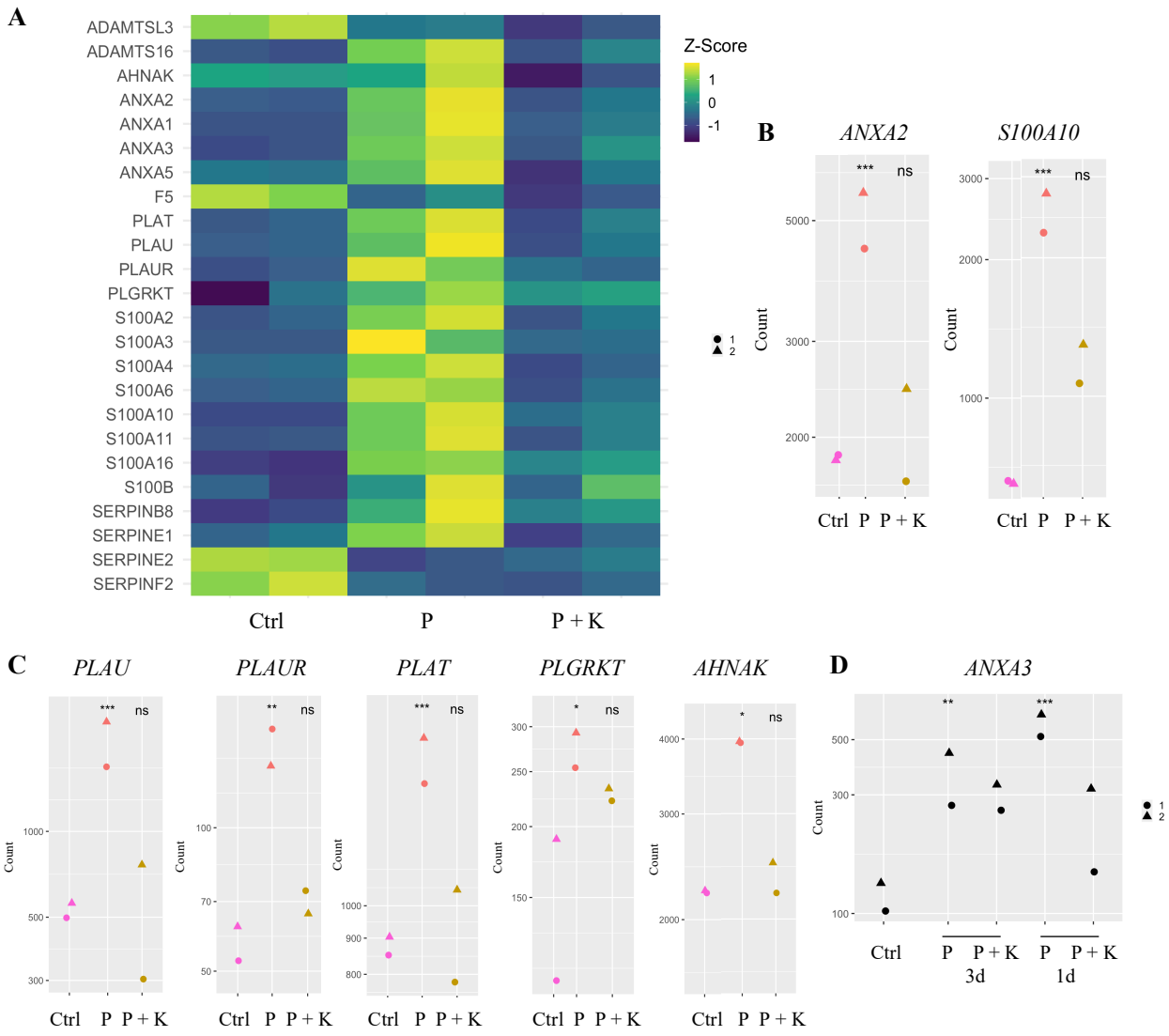

Figure 28. Upregulation of genes of the annexin A2 – S100A10 complex and associates by psilocin

(A) Heat map (z-scaled) and **(B-C)** TPM scaled RNAseq data, performed in biological duplicates of untreated condition (Ctrl), one day after 10 min psilocin administration (P) and psilocin co-treatment with ketanserin (P + K) revealed a significant increase of genes involved in plasmin generation such as the **(B)** *ANXA2, S100A10,* **(C)** *PLAU, PLAUR*, *PLAT, PLGRKT* and *AHNAK* gene, prevented by co-treatment with ketanserin. **(D)** *ANXA3* gene is significantly upregulated 1 day and still 3 days (3D) after psilocin administration. Significance levels against the respective control $*p < 0.05$, $**p < 0.01$, $***p < 0.001$. Heat map (z-scaled) illustration of RNA bulk seq data were generated by Dr. Anne Hoffrichter.

4.8.2 Psilocin increased annexin A2 and p11 protein level and complex formation

To elucidate whether not only the gene expression but also the protein levels of annexin A2 and p11 were increased I next stained for their expression by using ICC. Annexin A2 and p11 were expressed and co-localized, efficiently visible in high resolution with confocal and STED microscopy (**Fig. 29A-B**). I further investigated p11 density (particle per µm) and intensity and intracellular p11 and annexin

A2 co-localization using ICC, as the complex is built up intracellularly and is than shuttled to the surface. P11 intensity (from $M_{Ctrl} = 21.6$, $SD = 6.6$ to $M_{72hrs} = 25.85$, $SD = 9.25$, $p < 0.05$) and density (from $M_{Ctrl} = 0.4$, $SD = 0.24$ to $M_{72hrs} = 0.48$, $SD = 0.31$, $p < 0.05$) increased significantly three days after psilocin administration (**Fig. 29C, Appendix 29**). Annexin A2 and p11 co-localization (from $M_{Ctrl} = 0.11$, $SD = 0.09$ to $M_{72hrs} = 0.15$, $SD = 0.12$) non-significantly increased (**Fig. 29D-E, Appendix 29**).

In line with that, annexin A2 and p11 protein level measured with WB increased three days after psilocin administration that was reversed for annexin A2 by ketanserin co-treatment, suggesting a 5-HT2A-R involvement Annexin A2 (Annexin A2: $M_{Ctrl} = 1.14$, $SD = 0{,}38$ to $M_{Psi} = 1.63$, $SD = 0.51$ to $M_{Psi+Ket} = 1.55$, $SD = 0.65$; p11 from $M_{Ctrl} = 1.53$, $SD = 0{,}7$ to $M_{Psi} = 2{,}16$, $SD = 0{,}95$ to $M_{Psi+Ket} = 2{,}78$, $SD = 1{,}88$) (**Fig. 29F-G, Appendix 29**).

Notably, not only gene expression of the two major genes that built up the annexin A2 – S100A10 complex was increased. The increase in gene expression was also reflected by an increase on the protein level for p11 and annexin A2 and their A2 co-localization.

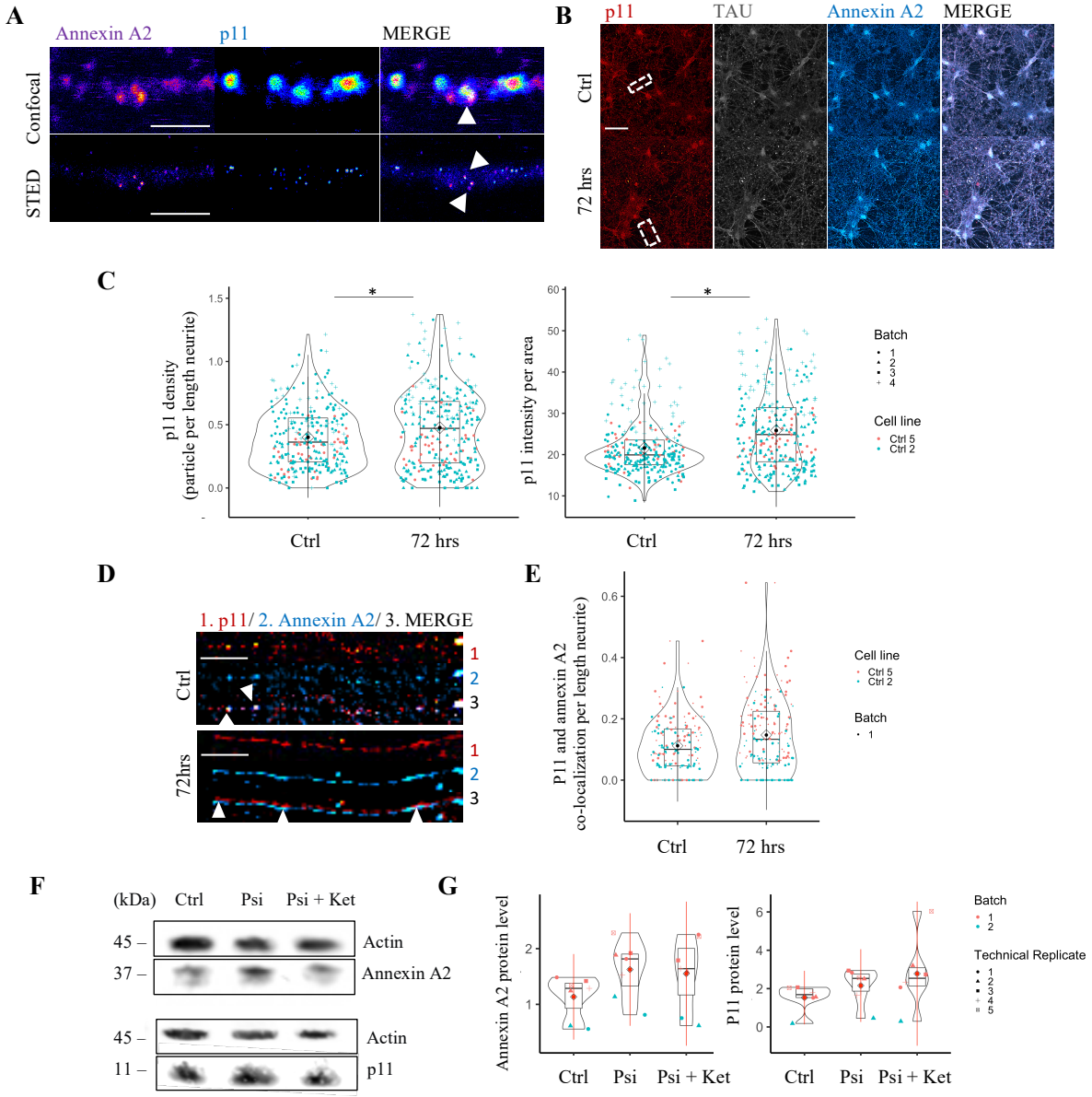

Figure 29. Psilocin induced upregulation of core proteins of the annexin A2 – S100A10 complex. **(A)** Confocal and STED microscope image showed close proximity of annexin A2 and p11(white arrows), scale bar: 2 μm. **(B)** Representative confocal image of control condition (Ctrl) and 72 hrs psilocin (72 hrs) administration, scale bar: 50 μM, **(C)** P11 density and p11 intensity per area were significantly increased 72 hrs after a after a 10 min psilocin trigger compared to an untreated control condition. Ctrl with N = 270 neurites; 72 hrs with N = 270 neurites. Two Ctrl cell lines were included in the analysis. **(D)** Close up of **(B)** showed an increase in annexin A2 and p11 co-localization (white arrows) for the 72 hrs psilocin condition, scale bar: 10 μm. **(E)** Annexin A2 – p11 co-localization increased three days after 10 min psilocin administration. Ctrl with N = 90 neurites; 72 hrs with N = 90 neurites. Two Ctrl cell lines were included in the analysis. **(F)** Representative WB for annexin A2 and p11 protein level 72 hrs after psilocin administration (Psi) and co-treatment with ketanserin (Psi + Ket). **(G)** Annexin A2 and p11 protein level was increased three days after 10 min psilocin administration prevented by ketanserin co-treatment only for annexin A2, suggesting a 5-HT2A-R involvement. One Ctrl cell line was included with two biological batches. Ctrl with N = 6 -7 data points; Psi with 6 - 7 data points; Psi + Ket with 6 - 7 data points. For all analyses Mann-Whitney-U test, respectively Kruskal-Wallis test (> 2 groups) for independent samples was calculated. Post hoc Wilcoxon rank sum test. Bonferroni-correction, adjusted $*p < .05$, mean ± SD.

4.9 Psilocin induced increase in p11-BDNF and p11-pro-BDNF co-localization

BDNF and p11 are associated with depression and their augmentation is associated with antidepressant response. Further both proteins seem to regulate each other's function (please refer to subchapter **1.6.2** and **1.7.1**).

In order to find out whether neurons that do express p11 also co-express BDNF I analyzed exploratively co-localization of pro-BDNF or BDNF with p11 before and after psilocin administration by using ICC. In first experiments I can confirm that psilocin provoked a significant increase not only in BDNF and p11 co-localization (from M_{Ctrl} = 0.23, SD = 0.12 to M_{72hrs} = 0.39, SD = 0.15) 3 days after psilocin administration (**Fig. 30A-C, Appendix 30A**) but also in pro-BDNF and p11 co-localization (from M_{Ctrl} = 0.1, SD = 0.09 to M_{48hrs} = 0.19, SD = 0.11) 2 days after psilocin administration (**Fig. 30D-E, Appendix 30B**).

Pro-BDNF density (particle per µm) significantly increased 2 days after psilocin administration (from M_{Ctrl} = 0.2, SD = 0.13 to M_{48hrs} = 0.3, SD = 0.15), same is true for intensity (from M_{Ctrl} = 11.4, SD = 4.92 to M_{48hrs} = 15.53, SD = 6.65) (**Fig. 30D-E, Appendix 30B**). 48 hrs after psilocin administration nuclear localization of pro-BDNF became visible (**Fig. 30F**). Also, endogenous pro-BDNF protein level increased 24 hrs after psilocin administration (**Fig. 30G**).

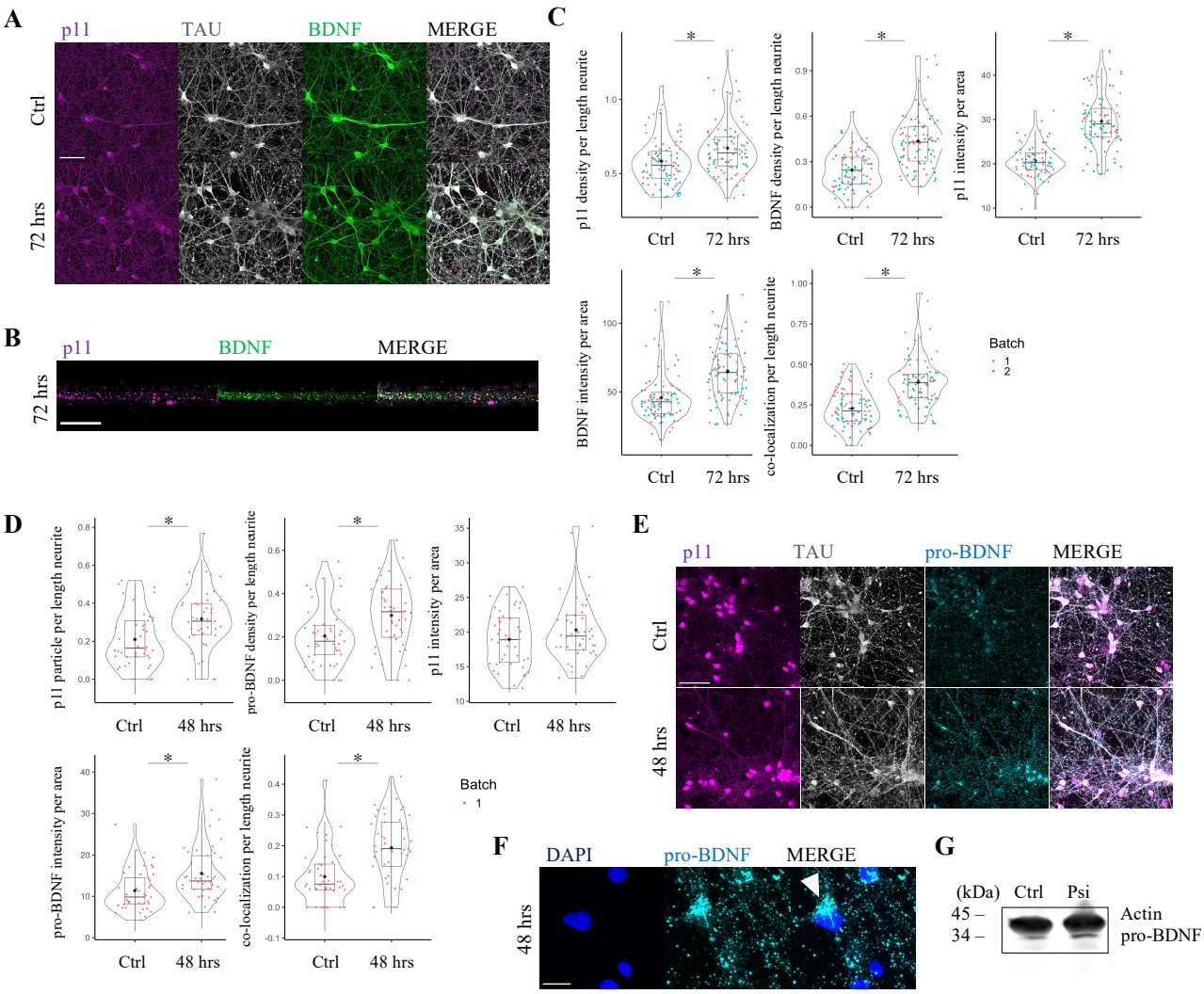

Figure 30. Psilocin induced increase in p11, BDNF and pro-BDNF and their co-localization.
(A) Representative image of a neuronal network for pre-treatment condition (Ctrl) and 72 hrs after a 10 min short psilocin trigger (72 hrs) for p11 and BDNF, scale bar: 50 µm. **(B)** STED microscopy image showed p11 and BDNF co-localization in high resolution, scale bar: 2.5 µm. **(C)** p11 and BDNF density and intensity per area as well as co-localized particle per length neurite were significantly increased 72 hrs after a 10 min 10 µM psilocin trigger compared to an untreated control condition. One Ctrl cell line with one biological batch replication was included in the analysis: Ctrl with $N = 90$ neurites; 72 hrs with $N = 90$ neurites. **(D)** p11 and pro-BDNF density and pro-BDNF intensity per area, as well as pro-BDNF and p11 co-localized particle were significantly increased 48 hrs after a after a 10 min 10 µM psilocin trigger (48 hrs) compared to an untreated control condition (Ctrl). One Ctrl cell line was included in the analysis: Ctrl with $N = 45$ neurites; 48 hrs with $N = 45$ neurites. **(E)** Representative image of a neuronal network for pre-treatment condition (Ctrl) and 48 hrs after a 10 min short psilocin trigger (48 hrs) for p11 and pro-BDNF. **(F)** Representative image 48 hrs after a 10 min short psilocin trigger reveals nuclear localization (arrow) for pro-BDNF, scale bar: 10 µm. **(G)** Endogenous pro-BDNF increased 24 hrs after psilocin (Psi) administration. For all analysis Kruskal-Wallis test for independent samples was calculated. Bonferroni-correction, adjusted $p < .05$, mean ± *SD*.

4.10 Psilocin fosters plasmin-mediated cleavage of pro-BDNF into m-BDNF

Plasmin, generated by the annexin A2 – S100A10 complex, mediates the cleavage of pro-BDNF into m-BDNF in the brain[291]. It is hypothesized that an imbalance or insufficient cleavage of m-BDNF-to-pro-BDNF transformation (higher pro-BDNF and lower m-BDNF levels) is involved in the etiology of psychiatric diseases[389,393,414–419] (please refer to subchapter **1.7.1**). An upregulation of genes and proteins of the annexin A2 – S100A10 complex and its assembly, like I found (see **Fig. 28-29**), is a necessary but not a sufficient requirement for the functionality of the complex. A proper functionality would be given if endogenous plasmin is generated by the complex and pro-BDNF is cleaved into m-BDNF by plasmin. In order to investigate this cleavage, I used an artificial system with a well-defined amount of recombinant pro-BDNF. The decision to work with artificial pro-BDNF was based on the fact that endogenous BDNF was repetitively under the detection limit in WB (only visible after psilocin or plasminogen treatment, see **Fig. 20D**). For WB I utilized an antibody that recognizes both, the pro-BDNF and the m-BDNF form. The ratio of the m-BDNF-to-pro-BDNF protein level was calculated as an indirect measurement of endogenous plasmin efficacy in our cells. Considering the previous shown data, I hypothesized that this cleavage is increased after psilocin treatment. Based on a higher number of complexes and plasminogen-into-plasmin cleaving enzymes after psilocin treatment (see **Fig. 28-29**) I expected an increase in endogenous plasmin generation, reflected by an increased cleavage of pro-BDNF in m-BDNF in the psilocin condition. Thus, cells of a control condition and cells treated for three days with psilocin were exposed to human recombinant pro-BDNF and plasminogen as RNA bulk seq data revealed that this precursor of plasmin and substrate of the annexin A2 – S100A10 complex, was expressed only at a low level in cortical neurons (**Fig. 31A**).

And in fact, as expected, there was increased cleavage of artificial pro-BDNF in m-BDNF in the psilocin condition (**Fig. 31B-C, Appendix 31**). That was visualizable by a non-significant decrease of artificial pro-BDNF level (from $M_{Ctrl} = 0.77$, $SD = 0.6$ to $M_{72hrs} = 0.49$, $SD = 0.38$) and an increase of cleaved m-BDNF (from $M_{Ctrl} = 1.38$, $SD = 0.68$ to $M_{72hrs} = 1.72$, $SD = 0.85$) in the psilocin condition. Therefore, the m-BDNF-to-pro-BDNF ratio increased (from $M_{Ctrl} = 5.13$, $SD = 6.12$ to $M_{72hrs} = 6.56$, $SD = 5.58$). Also, the BDNF dimer protein level increased non-significantly upon psilocin administration (from $M_{Ctrl} = 0.88$, $SD = 0.45$ to $M_{72hrs} = 1.05$, $SD = 0.3$).

I technically validated the former experiment by labelling Alexa Fluor-680 to recombinant human pro-BDNF to eliminate the influence of endogenous pro-BDNF and m-BDNF levels by detecting only Alexa Fluor 680^+ recombinant BDNF. Interestingly, I found again a non-significant decrease for the recombinant pro-BDNF-Alexa-680 labelled protein level 3 days after psilocin administration in plasminogen pretreated cells in three biological replicates of one cell line (from $M_{Ctrl} = 5.28$, $SD = 0.08$ to $M_{Psi} = 3.46$, $SD = 0.82$, **Fig. 31D, Appendix 31**). Confirmed also by an experiment where I used TCB-2 as a potent 5-HT2A-R agonist in plasminogen pretreated cells (from $M_{Ctrl} = 8.62$, $SD = 4.29$ to $M_{TCB-2} = 3.47$) (**Fig. 31E, Appendix 31**).

The detection of cleaved recombinant m-BDNF-Alexa-680 was only possible after adding plasminogen in a first experiment, confirming that this substrate is not expressed in cortical neurons but is needed for the enzymatical reaction. The level of cleaved recombinant m-BDNF-Alexa-680 was increased in psilocin pretreated cells (**Fig. 31F**), replicated also for 5-HT2A receptor agonist TCB-2 in a first experiment (**Fig. 31G**), in optimized incubation conditions.

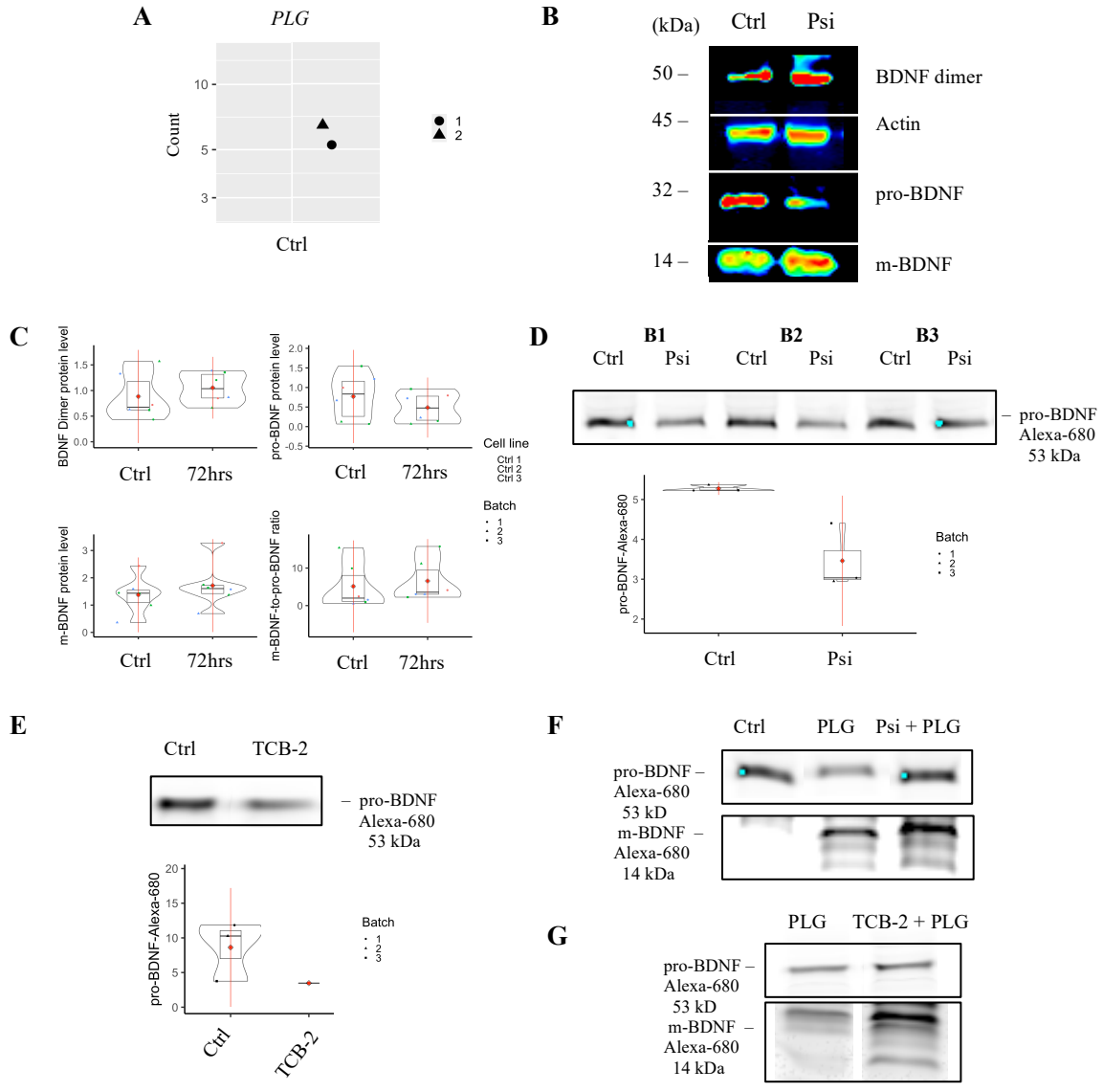

Figure 31. Psilocin increased plasmin-mediated cleavage of pro-BDNF into m-BDNF.
(A) TPM scaled RNA seq data of *PLG* gene, coding for PLG, the precursor of plasmin, is expressed only at low levels in cortical neurons. **(B)** Representative WB: increased cleavage of recombinant pro-BDNF into m-BDNF after addition of plasminogen in the psilocin treatment condition. Decrease of pro-BDNF level and increase level of cleaved m-BDNF and m-BDNF-to-pro-BDNF-ratio in the psilocin condition. BDNF dimer protein level increased. **(C)** Three Ctrl cell lines were included (Ctrl 1 with one biological batch; Ctrl 2 with three biological batches and Ctrl 3 with 3 biological batches). Ctrl with $N = 6$ data points; 72 hrs with 6 data points; Psi + Ket with 6 data points. Kruskal-Wallis test for independent samples was calculated. Post hoc Wilcoxon rank sum test. Bonferroni-correction, adjusted $p < .05$, mean ± SD. Significance levels against the respective control are $*p < 0.05$. **(D)** Representative WB: increased pro-BDNF-Alexa-680 cleavage 3 days after permanent psilocin

administration (in combination with PLG treatment) compared to a Ctrl condition. One Ctrl cell line was included (Ctrl 3 with three biological batches). Kruskal-Wallis test for independent samples was calculated. Post hoc Wilcoxon rank sum test. Bonferroni-correction, adjusted $p < .05$, mean ± SD. Significance levels against the respective control are $*p < 0.05$. **(E)** Representative WB: increased cleavage of recombinant pro-BDNF labelled to Alexa-680 3 days after permanent TCB-2 (5-HT2A-R agonist) administration (and PLG treatment). One Ctrl cell line was included for the TCB-2 conditions (Ctrl 3 with one biological batch), no statistics were calculated. **(F)** Cleavage of recombinant pro-BDNF labelled to Alexa-680 by endogenous plasmin into recombinant m-BDNF labelled to Alexa-680 occurred only after plasminogen treatment and increased for 3 days psilocin pretreated cells, **(G)** confirmed for TCB-2 pretreated cells. PLG, plasminogen.

Taken together, this data highlights that psilocin treatment leads to an increased number of annexin A2 – S100A10 complexes due to an augmentation of the complex components p11 and annexin A2 in human cortical neurons. As a result, the number of docking stations for plasminogen, the precursor of plasmin, were elevated. Moreover, the endogenous gene expression of plasminogen-cleaving enzymes like tPA and uPA were upregulated after psilocin administration. As a result, I first describe an elevated cleavage of pro-BDNF into m-BDNF after psilocin administration in human cortical neurons *in vitro*.

5 Discussion

The psychoplastogen[1] psilocybin develops as drug in the treatment of psychiatric disorders[2,120,254]. Especially in TRD and addiction psilocybin shows remarkable potential[2,45,120,143,144,146,148–153,155,156,254]. "*Brain network resetting*"[2] by restoration of neuronal and synaptic dysfunctions[1,181–188] and of reduced levels of neurotrophins[300,327–338] and IEGs[189–191](discussed to be associated with mental disorder pathophysiology) seems to be triggered by psychedelic administration. Remodeling of the neuronal architecture might be realized as a follow up of many neuroplastic events which modulate neuronal signaling and transmission. Prior to this study our knowledge about the molecular and cellular effects of psilocybin came mainly from animal studies and predictions of fMRI data.

In this doctoral thesis iPSC-derived human cortical neurons were employed for the first time to address the questions whether this model system is suitable to model the molecular mechanisms of psilocin as active metabolite of psilocybin. A second aim was the question whether insights, already known from animal studies can be translated to a human system. A superior question was also to get additional understandings about the potential therapeutic mechanism (e.g., antidepressant mode of action) of psilocybin behind. In the following, I will discuss that psilocin fosters neuroplasticity in iPSC-derived human cortical neurons (illustrated in **Fig. 32**) by modulating 5-HT2A-R presentation, by promoting structural and functional modifications (e.g., IEG and BDNF level augmentation) and by addressing the annexin A2 – S100A10 complex and I will mention potential implications of my research findings.

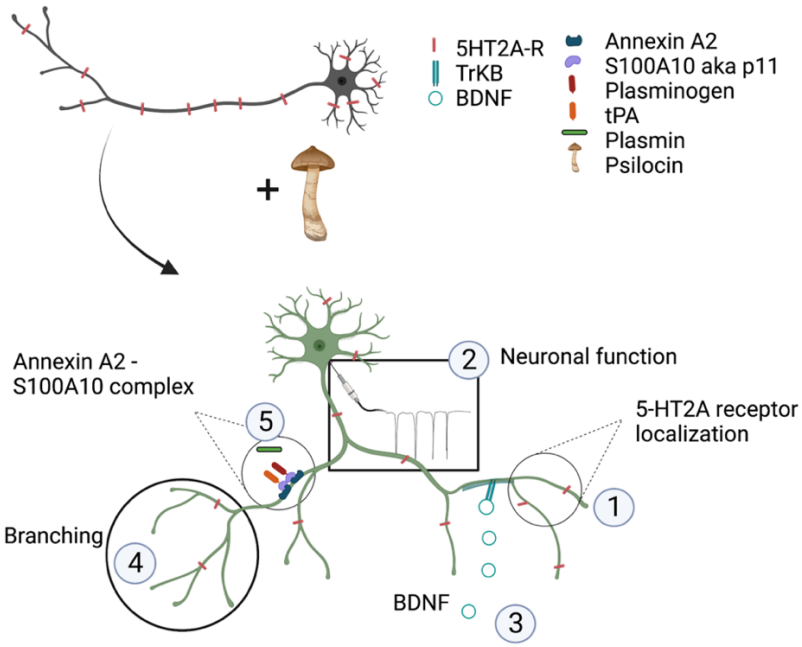

Figure 32. Psilocin modulates neuronal plasticity in iPSC-derived human cortical neurons.
Psilocin leads to structural and functional alterations that starts fast after administration and manifest over time. I observed modification in **1.** 5-HT2A receptor localization; **2.** neuronal function; **3.** BDNF levels; **4.** neurite branching and **5.** an upregulation of the annexin A2 – S100A10 complex. Graphic illustration generated with *Biorender.com.*

5.1 Prologue

I used a standardized differentiation protocol that leads to generation of functional and mature neurons of dorsal forebrain identity in high purity. The refined patterning of cortical progenitors into neurons with PFC identity[450,451] in order to increase the regional specificity and an accelerated neuronal maturation[452] is a constantly ongoing process in the research field and in our working group.

5.2 Psilocin provokes acute effects on the receptor presentation and a subacute downregulation of the 5-HT2A-R

The 5-HT2A receptor is expressed in iPSC-derived human cortical neurons which was already shown in iPSC-derived human cortical neurons[453]. Expression of the 5-HT2A receptor is an important precondition for the functioning of this model system as 5-HT2A-R activation plays a principal role in serotonergic psychedelic-mediated behavioral and cellular response[43,47,75,158,159,218,235–239].

I found clear evidence that psilocin leads to a subacute downregulation of the 5-HT2A-R already after 24 hrs in human cortical neurons. Serotonergic receptors use many different processes such as internalization, downregulation and recycling to self-regulate their system (please refer to subchapter **1.6.1**). Interestingly, LSD and psilocybin have been already shown to reduce 5-HT2A-R density in animal models[276,454,455]. Exemplarily, downregulation after chronic and acute administration with agonists, leading to a reduced receptor density on the surface, prevents overstimulation of the system and also explains that psychedelics are not addictive[53,232,269–271]. It has been shown that 5-HT2A-Rs are upregulated in inflammation and depression. For example, 5-HT2A-R abundance is increased in post mortem human brain tissue of suicide victim[372,456,457]. Research suggests that downregulation might contribute here to the therapeutical action of antidepressant drugs[271–276,280]. As I did not investigate how long this downregulation stays present further experiments should include prolonged time points after psilocin administration to focus on potential recovery mechanisms by receptor recycling-dependent or independent mechanisms.

To date, it is still unclear what happens to the 5-HT2A-R after acute psilocin administration. One obvious prediction is that the 5-HT2A-R internalizes after agonist binding. Internalization is a mechanism involved in the downregulation process[272,277] and has already been described to occur after binding of other serotonergic agonists and antagonists *in vivo* and *in vitro*[265,272,277–280]. For example, Bhattacharyya and colleagues described that dopamine as a partial agonist of the 5-HT2A-R induces, such as 5-HT, receptor internalization in human embryonic kidney (HEK) 293 cells[265]. I found evidence that psilocin stimulation decreased axonal extracellular 5-HT2A-R presentation already after 10 min. But whether this axonal decrease is a sign for receptor internalization has to be clarified. One doubting point comes from absent co-localization of the receptor with early endosome markers after the expected psilocin induced internalization. The early endosome is the first endocytic compartment for the incoming cargo[458]. It functions as a sorting station where the destination of the cargo will be determined.

Internalized receptors (such as the 5-HT2A-R[281]) appear in the early endosome already within min. Well characterized proteins of the early endosome are the RAB proteins and its effector the EEA1 protein, responsible for vesicle tethering, fusion, receiving cargo and vesicle budding[459–470]. But surprisingly there was not an increased co-localization of the receptor with early endosome markers, RAB5A and EEA1, although I analyzed different time points after acute psilocin administration (data not shown). Therefore, gapless evidence for an internalization process is still missing. Agonist induced 5-HT2A internalization is described to occur very fast within 2 min and is completed after 10 min post agonist treatment[277]. But receptor internalization and the velocity of this process after ligand binding seems to be functional selective for different agonists dependent on concentrations and affinities for the receptor and also in competition to other ligands[232]. Bhattacharyya and colleagues already showed that if both, 5-HT and dopamine, are present at the same time but with a higher concentration of dopamine to induce dopamine-specific internalization, internalization occurs much fast than described for monotreatment of one of the two drugs[265,277]. I also might have missed the right time point for the co-localization experiments. Further research should focus on the stability of the binding of psilocin to the receptor. A subsequent question would be whether psilocin is internalized together with the receptor, if internalization occurs.

Another explanation for the rapid decrease in axonal receptor density after psilocin administration might be due to a change of the surface receptor distribution. One potential explanation for that could be the formation of receptor multimers. 5-HT2 receptors can form homodimers with themselves or heterodimers with other serotonergic receptors *in vitro*[283,284]. But also, heteromeric GPCR complex formation is well-described, for example with mGluR2 [285,286]. Heteromeric complex formation of the 5-HT2A-R with mGluR2 is even involved in hallucinogenic induced neuropsychological responses and psychosis-like effects, induced by hallucinogenic 5-HT2A-R agonists in mice[286]. This receptor in on its own already associated with psychedelic induced response[221]. For example, mGluR2 receptor downregulation is restored after psilocybin administration in a rat model for addiction[188]. Undoubtedly, the mGluR2 receptor is an extremely interesting key candidate. Although I did not find the *GRM2* genes to be differentially regulated upon psilocin administration (data not shown), it might worth it to look for time-dependent structural modifications after psilocin administration. For example, it would be interesting to focus on mGluR2 receptor density and its potential role in 5-HT2A-R density reduction (due to a potential heteromeric complex formation). Future research should include microscopy techniques with higher resolution to identify for example an increase in complex formation after psilocin administration.

I further found evidence that retrograde receptor movement is induced by acute psilocin stimulation. Life cell imaging clearly demonstrates a retrograde movement of an artificial fluorescence-tagged 5-HT2A-R from the neurites to the soma. For follow-up experiments live cell imaging should include neuronal structure markers to differentiate between axonal and dendritic compartments for specifying the compartment origin of movement.

Conclusively, evidence that downregulation and acute decrease in axonal receptor density are associated with (or even essential for) the therapeutical action of the drug is missing. In the following discussion I will figure out that many proteins and signal cascades that are activated by psilocin are associated with neuroplasticity. Some of the described effects do not occur if the 5-HT2A-R is inhibited. If the therapeutical effect of the drug is based on (or at least mediated) by those neuroplastic events (a theory still under debate but in consideration of the literature widely accepted) I conclude that it is likely, that a 5-HT2A-R activation is involved. For example, I found STAT3 to be significantly upregulated one day after psilocin administration (data not shown). STAT3 is part of the JAK/STAT 5-HT2A downstream signaling pathway which is described to be activated after hallucinogenic 5-HT2A-R agonist administration[230,246] and 5-HT2A-R desensitization[471]. But whether the downregulation and an acute decrease in axonal receptor density (I on purpose avoid the terminus "internalization" because it is hypothesized but still under investigation) is necessary for those neuroplastic events (and the therapeutic action) or just a compensatory mechanism and effect-independent has to be investigated. Downregulation and acute decrease in axonal receptor density might also be an effect of the concentration of psilocin that I used. Following research should include different psilocin concentrations in order to see whether lower (and more physiological) doses also provoke the same effects.

Most importantly an outstanding experiment will be to inhibit the 5-HT2A-R with the antagonist ketanserin (with or without psilocin co-treatment) and check for downregulation and acute receptor presentation decrease, which it hypothesized to be inhibited. While I found that inhibition of the CME can prevent the acute decrease in receptor surface density (agonist induced internalization occurs via a dynamin-dependent and CME mechanism[281]), I did not test for ketanserin-prevented acute or subacute receptor downregulation. But as also antagonist induced internalization is described for 5-HT2A receptors (a quit unique feature of serotonergic receptors is that also the binding of antagonists could provoke effects that are usually described for agonists[265,272,277–280]) this hypothesis is explorative. In that case the concept of functional selectivity of those receptors might explain whether agonist binding, but not antagonist binding might induce downregulation, decrease in acute receptor presentation and/ or neuroplasticity associated events.

Finally, the 5-HT induced internalization is PKC-activation mediated[277]. For example, the activation of PKC with phorbol 12-myristate 13-acetate (PMA), a selective PKC activator, leads to efficient internalization of 5-HT2A-R in human embryonic kidney (HEK) 293 cells[277]. PKC inhibition with sphingosine prevents 5-HT induced internalization[277]. It is known that the process of internalization can vary depending on the ligand by which this process is induced. While for example the 5-HT induced internalization is PKC-dependent, the internalization induced by dopamine, another partial agonist of the receptor, is PKC-independent[265]. Inhibition of PKC with chelerythrine in presence of psilocin will show whether acute or subacute downregulation are PKC-dependent and still occur. Acute and subacute changes of the 5-HT2A-R are illustrated in **Figure 33**.

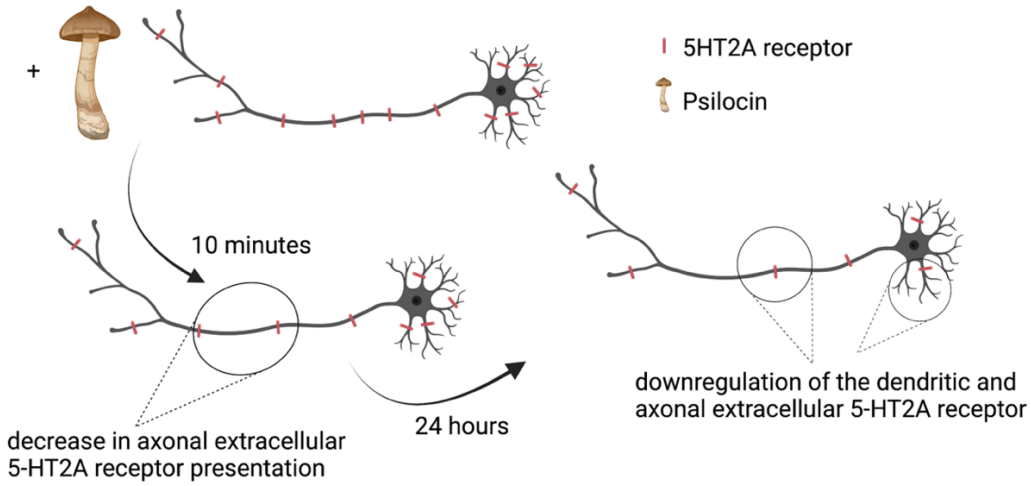

Figure 33. Psilocin provokes acute effects on receptor presentation and a subacute downregulation of the 5-HT2A-R.
There is a decrease in the axonal receptor presentation of the extracellular 5-HT2A receptor already 10 min after a psilocin trigger. The decrease in the extracellular 5-HT2A receptor presentation is present in the axonal and the dendritic compartment 24 hrs later in human cortical neurons *in vitro*. Graphic illustration generated with *Biorender.com.*

5.3 Psilocin fosters neuroplasticity in human cortical neurons

This doctoral thesis first provides data that psilocin fosters fast, long-lasting and enduring structural and functional plasticity in human cortical neurons *in vitro*.

Already 24 hrs after administration the intensity, but not the density, of the presynaptic vesicle proteins SV2 and synaptophysin and the postsynaptic scaffolding protein PSD-95 increased in neurites. That was accompanied by an enrichment of differentially expressed genes associated with synapse organization and synaptic vesicle cycle GO terms. An increase in intensity could be interpreted as increase in size (due to clustering of several proteins) or increase in the amount of protein per synapse. As the tool for measuring density works with a predefined particle size for proteins an underestimation might be caused by the impossibility to differentiate between clustering of several proteins (which are potentially recognized as one particle) or just one particle.

Moreover, my data underlines that even genes involved in spine and growth cone formation are modified. That is in line with current research where spinogenesis after psychedelic DMT, DOI, LSD, ketamine and psilocybin administration in rodent pyramidal neurons has been described[1,210]. Already a single DOI administration enhances cortical spine density, in detail of immature and transitional dendritic spines, which is 5-HT2A-R dependent[472]. So far, I was not able to detect changes in spine formation on a cellular level. For that high resolution microscopy on matured neurons should be applied in future experiments.

This doctoral thesis first moreover provides structural and functional evidence that psilocin rapidly reduces excitability in human cortical neurons *in vitro*. A morphological elongation and shift of the AIS (neuroplastic reaction of deprived neurons to become more excitable) to the soma was accompanied by functional changes, such a reduced AP amplitude and a reduced frequency of sEPSCs. This finding is interesting, particularity because there is a debate in research whether psilocybin decreases or increases brain activity and there is empirical evidence for both sides[198]. For example, it is known from animal and human fMRI studies that the serotonergic psychedelic DOI, psilocybin but also serotonin itself reduces brain activity and connectivity in the PFC[200–202]. But contrary, psilocybin increases PFC glucose metabolism in a PET study[158]. A reason for these contradictory findings might be that the 5-HT2A-R is present on excitatory pyramidal glutamatergic neurons and on inhibitory GABAergic interneurons[193–197,230,231,233,234]. This explains why extracellular GABA but also glutamate levels have been found to be increased after DOI, psilocybin and LSD administration[255,257,473].

In vitro data is also inconsistent and was based so far on animal studies. Two studies show that psilocybin or DMT increase excitatory neurotransmission, in detail the frequency and amplitude of mEPSCs, respectively sEPSCs in brain slices of rodents[1,210]. Shao and colleagues used putative layer 5 pyramidal neurons of the MFC. Ly and colleagues worked with neurons of the mPFC. One big difference to this experiment (except of the fact that those studies were performed in the animal system and there might be species-dependent dissociation kinetic differences of the drugs[210,474]) is that the animals received the drugs *in vivo* and were killed 24 hrs later for the electrophysiological brain recordings. The drug could therefore act on the whole brain and not just on selected cells. The electrophysiological outcome is thereby an interplay of interacting brain areas and association cortices. Also, the brain of a living animal contains a metabolic system and of cause much more cell types (neuronal and nonneuronal subcultures) than the homogenous culture of cortical neurons used. For example, it is discussed that the electrophysiological answer towards psychedelics is mediated by the presence of astrocytes[475] (psychedelics activate astrocytes and their response differ compared to the response of neuronal populations[224,476,477]). A third study that measured extracellular recordings in anaesthetized rats could clearly show that DOI depressed neuronal firing in raphe nuclei[478]. And interestingly, the direct bath-applied stimulation with selective 5-HT2A/2C receptor agonist DOI and serotonin reduced neuronal excitability (spontaneous APs and current-evoked-firing) in whole-cell patch clamp recordings of rat cultured cortical neurons[211].

Of importance, psilocin not only acts on the 5-HT2A-R but is also a partial agonist of the 5-HT1A receptor. 5-HT1A receptor activation has been shown to decrease excitability as it is an inhibitory GPCR[198,479]. It is known that 80% of pyramidal neurons co-express the 5-HT2A and the 5-HT1A receptor[233,234]. The 5-HT1A receptor is expressed by cortical neurons employed in this study (data not shown). Both receptors are mostly responsible for regulating the membrane excitability[480]. Selective inhibition of both receptors will show which are involved in decreasing excitability.

96 hrs after psilocin administration there is a significant increase in neuritic presynaptic synapsin and postsynaptic PSD-95 intensity. By focusing only on the dendritic compartment there is clear evidence for synaptogenesis promoting long-term effect by psilocin as co-localization of synapsin and PSD-95 augmented and endured even 6 days after administration. I further found an enrichment in differentially expressed genes associated with manifold GO terms linked to synaptogenesis (1 day and 3 days) after psilocin administration. Amongst those are GOs involved in synapse formation and specification. As dendritic PSD-95 (but not dendritic synapsin) intensity and density significantly increased 96 hrs and 6 days after 96 hrs psilocin treatment I conclude that synaptogenesis is mostly driven by postsynaptic modification. Consistent with effects on structural postsynaptic plasticity I found an enrichment in manifold GO terms associated with postsynaptic and asymmetric synapse specialization, postsynaptic organization and density one day but more prominent three days after psilocin administration.

This thesis thereby provides evidence that the postsynaptic density might need longer to undergo structural changes. PSD-95 density first significantly increased 48 hrs after psilocin administration. Confirmed by Ly and colleagues who showed that presynaptic vGLUT1 puncta but not PSD-95 puncta increased 24 hrs after DOI, DMT and LSD administration[1].

That psychedelics promote synaptogenesis is not novel. Recent research shows that serotonergic psychedelics foster synaptogenesis, defined by an increased co-localization of presynaptic marker vGLUT1 and the postsynaptic marker PSD-95[1]. That was confirmed on a genetic level by de la Fuente Revenga and colleagues who described amongst others epigenomic alterations related to synapse organization and synapse assembly GO terms after a single DOI administration[472].

Notably, I could associate those structural changes directly with functional changes. Interestingly, I found evidence that the short-term state of reduced excitability is reversed in the long-term. Already the shift of the AIS to the soma and its elongation (during a state of reduced excitability 24 hrs after psilocin administration) can be interpreted as compensatory mechanism in order to increase excitability. But moreover, sEPSC amplitude significantly increases 6 days following a 96 hrs psilocin administration, potentially based on the genetic alterations associated with postsynaptic cellular specializations.

PSD-95 controls activity-dependent AMPA receptor incorporation, meaning that PSD-95 is involved in trapping and anchoring synaptic AMPA receptors in the postsynapse[259,260]. This can modify the strength of excitatory synaptic transmission[481]. An increase in PSD-95 could be carefully interpreted with an increase in AMPA receptor incorporation and therefore an increased availability of docking stations for incoming glutamate burst which could explain excitatory sEPSC amplitude increase. That is not too much of interpretation as psilocybin targets the glutamatergic system directly. In humans the relative glutamate level was higher in the mPFC after psilocybin administration using an MRI approach[255]. Also, in rat cortex glutamate level was increased after ketamine, LSD and DOI administration[81,255–257,473]. Explainable also by 5-HT2A-R stimulation, which leads to the activation of

AMPA receptors that are associated with augmented glutamate concentrations[254]. And glutamate release itself stimulates AMPA receptors that activate synaptic plasticity associated pathways like the BDNF associated TrkB and mTORC1 pathway and BDNF expression (for review see[312,3131]). Of note, 5-HT2A co-localizes and thereby interacts with PSD-95[230,251,252]. But as there is not any information about an augmentation of cellular AMPA receptor incorporation nor an increase in extracellular glutamate concentrations in the used cortical neurons after psilocin administration this stays speculative and has to be investigated. But however, an enrichment in differentially expressed genes associated with glutamatergic signaling GO terms (1 day and three days) after psilocin administration supports this theory.

Further experiments and a development of the protocol is planned. An acute measurement of one cell following the electrophysiological changes before, while and after acute drug administration was already tried. That was so far not possible due to the stresses and strains for the cell based on the long measurement protocol. Also intended is to include the measurement of mEPCs 24 hrs after psilocin administration. Contrary to sEPSC, mEPCS are measured under the influence of tetrodotoxin (TTX). mEPCS therefore reflect the real spontaneous postsynaptic events as AP generation is prohibited. Interestingly, first experiments showed that 6 days and 10 days after one day psilocin administration the mEPCS amplitude was non-significantly increased, too (data not shown). Already one 24 hrs trigger (and not 96 hrs treatment duration) seems to be therefore enough to induce long-term functional changes. Corresponding sEPSCs data (6 or 10 days following 24 hrs psilocin administration) is also missing. Finally, it is definitely interesting to check for long-term effects on the AIS. One question would be whether it recovers to the baseline position or compensates in the opposite direction (shortening and shift away from the some) to reduce excitability again 6 days after 96 hrs administration.

Finally, an enrichment of differentially expressed genes associated with GO terms of learning, memory and cognition even suggest behavioral long-term effects of the drug which are based on such structural modifications. Of note psilocin administration leads to a significant enrichment of differentially expressed genes associated with nicotine, cocaine and amphetamine addiction, indicating its intervention in pathways related to addiction.

5.4 Psilocin induces increase in BDNF level and activation of prosurvival and neuroplasticity associated BDNF downstream cascades

BDNF plays an important role in neurogenesis, synaptogenesis, neuroprotection and the formation of synaptic interactions. As those processes are the basis of memory and cognition BDNF is modulating behavior. Particularly the m-BDNF/phosphorylated-TrkB receptor complex is involved in multiple pathways linked to prosurvival and synaptic plasticity (for review see[289,293,300–304] and subchapter **1.6.2).**

This doctoral thesis first describes that BDNF (and pro-BDNF) protein and gene expression level is strongly upregulated already one day after a short but strong psilocin stimulation in human cortical neurons *in vitro* and persists for at least 48 hrs. This finding is not new as it is already known that psychedelic increase neurotrophic factors and unfold their action over the BDNF linked TrkB and mTOR pathway[1,43,222,294,346–354]. But so far this has been exclusively described *in vitro* in non-human studies and in human blood plasma and serum.

Experimental evidence points towards an activation of BDNF associated neuroplasticity downstream cascades as I found a strong activation of the phosphorylated AKT protein after psilocin administration that has been described so far only after LSD treatment in mice[482]. This doctoral thesis further replicates an increase in neurite branching[1] after psilocin administration that could be explained by the activation of the BDNF downstream PI3K/AKT/mTOR cascade. That was supported by RNA bulk seq data that shows that there is an enrichment in differentially expressed genes associated with PI3K/AKT KEGG 24 hrs after psilocin administration. Further an enrichment in axonogenesis and axon guidance GO terms was present three days after psilocin administration. But an increase in neurite branching can also be explained by a significant increase in GAP 43 gene expression one day and three days after psilocin administration. GAP-43 is an important mediator of axonal outgrowth and neurite growth[483–486]. So far, I can only state on neurite branching as I cannot differentiate between axons and dendrites with the AAV that I used.

Moreover, this doctoral thesis can replicate an increase of IEGs[216,217,219–223] *cFOS* and *EGR1* gene expression upon psilocin administration that might speak for an activation of the MAPK/Ras BDNF downstream cascade. IEG cFOS expression increase is a sign for a procession of an external stimuli which induces neuronal activity. That was supported by RNA bulk seq data that shows that there is an enrichment in differentially expressed genes associated with MAPK KEGG. But in principle IEG increase can be also directly explained by 5-HT2A-R activation after psychedelic agonist administration[487]. Again, the psychedelic induced increase of IEGs and neurite branching was known from rodent studies[1,216–223]. But so far to my knowledge human data was missing. My work therefore confirms the postulation by the Olson group that psychedelics may promote plasticity through an evolutionary conserved mechanism[1].

It is obvious that those neuroplasticity effects provoked by psychedelic administration is hypothesized to be mediated by the release of BDNF. Unfortunately, measuring exogenous BDNF release has proven to be difficult as endogenous levels are low and do not reach the detection threshold of activity assays which was already tried in our working group. But exemplarily, in one study, both the single treatment with BDNF or DOI provoked neuritogenesis in cortical neurons of rats but co-treatment of both did not have an additional value in increasing neuritogenesis. The authors argue that both operate through similar mechanisms[1]. Inhibition of the TrkB receptor and mTOR pathway blocked neuritogenesis and spinogenesis[1] suggesting that BDNF downstream pathways are at least involved. Further research definitely should include inhibitors of the TrkB receptor (e.g., ANA-12) or inhibitors

of the mTOR pathway (e.g., rapamycin) in order to replicate the experiments done by the Olson group in my human neurons. Additionally, it makes sense to include an BDNF treatment condition to investigate whether BDNF provokes the same effects such as psilocin. With the aim to elucidate whether BDNF is the neuroplasticity-mediating factor or whether the increase in cFOS, pAKT and neurite branching are BDNF independent. Time-dependent experiments after psilocin administration can elucidate which comes first (or whether both occur simultaneously), BDNF increase an or increase in BDNF associated downstream pathways.

Interestingly, this doctoral thesis shows first evidence that PKC activation and endocytosis, two mechanisms contributing to 5-HT2A-R internalization[277,281] are at least involved in psilocin induced BDNF protein level increase. That is not completely new because serotonin induced increase in *BDNF* mRNA gene expression is PKC pathway dependent[326]. But so far, it is not clear at which step after psilocin application the activation of both mechanisms play a role. As I cannot find gapless evidence whether internalization occurs after psilocin administration (please see chapter **5.2**) it has to be elucidate whether I blocked an internalization process with dynasore and chelerythrine and subsequent whether this internalization process is essential for psilocin induced BDNF increase. PKC for example is not only important for the internalization process of serotonergic receptors, but is automatically activated by the m-BDNF/TrkB complex and also by 5-HT2A-R activation as it is downstream of both.

Moreover, I can show that the psilocin induced increase in BDNF protein and gene expression level does not occur if the 5-HT2A-R is inhibited by the receptor antagonist ketanserin, suggesting a 5-HT2A-mediated mechanism. Interestingly, the BDNF pathway is intertwined with serotonergic pathways. For example, serotonin, antidepressants and serotonergic receptor agonists efficiently increase BDNF levels[322–326]. And serotonin induced increase in *BDNF* mRNA gene expression is inhibited by ketanserin[326]. The involvement of this receptor in BDNF-mediated plasticity has already been shown in an animal model system. Exemplarily, antagonistic inhibition of the 5-HT2A-R in presence of DOI, LSD, DMT psilocin and MDMA prevents neuritogenesis and spinogenesis[1]. Further I can show that upregulation of IEGs *FOS*, *FOSL1* and *FOSL2* is prevented by ketanserin co-treatment. An effect already described for 5-HT2A-R antagonist MDL100907 which blocks LSD induced *cFOS* expression in the prefrontal cortex[250].

An important point that has to be discussed is the general problem of choosing the right concentration of the drugs used in this artificial system. I initially tested different psilocin concentration and treatment durations in their ability of increasing BDNF levels. 10 µM and 10 min treatment turned out to show maximal effects in increasing BDNF levels. But this dose and treatment duration is definitely not comparable to a physiological situation for neurons of the brain. Psychedelic effects start shortly after ingestion and last up to 6 hrs. Also influenced by the need of converting psilocybin in the intestine to psilocin which can than first cross the blood brain barrier. Taken that into account a more physiological treatment duration of the neurons would be 6 hrs and a more physiological treatment concentration would be 100 nM psilocin. Particularly at the beginning of studies it is in my opinion

justifiable to excess drugs in order to have the maximal outcome and to find interesting targets. Of course, this can provoke side effects and overshadows natural occurring effects. And my experiments also clearly demonstrate that there are no extensive differences between permanent psilocin administration, 100 nM (for 6 hrs) or 10 µM (for 10 min) psilocin concentration. A rapid decay of psilocin might result in a lack of treatment effects observed between acute and long-term treatment condition.

Future work may comprise more detailed pharmacological analysis to dissect the applied concentrations of chelerythrine, dynasore and ketanserin. At least there was an interference with psilocin treatment at the given concentrations. The concentrations might have been chosen too high (or too low) to simulate a natural blocking. For example, antagonistic effects of ketanserin to other receptors cannot be excluded at the given concentration. The recently often used 5-HT2A-R antagonist MDL100907 might be here an alternative drug for inhibiting the receptor in future studies.

5.5 BDNF levels are altered in cell lines derived from selected psychiatric disorder patients

The findings from the previous subchapter are of immense interest as there is striking evidence that BDNF signaling is impaired in psychiatric disorders. For example, the "neurotrophic hypothesis" states that the supply with neurotrophins is reduced in depression (for review see[342,488]). And in fact, BDNF levels are reduced in psychiatric disorder patients and stress[328–338]. For example, schizophrenia, depression, BD and SUD is associated with a reduction in serum and/ or plasma BDNF levels (for review see[300,327,343]). Moreover, stress as an important environmental factor which increases the susceptibility for psychiatric disorder etiology, is associated with BDNF level reduction in rodents and humans[339,489]. With the logic consequence that increasing BDNF levels can be used as a potential therapeutic mechanism[300,327]. It is already well known that BDNF level differences vanish after successful psychopharmacological treatment and ECT[105,332,338,340–345].

That lead to the question whether there is already a difference in the base BDNF level in cell lines of psychiatric patients compared to cell lines of healthy controls. For this purpose, I chose iPSC-derived cortical neurons from patients diagnosed for AUD and BD. I expected to see a decreased in BDNF baseline level. And in fact, this doctoral thesis replicates a reduced baseline BDNF density in cortical neurons-derived from patients suffering from AUD *in vitro*. Surprisingly, for cortical neurons-derived from BD patients I saw the opposite effect. Baseline BDNF levels were significantly increased, independent of a BD 1 or BD 2 diagnosis. But particularly for BD, in terms of BDNF level differences, research is inconsistent. Digging into literature there is research showing both, either a reduction but also an augmentation of BDNF levels, with an overall trend towards the former. Exemplarily, studies (amongst those a metanalysis) found a decreased BDNF serum and plasma level in acute mania and

depression[328,345,490]. But exemplarily one study shows BDNF plasma levels to be increased in BD 1 patients with long-term illness, in mania and remission[491].

That is one step closer in explaining the potential antidepressant effects of psilocybin with the knowledge that psilocin can increase BDNF levels in human cortical neurons. But the previous insights were shown in healthy control cells lines. Notably, the replication of those finding in cortical neurons-derived from psychiatric disorders patients was of main interest. Particularity for substance abuse (apart from TRD) psilocybin shows remarkable potential[149,150,153,155,156]. Therefore, I expected a BDNF "restoration" towards the baseline of Ctrl cell lines after psilocin administration in this patient group. For BD patient cell lines, the outcome was explorative. The risk of triggering mania or worsen manic symptoms might intuitively contradicts a psychedelic administration in BD. That's why participants with family background or a diagnosis of BD were excluded from clinical trials with psychedelics[49,492]. Also, because psychedelic LSD administration was long-time used as pharmacological model for psychosis as it could induce psychosis when administered in high doses[158–161,493].

This doctoral thesis further shows that BDNF intensity is increased after psilocin administration in BD patients and AUD patients, although the results for BDNF density were inconsistent in both patient groups. For BDs that was unexpected as psilocybin is discussed indeed in the treatment of AUD and not in BD patients. But current research does not strictly exclude psychedelics for the treatment of bipolar depression[125,492,494,495].

Further research with modern and standardized settings should test psilocybin in the treatment of bipolar depression in clinical trials or fMRI studies. At least based on this iPS-derived cortical neuron model system I would expect an effect after psilocybin administration in this patient group. Also, to solve the question whether an augmentation of an already increased baseline level of BDNF compared to healthy controls could be rated as "positive" (in terms of improving clinical symptoms) or even serve as a marker for inducing mania.

For both patient groups further research has to test whether subsequent or prolonged psilocin administration provokes an alteration of BDNF density and there is just a dose-dependent or time delayed onset of effects. As response to psilocybin is individual and dependent on personality traits and mood[42] and not all patients clinically benefit from psilocybin treatment equally it would be worth it to investigate biological differences in cortical neurons-derived from "responders" and "non-responders" of healthy controls or from patients.

Further studies should also include cells-derived from patients with TRD as psilocybin is mostly discussed as treatment in this patient group[143,146,148,151,152].

5.6 Psilocin mediates neuroplasticity by targeting the annexin A2 – S100A10 complex and associates

Most importantly my work first and clearly demonstrates that psilocin treatment directly addresses the plasmin-generating annexin A2 – S100A10 complex and its associates. This complex and its associates, widely known for their involvement in fibrinolysis in the body[369], is strongly associated with neuroplasticity in the brain as they are associated with antidepressant and anti-inflammatory effects[376] (please refer to subchapter **1.7.1**). Remarkably, an association between an impairment of the fibrinolytic system, inflammation and depression is already described by Idell and colleagues[376]. They further suggest that a restoration of disrupted fibrinolysis in depression by psilocybin might explains its therapeutical effects[376]. I can first support the assumption of this hypothetical paper with my experimental data. Not only the core proteins of the complex annexin A2 and p11 as docking station for plasminogen, the precursor of plasmin but also plasminogen-cleaving enzymes were upregulated upon psilocin administration. This upregulation occurs quickly (an alteration of the transcriptome occurs already within 24 hrs) and is 5-HT2A receptor mediated which again approves the importance of a 5-HT2A-R activation in psilocin-mediated neuroplasticity[1,349]. Many of those complex associated proteins can even explain psilocin induced neuroplasticity on their own.

One example is p11, besides annexin A2 one of the two main complex components. Gene expression and protein level are strongly upregulated after psilocin administration. P11 is considered to be one major protagonist in antidepressant response and therefore claimed as one promising drug target in depression[408–410]. One reason for this is that downregulation of *p11* serves as marker for depression and suicide[409,496]. And KO of the *p11* gene results in a depressive-like phenotype and worsen antidepressant treatment[325,411,412]. Interestingly, ECT or antidepressant therapy (but also BDNF administration) provoked an upregulation of *p11* gene and epigenetic modifications of the promotor while the behavior of mice overexpressing *p11* resembles mice treated with antidepressants[105,393,410,411,420,497–500]. Besides, layer 5 pyramidal neurons that express p11 are strongly and specifically responsive to antidepressants, those thereby mediate chronic treatment response[501]. A second reason is that p11 interacts with pathways that are associated by themselves with depression and/ or plasticity such as the serotonergic pathway and the BDNF signaling[325,413,502]. For example, *p11* gene and protein level is reduced in *BDNF* KO mice and serotonin induced *p11* gene expression is less efficient[325]. The other way around *p11* KO mice do not profit from antidepressant actions of BDNF[325,411,412]. I can first show in this doctoral thesis that p11 and BDNF colocalize in iPSC-derived cortical neurons and that colocalization (BDNF and pro-BDNF) is augmented upon psilocin administration. This spatial proximity is speaking for a functional cooperation of both proteins.

Further p11, modulates serotonergic signaling by regulating surface localization and trafficking of serotonin receptors that are associated with antidepressant actions[325,408,411,413,496,502–504]. For example, Svenningsson and colleague showed that co-transfection of cells with p11 and the 5-HT1B receptor increased the receptor presence at the cell surface compared to cells that were only transfected with 5-

HT1B. And the number of functional 5-HT1B receptors was reduced on the cell surface in *p11* KO mice[410]. By additionally interacting with the glutamatergic receptor mGluR5 p11 modulates its surface localization[505]. Interestingly, antagonistic inhibition of this receptor has antidepressant properties which is lacking in *p11* KO mice[420,505,506]. mGluR5 receptor is therefore an interesting target for further research. The interaction with the serotonergic system its own interesting as disturbances of the serotonergic signaling are associated with depression. Whether this can be modelled in human cortical neurons *in vitro* remains to be seen.

Interestingly already one paper describes that *p11* gene expression is significantly increased in the rat prefrontal cortex 90 min after a single dose of psilocybin[223]. Of note, a reduced expression of *p11* in rat model of stress can by reversed by ketamine administration[507]. And moreover, p11 levels could be used as predictor of ketamine treatment response[508]. By targeting p11 psilocin might intervene in the BDNF and the serotonergic signaling which might even unfold annexin A2 – S100A10 independent antidepressant effects.

Further, I found the expression of the plasmin cleaving enzyme genes *tPA* and *uPA* to be upregulated after psilocin administration. Both are strongly associated with synaptic plasticity. tPA is a neuronal activity induced IEG and neuromodulator of mood and behavior[380–382,384,388,509–511]. It is involved in structural and functional synapse restructuring as it triggers the synaptic vesicle cycle and synaptic growth[385–387,512]. tPA is also involved in NMDA-mediated signaling and long-term potentiation (LTP) and thus modulates learning, memory and cognitive functions[381,510,513–515]. Because tPA regulates glutamatergic neurotransmission[516] and it is known that psilocybin and other 5-HT2A agonist target the glutamatergic system directly[255–257], tPA might be one mediating player in the psilocybin-mediated glutamatergic response. Again, Idell and colleagues hypothetically predicted a endogenous tPA level upregulation for depression therapy[376]. A hypothetical conclusion that I can now underline with my experimental data.

Remarkably, tPA, uPA and its receptor are important neuro- and synapse protectants in neurological function recovery following and ischemic stroke, consequently both are discussed in stroke therapy[516–523]. tPA and uPA are found in synapses (tPA is stored in synaptic vesicles[512]) and released quickly following acute stroke ischemia and in the following recovery phase to protect neurons[519,524–526]. Not surprisingly, there is an association of tPA and uPA KO mice and decreased tPA levels with depression-like-phenotypes, MDD, inflammation and cognitive impairments[389,395,397–399]. Also, uPA is known as a suicidality and depression marker[395]. tPA level decrease is restored by antidepressant treatments such as SSRI, electroconvulsive seizures or physical exercise[341,389–394]. Psilocin might at least partially unfold its antidepressant effect by an activation of the plasmin cleaving enzymes tPA and uPA and thereby uses their role in synaptic plasticity, in remodeling and neuroprotection. So far, I only focused on difference on a gene expression level. Whether those are also increased on a protein level has to be investigated.

Another example is the Ahnak protein, the multimeric complex partner of annexin A2 – S100A10 (I found to be strongly upregulated by psilocin), that might promote synaptic plasticity by regulating L-type VGCC[401,402,497]. Calcium influx through those channels might activate CREB dependent gene transcription by activating MAPK pathway and thereby promoting synaptic plasticity[404,527]. Again, Ahnak KO in mice is associated with depression-like-phenotype, MDD, inflammation and cognitive impairments[404].

Another interesting target is the epigenetic modulator SMARCA3 that builds up the p11/Anxa2/Smarca3 complex, as well as its underdog neurensin-2[405–407,497]. SMARCA3 levels have been described to be increased after SSRI administration and the behavioral SSRI response is based on p11/SMARCA3-mediated repression of neurensin-2[400,528]. Overexpression of neurensin-2 is associated with depressive-like phenotype[528]. Interestingly, I found a significant downregulation of neurensin-1 (*NRSN1* gene), as paralogue of neurensin-2 after psilocin administration (data not shown). Further research should focus on the role of neurensin-1 (SMARCA3 dependent or independent) in the antidepressant effect by psilocin.

Finally, I found other *ANXA* and *S100* isoform genes, in particular the *ANXA3* gene (even in long-term) to be significantly increased after psilocin administration, mediated by 5-HT2A-R activation. Those isoforms are not known yet to be involved in fibrinolysis but annexin and S100 proteins are known to form complexes together. Particularity the *ANXA3* isoform is not well described yet and could be of immense interest in psilocin mediated effects.

Besides a disruption of the fibrinolytic system an overshooting of the coagulation system (the counterpart of fibrinolysis) could be a source for depression pathophysiology[376]. First, studies show that fibrinogen, as key factor involved in coagulation has pro-inflammatory properties and is negatively associated with plasticity linked neurite outgrowth[371,377,378]. Second, elevated levels of pro-inflammatory cytokines in neuroinflammation are linked to depression pathophysiology (for review see:[373,529,530]) and their inhibition improves depressed mood[371,374–376].

Psilocybin might restore impaired fibrinolysis as it might act anti-inflammatory[376]. This hypothetical conclusion is based on an association between fibrinolytic player PAI-1 (major inhibitor of fibrinolysis) and 5-HT2A-R upregulation in inflammation, suggested to be restored by psilocybin induced 5-HT2A-R downregulation[376]. Idell and colleagues refer to one paper which shows that upregulation of 5-HT2A-R expression in hypertrophic adipocytes is associated with an increased expression of PAI-1 which leads to an augmented inhibition of plasmin generation. Antagonistic inhibition of the 5-HT2A-R provokes a decrease in PAI-1 expression and thereby increases plasmin generation[531]. They conclude that 5-HT2A-R agonist psilocin might act similar by initiating receptor downregulation[376]. I can directly confirm this hypothesis with my work showing a 5-HT2A-R downregulation after psilocin administration. But in my data antagonistic inhibition of the 5-HT2A-R by ketanserin indeed leads to a decreased expression of the *SERPINE1* gene, coding for PAI-1 but contrary as expected psilocin provoked an upregulation of this gene.

Interestingly, there is a close relationship between serotonin and inflammation. Serotonin has pro-inflammatory properties and 5-HT2A-R activation with (R)-DOI leads to the inhibition of TNF-α mediated inflammation and downregulation of pro-inflammatory genes[532,533]. Remarkably, psychedelics have been already described to be anti-inflammatory. For example, DMT administration is associated with a reduction of brain ischemia and reduction of pro-inflammatory cytokines such as TNF-α and IL-6[351]. Another study performed on human cerebral organoids confirmed anti-inflammatory action of psychedelic 5-MeO-DMT[213]. I cannot find a significant downregulation neither of the *TNF* and *IL6* genes (coding for IL-6 and TNF-α), nor of the *FGB* gene (coding for fibrinogen) upon psilocin administration but expression of both genes was nearly not detectable in my RNA bulk seq data (data not shown). That is not surprising, even if neurons do express IL-6 and TNF-α, their production and release is enhanced in response to intrinsic or extrinsic injuries and insults of the CNS (for review see:[534,535]). Also, I performed these experiments with healthy donor cell lines and not cell lines-derived from depressed patients, where those levels have been described to be augmented. And fibrinogen is not even expressed in neurons. It is produced in the liver and can only enter the brain after a disruption of the blood brain barrier, for example due to a brain injury (e.g., stroke) (for review see:[536]). I thereby cannot confirm that psilocin restores an overshooting coagulation system in human cortical neurons *in vitro*.

I conclude that psilocin, at least in part, unfolds its neuroplastic effects by targeting the annexin A2 – S100A10 complex and associates. Whether a simultaneous activation of all above-mentioned proteins is necessary or even an activation of single players is sufficient will be part of future research. Also, if different 5-HT2A-R agonists can also activate this complex is an interesting question. It is recently debated whether 5-HT2A-R agonists that do have psychedelic mind-altering properties are necessary to induce neuroplasticity or whether non-psychedelic agonist (also newly chemically designed) could provoke the same effects.

5.7 The annexin A2 – S100A10 complex as novel antidepressant target

Besides the above-mentioned role in neuroplasticity the annexin A2 – S100A10 complex fulfills a significant task that provides a superior explanation why psilocybin has an antidepressant mode of action which makes it to an interesting target for antidepressant drugs. Plasmin, produced by the annexin A2 – S100A10 complex, provides the tPA-mediated extracellular cleavage of pro-BDNF in m-BDNF in the brain[291]. This insight is based on an experiment by Pang and colleagues. They showed that plasminogen or tPA KO mice showed impairments in in late phase of LTP (L-LTP), simultaneously pro-BDNF levels were increased[291]. When administered both, tPA and plasminogen, they were as efficient as plasmin in the cleavage of pro-BDNF into m-BDNF, indicating an indirect role of tPA in the cleavage of pro-BDNF and thereby in the generation of m-BDNF[291,537]. Interestingly, m-BDNF

application in those KO mice was sufficient to rescue the L-LTP deficient phenotype. They state that their results "*imply that m-BDNF is a key protein synthesis product, if not the only one, needed to carry on all the necessary functions for long-term modification of hippocampal synapses*"[291].

Remarkably, a deficient or insufficient pro-BDNF into m-BDNF cleavage (resulting in increased pro-BDNF and decreased m-BDNF levels) is considered to be involved in depression etiology[389,393,414–419]. This conclusion is based on studies which find elevated pro-BDNF levels and reduced m-BDNF levels in MDD[389,393,414–419]. Exemplarily, chronic pharmacological stress administration which induced depressive-like behaviors in rats, increased pro-BDNF levels, decreased m-BDNF levels and decreased the hippocampal m-BDNF-to-pro-BDNF-ratio[416] and is associated with a reduced spine density[417]. While pro-BDNF injection caused depressive-like behaviors and was also resulting in decrease in spine density, suggesting pro-BDNF-mediated effects, injection of exogenous BDNF reversed those effects[417]. And treatment with SSRI reversed pro-BDNF serum level elevations in MDD[389].

Interestingly, tPA-mediated pro-BDNF into m-BDNF cleavage can be influenced by environmental factors and treatment. For example, age associated decrease of hippocampal tPA expression could be reversed by an enriched environment in mice[514]. That is therefore that interesting because psychiatric disorders also emerge as interplay between environmental and genetic factors and are manifested after acute or chronic stress. Drugs that counteract and restore the m-BDNF-to-pro-BDNF imbalance are highly needed in depression therapy (for review see[300,415]).

My doctoral thesis first and clearly confirms that psilocin is one of those desperately needed drugs. Notably, in this doctoral thesis I can first show that cleavage of pro-BDNF into m-BDNF is elevated after psilocin administration in iPSC-derived human cortical neurons *in vitro.* That is based on an upregulation of annexin A2 – S100A10 complexes and plasminogen cleaving enzymes. Thereby endogenous plasmin levels are enhanced and the cleavage of pro-BDNF into m-BDNF is augmented (illustrated in **Fig. 34**). I conclude that psilocin exerts is antidepressant effect by restoring reduced m-BDNF levels in psychiatric disorder patients.

Further research should focus on the question how this cleavage process can be optimized. Recent research for example underlines the role of astrocytes in the plasminogen activation system. Astrocytes seem to be involved in plasmin formation (by providing the surface for plasminogen activation) and its clearance (by degrading plasmin and plasminogen)[538]. A co-culture of cortical neurons with astrocytes might enhance the cleavage process.

And treatment with different 5-HT2A-R agonists (such as TCB-2) (monotreatment or in combination with psilocin) might provoke similar or even augmented effects. Another possibility would be not to upregulate the annexin A2 – S100A10 complex first and then in the following indirectly augment the cleavage process (time delayed effect) but to directly intervene in the cleavage.

My work paves the way for novel antidepressant drug development and provides with annexin A2 – S100A10 an innovative drug target.

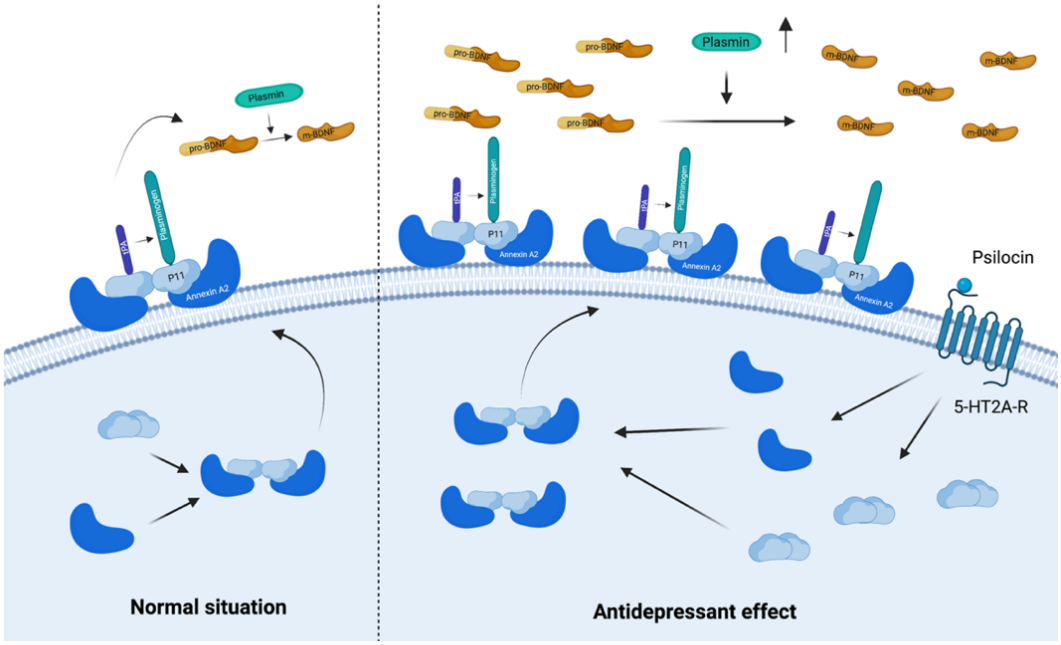

Figure 34. The annexin A2 – S100A10 complex as novel antidepressant drug target.
I can show that psilocin rapidly leads to an augmentation of annexin A2 and S100A10 on a gene expression and a protein level (main complex components) and their complex formation (docking station for plasminogen). Further, an upregulation of plasminogen cleaving enzyme genes like tPA and uPA and an altered gene regulation of complex associates (such as Ahnak, not shown) by a 5-HT2A-R mediation in human cortical neurons *in vitro*. Besides, psilocin treatment increases endogenous pro-BDNF levels as substrate for plasmin. As a consequence, plasmin levels are increased (arrow pointing upwards) after psilocin treatment, leading to on an elevated cleavage of pro-BDNF in m-BDNF, suggesting functional complex formation *in vitro*. I hypothesize that psilocin exerts is antidepressant effect by restoring reduced m-BDNF levels in psychiatric disorder patients. Image was created with *Biorender.com*

5.8 Summary

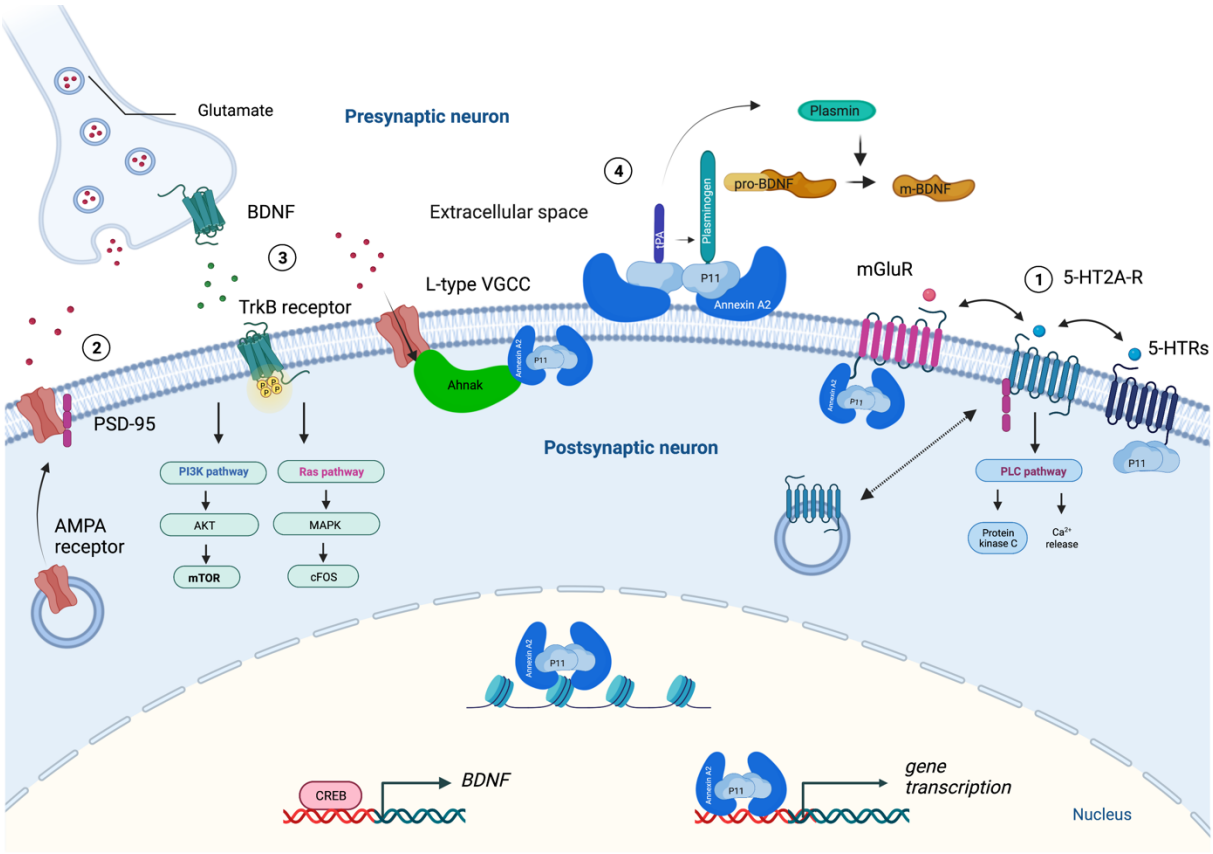

Figure 35. The psychedelic psilocin fosters neuroplasticity in iPSC-derived human cortical neurons.
In bold the key findings of my doctoral thesis (incomplete graphic illustration, supplemented by already known research results). Image was created with *Biorender.com*.

- 1. Psilocin binds to the **5-HT2A-R** that in the following **is downregulated**. This process starts already within min in the axonal compartment. Downregulation of the 5-HT2A-R presumably regulates an overshooting of serotonergic signaling in depression and might contribute to its therapeutical action. 5-HT2A-R could also form homo-or heterodimers with other serotonergic receptors and/ or mGluR.
- Psilocin **reduces in short-term excitability** in human cortical neurons *in vitro*.
- 2. A psilocin-mediated PSD-95 upregulation (co-localizes with 5-HTR2A-R) might increase AMPA receptor incorporation that could explain **increase of excitatory sEPSCs amplitude in long-term**, as a potential result of increased glutamatergic signaling.
- Psilocin leads to a fast and lasting enrichment of GO gene terms that are associated with synapse formation and synapse specialization and promotes **synaptogenesis**.

- 3. Activation of the 5-HT2A receptor provokes **BDNF increase** and the **stimulation of m-BDNF/pTrkB downstream pathways** such as the MAPK and AKT pathway, that could explain IEG expression and increase in neurite branching after psilocin administration.
- BDNF levels are **reduced in** cortical neurons derived from **AUD** patients. A BDNF restorage might explain its therapeutical efficacy in this patient group.
- 4. Psilocin directly targets the **annexin A2 – S100A10 complex** and promotes **neuroplasticity** by
  - **upregulation of p11**, known to mediate SSRI antidepressant response by increasing serotonergic signaling and by its interference with BDNF signaling and a potential interaction with mGluR receptors that mediate hallucinogenic responses.
  - **upregulation of plasminogen-cleaving enzymes**, such as the synapse protectant and neuromodulator **tPA**.
  - interaction with **Ahnak** that controls L-type VGCC. The increase in Ca^{2+} influx might trigger CREB-mediated BDNF transcription.
  - its potential involvement in gene transcription and epigenetics.
  - mediation of the extracellular **cleavage of pro-BDNF into m-BDNF** by plasmin, thereby fosters an **increase in m-BDNF level**, which is reduced in psychiatric disorders.
- An interconnection of the 5-HT2A and the BDNF pathway makes it impossible to predict which plasticity events is the logic consequence of the activation of one key pathway or whether these pathways are activated simultaneously.

This doctoral thesis is the first study that employs iPSC-derived human cortical neurons to investigate the effects of psilocin. It supports the importance of this model system in drug investigation and disease modeling. I first show that psilocin leads to fast upregulation of genes and proteins that are linked to neuroplasticity in a human *in vitro* system. The antidepressant effect of psilocin might be achieved by a normalization of increased 5-HT2A density levels and/ or a rescue of neuro-and synaptopaties. This doctoral thesis first identifies with the annexin A2 – S100A10 complex a novel antidepressant drug target in mental illness.

6 Appendix

A

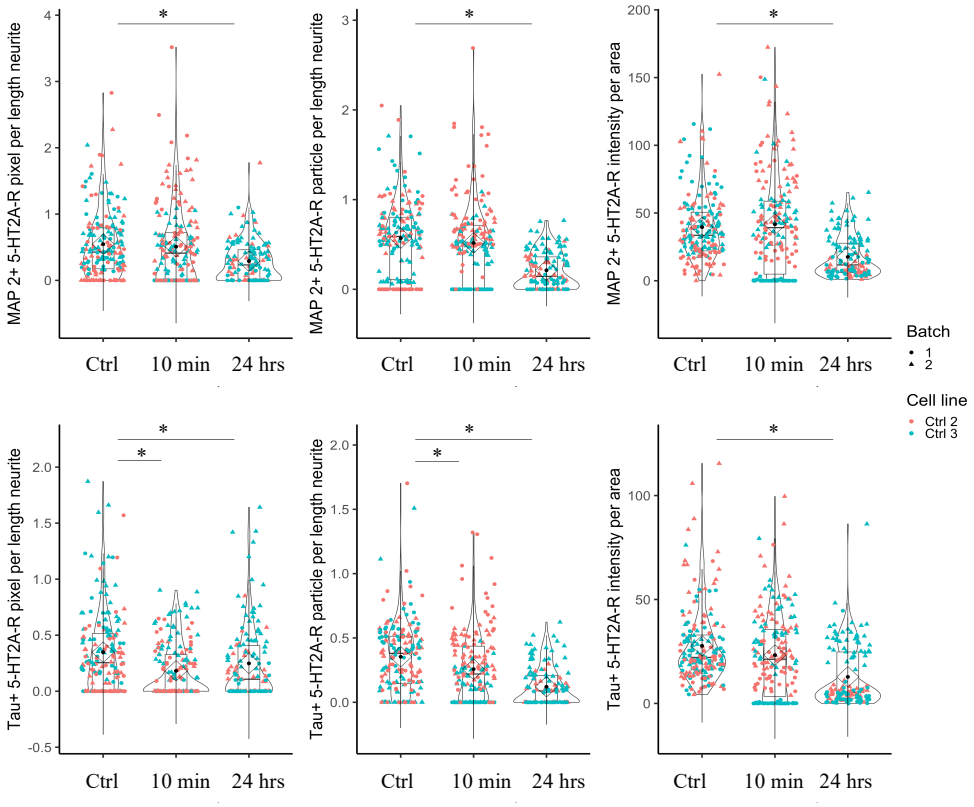

B

MAP2+ 5-HT2A-R								
Pixel	**N**	**Mean**	**SD**	**Median**	**Min**	**Max**	**Range**	**Statistic Ctrl vs.**
Ctrl	180	0.55	0.5	0.43	0	2.83	2.83	
10 min	180	0.51	0.58	0.41	0	3.52	3.52	0.30
24 hrs	135	0.29	0.3	0.23	0	1.77	1.77	4.00E-06
Particle								
Ctrl	180	0.57	0.42	0.59	0	2.05	2.05	
10 min	180	0.52	0.45	0.51	0	2.69	2.69	0.092
24 hrs	135	0.21	0.20	0.14	0	0.77	0.77	7.8e-15
Intensity								
Ctrl	180	39.55	25.55	33.55	0	152.4	152.4	
10 min	180	41.68	36.53	39.19	0	172.39	172.39	1.00E+00
24 hrs	135	17.53	14.97	11.68	0	65.23	64.21	<2e-16
TAU+ 5-HT2A-R								
Pixel	**N**	**Mean**	**SD**	**Median**	**Min**	**Max**	**Range**	**Statistic**
Ctrl	180	0.35	0.37	0.25	0	1.87	1.87	
10 min	180	0.18	0.24	0	0	0.9	0.9	4.00E-06
24 hrs	140	0.25	0.34	0.11	0	1.64	1.64	0.0059
Particle								
Ctrl	180	0.35	0.28	0.38	0	1.7	1.7	
10 min	180	0.26	0.27	0.22	0	1.32	1.32	0.00034
24 hrs	140	0.12	0.15	0.09	0	0.62	0.62	<2e-16
Intensity								
Ctrl	180	27.72	18.46	22.15	4.25	115.42	111.17	
10 min	180	23.24	20.13	21.26	0	99.6	99.6	0.0752
24 hrs	140	12.77	14.41	5.37	0	86.33	86.33	<2e-16

Figure 36. Appendix 12 of Figure 12I. Effect of psilocin on 5-HT2A-R presentation.
(A) The acute 10 µM psilocin exposure for 10 min (10 min) led to a significant decrease in TAU$^+$ axonal extracellular 5-HT2A (ex5-HT2A-R) receptor presentation (pixel per length neurite, particle per length neurite, non-significantly for intensity per area). 24 hrs after a 10 min 10 µM psilocin trigger (24 hrs) dendritic MAP 2$^+$ and axonal TAU$^+$ extracellular 5-HT2A-R presentation was significantly decreased compared to an untreated control condition (Ctrl) (pixel per length neurite, particle per length neurite and intensity per area). For Ctrl N = 180 neurites, for 10 min N = 180 neurites, for 24 hrs N = 135 - 140 neurites with 2 biological batches for MAP2+ and TAU$^+$ 5-HT2A-R were included. Kruskal-Wallis test for independent samples was calculated. Post hoc Wilcoxon rank sum test. Bonferroni-correction, adjusted $p < .05$, mean ± *SD*. **(B)** Descriptive statistics and post hoc *p*-values for data shown in **(A)** Marked in yellow, if significant. Significance levels against the respective control are *$p < 0.05$. **(C)** Two control cell lines each with two biological batches were included (except of 24 hrs for Ctrl 3 with one biological batch). Ctrl 2: For Ctrl N = 90 neurites, for 10 min N = 90 neurites, for 24 hrs N = 45 neurites with two biological batches for MAP2$^+$ and TAU$^+$ 5-HT2A-R were included. Ctrl 3: For Ctrl N = 90 neurites, for 10 min N = 90 neurites, for 24 hrs N = 90 - 95 neurites with two biological batches were included. Kruskal-Wallis test for independent samples was calculated. Post hoc Wilcoxon rank sum test. Bonferroni-correction, adjusted $p < .05$, mean ± *SD*. Significance levels against the respective control are *$p < 0.05$.

C

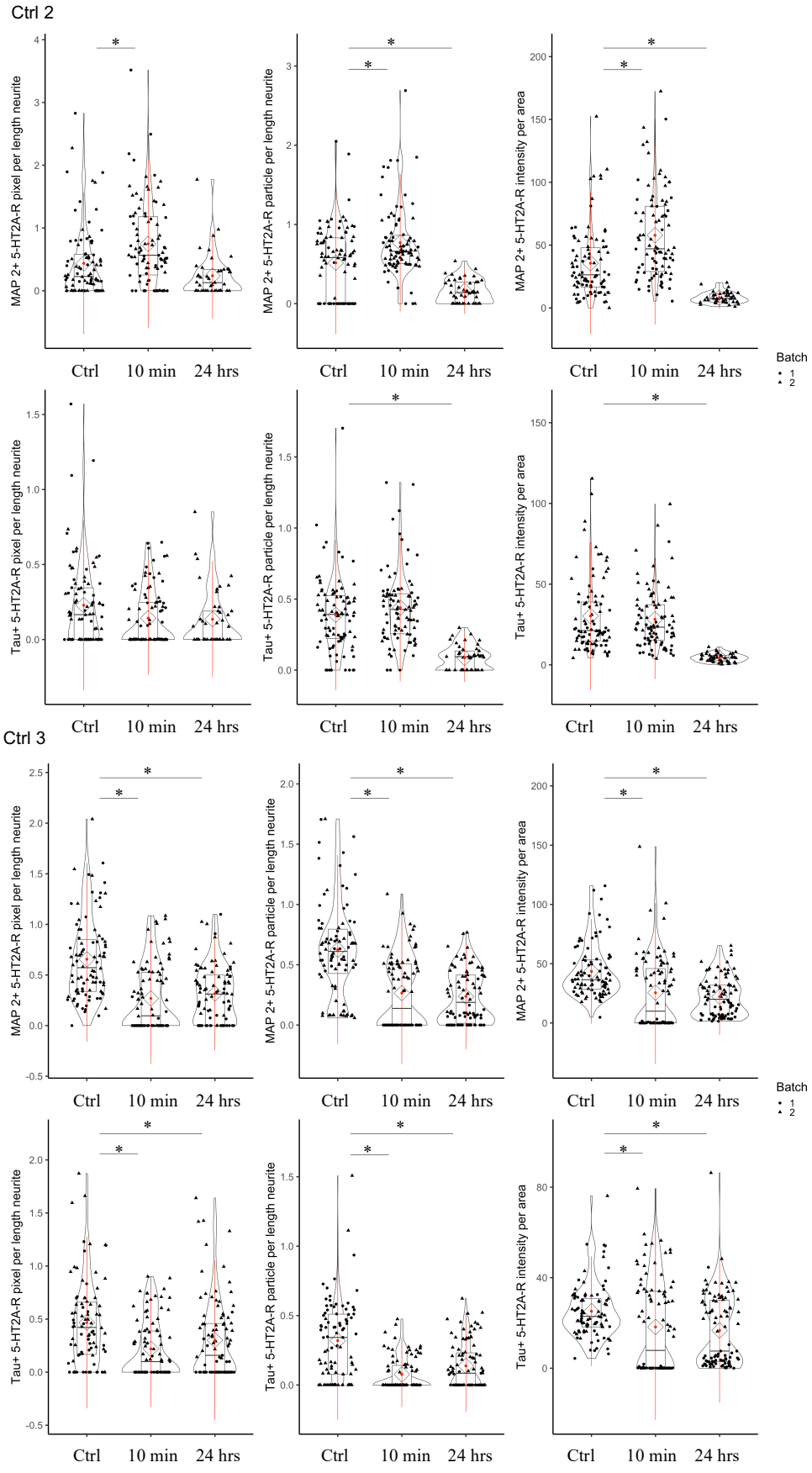
Ctrl 2
MAP 2+ 5-HT2A-R pixel per length neurite
MAP 2+ 5-HT2A-R particle per length neurite
MAP 2+ 5-HT2A-R intensity per area
Tau+ 5-HT2A-R pixel per length neurite
Tau+ 5-HT2A-R particle per length neurite
Tau+ 5-HT2A-R intensity per area
Ctrl
10 min
24 hrs
Batch
1
2
Ctrl 3

A

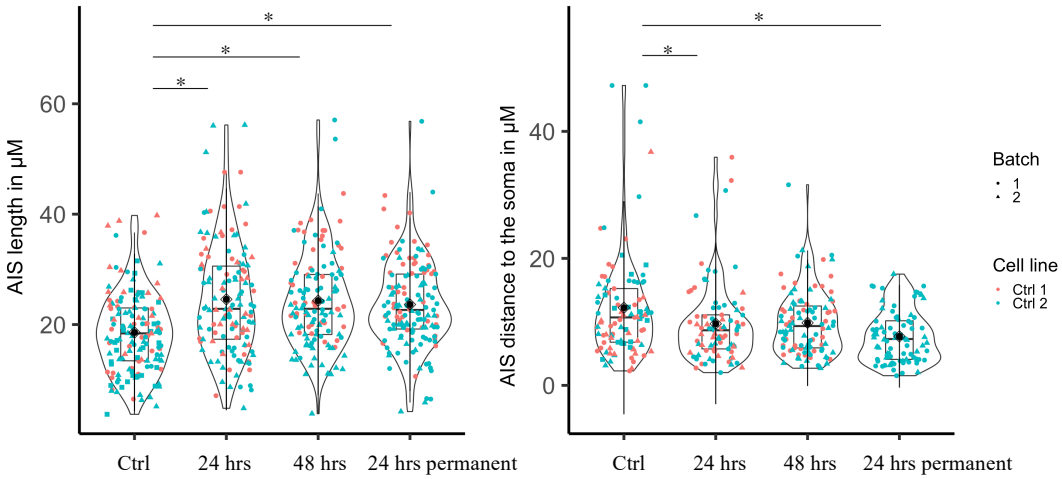

B

AIS length	N	Mean	SD	Median	Min	Max	Range	Statistic Ctrl vs.
Ctrl	119	18,57	7,13	18,4	3,74	39,77	36,03	
24 hrs	134	24,56	10,05	22,84	4,83	56,16	51,33	1,7 E-06
48 hrs	128	24,33	8,54	22,86	3,85	57,07	53,22	1,00E-07
24 hrs permanent	145	23,63	7,84	22,64	4,23	56,82	52,59	1,20E-07
AIS distance to the soma								
Ctrl	81	12,23	8,39	10,7	2,28	47,23	44,95	
24 hrs	85	9,71	6,34	8,67	2,01	35,93	33,91	5,80E-02
48 hrs	103	9,85	4,98	9,34	2,7	31,59	28,89	4,20E-01
24 hrs permanent	80	7,72	4,03	7,3	1,52	17,52	16,00	5,70E-05

C

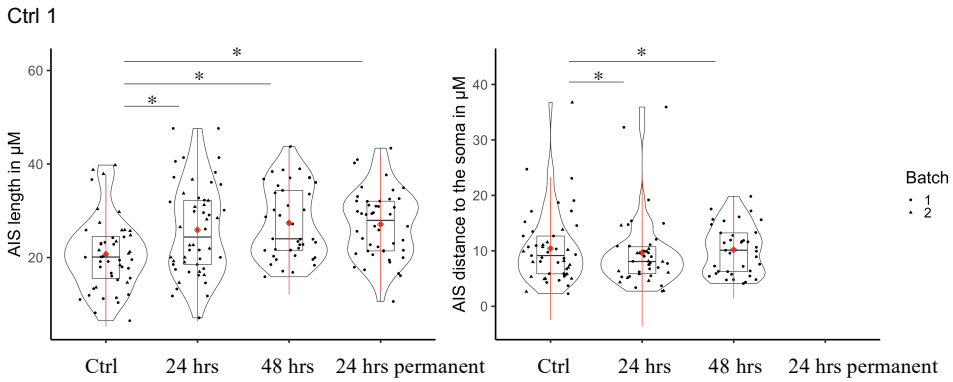

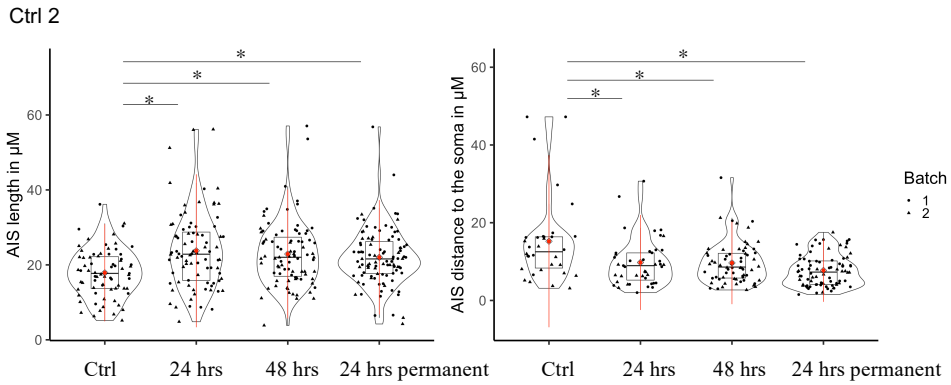

Figure 37. Appendix 14 of Figure 14C-D. Psilocin-induced AIS length increase and AIS shift to the soma.

(A) AIS length was significantly increased 24 hrs and 48 hrs after a 10 min 10 µM psilocin trigger (24 hrs, 48 hrs) and 24 hrs after permanent psilocin administration (24 hrs permanent). AIS distance to the soma was significantly decreased 24 hrs after a 10 min 10 µM psilocin trigger and 24 hrs after permanent psilocin administration. Two Ctrl cell lines were included in the analysis each with two biological batches. AIS distance to the soma: Ctrl with $N = 81$ neurites; 24 hrs with $N = 85$ neurites; 48 hrs with $N = 103$ neurites and 24 hrs permanent with $N = 80$. AIS length: Ctrl with $N = 119$ neurites; 24 hrs with $N = 134$ neurites; 48 hrs with $N = 128$ neurites and 24 hrs permanent with $N = 145$. **(B)** Descriptive statistics and post hoc p-values for data shown in **(A)** Marked in yellow, if significant. **(C)** Ctrl 1: AIS distance to the soma: Ctrl with $N = 47$ neurites; 24 hrs with $N = 42$ neurites; 48 hrs with $N = 37$ neurites. AIS length: Ctrl with $N = 48$ neurites; 24 hrs with $N = 50$ neurites; 48 hrs with $N = 41$ neurites and 24 hrs permanent with $N = 46$. Ctrl 2: AIS distance to the soma: Ctrl with $N = 34$ neurites; 24 hrs with $N = 43$ neurites; 48 hrs with $N = 66$ neurites; 24 hrs permanent with $N = 80$ neurites. AIS length: Ctrl with $N = 71$ neurites; 24 hrs with $N = 84$ neurites; 48 hrs with $N = 87$ neurites and 24 hrs permanent with $N = 99$. Kruskal-Wallis test for independent samples was calculated. Bonferroni-correction, adjusted $p < .05$, mean ± *SD*. Post hoc Wilcoxon rank sum test. Significance levels against the respective control are $*p < 0.05$.

Appendix

A

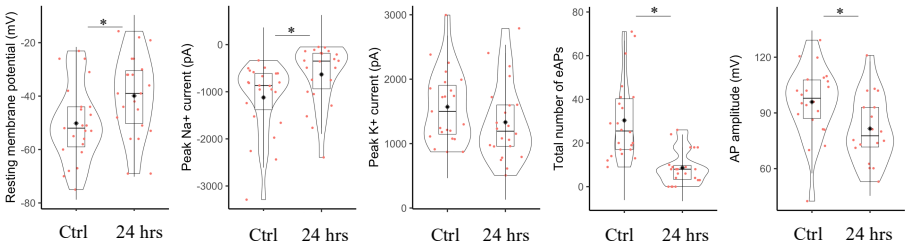

B

	N	Mean	SD	Median	Min	Max	Range	Statistic Ctrl vs.
Resting membrane potential								
Ctrl	23	-50,18	14,29	-52	-75	-23,1	51,9	
24 hrs	22	-39,9	15,13	-39	-69	-15,7	53,3	2,90E-02
Peak Na+ current (pA)								
Ctrl	23	-1121,9	743,27	-868	-3290	-334,8	2955,2	
24 hrs	22	-632,82	630,53	-349,55	-2393	-49	2344	4,00E-03
Peak K+ current (pA)								
Ctrl	23	1570,11	553,06	1500	871,1	2996	2124,9	
24 hrs	22	1331,73	600,96	1192,5	507	2789	2282	1,20E-01
Total number of evoked APs								
Ctrl	22	30,36	18,25	25,50	9	71	62	
24 hrs	22	8,64	7,63	8	0	26	26	3,70E-06
AP amplitude (mV)								
Ctrl	22	95,91	19,22	97,9	42,5	129,2	86,7	
24 hrs	18	81,54	18,09	77,7	53	121	68	1,50E-02

C

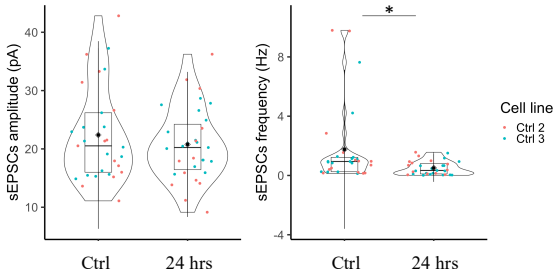

D

Amplitude	N	Mean	SD	Median	Min	Max	Range	Statistic Ctrl vs.
Ctrl	29	22,39	8,04	20,53	21,78	42,82	31,72	
24 hrs	31	20,77	6,22	20,24	20,45	36,24	27,09	6,40E-01
Frequency								
Ctrl	29	1,76	2,68	0,94	1,25	9,79	9,66	
24 hrs	31	0,51	0,47	0,34	0,45	1,57	1,56	3,30E-03

E

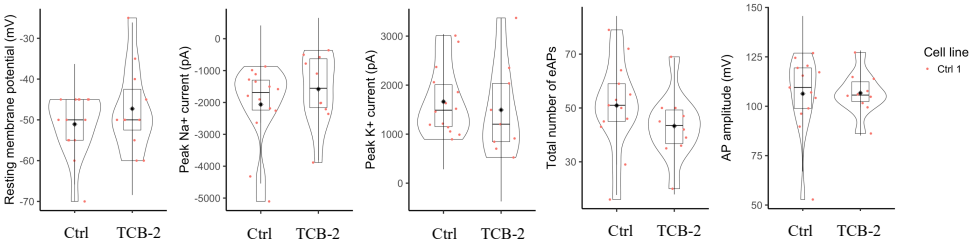

F

	N	Mean	SD	Median	Min	Max	Range	Statistic Ctrl vs.
Resting membrane potential								
Ctrl	14	-51,07	7,38	-50	-70	-45	25	
TCB-2	11	-47,27	10,57	-50	-60	-25	35	6,50E-01
Peak Na+ current (pA)								
Ctrl	14	-2063,34	1239,34	-1687	-5105	-870,8	4234,2	
TCB-2	10	-1580,87	-1580,87	-1555	-3885	-362,4	3522,6	3,40E-01
Peak K+ current (pA)								
Ctrl	14	1662,41	689,33	1488,5	893,7	3010	2116,3	
TCB-2	9	1493,5	932,98	1203	523,8	3371	2847,2	3,70E-01
Total number of evoked APs								
Ctrl	13	50,92	16,62	51	16	79	63	
TCB-2	10	43,3	12,7	43,5	20	69	49	1,20E-01
AP amplitude (mV)								
Ctrl	13	106,33	19,67	109,5	52,8	126,9	74,1	
TCB-2	10	106,7	10,77	105,65	86,21	127,2	40,99	6,50E-01

Figure 38. Appendix 15 of Figure 15A, C, E. Psilocin and TCB-2 reduced excitability in short-term.

(A-B) Effect of psilocin on intrinsic properties. **(A)** Significant decrease in AP amplitude, total AP number, resting membrane potential and peak Na^+ current 24 hrs after 10-min exposure to 10 µM psilocin (24 hrs), confirmed reduced excitability. No effect on peak K^+ current. For Ctrl $N = 22$ - 23 neurites, for 24 hrs $N = 18$ - 22 cells were measured, Mann-Whitney-U-test for independent samples was calculated, ± *SD*. **(B)** Descriptive statistics and post hoc *p*-values for data shown in **(A)** Marked in yellow, if significant. **(C-D)** Short-term effect of psilocin on synaptic properties. **(C)** Significant decrease in sEPSCs frequency, with unchanged amplitude 24 hrs after permanent 10 µM psilocin administration (24 hrs). Two Ctrl cell lines were included in the analysis. Ctrl with $N = 29$ cells, 24 hrs with $N = 31$ cells. Ctrl 2 Ctrl $N = 14$ cells, 24 hrs with $N = 13$ cells. Ctrl 3 with Ctrl $N = 15$ cells, 24 hrs with $N = 18$ cells. (**D**) Descriptive statistics and post hoc *p*-values for data shown in **(C)** Marked in yellow, if significant. **(E)** 24 hrs permanent treatment with 5-HT2A-R agonist TCB-2 reduced total number of APs, peak Na^+ current and peak K^+ current. One Ctrl cell line was included in the analysis. Ctrl with $N = 13$ - 14 cells, TCB-2 with $N = 9$ - 11 cells. Mann-Whitney-U-test for independent samples was calculated, ± *SD*. **(F)** Descriptive statistics and post hoc *p*-values for data shown in **(E)**. Significance levels against the respective control are $*p < 0.05$. AP, action potential; eAP, evoked action potential; sEPSCs**,** spontaneous excitatory postsynaptic current. Electrophysical measurements were performed by Dr. Mahnaz Davoudi.

A

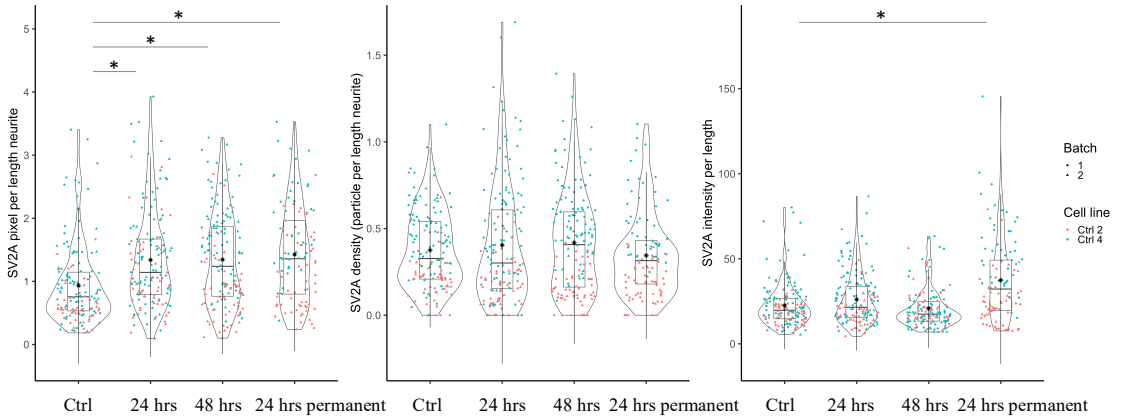

B

SV2A pixel	N	Mean	SD	Median	Min	Max	Range	Statistic Ctrl vs.
Ctrl	150	0,93	0,62	0,76	0,18	3,41	3,22	
24 hrs	150	1,34	0,77	1,14	0,09	3,93	3,84	5,70E-07
48 hrs	150	1,35	0,75	1,24	0,1	3,28	3,18	1,50E-06
24 hrs permanent	105	1,43	0,76	1,36	0,24	3,53	3,29	2,50E-07
SV2A particle								
Ctrl	150	0,38	0,22	0,33	0	1,1	1,1	1,00E+00
24 hrs	150	0,4	0,34	0,3	0	1,69	1,69	1,00E+00
48 hrs	150	0,42	0,29	0,41	0	1,39	1,39	8,40E-01
24 hrs permanent	105	0,34	0,24	0,31	0	1,1	1,1	
SV2A intensity								
Ctrl	150	22,6	12,84	19,73	5,36	80,23	74,87	
24 hrs	150	26,05	15	21,48	4,41	86,77	82,36	3,91E-01
48 hrs	150	20,85	11,72	17,47	6,94	63,28	56,34	4,84E-01
24 hrs permanent	105	37,42	24,57	32,22	7,58	145,48	137,89	8,90E-07

C

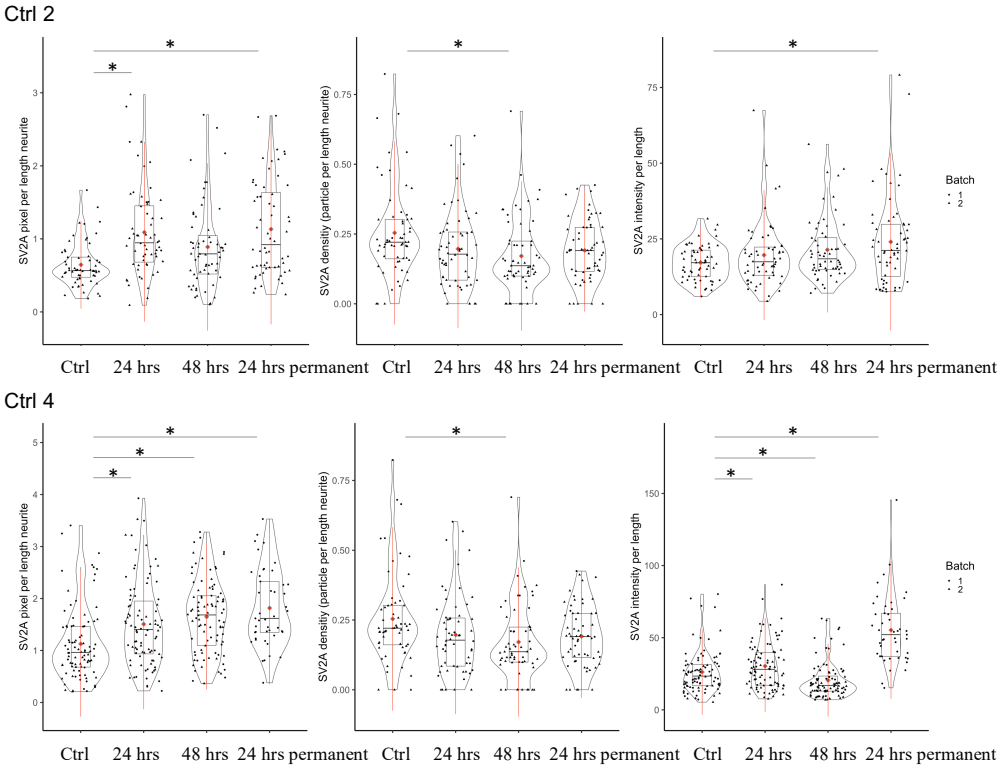

Figure 39. Appendix 16A of Figure 16C. Effect of psilocin on neuritic presynaptic SV2A.
(A) SV2A pixel per length neurite were significantly increased 24 and 48 hrs after a 10 min 10 µM psilocin trigger (24 hrs; 48 hrs) and 24 hrs after permanent psilocin administration (24 hrs permanent). SV2A intensity per area was significantly increased 24 hrs after permanent psilocin administration. (Ctrl with $N = 150$ neurites; 24 hrs with $N = 150$ neurites; 48 hrs with $N = 150$ neurites and 24 hrs permanent with $N = 105$ neurites). **(B)** Descriptive statistics and post hoc p-values for data shown in **(A)** Marked in yellow, if significant. **(C)** Two Ctrl cell lines were included in the analysis. Ctrl 2 with (Ctrl with $N = 60$ neurites; 24 hrs with $N = 60$ neurites; 48 hrs with $N = 60$ neurites and 24 hrs permanent with $N = 60$ neurites with 2 biological batches. Ctrl 4 with (Ctrl with $N = 90$ neurites; 24 hrs with $N = 90$ neurites; 48 hrs with $N = 90$ neurites and 24 hrs permanent with $N = 45$ neurites with 2 biological batches, mean ± *SD*. For all statistical analysis Kruskal-Wallis test for independent samples was calculated. Bonferroni-correction, adjusted $p < .05$, mean ± *SD*. Significance levels against the respective control are $*p < 0.05$.

A

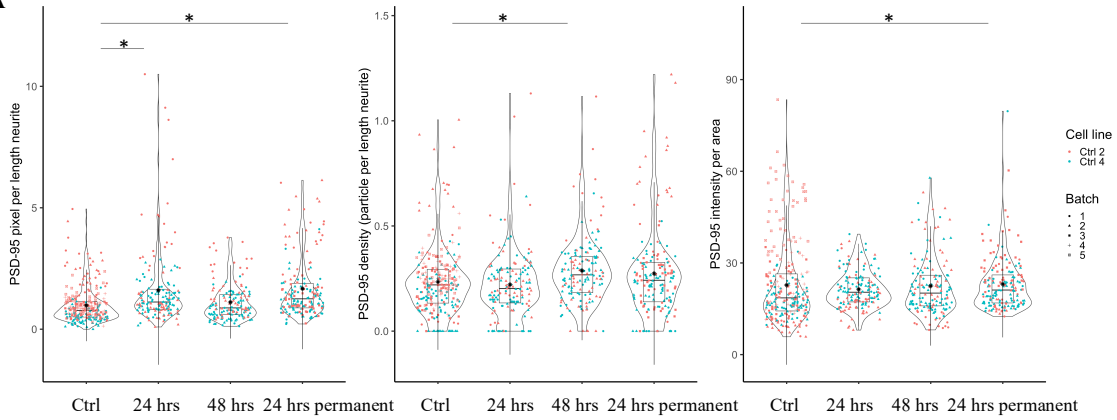

B

PSD-95 pixel	N	Mean	SD	Median	Min	Max	Range	Statistic Ctrl vs.
Ctrl	261	0,98	0,74	0,74	0	4,95	4,95	
24 hrs	155	1,61	1,53	1,12	0,09	10,5	10,41	2,20E-09
48 hrs	150	1,11	0,75	0,88	0,12	3,77	3,65	1,43E-01
24 hrs permanent	170	1,67	1,25	1,25	0,22	6,13	5,92	1,40E-13
PSD-95 particle								
Ctrl	260	0,23	0,16	0,22	0	1	1	
24 hrs	155	0,22	0,17	0,2	0	1,13	1,13	1,00E+00
48 hrs	150	0,29	0,17	0,27	0	1,12	1,12	3,60E-04
24 hrs permanent	170	0,27	0,22	0,24	0	1,22	1,22	5,16E-01
PSD-95 intensity								
Ctrl	260	22,75	13,03	18,57	5,83	83,43	77,6	
24 hrs	155	21,37	6,07	20,41	8,03	39,43	31,4	3,60E-01
48 hrs	150	22,48	9,77	20,13	8,08	57,82	49,74	1,00E+00
24 hrs permanent	170	23,07	8,71	21,14	12,49	79,66	67,17	2,00E-02

C

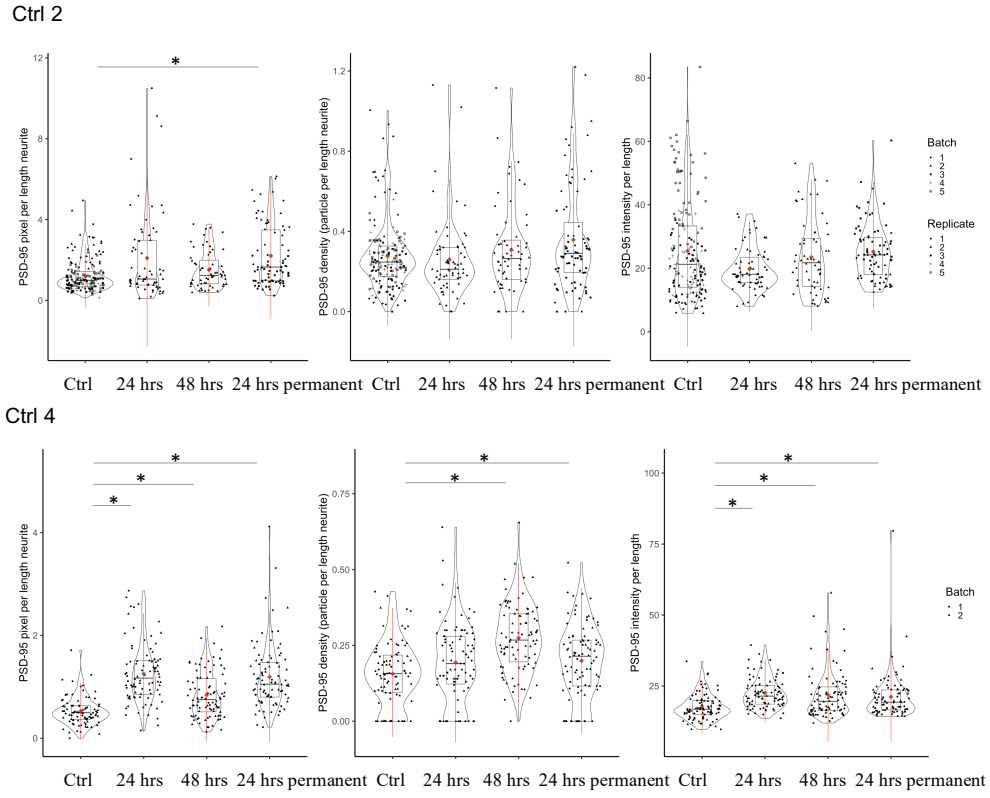

Figure 40. Appendix 16B of Figure 16D. Effect of psilocin on neuritic postsynaptic PSD-95.
(A) Significant increase in PSD-95 pixel per length neurite and intensity per area 24 hrs after permanent (24 hrs permanent) psilocin administration. Significant increase in PSD-95 pixel per length neurite 24 hrs after 10 min psilocin administration (24 hrs) and permanent psilocin administration (24 hrs permanent). Significant increase in PSD-95 particle per length neurite 48 hrs after 10 min psilocin administration (48 hrs). **(B)** Descriptive statistics and post hoc *p*-values for data shown in **(A)**. Marked in yellow, if significant. **(C)** For Ctrl $N = 260$ - 261 neurites, for 24 hrs $N = 155$ neurites, for 48 hrs $N = 150$ neurites, for 24 hrs permanent $N = 170$ neurites were calculated. Two control cell lines were included. Ctrl 2 with (Ctrl $N = 90$ neurites, for 24 hrs $N = 90$ neurites, for 48 hrs $N = 90$ neurites, for 24 hrs permanent $N = 90$ neurites); Ctrl 4 with (Ctrl $N = 170$ - 171 neurites, for 24 hrs $N = 65$ neurites, for 48 hrs $N = 60$ neurites, for 24 hrs permanent $N = 80$ neurites). Kruskal-Wallis test for independent samples was calculated. Post hoc Wilcoxon rank sum test. Bonferroni-correction, adjusted $p < .05$, mean ± *SD*. Significance levels against the respective control are $*p < 0.05$.

Appendix

A

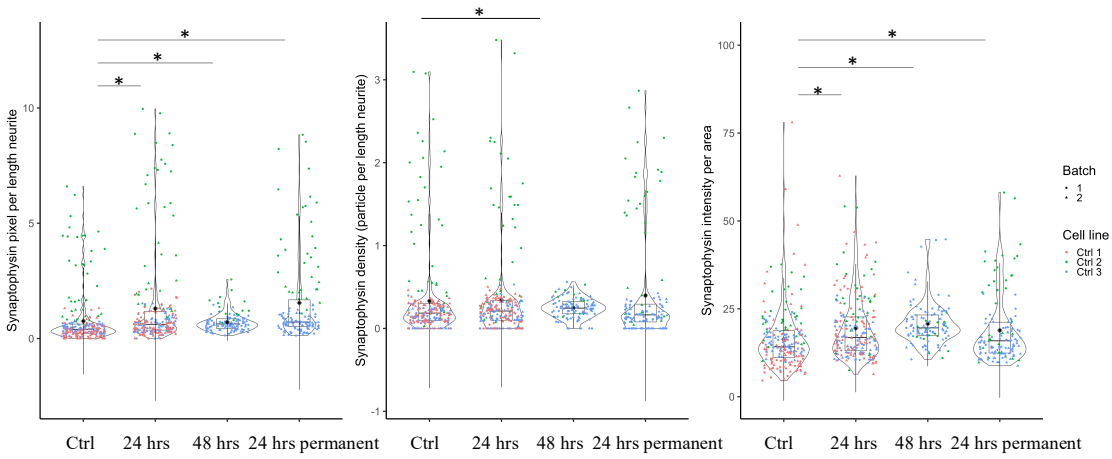

B

Synaptophysin pixel	N	Mean	SD	Median	Min	Max	Range	Statistic Ctrl vs.
Ctrl	215	0,75	1,16	0,4	0	6,6	6,6	
24 hrs	215	1,3	2	0,62	0	9,96	9,96	4,60E-07
48 hrs	105	0,71	0,4	0,63	0,13	2,56	2,43	5,70E-07
24 hrs permanent	126	1,55	1,88	0,72	0,13	8,84	8,71	4,60E-12
Synaptophysin particle								
Ctrl	215	0,33	0,53	0,19	0	3,1	3,1	
24 hrs	215	0,34	0,53	0,21	0	3,48	3,48	1,00E+00
48 hrs	105	0,25	0,12	0,24	0	0,56	0,56	1,83E-02
24 hrs permanent	125	0,4	0,64	0,16	0	2,87	2,87	1,00E+00
Synaptophysin intensity								
Ctrl	215	16,31	8,73	14,2	4,6	78,06	73,46	
24 hrs	215	19,51	9,12	16,85	6,42	62,81	56,39	6,10E-05
48 hrs	105	20,76	6,03	19,59	10,64	44,78	34,14	2,20E-12
24 hrs permanent	125	18,88	9,59	15,91	8,8	58,08	49,28	5,43E-02

C

Ctrl 1

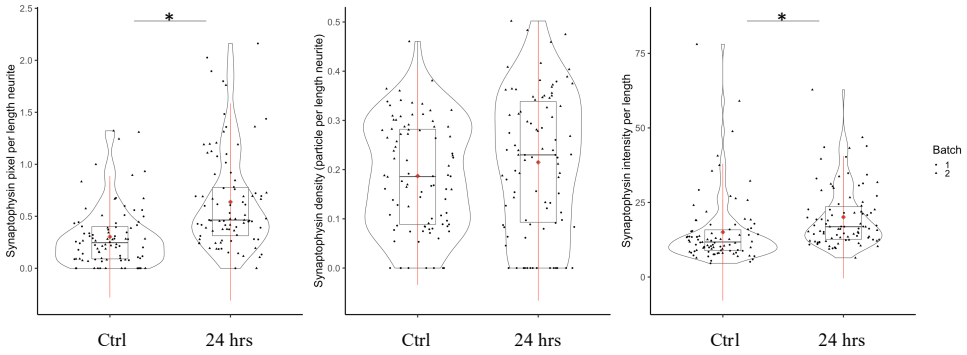

Ctrl 2

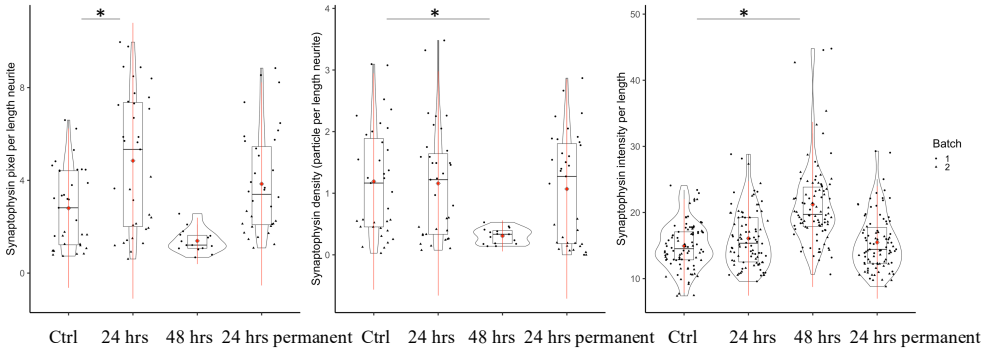

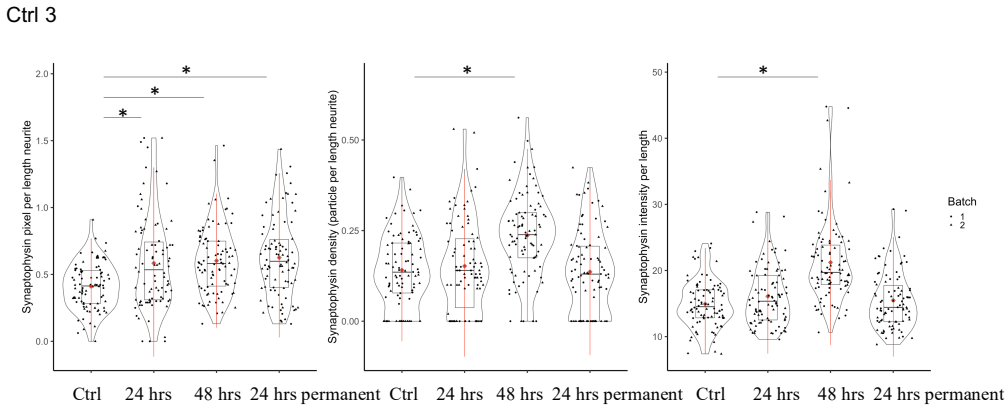

Figure 41. Appendix 16C of Figure 16G. Effect of psilocin on neuritic presynaptic synaptophysin.
(A) Synaptophysin pixel per length neurite and synaptophysin intensity per area were significantly increased 24 and 48 hrs after a 10 min 10 µM psilocin trigger (24 hrs; 48 hrs) and 24 hrs after permanent psilocin administration (24 hrs permanent). Synaptophysin particle per length neurite was significantly decreased 48 hrs after a 10 min 10 µM psilocin trigger (48 hrs). Three Ctrl cell lines were included in the analysis. (Ctrl with $N = 215$ neurites; 24 hrs permanent with $N = 215$ neurites; 48 hrs with $N = 105$ neurites and 24 hrs permanent with $N = 125 – 126$ neurites). **(B)** Descriptive statistics and post hoc p-values for data shown in **(A)**. Marked in yellow, if significant. **(C)** Ctrl 1 with (Ctrl with $N = 90$ neurites; 24 hrs with $N = 90$ neurites) with 2 biological batches. Ctrl 2 with (Ctrl with $N = 35$ neurites; 24 hrs with $N = 35$ neurites; 48 hrs with $N = 15$ neurites and 24 hrs permanent with $N = 35$ - 36 neurites) with 2 biological batches. Ctrl 4 with (Ctrl with $N = 90$ neurites; 24 hrs with $N = 90$ neurites; 48 hrs with $N = 90$ neurites and 24 hrs permanent with $N = 90$ neurites) with 2 biological batches. For all statistical analysis Kruskal-Wallis test for independent samples was calculated. Bonferroni-correction, adjusted $p < .05$, mean ± *SD*. Significance levels against the respective control are *$p < 0.05$.

A

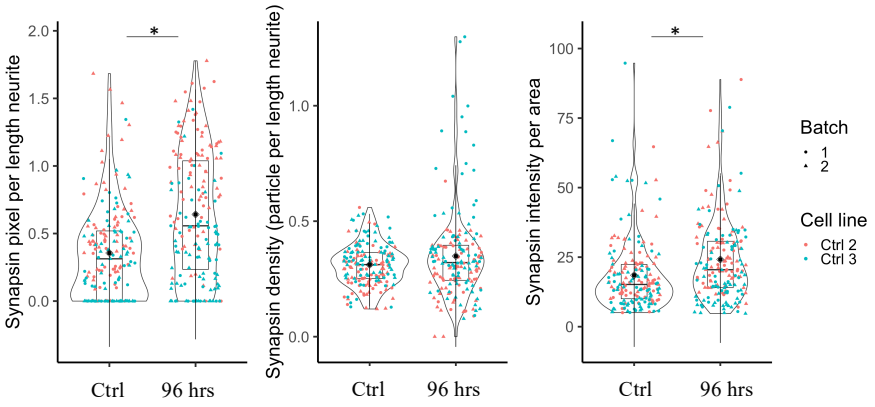

B

Synapsin pixel	N	Mean	SD	Median	Min	Max	Range	Statistic Ctrl vs.
Ctrl	181	0,36	0,35	0,31	0	1,68	1,68	
96 hrs	180	0,64	0,46	0,62	0	1,78	1,78	2,00E-09
Synapsin particle								
Ctrl	181	0,31	0,09	0,31	0,12	0,56	0,44	
96 hrs	180	0,35	0,2	0,32	0,1	1,3	1,3	3,00E-01
Synapsin intensity								
Ctrl	181	18,5	12,88	15,18	5,04	94,75	89,7	
96 hrs	180	24,16	15	20,49	4,72	88,86	84,14	7,2E-06

C

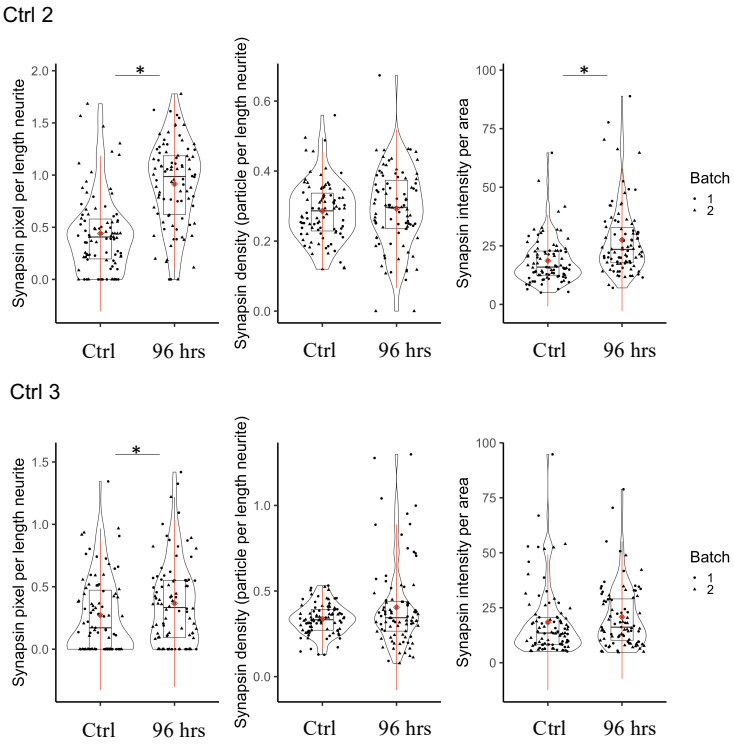

Figure 42. Appendix 17A of Figure 17C-D. Long-term effect of psilocin on neuritic presynaptic synapsin.

(A) Significant increase in synapsin pixel per length neurite and intensity per area and non-significant increase in particle per length neurite. For Ctrl $N = 181$ neurites, for 96 hrs $N = 180$ neurites were included. Two control cell lines each with two biological batches were included. **B)** Descriptive statistics and post hoc p-values for data shown in **(A).** Marked in yellow, if significant. **(C)** Ctrl 2 with (Ctrl with $N = 91$ neurites; 96 hrs with $N = 90$ neurites); Ctrl 3 with (Ctrl with $N = 90$ neurites; 96 hrs with $N = 90$ neurites). Kruskal-Wallis test for independent samples was calculated. Post hoc Wilcoxon rank sum test. Bonferroni-correction, adjusted $p < .05$, mean ± SD. Significance levels against the respective control are *$p < 0.05$.

A

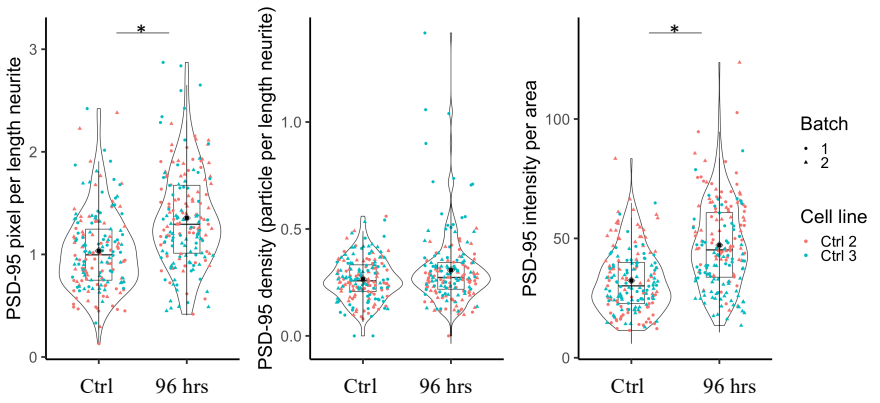

B

PSD-95 pixel	N	Mean	SD	Median	Min	Max	Range	Statistic Ctrl vs.
Ctrl	181	1,03	0,39	1	0,13	2,42	2,29	
96 hrs	180	1,36	0,47	1,29	0,42	2,87	2,45	9,70E-12
PSD-95 particle								
Ctrl	181	0,27	0,1	0,26	0	0,56	0,56	
96 hrs	180	0,31	0,17	0,27	0	1,42	1,42	7,50E-02
PSD-95 intensity								
Ctrl	181	32,34	13,23	30,14	11,46	83,43	71,97	
96 hrs	180	47,16	18,27	45,19	13,52	123,68	110,16	7,90E-16

C

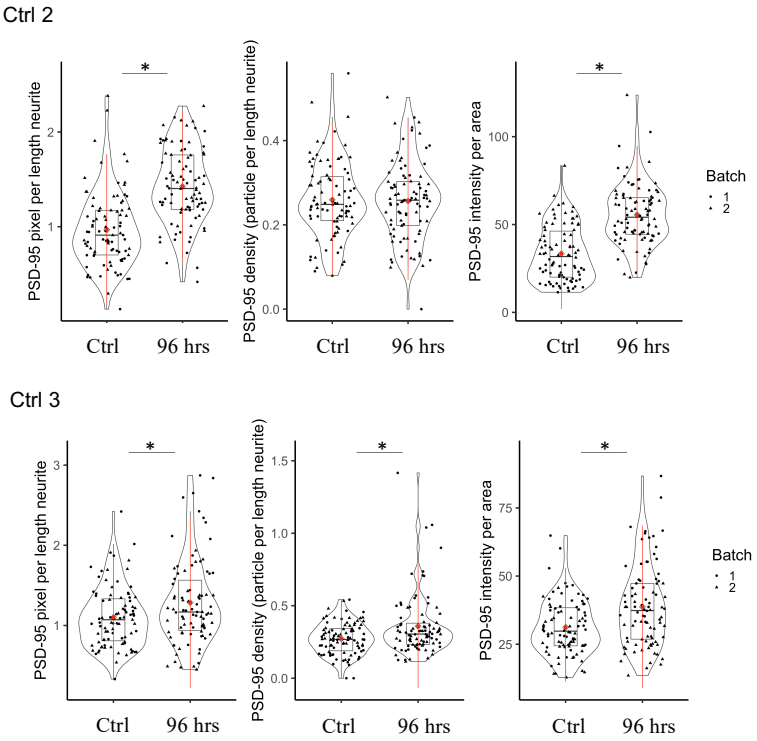

Figure 43. Tbc. Appendix 17A of Figure 17E-F. Long-term effect of psilocin on neuritic postsynaptic PSD-95.

(A) Significant increase in PSD-95 pixel per length neurite and intensity per area and non-significant increase in particle per length neurite. For Ctrl $N = 181$ neurites, for 96 hrs $N = 180$ neurites were included. Two control cell lines each with two biological batches were included. **B)** Descriptive statistics and post hoc p-values for data shown in **(A)**. Marked in yellow, if significant. **(C)** Ctrl 2 with (Ctrl with $N = 91$ neurites; 96 hrs with $N = 90$ neurites); Ctrl 3 with (Ctrl with $N = 90$ neurites; 96 hrs with $N = 90$ neurites). Kruskal-Wallis test for independent samples was calculated. Post hoc Wilcoxon rank sum test. Bonferroni-correction, adjusted $p < .05$, mean ± *SD*. Significance levels against the respective control are *$p < 0.05$.

A

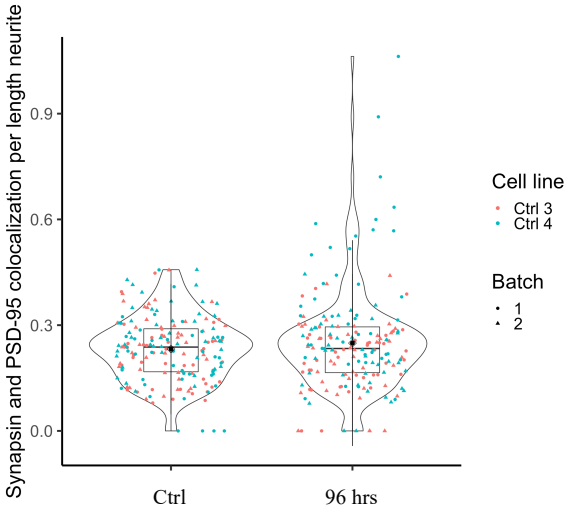

B

Synapsin/ PSD-95 co-localization per length neurite	N	Mean	SD	Median	Min	Max	Range	Statistic Ctrl vs.
Ctrl	181	0.23	0.09	0.24	0	0.46	0.46	
96 hrs	180	0.25	0.15	0.23	0	1.06	1.06	2.30E-01

C

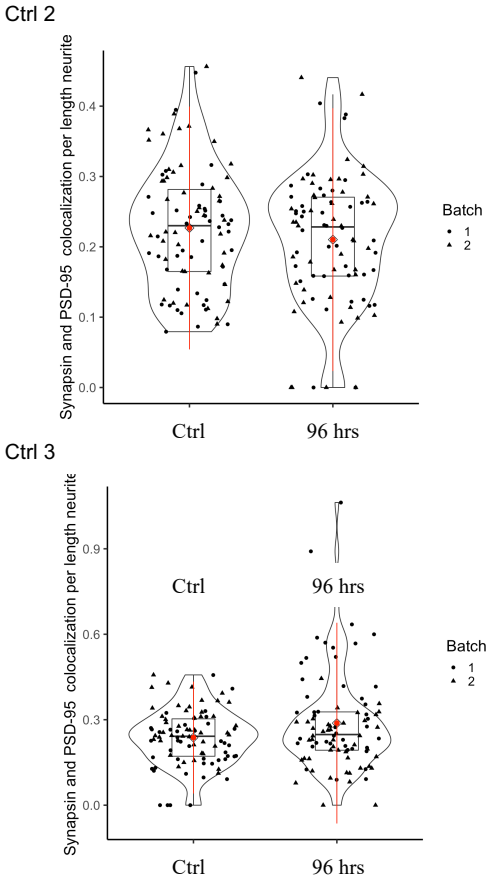

Figure 44. Tbc. Appendix 17A of Figure 17G. Long-term effect of psilocin on neuritic synapsin and PSD-95 co-localization.

(A) Non-significant increase in synapsin and PSD-95 co-localized particle per length neurite. For Ctrl $N = 181$ neurites, for 96 hrs $N = 180$ neurites were included. Two control cell lines each with two biological batches were included. **(B)** Descriptive statistics and post hoc p-values for data shown in **(A)**. Marked in yellow, if significant. **(C)** Ctrl 2 with (Ctrl with $N = 91$ neurites; 96 hrs with $N = 90$ neurites); Ctrl 3 with (Ctrl with $N = 90$ neurites; 96 hrs with $N = 90$ neurites); Kruskal-Wallis test for independent samples was calculated. Bonferroni-correction, adjusted $p < .05$, mean ± *SD*. Significance levels against the respective control are $*p < 0.05$.

Appendix

A

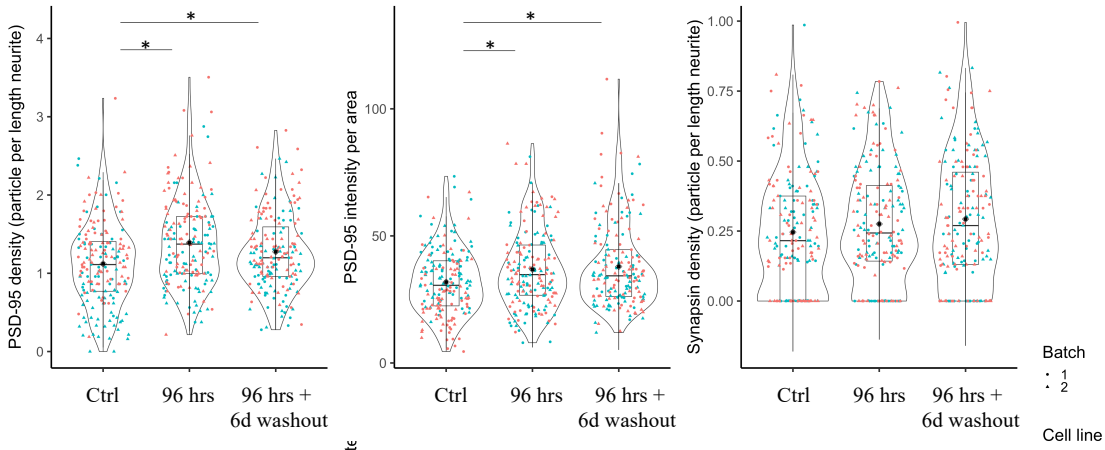

B

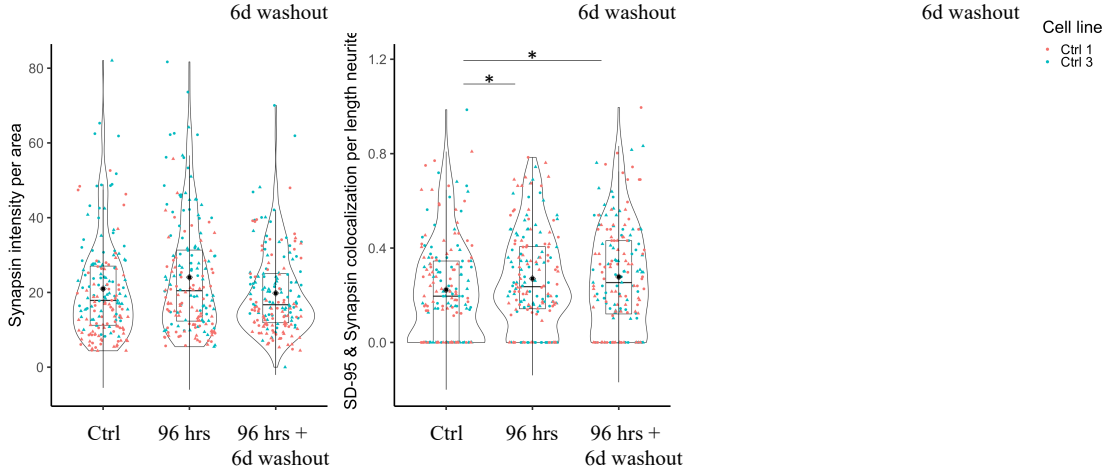

C

Synapsin particle	N	Mean	SD	Median	Min	Max	Range	Statistic Ctrl vs.
Ctrl	180	0,25	0,21	0,22	0	0,99	0,99	
96 hrs	180	0,28	0,21	0,24	0	0,78	0,78	4,10E-01
96 hrs + 6d washout	180	0,29	0,23	0,27	0	1	1	1,70E-01
Synapsin intensity								
Ctrl	180	20,98	13,26	17,86	4,38	82,05	77,67	
96 hrs	180	24,06	15,04	20,47	5,47	81,68	76,21	2,11E-01
96 hrs + 6d washout	180	19,79	10,93	16,72	0	70,04	70,04	1,00E+03
PSD-95 particle								
Ctrl	180	1,12	0,53	1,11	0	3,24	3,24	
96 hrs	180	1,39	0,57	1,37	0,22	3,5	3,29	4,5E-05
96 hrs + 6d washout	180	1,27	0,5	1,2	0,28	2,83	2,55	3,70E-02
PSD-95 intensity								
Ctrl	180	31,83	12,92	30,56	4,5	73,44	68,94	
96 hrs	180	36,81	15,35	34,77	7,96	86,33	78,37	1,37E-02
96 hrs + 6d washout	180	37,95	16,4	34,29	11,93	111,69	99,76	5,90E-03
Synapsin/ PSD-95 co-localization per length neurite								
Ctrl	180	0,22	0,21	0,2	0	0,99	0,99	
96 hrs	180	0,27	0,2	0,24	0	0,78	0,78	4,30E-02
96 hrs + 6d washout	180	0,28	0,22	0,25	0	1	1	4,70E-02

Ctrl 1

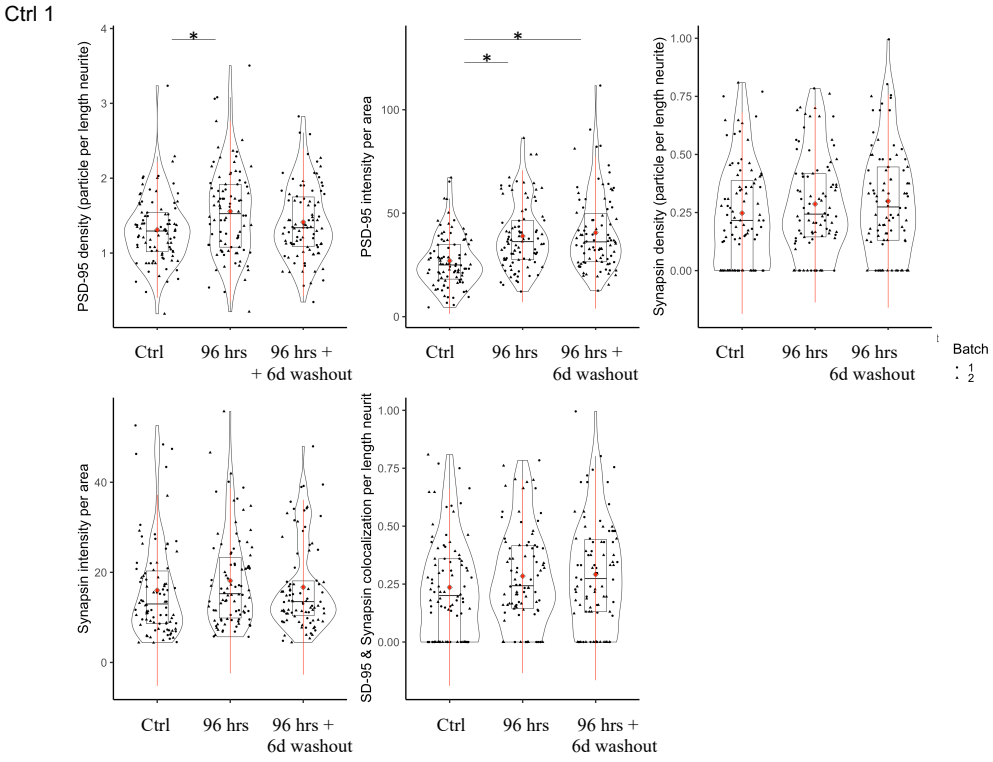

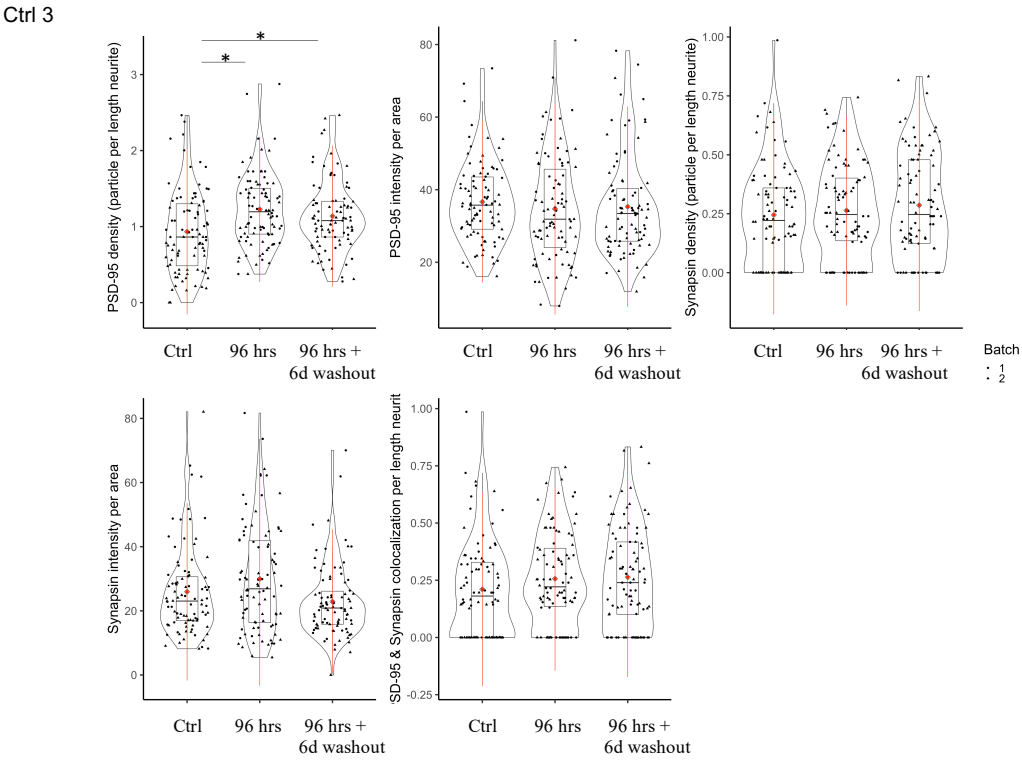

Figure 45. Appendix 17B of Figure 17J-N. Long-term effect of psilocin on dendritic synapsin and PSD-95 co-localization.

(A) PSD-05 particle per length neurite and intensity per area and synapsin/ PSD-95 co-localization was significantly increased 96 hrs after permanent 10 µM psilocin treatment (96 hrs) and 6 days after 96 hrs permanent psilocin (96 hrs + 6d washout) treatment compared to an untreated control condition (Ctrl). Ctrl with $N = 180$ neurites; 96 hrs with $N = 180$ neurites, 96 hrs + 6d washout with $N = 180$ neurites. **(B)** Descriptive statistics and post hoc p-values for data shown in **(A)**. **(C)** Two Ctrl cell lines were included in the analysis: Ctrl 1 (Ctrl with $N = 90$ neurites; 96 hrs with $N = 90$ neurites, 96 hrs + 6d washout with $N = 90$ neurites). Ctrl 3 (Ctrl with $N = 90$ neurites; 96 hrs with $N = 90$ neurites, 96 hrs + 6d washout with $N = 90$ neurites); Kruskal-Wallis-Test for independent samples was calculated. Bonferroni-correction, adjusted $p < .05$, mean ± SD. Significance levels against the respective control are $*p < 0.05$.

A

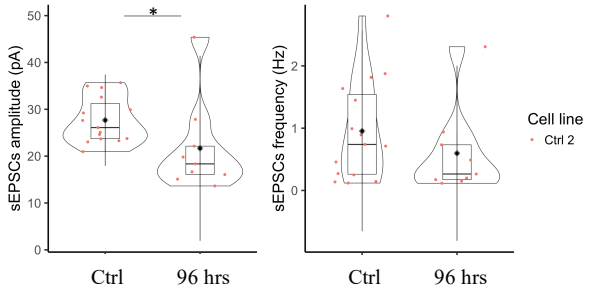

B

Amplitude	N	Mean	SD	Median	Min	Max	Range	Statistic Ctrl vs.
Ctrl	15	27,68	4,88	26,1	20,96	35,68	14,72	
96 hrs	9	21,66	9,87	18,35	13,64	45,38	31,75	1,00E-02
Frequency								
Ctrl	15	0,95	0,8	0,74	0,12	2,8	2,68	
96 hrs	9	0,6	0,7	0,26	0,12	2,31	2,19	2,90E-01

C

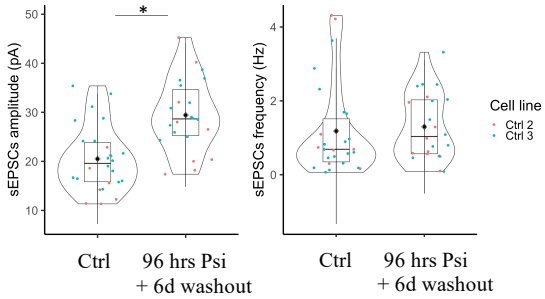

D

Amplitude	N	Mean	SD	Median	Min	Max	Range	Statistic Ctrl vs.
Ctrl	26	20,5	6,63	19,59	11,33	35,39	24,06	
96 hrs Psi + 6d washout	22	29,43	7,32	28,66	17,38	45,24	27,86	8,10E-05
Frequency								
Ctrl	26	1,18	1,26	0,69	0,07	4,31	4,25	
96 hrs Psi + 6d washout	22	1,3	0,9	1,04	0,09	3,32	3,23	3,20E-01

Figure 46. Appendix 18 of Figure 18A, C. Psilocin induced electrophysiological changes in synaptic properties over time.
(A) Significant decrease in sEPSCs amplitude, with unchanged frequency after 96 hrs permanent 10 µM psilocin administration (96 hrs). One Ctrl cell lines was included in the analysis. Ctrl with $N = 15$ cells, 96 hrs with $N = 9$ cells were measured. (**B**) Descriptive statistics and post hoc *p*-values for data shown in **(A)**. Marked in yellow, if significant. (**C**) Significant increase in sEPSCs amplitude, with unchanged frequency, 6 days washout after 96 hrs permanent 10 µM psilocin administration (96 hrs Psi + 6d washout). Two Ctrl cell lines were included in the analysis. Ctrl with $N = 26$ cells, 96 hrs Psi + 6d washout with $N = 22$ cells were measured. Ctrl 2 Ctrl $N = 8$ cells, 96 hrs Psi + 6d washout with $N = 9$ cells. Ctrl 3 with Ctrl $N = 18$ cells, 96 hrs Psi + 6d washout with $N = 13$ cells. (**D**) Descriptive statistics and post hoc *p*-values for data shown in **(C)**. Marked in yellow, if significant. For all experiments Mann-Whitney-U-test for independent samples was calculated, ± *SD*. Significance levels against the respective control are $*p < 0.05$. Marked in yellow, if significant. Electrophysical measurements were performed by Dr. Mahnaz Davoudi.

A

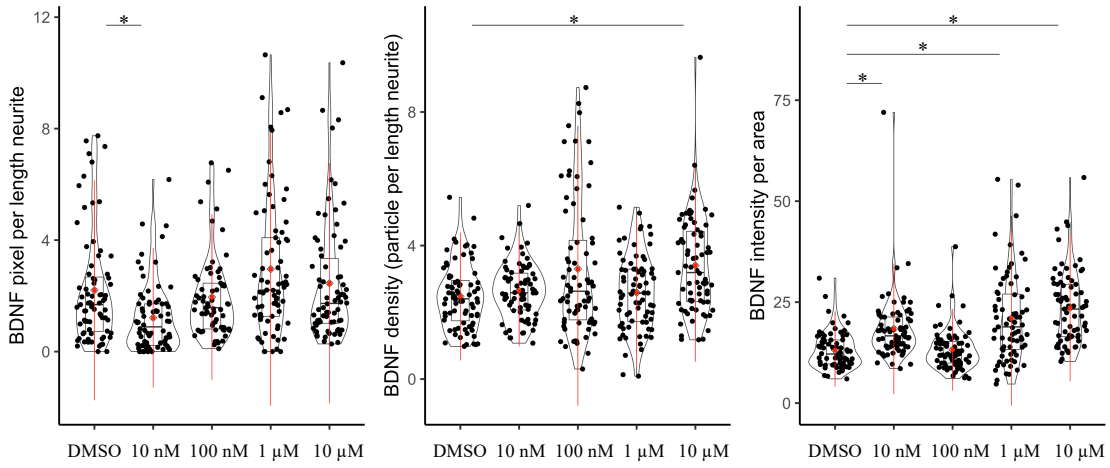

B

BDNF								
Pixel	**N**	**Mean**	**SD**	**Median**	**Min**	**Max**	**Range**	**Statistic Ctrl vs.**
DMSO	76	2,2	1,97	1,69	0	7,74	7,74	
10 nM	74	1,21	1,25	0,89	0	6,17	6,17	2,00E-03
100 nM	69	1,95	1,49	1,58	0,1	6,77	6,67	1,00E+00
1 µM	73	2,96	2,45	2,21	0	10,65	10,65	3,43E-01
10 µM	74	2,45	2,16	1,73	0,27	10,36	10,09	1,00E+00
Particle								
DMSO	76	2,48	0,96	2,4	0,98	5,45	4,47	1,00E+00
10 nM	75	2,65	0,83	2,58	1,08	5,2	4,12	6,85E-01
100 nM	75	3,3	2,05	2,63	0,3	8,73	8,43	1,00E+00
1 µM	75	2,59	1,12	2,58	0,09	5,15	5,06	2,80E-04
10 µM	75	3,4	1,44	3,19	1,18	9,64	8,46	
Intensity								
DMSO	76	13,12	4,51	12,15	6	30,94	24,94	
10 nM	75	18,38	8,09	16,65	8,54	71,98	63,44	1,30E-07
100 nM	75	13,21	5,07	12,03	6,1	38,74	32,64	1,00E+00
1 µM	75	20,91	10,78	18,87	4,72	55,4	50,68	3,30E-06
10 µM	75	23,63	9,1	23,29	10,33	55,86	45,53	5,10E-14

Figure 47. Appendix 19A of Figure 19B. Influence of different psilocin concentrations on BDNF level.

(A) BDNF particle per length neurite and BDNF intensity per area were significantly increased 24 hrs after 10 min 10 µM Psilocin trigger (10 µM). 10 min after a 10 nM and a 1 µM Psilocin trigger BDNF intensity per area was significantly increased compared to the DMSO control condition. One Ctrl cell line was included in the analysis, with one biological batch. (DMSO Ctrl with $N = 76$ neurites; 24 hrs after a 10 min 10 nM with $N = 74$ - 75 neurites, respectively 100 nM with $N = 69$ - 75 neurites, respectively 1 µM with $N = 73$ - 75 neurites, respectively 10 µM with $N = 74$ - 75 neurites psilocin trigger. Kruskal-Wallis test for independent samples was calculated. Post hoc Wilcoxon rank sum test. Bonferroni-correction, adjusted $p < .05$, mean ± *SD*. Significance levels against the respective control are $*p < 0.05$ **(B)** Descriptive statistics and post hoc *p*-values for data shown in **(A)**. Marked in yellow, if significant.

A

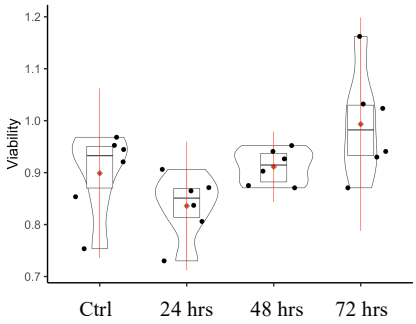

B

Cell viability	*N*	Mean	SD	Median	Min	Max	Range	Statistic Ctrl vs.
Ctrl	6	0,9	0,08	0,93	0,75	0,97	0,21	
24 hrs	6	0,84	0,06	0,85	0,73	0,91	0,18	7,92E-01
48 hrs	6	0,91	0,03	0,91	0,87	0,95	0,08	1,00E+00
72 hrs	6	0,99	0,1	0,98	0,87	1,16	0,29	1,00E+00

Figure 48. Appendix 19B of Figure 19C. Influence of psilocin concentrations on cell viability.
(A) Cell viability assay demonstrates no significant change in cell viability up to 72 hrs after 10 min 10 µM psilocin treatment. One Ctrl cell line 3 was included in the analysis. For each condition $N = 6$ technical replicates were included. (**B**) Descriptive statistics and post hoc *p*-values for data shown in **(A)**. Post hoc Wilcoxon rank sum test. Kruskal-Wallis test for independent samples was calculated. Bonferroni-correction, adjusted $p < .05$, mean ± *SD*. Significance levels against multiple group comparisons are $*p < 0.05$. Marked in yellow, if significant.

A

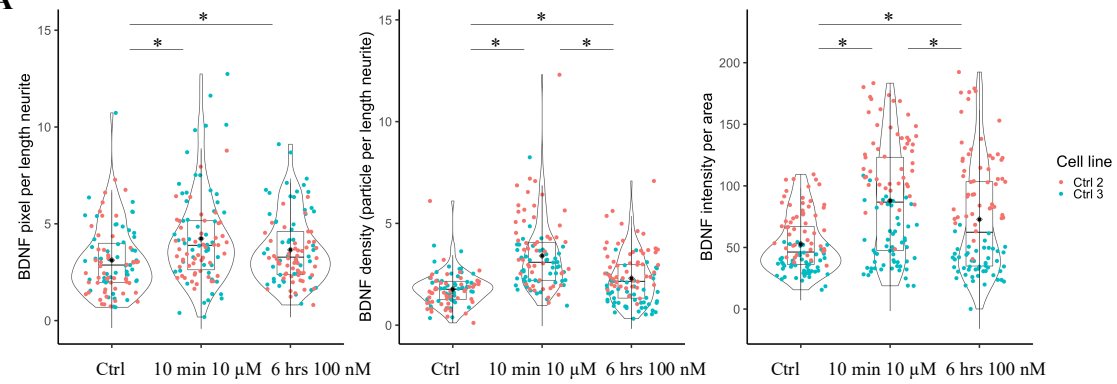

B

Pixel	N	Mean	SD	Median	Min	Max	Range	Statistic Ctrl vs.	10 min vs. 6 hrs
Ctrl	99	3,12	1,75	2,87	0,69	10,73	10,4		
10 min 10 µM	102	4,24	2,33	3,89	0,19	12,74	12,55	3,40E-04	
6 hrs 100 nM	102	3,66	1,74	3,28	0,81	9,11	8,3	4,08E-02	2,12E-01
Particle									
Ctrl	99	1,77	0,83	1,76	0,11	6,1	5,99		
10 min 10 µM	102	3,41	1,72	3,09	0,96	12,3	11,35	< 2E-16	
6 hrs 100 nM	102	2,3	1,24	2,15	0,32	7,08	6,77	7,30E-03	5,22E-07
Intensity									
Ctrl	102	52,77	22,83	46,29	15,59	109,35	93,76		
10 min 10 µM	104	88,05	44,86	86,8	18,84	183,4	164,56	3,10E-08	
6 hrs 100 nM	104	72,78	44,41	62,33	0,06	192, 41	192,35	2,70E-02	2,50E-02

C

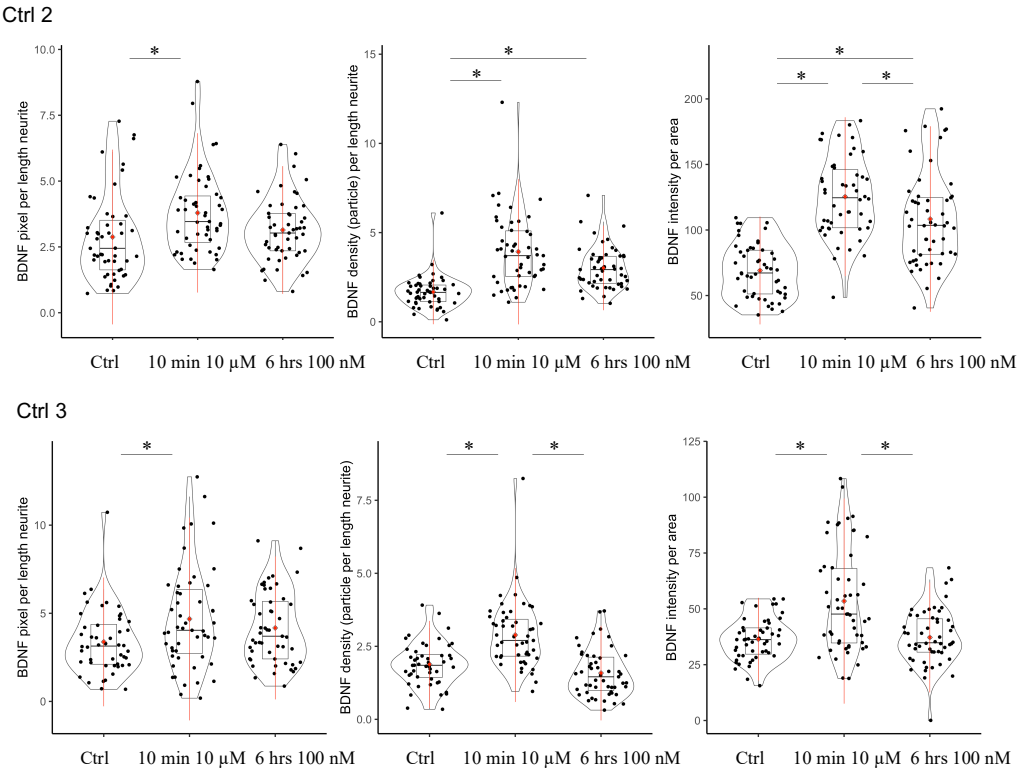

Figure 49. Appendix 19C of Figure 19E. Influence of artificial (10 min 10 µM) psilocin trigger versus physiological (6 hrs 100 nM) psilocin stimulation on BDNF level.
(A) BDNF pixel, particle per length neurite and intensity per area were significantly increased 24 hrs after a 10 min 10 µM psilocin trigger (10 min 10 µM) and 24 hrs after a 6 hrs 100 nM psilocin stimulation (6 hrs 100 nM). BDNF particle per length neurite and intensity per area were significantly increased for the artificial compared to the physiological stimulation. (Ctrl with $N = 99$ - 102 neurites; 10 min 10 µM with $N = 102$ - 104 neurites; 6 hrs 100 nM with $N = 102$ - 104 neurites). **(B)** Descriptive statistics and post hoc p-values for data shown in **(A).** Marked in yellow, if significant. **(C)** Two Ctrl cell lines were included in the analysis, each with one biological batch. Ctrl 2 with (Ctrl with $N = 51$ neurites; 10 min 10 µM with $N = 50$ - 51 neurites; 6 hrs 100 nM with $N = 51$ - 52 neurites). Ctrl 3 with (Ctrl with $N = 48$ - 51 neurites; 10 min 10 µM with $N = 51$ - 54 neurites; 6 hrs 100 nM with $N = 51$ - 52 neurites). Post hoc Wilcoxon rank sum test. Kruskal-Wallis test for independent samples was calculated. Bonferroni-correction, adjusted $p < .05$, mean ± *SD*. Significance levels against multiple group comparisons are $*p < 0.05$.

A

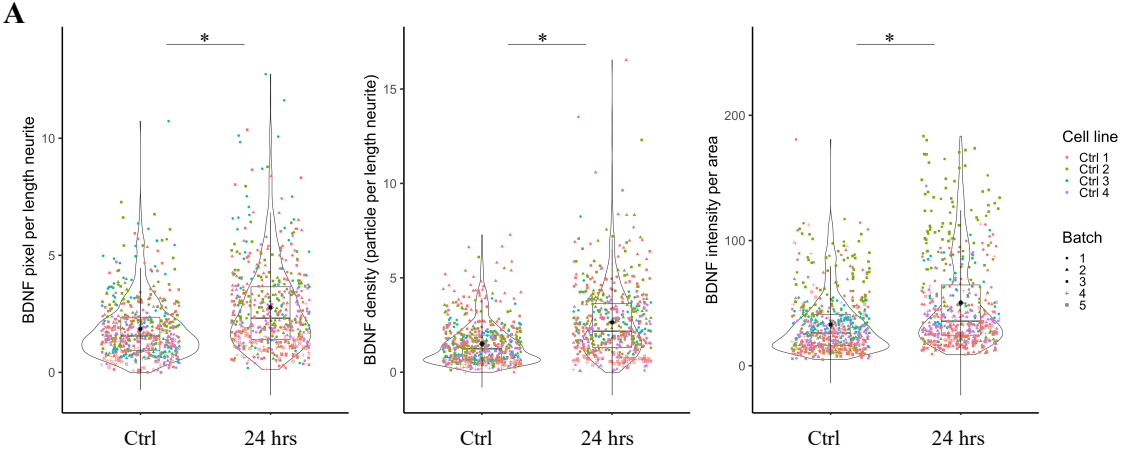

B

Pixel	N	Mean	SD	Median	Min	Max	Range	Statistic Ctrl vs.
Ctrl	564	1,86	1,3	1,55	0	10,73	10,73	
24 hrs	527	2,77	1,88	2,32	0,13	12,74	12,61	< 2E-16
Particle								
Ctrl	613	1,5	1,16	1,24	0	7,28	7,28	
24 hrs	529	2,64	1,93	2,17	0	16,54	16,54	< 2E-16
Intensity								
Ctrl	616	32,84	23,41	26,19	4,96	180,78	175,82	
24 hrs	531	50,23	36,92	35,67	8,9	183,4	174,5	< 2E-16

C

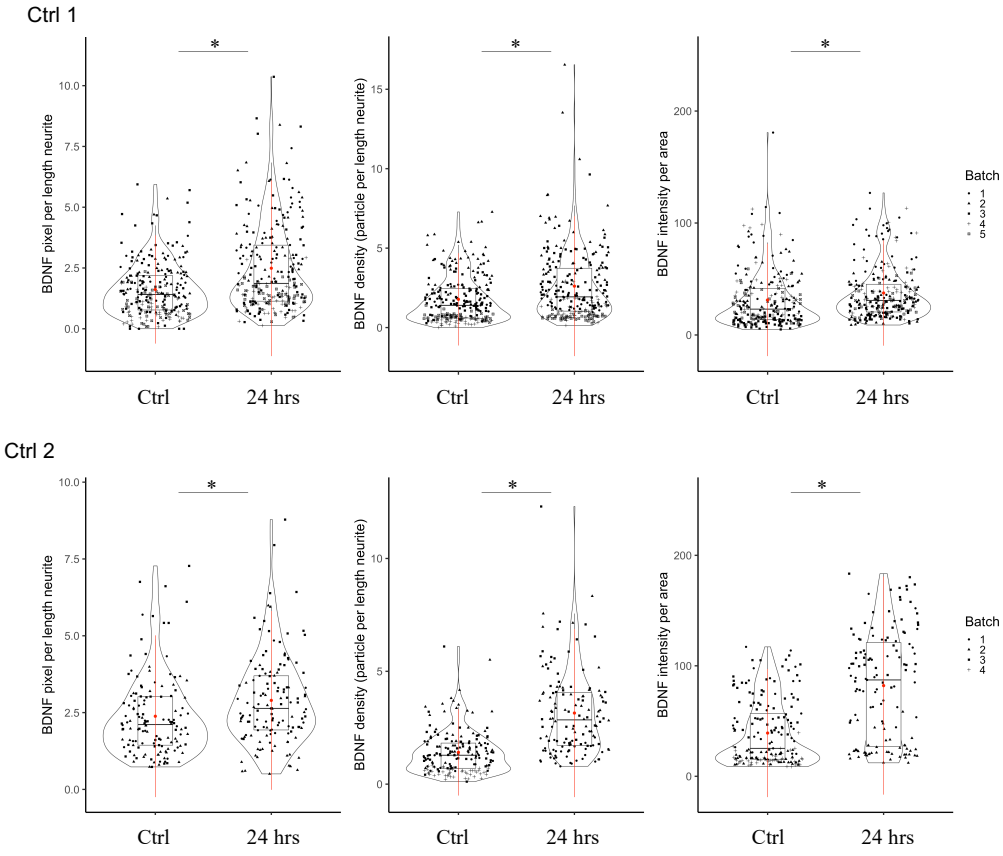

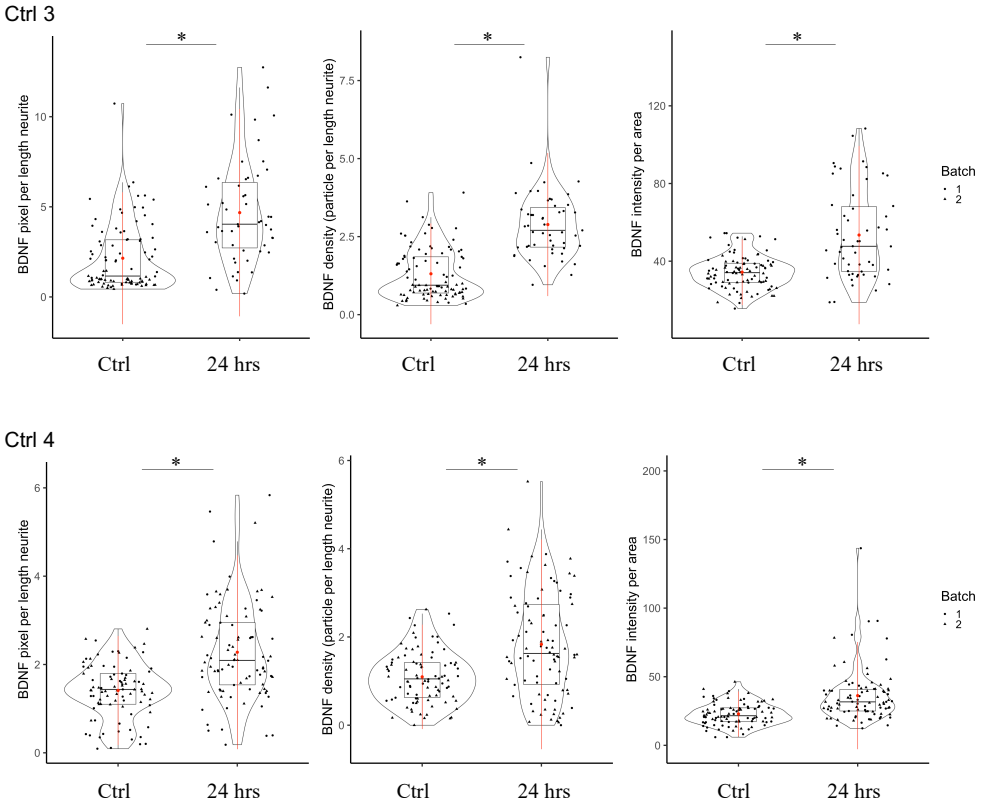

Figure 50. Appendix 20A of Figure 20C. Psilocin induced BDNF level increase.
(A) BDNF pixel and particle per length neurite and BDNF intensity were significantly increased 24 hrs after a 10 min 10 µM psilocin trigger (24 hrs). Four Ctrl cell lines were included in the analysis (Ctrl with N = 564 - 616 neurites; 24 hrs with N = 527 - 531 neurites). **(B)** Descriptive statistics and post hoc p-values for data shown in **(A)**. Marked in yellow, if significant. **(C)** Ctrl 1 with 5 biological batches (Ctrl with N = 245 - 249 neurites; 24 hrs with N = 251 - 252); Ctrl 2 with 4 (3 for BDNF pixel per length neurite) biological batches (Ctrl with N = 136 - 181 neurites; 24 hrs with N = 135 - 136 neurites); Ctrl 3 with 2 biological batches (Ctrl with N = 93 - 96 neurites; 24 hrs with N = 51 – 54 neurites); Ctrl 4 with 2 biological batches (Ctrl with N = 90 neurites; 24 hrs with N = 90 neurites). Kruskal-Wallis test for independent samples was calculated. Post hoc Wilcoxon rank sum test. Bonferroni-correction, adjusted $p < .05$, mean ± SD. Significance levels against the respective control are *$p <$ 0.05.

A

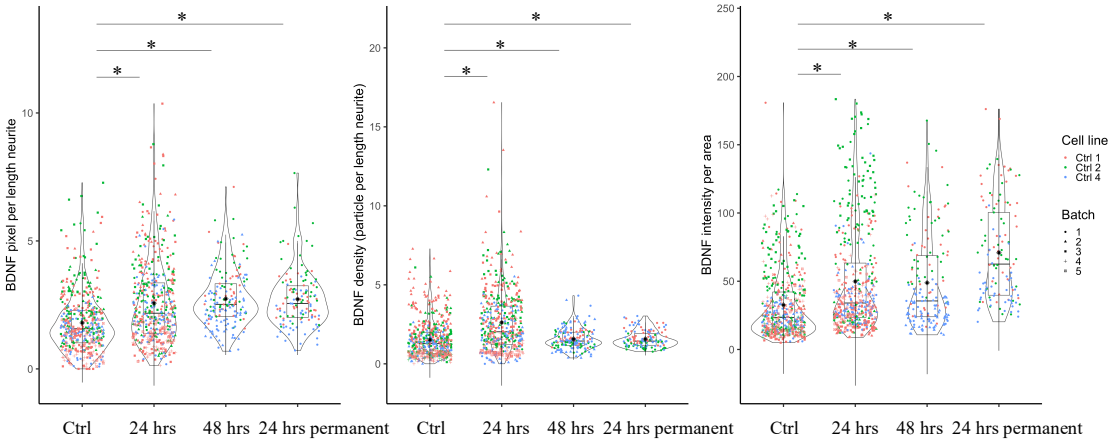

B

Pixel	N	Mean	SD	Median	Min	Max	Range	Statistic Ctrl vs.
Ctrl	471	1,8	1,16	1,57	0	7,27	7,27	
24 hrs	476	2,57	1,61	2,18	0,13	10,36	10,23	1,90E-14
48 hrs	170	2,74	1,1	2,52	0,69	7,11	6,42	<2 E-16
24 hrs permanent	130	2,72	1,09	2,56	0,72	7,65	6,93	<2 E-16
Particle								
Ctrl	520	1,53	1,21	1,28	0	7,28	7,28	
24 hrs	478	2,62	2	2,03	0	16,54	16,54	< 2E-16
48 hrs	170	1,58	0,66	1,44	0,37	4,32	3,94	3,40E-03
24 hrs permanent	125	1,58	0,52	1,44	0,77	3,03	2,26	2,10E-03
Intensity								
Ctrl	520	32,57	25,21	23,47	4,96	180,78	175,82	
24 hrs	477	49,86	38,18	34,04	8,9	183,4	174,5	< 2E-16
48 hrs	170	48,87	33,48	35,56	10,72	167,69	156,97	1,4 E-11
24 hrs permanent	125	70,9	55,91	62,56	20,26	176,13	155,87	< 2E-16

C

Ctrl 1

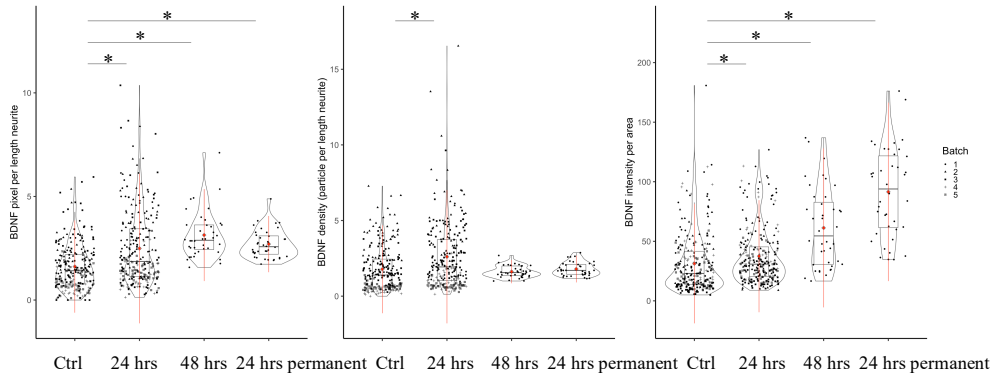

Ctrl 2

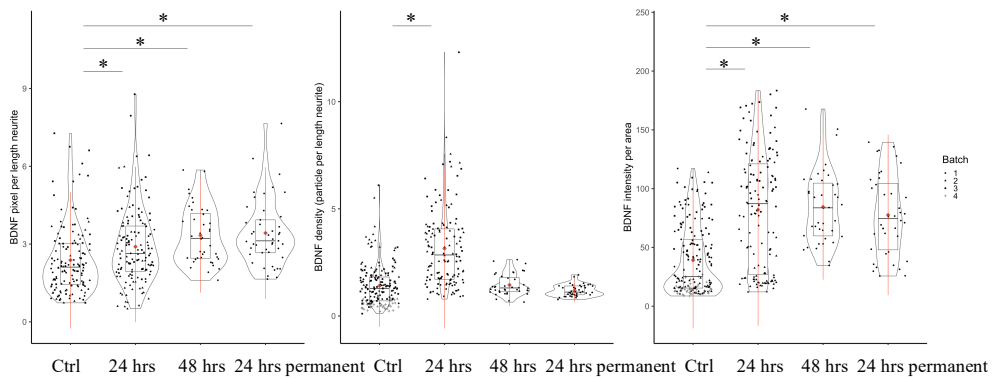

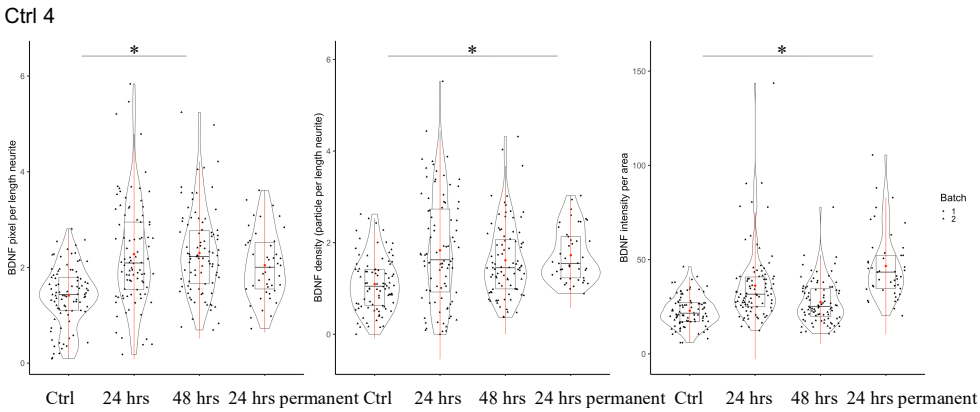

D

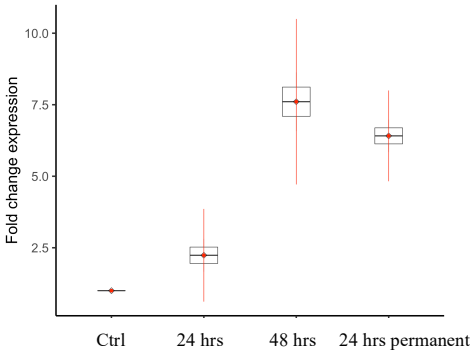

E

BDNF	*N*	Mean	SD	Median	Min	Max	Range
Ctrl	2	1	0	1	1	1	0
24 hrs	2	2,24	0,81	2,24	1,66	2,81	1,15
48 hrs	2	7,61	1,45	7,61	6,58	8,63	2,04
24 hrs permanent	2	6,41	0,79	6,41	5,85	6,95	1,12

Figure 51. Appendix 20B of Figure 20E-F. Psilocin-induced BDNF level increase for different treatment conditions.

(A) BDNF pixel and particle per length neurite and BDNF intensity were significantly increased 24 and still 48 hrs after a 10 min 10 µM psilocin trigger (24 hrs; 48 hrs) and after permanent psilocin administration (24 hrs permanent). Three Ctrl cell lines were included in the analysis (Ctrl with N = 471- 520 neurites; 24 hrs with N = 476 - 478 neurites; 48 hrs with N = 170 neurites; 24 hrs permanent with N = 125 - 130 neurites). **(B)** Descriptive statistics and post hoc p-values for data shown in **(A)**. Marked in yellow, if significant. **(C)** Ctrl 1 with 5 biological batches (Ctrl with N = 245 - 249 neurites; 24 hrs with N = 251 - 252 neurites; 48 hrs with N = 40 neurites; 24 hrs permanent with N = 40 neurites); Ctrl 2 with 4 (3 for BDNF pixel per length neurite) biological batches (Ctrl with N = 136 - 181 neurites; 24 hrs with N = 135 - 136 neurites; 48 hrs with N = 40 neurites; 24 hrs permanent with N = 45 neurites); Ctrl 4 with 2 biological batches (Ctrl with N = 90 neurites; 24 hrs with N = 90 neurites; 48 hrs with N = 90 neurites; 24 hrs permanent with N = 45 neurites). Kruskal-Wallis test for independent samples was calculated. Post hoc Wilcoxon rank sum test. Bonferroni-correction, adjusted $p < .05$, mean ± SD. Significance levels against the respective control are *$p < 0.05$. **(D)** RT-qPCR revealed increase in *BDNF* gene expression 24 and still 48 hrs after a 10 min 10 µM psilocin trigger and after permanent psilocin administration. One BD1 3 cell line was included (Ctrl with N = 2 technical replicates; 24 hrs with N = 2 technical replicates; 48 hrs with N = 2 technical replicates, 24 hrs permanent with N = 2 technical replicates). **(E)** Descriptive statistics for data shown in **(D)**, no statistics were calculated.

A

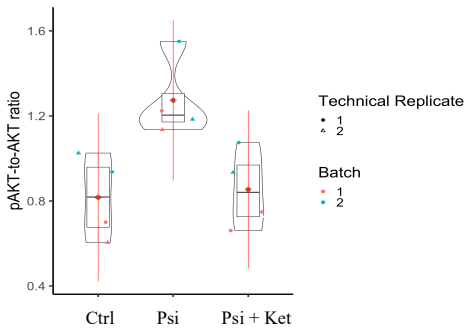

B

pAkt-to-Akt ratio	*N*	Mean	SD	Median	Min	Max	Range	Statistic Ctrl vs.
Ctrl	4	0,82	0,2	0,82	0,6	1,03	0,42	
Psi	4	1,27	0,19	1,2	1,14	1,55	0,42	8,60E-02
Psi + Ket	4	0,85	0,19	0,84	0,66	1,07	0,41	1,00E+00

Figure 52. Appendix 21 of Figure 21E. Psilocin induced activation of prosurvival AKT downstream cascade.

(A) pAKT protein level was non significantly increased 72 hrs after psilocin exposure (Psi), not significantly reversed by ketanserin (selective 5-HT2A-R antagonist) co-treatment (Psi + Ket). Ctrl cell line 3 with two biological batches was included in the analysis (Ctrl with $N = 4$ data points, Psi with $N = 4$ data points; Psi + Ket with $N = 4$ data points). For analysis Kruskal-Wallis test for independent samples was calculated. Post hoc Wilcoxon rank sum test. Bonferroni-correction, adjusted $p < .05$, mean ± *SD*. Significance levels against the respective control are $*p < 0.05$. **(B)** Descriptive statistics and post hoc *p*-values for data shown in **(A)**. Marked in yellow, if significant. pAKT, phosphorylated AKT.

A

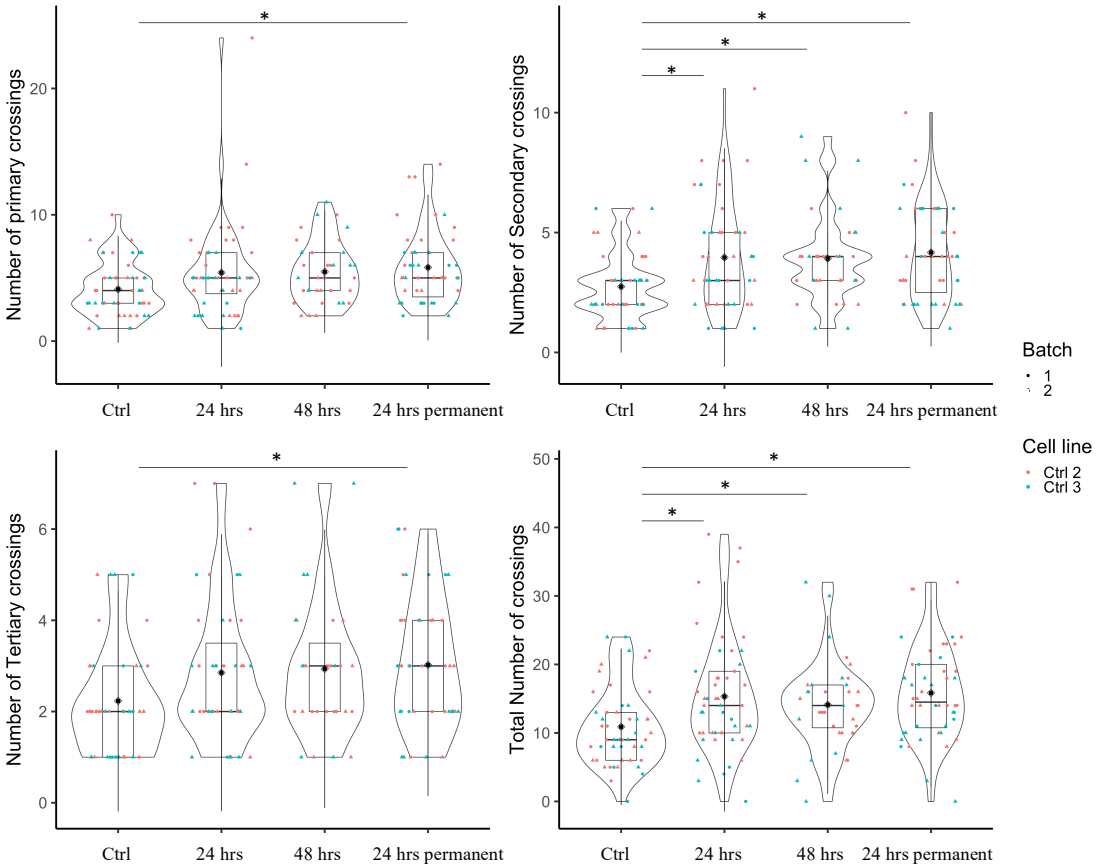

B

R1	N	Mean	SD	Median	Min	Max	Range	Statistic Ctrl vs.
Ctrl	48	4,10	2,12	4	1	10	9	
24 hrs	48	5,42	3,72	5	2	24	23	2,72E-01
48 hrs	35	5,49	2,42	5	2	11	9	6,00E-02
24 hrs permanent	47	5,83	2,88	5	2	14	12	1,30E-02
R2								
Ctrl	47	2,74	1,37	3	2,62	6	5	
24 hrs	48	3,96	2,28	3	3,78	11	10	4,87E-02
48 hrs	34	3,91	1,83	4	3,71	9	8	7,70E-03
24 hrs permanent	47	4,17	1,96	4	4,03	10	9	1,40E-03
R3								
Ctrl	43	2,23	1,21	2	1	5	4	
24 hrs	47	2,85	1,52	2	1	7	6	2,09E-01
48 hrs	31	2,94	1,53	3	1	7	6	1,57E-01
24 hrs permanent	46	3,02	1,44	3	1	6	5	3,70E-02
R4								
Ctrl	35	1,86	0,91	2	1	5	4	
24 hrs	45	2,16	1,35	2	1	7	6	1,00E+00
48 hrs	25	2,12	0,97	2	1	4	3	1,00E+00
24 hrs permanent	42	2,07	1,07	2	1	6	5	1,00E+00
R5								
Ctrl	29	1,62	0,73	2	1	4	3	
24 hrs	43	1,63	0,93	1	1	5	4	1,00E+00
48 hrs	22	1,77	0,61	2	1	3	2	1,00E+00
24 hrs permanent	37	1,73	0,93	2	1	5	4	1,00E+00
Sum								
Ctrl	49	10,90	5,71	9	0	24	24	
24 hrs	49	15,33	8,40	14	0	39	39	1,58E-02
48 hrs	36	14,11	6,50	14	0	32	32	4,39E-02
24 hrs permanent	48	15,83	6,83	14,5	0	32	32	7,30E-04

C

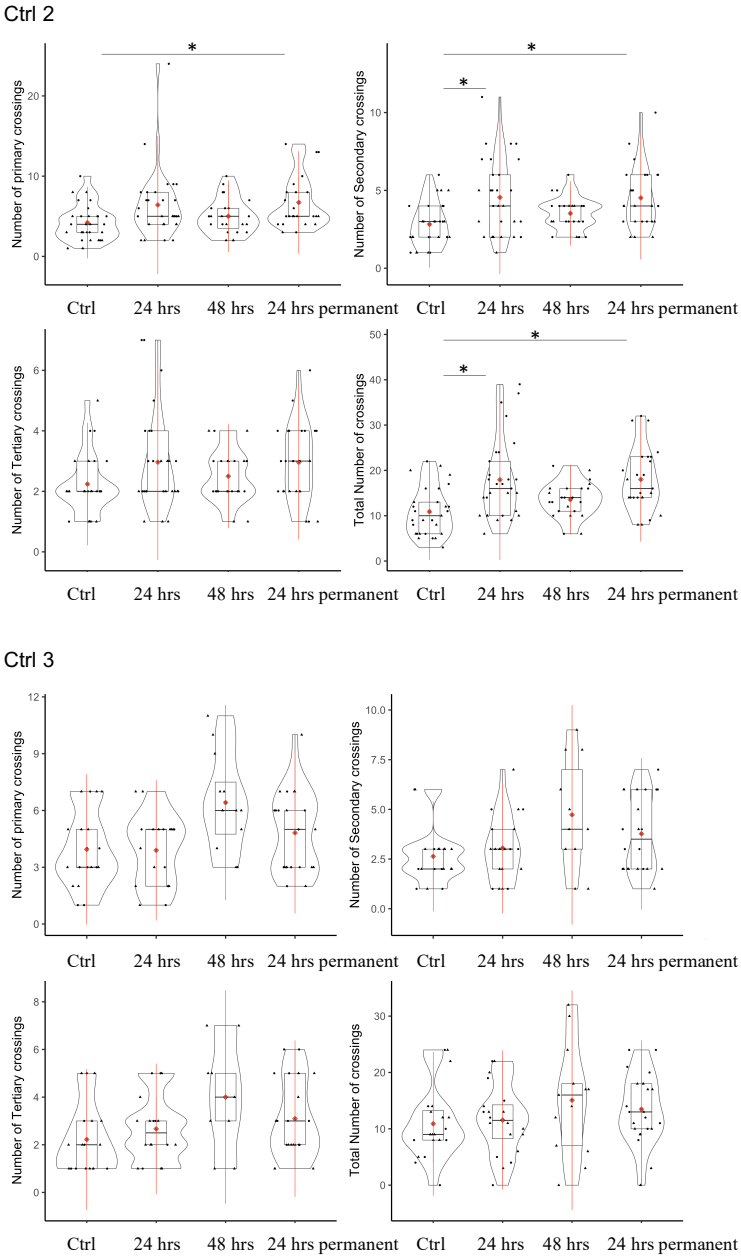

Figure 53. Appendix 22 of Figure 22B. Psilocin induced increase in neurite complexity.
(A) Sholl singular analysis: 24 hrs after permanent psilocin administration (24 hrs permanent) the number of primary (25 µm distance from soma) and tertiary (75 µM distance to the soma) crossings significantly increased compared to the untreated control condition (Ctrl). The number of secondary crossings (50 µm distance from soma) and the total number of neurite crossings significantly increased 24 (short and permanent) and 48 hrs after a 10 min 10 µM psilocin trigger. Two Control cell lines with two biological batches (Ctrl with $N = 43$ - 48 neurites; 24 hrs with $N = 47$ - 48 neurites; 48 hrs with $N = 31$ - 35 and 24 hrs permanent with $N = 46$ - 47 neurites were included. **(B)** Descriptive statistics and post hoc p-values for data shown in **(A)**. Marked in yellow, if significant. **(C)** Ctrl 2 with Ctrl with $N = 25$ - 29 neurites; 24 hrs with $N = 29$ neurites; 48 hrs with $N = 22$ - 23 and 24 hrs permanent with $N = 25$ neurites; Ctrl 3 with Ctrl with $N = 18$ - 20 neurites; 24 hrs with $N = 18$ - 20 neurites; 48 hrs with $N = 9$ - 13 and 24 hrs permanent with $N = 21$ - 23 neurites. For all statistical analysis Kruskal-Wallis test for independent samples was calculated. Bonferroni-correction, adjusted $p < .05$, mean ± *SD*. Significance levels against the respective control are $*p < 0.05$.

A

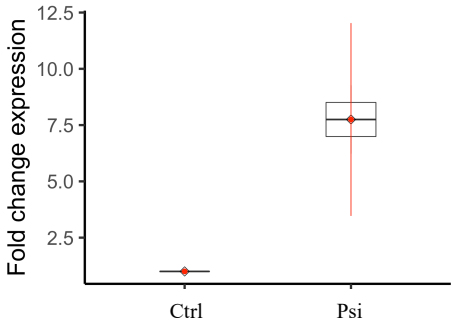

B

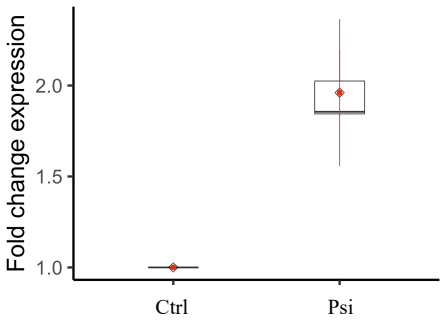

C

cFOS	*N*	Mean	SD	Median	Min	Max	Range
Ctrl	3	1	0	1	1	1	0
Psi	2	7,75	2,14	7,74	6,23	9,26	3,03

D

EGR2	*N*	Mean	SD	Median	Min	Max	Range
Ctrl	3	1	0	1	1	1	0
Psi	3	1,96	0,2	1,86	1,83	2,19	0,36

Figure 54. Appendix 23 of Figure 23B, E. Psilocin induced increase in immediate early genes.
(A) *cFOS* gene expression 24 hrs after permanent 10 µM psilocin administration was increased, validated by RT-qPCR. One control cell line was included (Ctrl with N = 3 technical replicates; Psi with N = 2-3 technical replicates). **(B)** RT-qPCR revealed an increase in *EGR2* gene expression 24 after permanent 10 µM psilocin administration. One control cell line was included (Ctrl with N = 3 technical replicates; Psi with N = 2 - 3 technical replicates). **(C-D)** Descriptive statistics for data shown in **(A-B)**, no statistics were calculated.

A

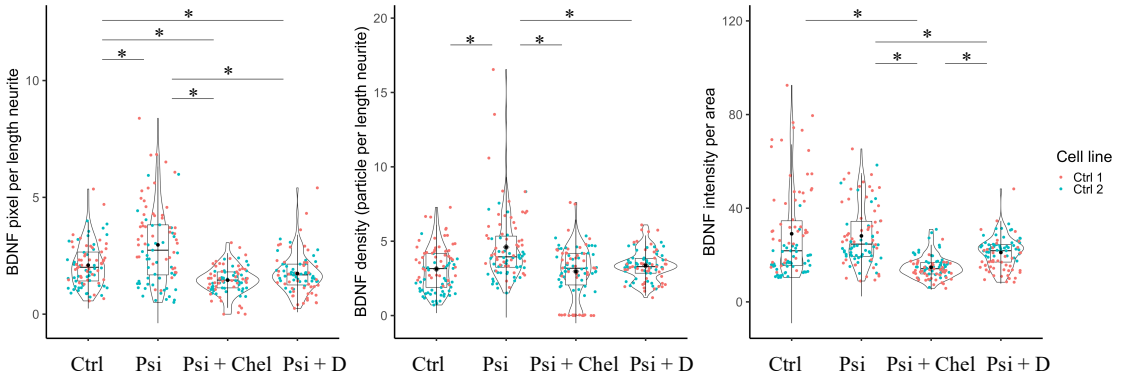

B

Pixel	N	Mean	SD	Median	Min	Max	Range	Statistic Ctrl vs.	Psi vs.
Ctrl	90	2.01	0.93	2	0.57	5.36	4.79		
Psi	89	2.97	1.68	2.74	0.5	8.39	7.88	2.80E-02	
Psi + Chel	90	1.45	0.58	1.46	0	3.06	3.06	1.10E-05	3.80E-10
Psi + D	90	1.74	0.83	1.68	0.25	5.41	5.16	3.92E-02	1.00E-06
Particle									
Ctrl	90	3.13	1.48	3.16	0.71	7.28	6.57		
Psi	90	4.6	2.37	3.95	1.52	16.54	15.03	1.5E-05	
Psi + Chel	90	2.97	1.74	3.18	0	7.60	7.60	1.00E+00	6.1E-05
Psi + D	90	3.36	1.01	3.29	1.2	6.10	4.89	1.00E+00	0.00022
Intensity									
Ctrl	90	29.08	19.09	21.84	10.38	92.5	82.12		
Psi	90	28.18	12.91	24.66	8.9	65.34	56.44	1.00E+00	
Psi + Chel	90	14.79	4.8	14.19	5.77	30.97	25.2	4.6E-10	6.30E-16
Psi + D	90	21.1	6.66	21.86	8.4	48.25	39.85	8.14E-01	2.70E-03

C

Ctrl 1

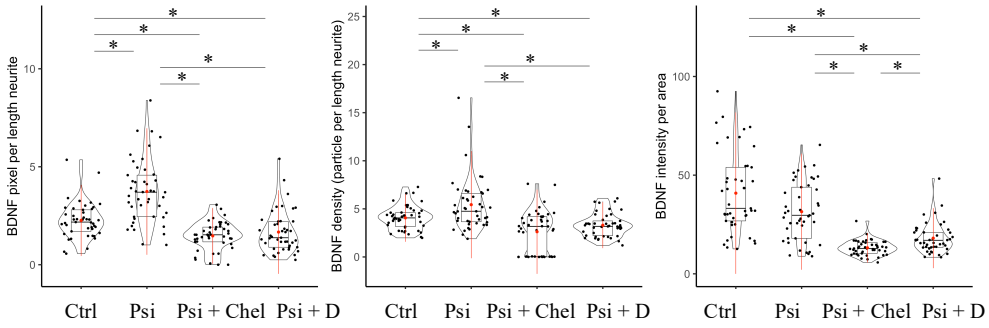

Ctrl 2

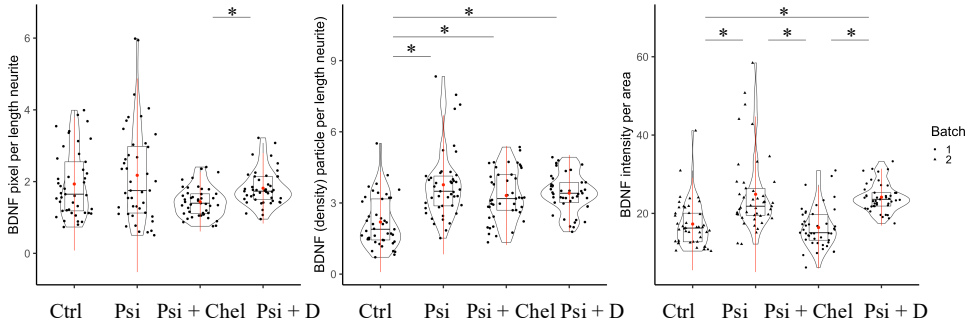

D

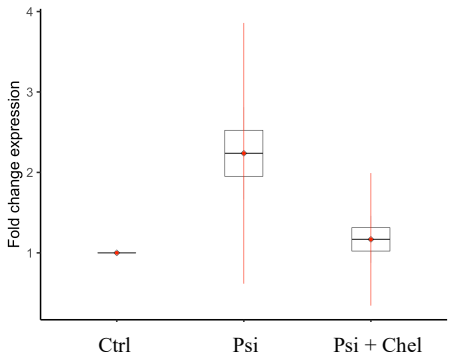

E

BDNF	*N*	Mean	SD	Median	Min	Max	Range
Ctrl	2	1	0	1	1	1	0
Psi	2	2,24	0,81	2,24	1,66	2,81	1,15
Psi + Chel	2	1,17	0,41	1,17	0,88	1,46	0,58

Figure 55. Appendix 24 of Figure 24B, D. Influence of chelerythrine and dynasore co-treatment on BDNF level.

(A) BDNF pixel and particle per length neurite were significantly increased 24 after a 10 min 10 µM psilocin trigger (Psi) compared to a Ctrl condition (Ctrl). BDNF intensity per area increased non-significantly. For chelerythrine (Psi + Chel) and dynasore (Psi + D) co-treatment pixel and particle per length neurite and BDNF intensity per area were significantly reduced compared to the psilocin condition. BDNF intensity per area for the chelerythrine co-treatment was significantly reduced compared to the dynasore co-treatment condition. BDNF pixel per length neurite were significantly reduced for the chelerythrine and dynasore co-treatment compared to the Ctrl condition. BDNF intensity per area was significantly reduced for the chelerythrine co-treatment to the Ctrl condition. Two Ctrl cell lines were included in the analysis, each with one biological batch. (Ctrl with $N = 90$ neurites; Psi with $N = 89$ - 90 neurites; Psi + Chel with $N = 90$ neurites; Psi + D with $N = 90$ neurites). **(B)** Descriptive statistics and post hoc *p*-values for data shown in **(A)**. Marked in yellow, if significant. **(C)** Ctrl 1 (Ctrl with $N = 45$ neurites; Psi with $N = 45$ neurites; Psi + Chel with $N = 45$ neurites; Psi + D with $N = 45$ neurites); Ctrl 2 (Ctrl with $N = 45$ neurites; Psi with $N = 44$ - 45 neurites; Psi + Chel with $N = 45$ neurites; Psi + D with $N = 45$ neurites). Kruskal-Wallis test for independent samples was calculated. Post hoc Wilcoxon rank sum test. Bonferroni-correction, adjusted $p < .05$, mean ± *SD*. Significance levels against multiple group comparisons are $*p < 0.05$. **(D)** RT-qPCR revealed increase in *BDNF* gene expression, reversed by chelerythrine co-treatment. One BD1 3 cell line was included (Ctrl with $N = 2$ technical replicates; Psi with $N = 2$ technical replicates; Psi + Chel with $N = 2$ technical replicates). **(E)** Descriptive statistics for data shown in **(D)**, no statistics were calculated.

A

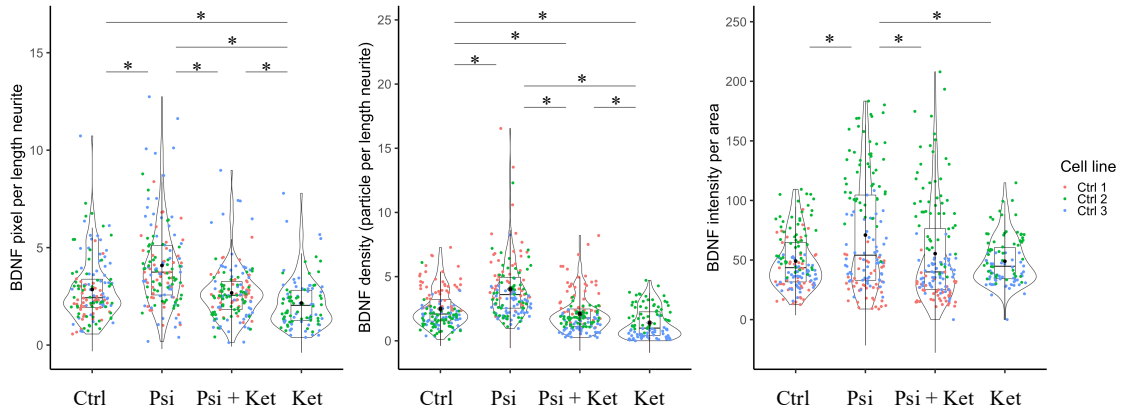

B

Pixel	N	Mean	SD	Median	Min	Max	Range	Statistic Ctrl vs.	Psi vs.	Psi + Ket vs. Ket
Ctrl	144	2,85	1,59	2,43	0,57	10,73	10,16			
Psi	147	4,08	2,14	3,74	0,19	12,74	12,55	3,90E-08		
Psi + Ket	147	2,68	1,38	2,55	0,13	8,96	8,84	1,00E+00	1,60E-10	
Ket	102	2,16	1,28	2,04	0,39	7,79	7,4	9,30E-04	1,10E-15	1,46E-03
Particle										
Ctrl	144	2,49	1,44	2,09	0,11	7,28	7,17			
Psi	147	4,03	2,3	3,6	0,96	16,54	15,59	7,50E-12		
Psi + Ket	147	2,11	1,44	1,79	0,25	8,20	7,95	3,70E-02	< 2E-16	
Ket	102	1,4	1,17	0,99	0	4,71	4,71	3,80E-09	< 2E-16	5,70E-05
Intensity										
Ctrl	147	49,13	22,73	43,63	12,62	109,35	96,74			
Psi	149	70,96	46,3	54,05	8,9	183,4	174,5	4,90E-03		
Psi + Ket	148	55,38	41,61	40,04	0,01	207,95	207,94	1,00E+00	7,50E-03	
Ket	102	48,99	19,72	44,77	0,05	114,75	114,75	1,00E+00	4,92E-02	1,00E+00

C

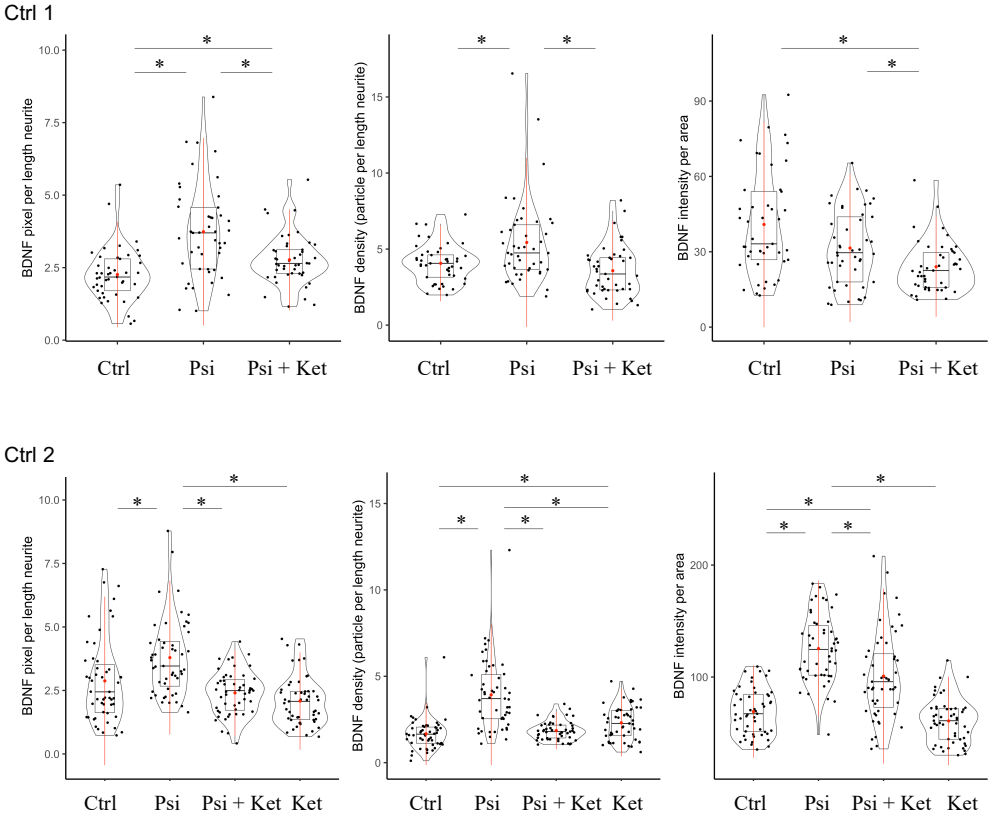

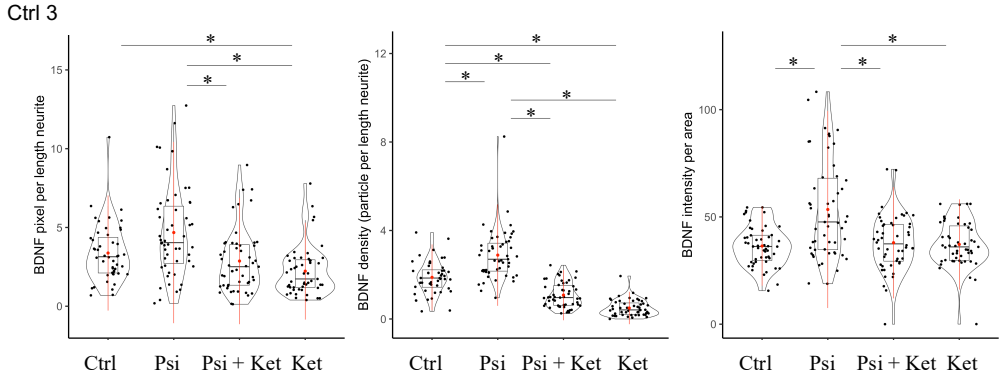

Figure 56. Appendix 25 of Figure 25B. Influence of ketanserin treatment on BDNF level.
(A) BDNF pixel, particle per length neurite and intensity per area were significantly increased 24 after a 10 min 10 µM psilocin trigger (Psi) compared to a control condition (Ctrl). Ketanserin co-treatment (Psi + Ket) and ketanserin monotreatment (Ket) significantly reduced pixel and particle per length neurite and BDNF intensity per area compared to the psilocin condition. Ketanserin monotreatment provoked a significant reduction in in BDNF pixel and particle per length neurite compared to ketanserin co-treatment with Psilocin. Ketanserin co-treatment and ketanserin monotreatment significantly reduced particle per length neurite to the Ctrl condition. Ketanserin monotreatment (24h Ket) significantly reduced pixel per length neurite to the Ctrl condition. Three Ctrl cell lines were included in the analysis, each with one biological batch. (Ctrl with $N = 144$ - 147 neurites; Psi with $N = 147$ - 149; Psi + Ket with $N = 147$ - 148 neurites; Ket with $N = 102$ neurites). **(B)** Descriptive statistics and post hoc p-values for data shown in **(A)**. Marked in yellow, if significant. **(C)** Ctrl 1: (Ctrl with $N = 45$ neurites; Psi with $N = 45$ neurites; Psi + Ket with $N = 45$ neurites). Ctrl 2: (Ctrl with $N = 51$ neurites; Psi with $N = 50$ - 51 neurites; Psi + Ket with $N = 51$ neurites; Ket with $N = 51$ neurites); Ctrl 3: (Ctrl with $N = 48$ - 51 neurites; Psi with $N = 51$ - 54 neurites; Ket with $N = 51$ - 52 neurites; Ket with $N = 51$ neurites). Kruskal-Wallis test for independent samples was calculated. Post hoc Wilcoxon rank sum test. Bonferroni-correction, adjusted $p < .05$, mean ± *SD*. Significance levels against multiple group comparisons are *$p < 0.05$.

A

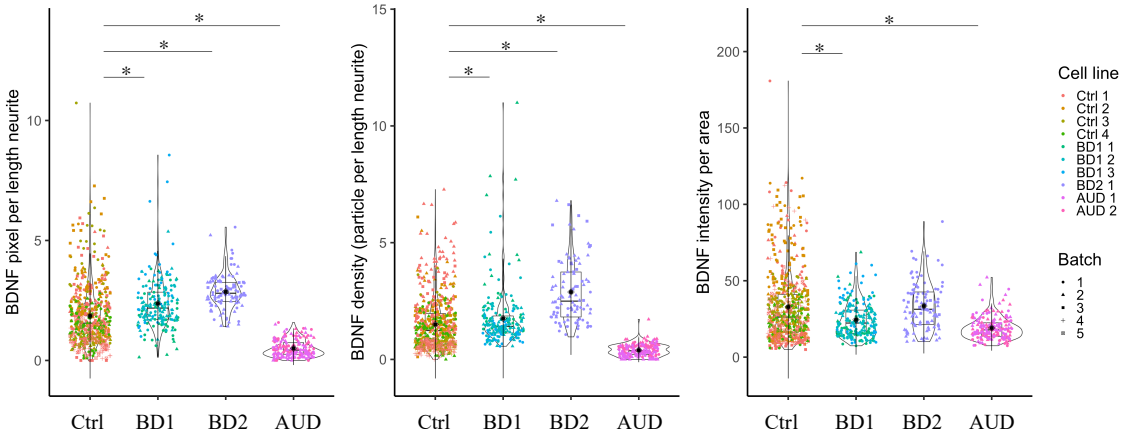

B

Pixel	N	Mean	SD	Median	Min	Max	Range	Statistic Ctrl vs.	BD 1 vs.	BD 2 vs.
Ctrl	564	1,86	1,3	1,55	0	10,73	10,73			
BD 1	185	2,38	1,1	2,18	0,13	8,56	8,43	1,10E-11		
BD 2	100	2,87	0,74	2,8	1,42	5,56	4,14	< 2E-16	4,90E-07	
AUD	180	0,51	0,35	0,43	0	1,58	1,58	< 2E-16	< 2E-16	< 2E-16
Particle										
Ctrl	613	1,5	1,16	1,24	0	7,28	7,28			
BD 1	203	1,75	1,28	1,41	0,56	10,99	10,43	6,80E-05		
BD 2	100	2,89	1,35	2,5	0,96	6,80	5,83	< 2E-16	< 2E-16	
AUD	180	0,39	0,26	0,37	0	1,72	1,72	< 2E-16	< 2E-16	< 2E-16
Intensity										
Ctrl	616	32,84	23,41	26,19	4,96	180,78	175,82			
BD 1	203	24,44	11,42	22,3	7,41	68,66	61,25	3,30E-03		
BD 2	100	33,46	15,52	31,31	10,12	88,74	78,62	1,58E-01	2,90E-06	
AUD	180	19,08	7,43	17,84	7,44	52,21	44,77	1,00E-13	2,00E-05	2,40E-15

C

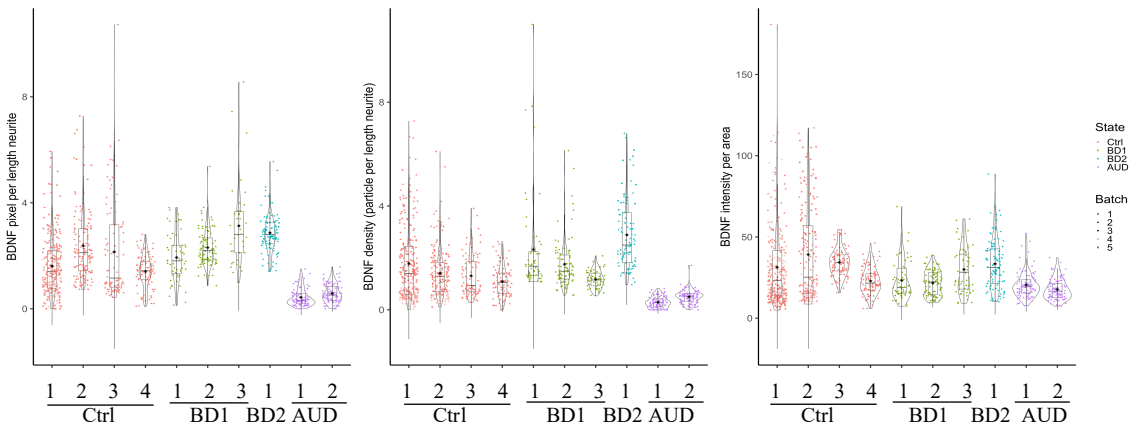

Figure 57. Appendix 26A of Figure 26A, B. BDNF base level differences in BD and AUD patients.

(A) Significantly increased BDNF pixel and particle per length neurite in BD 1 and BD 2 patients compared to healthy controls. AUD patients show a significantly reduced BDNF pixel and particle per length neurite and BDNF intensity compared to healthy controls. Ctrl with $N = 564$ - 616 neurites; BD 1 with $N = 185$ - 203 neurites, BD 2 with $N = 100$ neurites, AUD with $N = 180$ neurites. **(B)** Descriptive statistics and post hoc p-values for data shown in **(A)**. Marked in yellow, if significant. **(C)** Four Ctrl cell lines were included (Ctrl 1 with $N = 245$ - 249 neurites and 5 biological batches; Ctrl 2 with $N = 136$ - 181 neurites and 4 (3 for BDNF pixel per length neurite) biological batches; Ctrl 3 with $N = 93$ - 96 neurites and 2 biological batches and Ctrl 4 with $N = 90$ neurites and two biological batches). Three BD cell lines were included in the analysis. BD1 1: Ctrl with $N = 55$ - 57 neurites and 2 biological batches. BD1 2: Ctrl with $N = 90$ neurites and 2 biological batches. BD1 3 with $N = 40$ - 56 neurites and 1 biological batch. BD2 1 with $N = 100$ neurites and 3 biological batches. For analysis two AUD cell lines were included. AUD 1 with $N = 90$ neurites and 2 biological batches. AUD 2 with $N = 90$ neurites and 2 biological batches. Kruskal-Wallis test for independent samples was calculated. Post hoc Wilcoxon rank sum test. Bonferroni-correction, adjusted $p < .05$, mean ± *SD*. Significance levels against the respective control are $*p < 0.05$.

Appendix

A

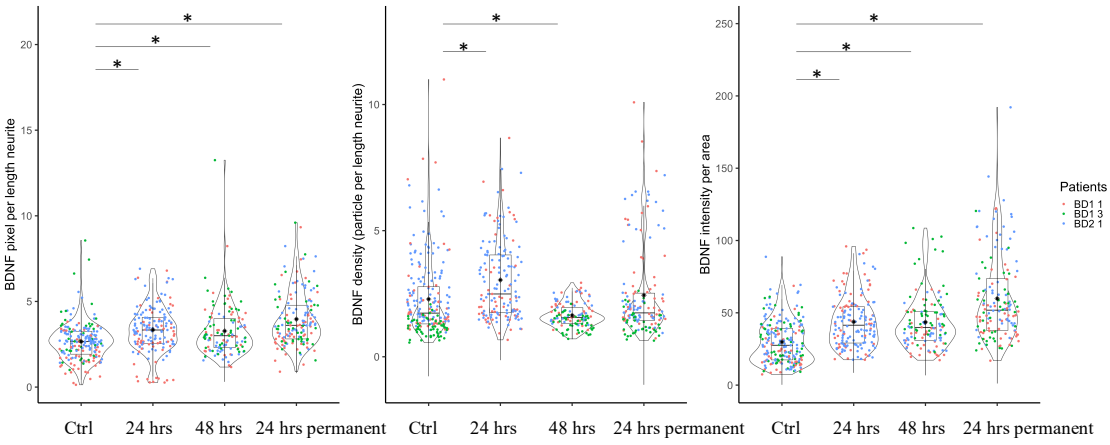

B

BDNF pixel	N	Mean	SD	Median	Min	Max	Range	Statistic Ctrl vs.
Ctrl	195	2,66	1,11	2,66	0,13	8,56	8,43	
24 hrs	156	3,34	1,36	3,33	0,27	6,91	6,64	1,10E-07
48 hrs	127	3,27	1,48	3	1,17	13,25	12,08	6,80E-04
24 hrs permanent	152	3,97	1,58	3,6	0,9	9,6	8,7	< 2E-16
BDNF particle								
Ctrl	213	2,29	1,53	1,73	0,56	10,99	10,43	
24 hrs	155	3,04	1,59	2,49	0,67	8,67	8	4,70E-08
48 hrs	128	1,64	0,47	1,56	0,71	2,93	2,23	3,66E-02
24 hrs permanent	150	2,44	1,77	1,74	0,64	10,09	9,45	1,00E+00
BDNF intensity								
Ctrl	213	29,82	14,8	27,52	7,41	88,74	81,33	
24 hrs	155	43,76	17,64	41,41	17,52	95,95	78,43	1,00E-13
48 hrs	128	43,54	18,39	39,84	17,25	108,6	91,35	5,80E-12
24 hrs permanent	150	59,86	29,37	51,81	16,89	192,11	175,22	< 2E-16

C

BD1 1

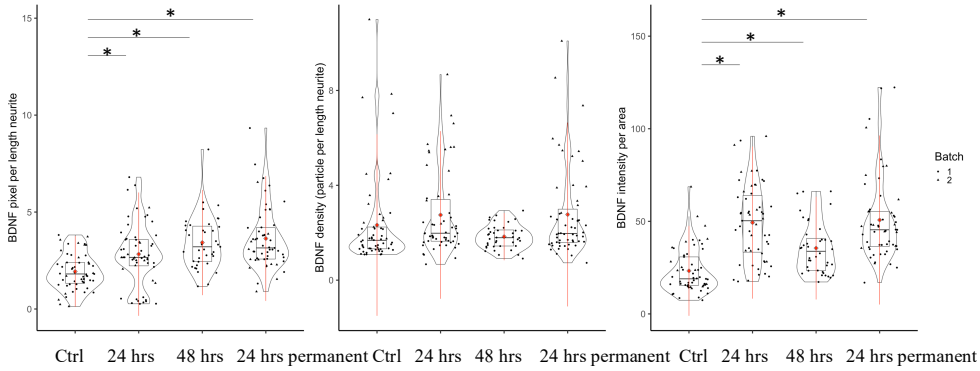

BD1 3

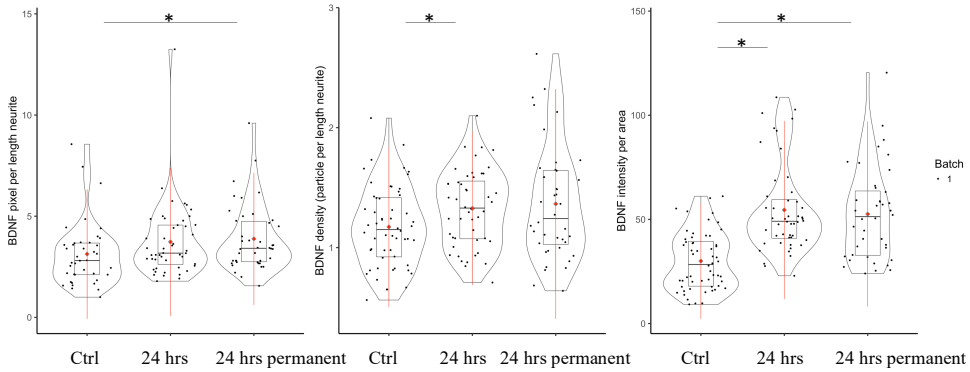

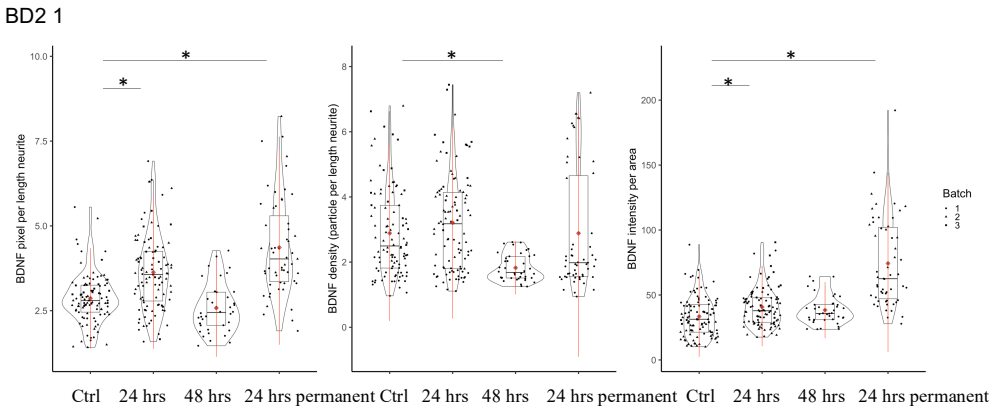

Figure 58. Appendix 26B of Figure 26D. Effect of psilocin on BDNF level of neurons derived from BD patients.

(A) BDNF pixel per length neurite and intensity per area were significantly increased 24 and 48 hrs after a 10 min 10 µM psilocin trigger (24 hrs; 48 hrs) and after 24 hrs permanent 10 µM psilocin administration (24 hr permanent). BDNF particle per length neurite were significantly increased 24 hrs and significantly decreased 48 hrs after a 10 min 10 µM psilocin trigger. Three BD cell lines were included in the analysis (Ctrl with N = 195 - 213 neurites; 24 hrs with N = 155 - 156 neurites; 48 hrs with N = 127 - 128 neurites; 24 hrs permanent with N = 150 - 152 neurites). **(B)** Descriptive statistics and post hoc p-values for data shown in **(A)**. Marked in yellow, if significant. **(C)** BD 1 1: Ctrl with N = 55 - 57 neurites; 24 hrs PS with N = 55 - 56 neurites; 48 hrs with N = 39 - 40 neurites; 24 hrs permanent with N = 55 neurites with 2 biological batches. BD 1 3: Ctrl with N = 40 - 56 neurites; 48 hrs with N = 48 neurites; 24 hrs permanent with N = 40 - 42 neurites) with 1 biological batch. BD 2 1: Ctrl with N = 100 neurites; 24 hrs with N = 100 neurites; 48 hrs with N = 40 neurites; 24 hrs permanent with N = 55 neurites) with 3 biological batches. For all statistical analysis Kruskal-Wallis test for independent samples was calculated. Bonferroni-correction, adjusted $p < .05$, mean ± SD. Significance levels against the respective control are *$p <$ 0.05.

A

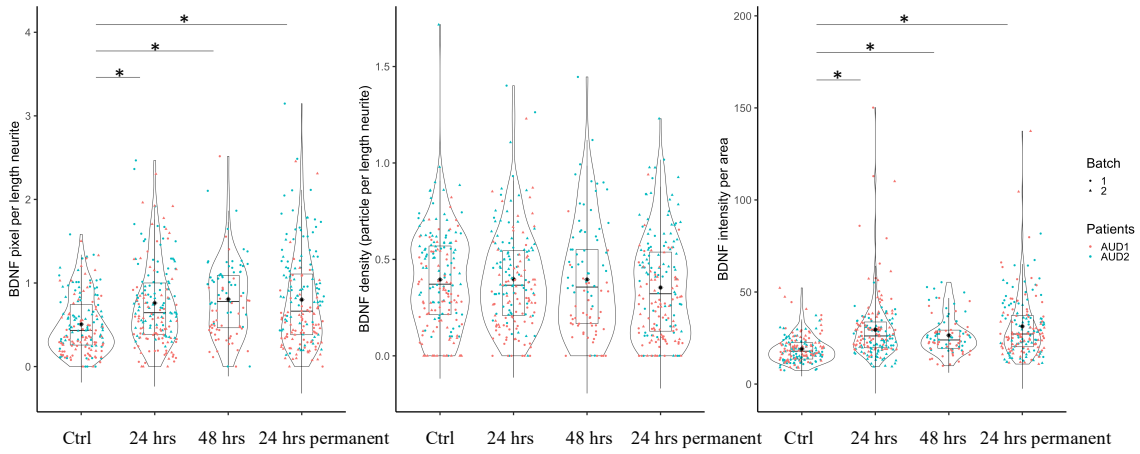

B

BDNF pixel	N	Mean	SD	Median	Min	Max	Range	Statistic Ctrl vs.
Ctrl	180	0,51	0,35	0,43	0	1,58	1,58	
24 hrs	180	0,76	0,5	0,64	0	2,46	2,47	1,50E-06
48 hrs	90	0,81	0,46	0,78	0	2,52	2,52	3,20E-07
24 hrs permanent	180	0,8	0,56	0,66	0	3,15	3,15	1,40E-06
BDNF particle								
Ctrl	180	0,39	0,26	0,37	0	1,72	1,72	
24 hrs	180	0,4	0,26	0,37	0	1,4	1,4	1,00E+00
48 hrs	90	0,4	0,3	0,36	0	1,45	1,45	1,00E+00
24 hrs permanent	180	0,35	0,32	0,32	0	1,23	1,23	4,70E-01
BDNF intensity								
Ctrl	180	19,08	7,43	17,84	7,44	52,21	44,77	
24 hrs	180	29,55	17,32	26,13	9,44	150,16	140,72	< 2E-16
48 hrs	90	26,45	10,15	23,95	9,92	55,3	45,38	1,30E-09
24 hrs permanent	180	31,33	16,93	27,18	10,86	137,4	137,4	<2E-16

C

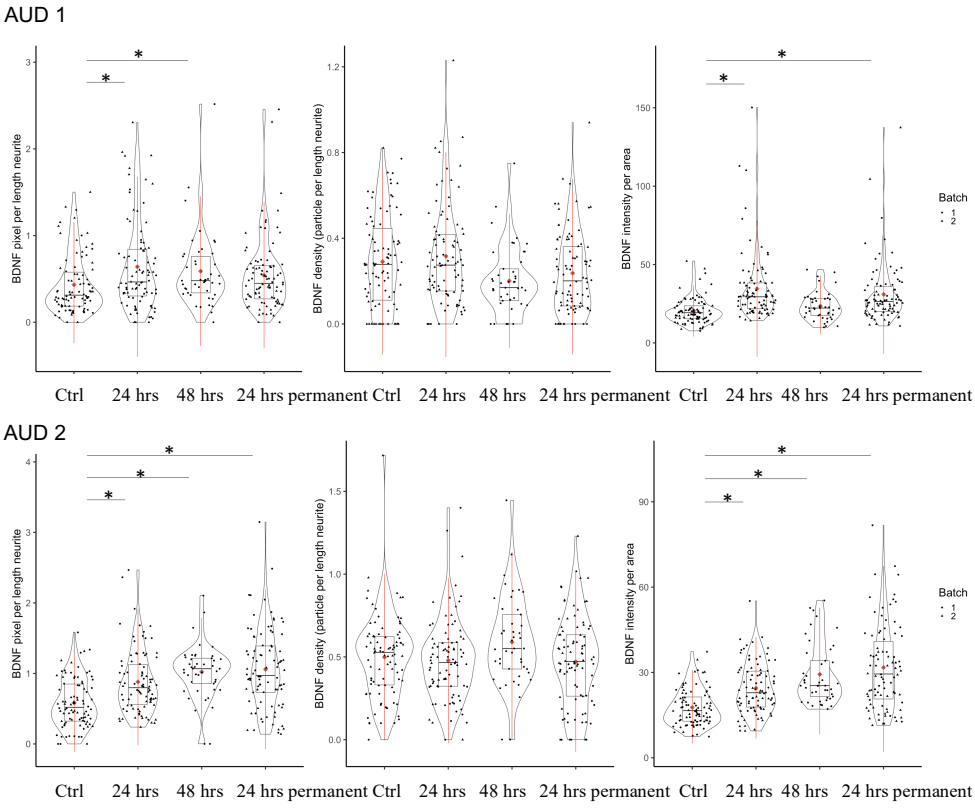

Figure 59. Appendix 26C of Figure 26E. Effect of psilocin on BDNF level of neurons derived from AUD patients.

(A) BDNF pixel per length neurite and intensity per area were significantly increased 24 and 48 hrs after a 10 min 10 µM psilocin trigger (24 hrs; 48 hrs) and after 24 hrs permanent 10 µM psilocin administration (24 hrs permanent). For analysis two AUD cell lines were included. Neurites counted: Ctrl with $N = 180$ neurites; 24 hrs with $N = 180$ neurites; 48 hrs with $N = 90$ neurites and 24 hrs permanent with $N = 180$ neurites. **(B)** Descriptive statistics and post hoc p-values for data shown in **(A)**. Marked in yellow, if significant. **(C)** AUD 1: Ctrl with $N = 90$ neurites; 24 hrs with $N = 90$ neurites; 48 hrs with $N = 45$ neurites; 24 hrs permanent with $N = 90$ neurites with 2 biological batches. AUD 2: Ctrl with $N = 90$ neurites; 24 hrs with $N = 90$ neurites; 48 hrs with $N = 45$ neurites; 24 hrs permanent with $N = 90$ neurites with 2 biological batches. For all statistical analysis Kruskal-Wallis test for independent samples was calculated. Bonferroni-correction, adjusted $p < .05$, mean ± *SD*. Significance levels against the respective control are *$p < 0.05$.

A

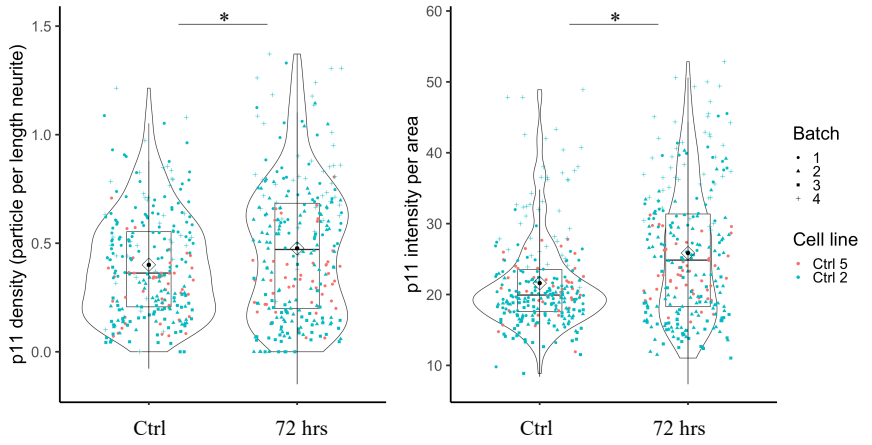

B

P11 particle	N	Mean	SD	Median	Min	Max	Range	Statistic Ctrl vs.
Ctrl	270	0,4	0,24	0,36	0	1,21	1,21	
72 hrs	270	0,48	0,31	0,47	0	1,37	1,37	1,10E-02
p11 intensity								
Ctrl	270	21,6	6,6	19,92	8,86	48,9	40,04	
72 hrs	270	25,85	9,25	24,85	11,04	52,85	52,85	2,00E-07

C

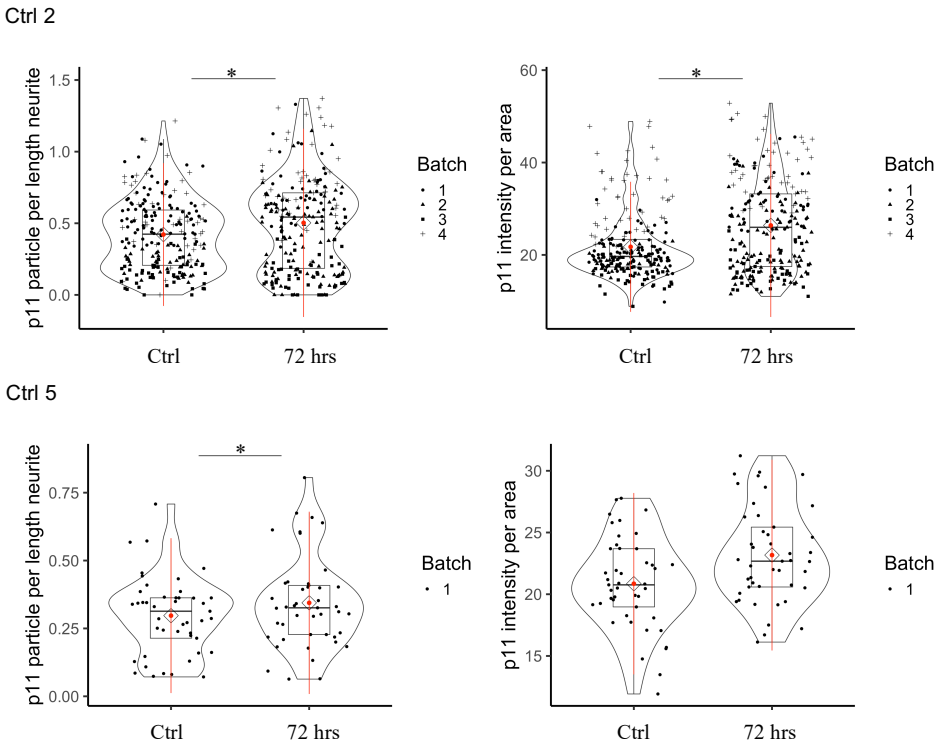

Figure 60. Appendix 29 of Figure 29C. Psilocin induced p11 level increase.
(A) P11 particle per length neurite and p11 intensity per area were significantly increased 72 hrs after a after a 10 min 10 µM psilocin trigger (72 hrs) compared to an untreated control condition (Ctrl). Ctrl with $N = 270$ neurites; 72 hrs with $N = 270$ neurites. **(B)** Descriptive statistics and post hoc p-values for data shown in **(A)**. Marked in yellow, if significant. **(C)** Two Ctrl cell lines were included in the analysis: Ctrl 2 (Ctrl with $N = 225$ neurites; 72 hrs with N = 225 neurites). Ctrl 5 (Ctrl with $N = 45$ neurites; 72 hrs with $N = 45$ neurites); Kruskal-Wallis test for independent samples was calculated. Bonferroni-correction, adjusted $p < .05$, mean ± *SD*. Significance levels against the respective control are *$p < 0.05$.

A

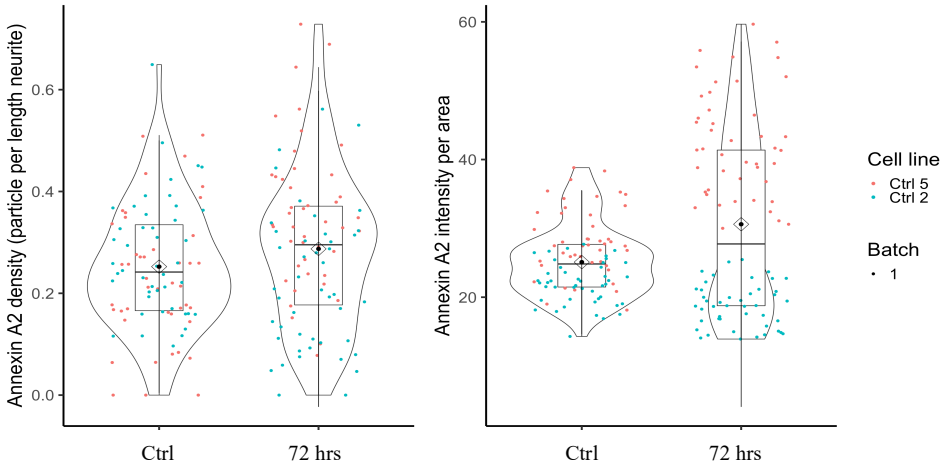

B

C

Annexin A2 particle	N	Mean	SD	Median	Min	Max	Range	Statistic Ctrl vs.
Ctrl	90	0,25	0,12	0,24	0	0,65	0,65	
72 hrs	90	0,29	0,16	0,3	0	0,73	0,73	1,30E-01
Annexin A2 intensity								
Ctrl	90	25,1	5,23	24,83	14,3	38,82	24,52	
72 hrs	90	30,6	13,27	27,74	13,92	59,66	45,74	1,60E-01

D

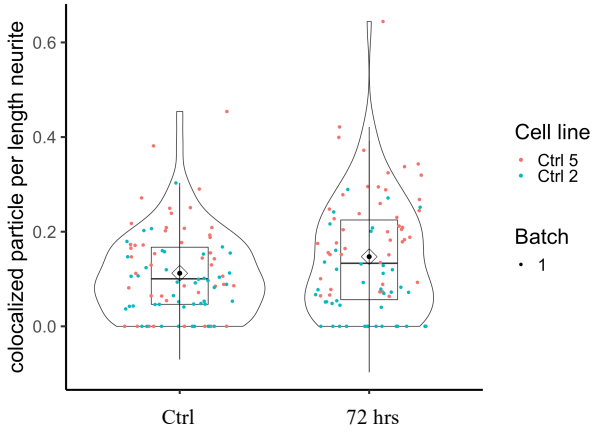

p11 Annexin co-localized particle	N	Mean	SD	Median	Min	Max	Range	Statistic Ctrl vs.
Ctrl	90	0,11	0,09	0,1	0	0,45	0,45	
72 hrs	90	0,15	0,12	0,13	0	0,64	0,64	6,90E-02

Figure 61. Tbc. Appendix 29 of Figure 29E. Influence of psilocin on annexin A2 and p11 – annexin A2 co-localization.

(A) Annexin A2 particle per length neurite were increased 72 hrs after a after a 10 min 10 µM psilocin trigger (72 hrs). Ctrl with $N = 90$ neurites; 72 hrs with $N = 90$ neurites. The effect is mostly based on Ctrl 5. Two Ctrl cell lines were included in the analysis: Ctrl 5 (Ctrl with $N = 45$ neurites; 72 hrs with $N = 45$ neurites); Ctrl 2 (Ctrl with $N = 45$ neurites; 72 hrs with $N = 45$ neurites). **(B)** Descriptive statistics and post hoc *p*-values for data shown in **(A)**. Marked in yellow, if significant. **(C)** Annexin A2 – p11 co-localization increased three days after 10 min 10 µM psilocin administration (72 hrs). Ctrl with $N = 90$ neurites; 72 hrs with $N = 90$ neurites. Two Ctrl cell lines were included in the analysis: Ctrl 5 (Ctrl with $N = 45$ neurites; 72 hrs with $N = 45$ neurites); Ctrl 2 (Ctrl with $N = 45$ neurites; 72 hrs with $N = 45$ neurites). **(D)** Descriptive statistics and post hoc *p*-values for data shown in **(C)**. Marked in yellow, if significant. For all analyses Kruskal-Wallis test for independent samples was calculated. Bonferroni-correction, adjusted $p < .05$, mean ± *SD*. Post hoc Wilcoxon rank sum test. Significance levels against the respective control are $*p < 0.05$.

A

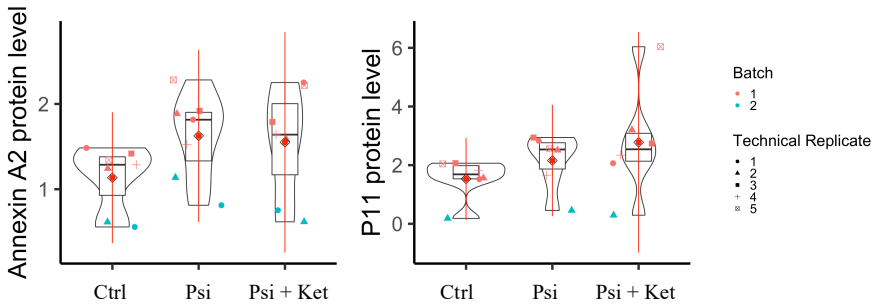

B

p11 protein level	N	Mean	SD	Median	Min	Max	Range	Statistic Ctrl vs.
Ctrl	6	1,53	0,7	1,69	0,18	2,07	1,88	
Psi	6	2,16	0,95	2,53	0,46	2,94	2,48	4,00E-01
Psi + Ket	6	2,78	1,88	2,54	0,29	6,04	5,74	1,90E-01
Annexin A2 protein level								
Ctrl	7	1,14	0,38	1,29	0,56	1,48	0,93	
Psi	7	1,63	0,51	1,82	0,81	2,28	1,47	2,20E-01
Psi + Ket	7	1,55	0,65	1,64	0,62	2,25	1,63	2,20E-01

Figure 62. Tbc. Appendix 29 of Figure 29H. Psilocin induced upregulation of core proteins of the AIIt complex.
(A) Annexin A2 and p11 protein level was increased three days after 10 min 10 µM psilocin administration (Psi) prevented by ketanserin (Psi + Ket), co-treatment only for annexin A2, suggesting a 5-HT2A-R involvement. One Ctrl cell line was included with two biological batches. Ctrl with $N = 6$ - 7 data points; Psi with 6 - 7 data points; Psi + Ket with 6 - 7 data points. For analysis Kruskal-Wallis test for independent samples was calculated. Post hoc Wilcoxon rank sum test. Bonferroni-correction, adjusted $*p < .05$, mean ± *SD*. **(B)** Descriptive statistics and post hoc *p*-values for data shown in **(A)**. Marked in yellow, if significant.

A

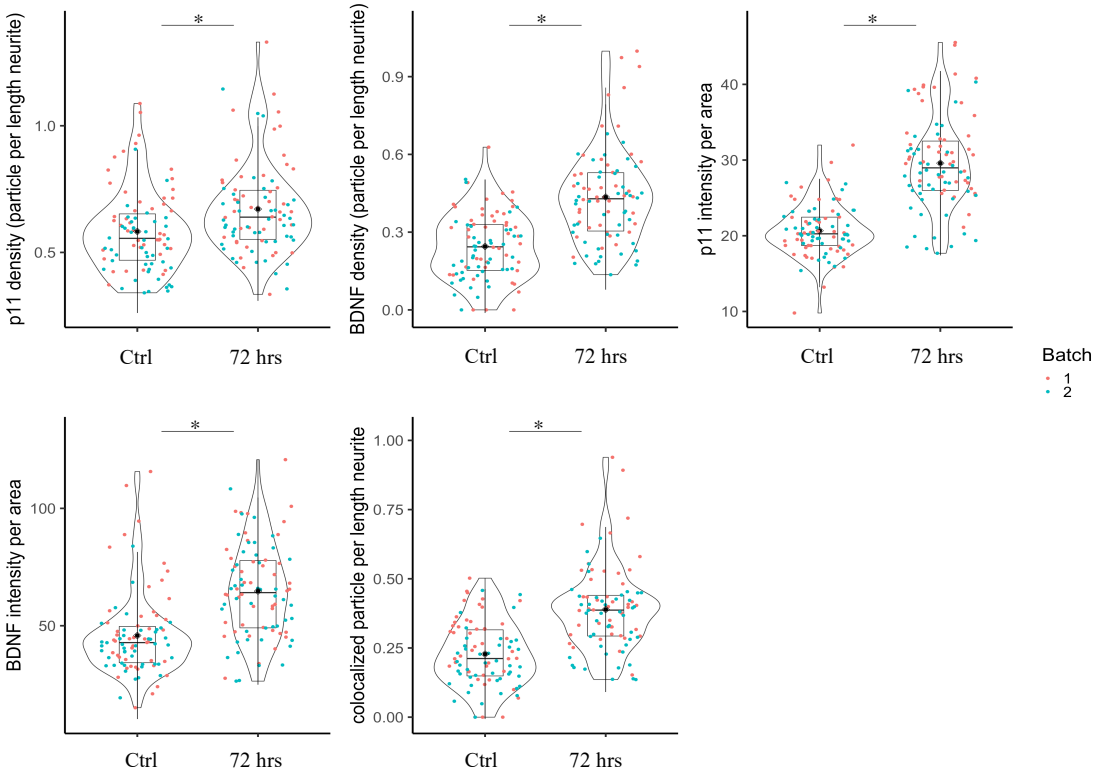

B

Co-localized particle	N	Mean	SD	Median	Min	Max	Range	Statistic Ctrl vs.
Ctrl	90	0,23	0,12	0,21	0	0,5	0,5	
72 hrs	90	0,39	0,15	0,39	0,14	0,9	0,8	1,6 E-12
P11 particle								
Ctrl	90	0,58	0,16	0,56	0,34	1,09	0,75	
72 hrs	90	0,67	0,18	0,64	0,33	1,33	1,00	2,90E-04
BDNF particle								
Ctrl	90	0,24	0,13	0,24	0	0,63	0,63	
72 hrs	90	0,44	0,18	0,43	0,14	0,86	0,86	3,10E-13
P11 intensity								
Ctrl	90	20,67	5,43	20,26	9,8	31,98	22,18	
72 hrs	90	29,58	6,09	28,97	17,69	45,53	27,85	< 2E-16
BDNF intensity								
Ctrl	90	45,83	17,8	42,82	15,06	115,7	100,64	
72 hrs	90	64,74	19,94	64,11	26,4	120,76	94,35	3,8 E-11

Figure 63. Appendix 30A of Figure 30C.Psilocin-induced p11 and BDNF increase and their co-localization.

(A) P11 and BDNF particle per length neurite and BDNF and p11 intensity per area as well as BDNF and p11 co-localized particle per length neurite were significantly increased 72 hrs after a after a 10 min 10 µM psilocin trigger (72 hrs) compared to an untreated control condition (Ctrl). One Ctrl cell line with two biological batch replications were included in the analysis: Ctrl with $N = 90$ neurites; 72 hrs with $N = 90$ neurites. Kruskal-Wallis test for independent samples was calculated. Bonferroni-correction, adjusted $p < .05$, mean ± *SD*. Post hoc Wilcoxon rank sum test. Significance levels against the respective control are $*p < 0.05$. **(B)** Descriptive statistics and post hoc *p*-values for data shown in **(A)**. Marked in yellow, if significant.

A

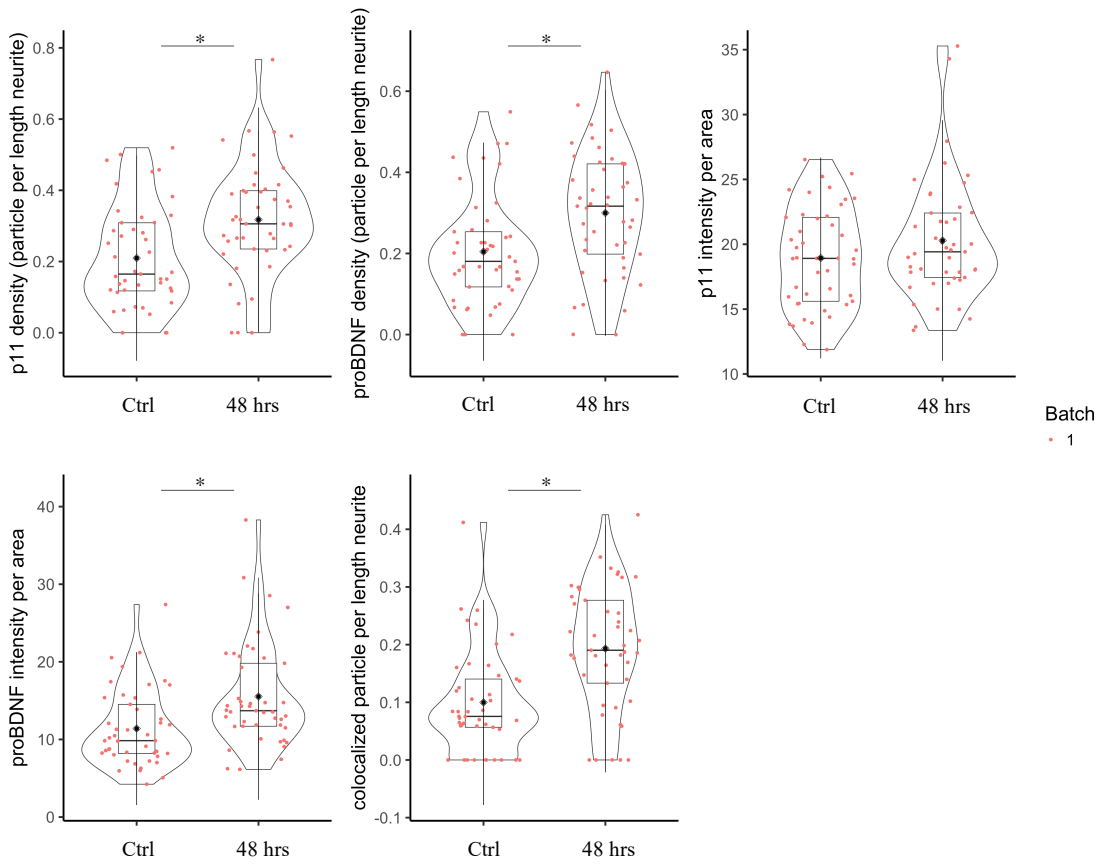

B

Co-localized particle	N	Mean	SD	Median	Min	Max	Range	Statistic Ctrl vs.
Ctrl	45	0,1	0,09	0,08	0	0,41	0,41	
48 hrs	45	0,19	0,11	0,19	0	0,43	0,43	2,30E-05
P11 particle								
Ctrl	45	0,21	0,14	0,16	0	0,52	0,52	
48 hrs	45	0,32	0,16	0,31	0	0,77	0,77	1,20E-03
proBDNF particle								
Ctrl	45	0,2	0,13	0,18	0	0,55	0,55	
48 hrs	45	0,3	0,15	0,32	0	0,65	0,65	2,10E-03
P11 intensity								
Ctrl	45	18,94	3,87	18,91	11,88	26,53	14,65	
48 hrs	45	20,29	4,63	19,42	13,36	35,28	21,92	2,80E-01
proBDNF intensity								
Ctrl	45	11,4	4,92	9,84	4,23	27,38	23,15	
48 hrs	45	15,53	6,65	13,7	6,14	38,28	32,14	6,20E-04

Figure 64. Appendix 30B of Figure 30D. Psilocin induced p11 and pro-BDNF increase and their co-localization.

(A) P11 and pro-BDNF particle per length neurite and pro-BDNF intensity per area as well as pro-BDNF and p11 co-localized particle per length neurite were significantly increased 48 hrs after a 10 min 10 µM psilocin trigger (48 hrs) compared to an untreated control condition (Ctrl). One Ctrl cell line was included in the analysis: Ctrl with $N = 45$ neurites; 48 hrs with $N = 45$ neurites. Kruskal-Wallis test for independent samples was calculated. Bonferroni-correction, adjusted $p < .05$, mean ± *SD*. Post hoc Wilcoxon rank sum test. Significance levels against the respective control are $*p < 0.05$. **(B)** Descriptive statistics and post hoc *p*-values for data shown in **(A)**. Marked in yellow, if significant.

A

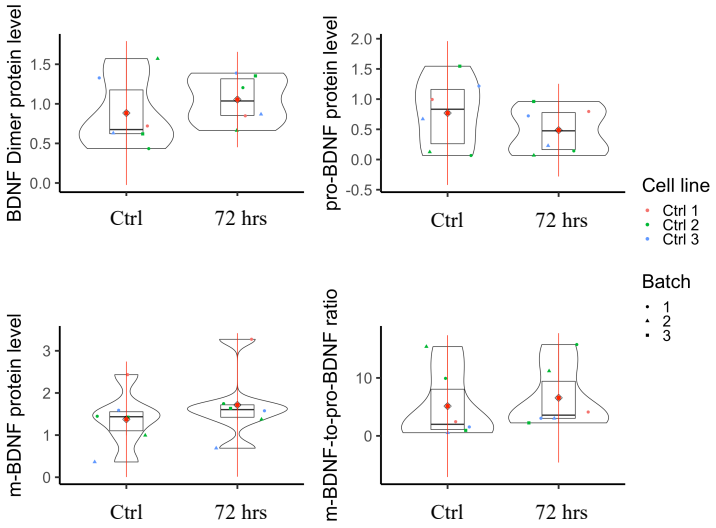

B

BDNF dimer	N	Mean	SD	Median	Min	Max	Range	Statistic Ctrl vs.
Ctrl	6	0,88	0,45	0,67	0,43	1,57	1,14	
72 hrs	6	1,05	0,3	1,04	0,66	1,39	0,73	3,10E-01
proBDNF								
Ctrl	6	0,77	0,6	0,83	0,07	1,55	1,48	
72 hrs	6	0,49	0,38	0,48	0,07	0,96	0,89	5,90E-01
mBDNF								
Ctrl	6	1,38	0,68	1,44	0,36	2,43	2,07	
72 hrs	6	1,72	0,85	1,6	0,69	3,27	2,58	4,80E-01
mBDNF-to-proBDNF-ratio								
Ctrl	6	5,13	6,12	1,99	0,54	15,4	15,4	2,40E-01
72 hrs	6	6,56	5,58	3,58	2,24	15,76	15,76	

C

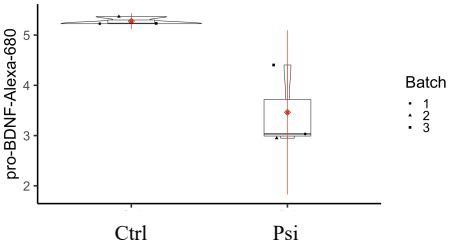

D

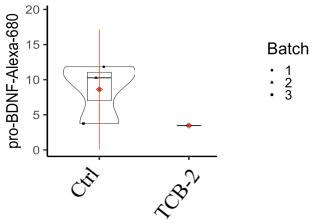

E

proBDNF-Alexa-680	N	Mean	SD	Median	Min	Max	Range	Statistic Ctrl vs.
Ctrl	3	5,28	0,08	5,23	5,23	5,37	0,14	
Psi	3	3,46	0,82	3,03	2,95	4,41	1,46	0,1

F

proBDNF-Alexa-680	N	Mean	SD	Median	Min	Max	Range
Ctrl	3	8,62	4,29	10,27	3,76	11,84	8,08
TCB-2	1	3,47	0	3,47	3,47	3,47	0

Figure 65. Appendix 31 of Figure 31C-E. Psilocin increases plasmin mediated cleavage of pro-BDNF into m-BDNF.

(A) Increased cleavage of pro-BDNF into m-BDNF after addition of plasminogen (PLG) in the psilocin treatment condition (72 hrs). Decrease of pro-BDNF level and increase of cleaved m-BDNF and m-BDNF-to-pro-BDNF-ratio in the psilocin condition. BDNF dimer protein level increased. Three Ctrl cell lines were included (Ctrl 1 with one biological batch; Ctrl 2 with three biological batches and Ctrl 3 with 3 biological batches. Ctrl with N = 6 data points; Psi with 6 data points; Psi + Ket with 6 data points. **(B)** Descriptive statistics and post hoc p-values for data shown in **(A)**. **(C)** Increased cleavage of recombinant pro-BDNF labelled to Alexa-680 after addition of PLG 3 days after permanent psilocin administration (Psi). One Ctrl cell line was included (Ctrl 3 with three biological batches). For all analyses Kruskal-Wallis test for independent samples was calculated. Post hoc Wilcoxon rank sum test. Bonferroni-correction, adjusted $p < .05$, mean ± SD. Significance levels against the respective control are *$p < 0.05$. **(D)** Increased cleavage of recombinant pro-BDNF labelled to Alexa-680 after addition 3 days after permanent TCB-2 (5-HT2A-R agonist) administration in PLG pretreated cells. One Ctrl cell line was included (Ctrl 3 with one biological batch), no statistics were calculated. **(E-F)** Descriptive statistics and/or post hoc p-values for data shown in **(C-D)**

7 References

1. Ly C, Greb AC, Cameron LP, et al. Psychedelics Promote Structural and Functional Neural Plasticity. *Cell Rep*. 2018;23(11):3170-3182. doi:10.1016/j.celrep.2018.05.022
2. Nichols D, Johnson M, Nichols C. Psychedelics as Medicines: An Emerging New Paradigm. *Clin Pharmacol Ther*. 2017;101(2):209-219. doi:10.1002/cpt.557
3. Pakkenberg B, Gundersen HJ. Neocortical neuron number in humans: effect of sex and age. *J Comp Neurol*. 1997;384(2):312-320.
4. Stiles J, Jernigan TL. The Basics of Brain Development. *Neuropsychol Rev*. 2010;20(4):327-348. doi:10.1007/s11065-010-9148-4
5. Ming G li, Song H. Adult Neurogenesis in the Mammalian Brain: Significant Answers and Significant Questions. *Neuron*. 2011;70(4):687-702. doi:10.1016/j.neuron.2011.05.001
6. Stiles J. *The Fundamentals of Brain Development*. Harvard University Press; 2008.
7. Bayer SA, Altman J, Russo RJ, Zhang X. Timetables of neurogenesis in the human brain based on experimentally determined patterns in the rat. *Neurotoxicology*. 1993;14(1):83-144.
8. Rakic P. Corticogenesis in human and nonhuman primates. In: In M. S. Gazzaniga, ed. *The Cognitive Neurosciences*. The MIT Press; 1995:127-145.
9. Rakic P. Evolution of the neocortex: a perspective from developmental biology. *Nat Rev Neurosci*. 2009;10(10):724-735. doi:10.1038/nrn2719
10. Weissman T. Neurogenic Radial Glial Cells in Reptile, Rodent and Human: from Mitosis to Migration. *Cerebral Cortex*. 2003;13(6):550-559. doi:10.1093/cercor/13.6.550
11. Clancy B, Darlington RB, Finlay BL. Translating developmental time across mammalian species. *Neuroscience*. 2001;105(1):7-17. doi:10.1016/S0306-4522(01)00171-3
12. Bystron I, Blakemore C, Rakic P. Development of the human cerebral cortex: Boulder Committee revisited. *Nat Rev Neurosci*. 2008;9(2):110-122. doi:10.1038/nrn2252
13. Cooper JA. A mechanism for inside-out lamination in the neocortex. *Trends Neurosci*. 2008;31(3):113-119. doi:10.1016/j.tins.2007.12.003
14. Subramanian L, Calcagnotto ME, Paredes MF. Cortical Malformations: Lessons in Human Brain Development. *Front Cell Neurosci*. 2020;13. doi:10.3389/fncel.2019.00576
15. Hornung JP, Tribolet N. Distribution of GABA-containing neurons in human frontal cortex: a quantitative immunocytochemical study. *Anat Embryol (Berl)*. 1994;189(2). doi:10.1007/BF00185772
16. Sahara S, Yanagawa Y, O'Leary DDM, Stevens CF. The Fraction of Cortical GABAergic Neurons Is Constant from Near the Start of Cortical Neurogenesis to Adulthood. *Journal of Neuroscience*. 2012;32(14):4755-4761. doi:10.1523/JNEUROSCI.6412-11.2012
17. O'Leary DDM, Chou SJ, Sahara S. Area Patterning of the Mammalian Cortex. *Neuron*. 2007;56(2):252-269. doi:10.1016/j.neuron.2007.10.010
18. Marin O, Valiente M, Ge X, Tsai LH. Guiding Neuronal Cell Migrations. *Cold Spring Harb Perspect Biol*. 2010;2(2):a001834-a001834. doi:10.1101/cshperspect.a001834
19. Anderson SA, Eisenstat DD, Shi L, Rubenstein JLR. Interneuron Migration from Basal Forebrain to Neocortex: Dependence on Dlx Genes. *Science (1979)*. 1997;278(5337):474-476. doi:10.1126/science.278.5337.474
20. Lavdas AA, Grigoriou M, Pachnis V, Parnavelas JG. The Medial Ganglionic Eminence Gives Rise to a Population of Early Neurons in the Developing Cerebral Cortex. *The Journal of Neuroscience*. 1999;19(18):7881-7888. doi:10.1523/JNEUROSCI.19-18-07881.1999
21. Takahashi K, Yamanaka S. Induction of pluripotent stem cells from mouse embryonic and adult fibroblast cultures by defined factors. *Cell*. 2006;126(4):663-676. doi:10.1016/j.cell.2006.07.024
22. Yamanaka S, Takahashi K, Tanabe K, et al. Induction of pluripotent stem cells from adult human fibroblasts by defined factors. *Cell*. 2007;131(5):861-872. doi:10.1016/j.cell.2007.11.019
23. Yu J, Vodyanik MA, Smuga-Otto K, et al. Induced Pluripotent Stem Cell Lines Derived from Human Somatic Cells. *Science (1979)*. 2007;318(5858):1917-1920. doi:10.1126/science.1151526
24. Ladewig J, Koch P, Brüstle O. Leveling Waddington: the emergence of direct programming and the loss of cell fate hierarchies. *Nat Rev Mol Cell Biol*. 2013;14(4):225-236. doi:10.1038/nrm3543
25. Howe JR, Bear MF, Golshani P, et al. The mouse as a model for neuropsychiatric drug development. *Current Biology*. 2018;28(17):R909-R914. doi:10.1016/j.cub.2018.07.046
26. Lancaster MA, Knoblich JA. Organogenesis in a dish: Modeling development and disease using organoid technologies. *Science (1979)*. 2014;345(6194). doi:10.1126/science.1247125
27. Lindvall O, Björklund A. Cell replacement therapy: helping the brain to repair itself. *NeuroRx*. 2004;1(4):379-381. doi:10.1602/neurorx.1.4.379
28. Shi Y, Inoue H, Wu JC, Yamanaka S. Induced pluripotent stem cell technology: a decade of progress. *Nat Rev Drug Discov*. 2017;16(2):115-130. doi:10.1038/nrd.2016.245

29. Zahumenska R, Nosal V, Smolar M, et al. Induced Pluripotency: A Powerful Tool for In Vitro Modeling. *Int J Mol Sci*. 2020;21(23):8910. doi:10.3390/ijms21238910
30. Chambers SM, Fasano CA, Papapetrou EP, Tomishima M, Sadelain M, Studer L. Highly efficient neural conversion of human ES and iPS cells by dual inhibition of SMAD signaling. 2009;27(3). doi:10.1038/nbt.1529
31. Li XJ, Zhang X, Johnson MA, Wang ZB, LaVaute T, Zhang SC. Coordination of sonic hedgehog and Wnt signaling determines ventral and dorsal telencephalic neuron types from human embryonic stem cells. *Development*. 2009;136(23):4055-4063. doi:10.1242/dev.036624
32. Shi Y, Kirwan P, Livesey FJ. Directed differentiation of human pluripotent stem cells to cerebral cortex neurons and neural networks. *Nat Protoc*. 2012;7(10):1836-1846. doi:10.1038/nprot.2012.116
33. Vierbuchen T, Ostermeier A, Pang ZP, Kokubu Y, Südhof TC, Wernig M. Direct conversion of fibroblasts to functional neurons by defined factors. *Nature*. 2010;463(7284):1035-1041. doi:10.1038/nature08797
34. Pang ZP, Yang N, Vierbuchen T, et al. Induction of human neuronal cells by defined transcription factors. *Nature*. 2011;476(7359):220-223. doi:10.1038/nature10202
35. Son EY, Ichida JK, Wainger BJ, et al. Conversion of Mouse and Human Fibroblasts into Functional Spinal Motor Neurons. *Cell Stem Cell*. 2011;9(3):205-218. doi:10.1016/j.stem.2011.07.014
36. Liu ML, Zang T, Zou Y, et al. Small molecules enable neurogenin 2 to efficiently convert human fibroblasts into cholinergic neurons. *Nat Commun*. 2013;4(1):2183. doi:10.1038/ncomms3183
37. Jaffe JH. Drug addiction and drug abuse. In: Gilman AG, Ralt TW, Nies AS TP, eds. *Goodman and Gilmans the Pharmacological Basis of Therapeutics.* Pergamon; 1990:522-573.
38. Turton S, Nutt DJ, Carhart-Harris RL. A Qualitative Report on the Subjective Experience of Intravenous Psilocybin Administered in an fMRI Environment. *Curr Drug Abuse Rev*. 2015;7(2):117-127. doi:10.2174/1874473708666150107120930
39. Schmid Y, Enzler F, Gasser P, et al. Acute Effects of Lysergic Acid Diethylamide in Healthy Subjects. *Biol Psychiatry*. 2015;78(8):544-553. doi:10.1016/j.biopsych.2014.11.015
40. Hartogsohn I. Constructing drug effects: A history of set and setting. *Drug Sci Policy Law*. 2017;3:205032451668332. doi:10.1177/2050324516683325
41. Studerus E, Kometer M, Hasler F, Vollenweider FX. Acute, subacute and long-term subjective effects of psilocybin in healthy humans: a pooled analysis of experimental studies. *Journal of Psychopharmacology*. 2011;25(11):1434-1452. doi:10.1177/0269881110382466
42. Studerus E, Gamma A, Kometer M, Vollenweider FX. Prediction of Psilocybin Response in Healthy Volunteers. *PLoS One*. 2012;7(2):e30800. doi:10.1371/journal.pone.0030800
43. Holze F, Vizeli P, Ley L, et al. Acute dose-dependent effects of lysergic acid diethylamide in a double-blind placebo-controlled study in healthy subjects. *Neuropsychopharmacology*. 2021;46(3):537-544. doi:10.1038/s41386-020-00883-6
44. Griffiths RR, Richards WA, McCann U, Jesse R. Psilocybin can occasion mystical-type experiences having substantial and sustained personal meaning and spiritual significance. *Psychopharmacology (Berl)*. 2006;187(3):268-283. doi:10.1007/s00213-006-0457-5
45. Griffiths RR, Johnson MW, Richards WA, Richards BD, McCann U, Jesse R. Psilocybin occasioned mystical-type experiences: immediate and persisting dose-related effects. *Psychopharmacology (Berl)*. 2011;218(4):649-665. doi:10.1007/s00213-011-2358-5
46. Nichols DE. Hallucinogens. *Pharmacol Ther*. 2004;101(2):131-181. doi:10.1016/j.pharmthera.2003.11.002
47. Nichols DE. Psychedelics. *Pharmacol Rev*. 2016;68(2):264-355. doi:10.1124/pr.115.011478
48. Griffiths R, Richards W, Johnson M, McCann U, Jesse R. Mystical-type experiences occasioned by psilocybin mediate the attribution of personal meaning and spiritual significance 14 months later. *Journal of Psychopharmacology*. 2008;22(6):621-632. doi:10.1177/0269881108094300
49. Studerus E, Kometer M, Hasler F, Vollenweider FX. Acute, subacute and long-term subjective effects of psilocybin in healthy humans: a pooled analysis of experimental studies. *Journal of Psychopharmacology*. 2011;25(11):1434-1452. doi:10.1177/0269881110382466
50. MacLean KA, Johnson MW, Griffiths RR. Mystical experiences occasioned by the hallucinogen psilocybin lead to increases in the personality domain of openness. *Journal of Psychopharmacology*. 2011;25(11):1453-1461. doi:10.1177/0269881111420188
51. McGlothlin WH. LSD Revisited. *Arch Gen Psychiatry*. 1971;24(1):35. doi:10.1001/archpsyc.1971.01750070037005
52. Strassman RJ. Adverse reactions to psychedelic drugs. A review of the literature. *J Nerv Ment Dis*. 1984;172(10):577-595. doi:10.1097/00005053-198410000-00001
53. O'Brien CP. Drug addiction. In: Brunton L.L., Chabner B.A., Knollmann B.C, eds. *Goodman & Gilman's: The Pharmacological Basis of Therapeutics*. 12th ed. ; 2022.

54. Carbonaro TM, Bradstreet MP, Barrett FS, et al. Survey study of challenging experiences after ingesting psilocybin mushrooms: Acute and enduring positive and negative consequences. *Journal of Psychopharmacology*. 2016;30(12):1268-1278. doi:10.1177/0269881116662634
55. Cooper H. Hallucinogenic drugs. *Lancet*. 1955;1:1078-1079.
56. American Psychiatric Association. *Diagnostic and Statistical Manual of Mental Disorders* . 5th ed. (American Psychiatric Association, ed.).; 2013.
57. The ICD-10 Classification of Mental and Behavioural Disorders Diagnostic criteria for research.
58. Halpern J. Hallucinogen persisting perception disorder: what do we know after 50 years? *Drug Alcohol Depend*. 2003;69(2):109-119. doi:10.1016/S0376-8716(02)00306-X
59. Hermle L, Ruchsow M, Täschner K. Halluzinogen-induzierte Persistierende Wahrnehmungsstörung (HPPD) und Flashback-Phänomene – Differenzialdiagnose und Erklärungsmodelle. *Fortschritte der Neurologie · Psychiatrie*. 2015;83(09):506-515. doi:10.1055/s-0035-1553717
60. Johnson M, Richards W, Griffiths R. Human hallucinogen research: guidelines for safety. *Journal of Psychopharmacology*. 2008;22(6):603-620. doi:10.1177/0269881108093587
61. Nichols DE. Hallucinogens. *Pharmacol Ther*. 2004;101(2):131-181. doi:10.1016/j.pharmthera.2003.11.002
62. Gable RS. Comparison of acute lethal toxicity of commonly abused psychoactive substances. *Addiction*. 2004;99(6):686-696. doi:10.1111/j.1360-0443.2004.00744.x
63. Gable RS. Toward a Comparative Overview of Dependence Potential and Acute Toxicity of Psychoactive Substances Used Nonmedically. *Am J Drug Alcohol Abuse*. 1993;19(3):263-281. doi:10.3109/00952999309001618
64. Hasler F, Grimberg U, Benz MA, Huber T, Vollenweider FX. Acute psychological and physiological effects of psilocybin in healthy humans: a double-blind, placebo-controlled dose-effect study. *Psychopharmacology (Berl)*. 2004;172(2):145-156. doi:10.1007/s00213-003-1640-6
65. Halpern JH, Pope HG. Do hallucinogens cause residual neuropsychological toxicity? *Drug Alcohol Depend*. 1999;53(3):247-256. doi:10.1016/S0376-8716(98)00129-X
66. Hoffer A. A program for the treatment of alcoholism: LSD, malvaria and nicotinic acid. In: Abramson HA, ed. *The Use of LSD in Psychotherapy and Alcoholism*. Bobbs-Merrill; 1967.
67. Nichols DE. Differences Between the Mechanism of Action of MDMA, MBDB, and the Classic Hallucinogens. Identification of a New Therapeutic Class: Entactogens. *J Psychoactive Drugs*. 1986;18(4):305-313. doi:10.1080/02791072.1986.10472362
68. Hartogsohn I. *The Psycho-Social Construction of LSD: How Set and Setting Shaped the American Psychedelic Experience 1950–1970*. Bar Ilan University; 2015.
69. Osmond H. A review of the clinical effects of psychotomimetic agents. *Ann N Y Acad Sci*. 1957;66(3):418-434. doi:10.1111/j.1749-6632.1957.tb40738.x
70. Thompson C, Szabo A. Psychedelics as a novel approach to treating autoimmune conditions. *Immunol Lett*. 2020;228:45-54. doi:10.1016/j.imlet.2020.10.001
71. Twarog BM, Page IH. Serotonin Content of Some Mammalian Tissues and Urine and a Method for Its Determination. *American Journal of Physiology-Legacy Content*. 1953;175(1):157-161. doi:10.1152/ajplegacy.1953.175.1.157
72. Hofmann A. *My Problem Child*. Tarcher; 1979.
73. Woolley DW, Shaw E. A biochemical and pharmacological suggestion about certain mental disorders. *Proceedings of the National Academy of Sciences*. 1954;40(4):228-231. doi:10.1073/pnas.40.4.228
74. Rickli A, Moning OD, Hoener MC, Liechti ME. Receptor interaction profiles of novel psychoactive tryptamines compared with classic hallucinogens. *European Neuropsychopharmacology*. 2016;26(8):1327-1337. doi:10.1016/j.euroneuro.2016.05.001
75. Glennon RA, Titeler M, McKenney JD. Evidence for 5-HT2 involvement in the mechanism of action of hallucinogenic agents. *Life Sci*. 1984;35(25):2505-2511. doi:10.1016/0024-3205(84)90436-3
76. Hofmann A, Heim R, Brack A, Kobel H. Psilocybin, ein psychotroper Wirkstoff aus dem mexikanischen Rauschpilz Psilocybe mexicana Heim. *Experientia*. 1958;14(3):107-109. doi:10.1007/BF02159243
77. Hofmann A, Frey A, Ott H, Petrzilka Th, Troxler F. Konstitutionsaufklärung und Synthese von Psilocybin. *Experientia*. 1958;14(11):397-399. doi:10.1007/BF02160424
78. Hofmann A, Heim R, Brack A, et al. Psilocybin und Psilocin, zwei psychotrope Wirkstoffe aus mexikanischen Rauschpilzen. *Helv Chim Acta*. 1959;42(5):1557-1572. doi:10.1002/hlca.19590420518
79. Dinis-Oliveira RJ. Metabolism of psilocybin and psilocin: clinical and forensic toxicological relevance. *Drug Metab Rev*. 2017;49(1):84-91. doi:10.1080/03602532.2016.1278228
80. Passie T, Seifert J, Schneider U, Emrich HM. The pharmacology of psilocybin. *Addiction Biology*. 2002;7(4):357-364. doi:10.1080/1355621021000005937
81. de Vos CMH, Mason NL, Kuypers KPC. Psychedelics and Neuroplasticity: A Systematic Review Unraveling the Biological Underpinnings of Psychedelics. *Front Psychiatry*. 2021;12:724606. doi:10.3389/fpsyt.2021.724606

82. Schultes RE. Hallucinogens of Plant Origin. *Science (1979)*. 1969;163(3864):245-254. doi:10.1126/science.163.3864.245
83. Schultes RE, Hoffman A, Rätsch C. *Plants of the Gods: Their Sacred, Healing, and Hallucinogenic Powers*. Revised Edition. Healing Arts Press; 2001.
84. Kast E. Attenuation of anticipation: A therapeutic use of lysergic acid diethylamide. *Psychiatr Q*. 1967;41(4):646-657. doi:10.1007/BF01575629
85. Cohen S. LSD and the anguish of dying. *Harper's Magazine*. 1965;231:69-78.
86. Kast E, Collins V. Study of lysergic acid diethylamide as an analgesic agent. *Anesth Analg*. 1964;43:285-291.
87. Stockings GT. A Clinical Study of the Mescaline Psychosis, with Special Reference to the Mechanism of the Genesis of Schizophrenic and Other Psychotic States. *Journal of Mental Science*. 1940;86(360):29-47. doi:10.1192/bjp.86.360.29
88. Hoch PH, Pennes HH, Cattell JP. Psychoses produced by administration of drugs. *Res Publ Assoc Res Nerv Ment Dis*. 1953;32:287-296.
89. Hoffer A, Callbeck MJ. Drug-Induced Schizophrenia. *Journal of Mental Science*. 1960;106(442):138-159. doi:10.1192/bjp.106.442.138
90. Leuner H. *Die Experimentelle Psychose*. Springer; 1962.
91. Kuramochi H. Psychopathology Of LSD Intoxication. *Arch Gen Psychiatry*. 1964;11(2):151. doi:10.1001/archpsyc.1964.01720260045006
92. Smart RG, Storm T, Baker EF, Solursh L. A controlled study of lysergide in the treatment of alcoholism. 1. The effects on drinking behavior. *Q J Stud Alcohol*. 1966;27(3):469-482.
93. Ludwig A, Levine J, Stark L, Lazar R. A Clinical Study of LSD Treatment in Alcoholism. *American Journal of Psychiatry*. 1969;126(1):59-69. doi:10.1176/ajp.126.1.59
94. Kurland A, Savage C, Pahnke WN, Grof S, Olsson JE. LSD in the Treatment of Alcoholics. *Pharmacopsychiatry*. 1971;4(02):83-94. doi:10.1055/s-0028-1094301
95. Savage C. Residential Psychedelic (LSD) Therapy for the Narcotic Addict. *Arch Gen Psychiatry*. 1973;28(6):808. doi:10.1001/archpsyc.1973.01750360040005
96. Hollister LE, Shelton J, Krieger G. A Controlled Comparison of Lysergic Acid Diethylamide (LSD) and Dextroamphetamine in Alcoholics. *American Journal of Psychiatry*. 1969;125(10):1352-1357. doi:10.1176/ajp.125.10.1352
97. Kurland AA, Grof S, Pahnke WN, Goodman LE. Psychedelic drug assisted psychotherapy. In: Goldberg IK, Malitz S, Kutscher AH, eds. *Patients With Terminal Cancer Psychotheramacological Agents for the Terminally Ill and Bereaved*. Columbia University Press; 1973:86-133.
98. Pahnke WN, Kurland AA, Goodman LE, Richards WA. LSD-assisted psychotherapy with terminal cancer patients. *Curr Psychiatr Ther*. 1969;9:144-152.
99. Richards WA GSGLKA. LSD-Assisted psychotherapy and the human encounter with death. *Journal of Transpersonal Psychology*. Published online 1972:121-150.
100. Grof S, Goodman LE, Richards WA, Kurland AA. LSD-Assisted Psychotherapy in Patients with Terminal Cancer. *Int Pharmacopsychiatry*. 1973;8(3):129-144. doi:10.1159/000467984
101. Kurland AA, Pahnke WN, Unger S, Savage C, Goodman E. Psychedelic psychotherapy (LSD) in the treatment of the patient with a malignancy. In: Cerletti A, Bove FJ, eds. *The Present Status of Psychotropic Drugs: Pharmacological and Clinical Aspects*. Excerpta Medica; 1969:432-434.
102. Grof S, Halifax J. *The Human Encounter with Death*. EP Dutton; 1977.
103. Richards WA, Rhead JC, Dileo FB, Yensen R, Kurland AA. The Peak Experience Variable in DPT-Assisted Psychotherapy with Cancer Patients. *J Psychedelic Drugs*. 1977;9(1):1-10. doi:10.1080/02791072.1977.10472020
104. Richards WA, Rhead JC, Grof S, Goodman LE, di Leo F, Rush L. DPT as an Adjunct in Brief Psychotherapy with Cancer Patients. *OMEGA - Journal of Death and Dying*. 1980;10(1):9-26. doi:10.2190/NGUB-V4RM-T7DC-XTH3
105. Alboni S, van Dijk RM, Poggini S, et al. Fluoxetine effects on molecular, cellular and behavioral endophenotypes of depression are driven by the living environment. *Mol Psychiatry*. 2017;22(4):552-561. doi:10.1038/mp.2015.142
106. Gueorguieva R. Trajectories of Depression Severity in Clinical Trials of Duloxetine. *Arch Gen Psychiatry*. 2011;68(12):1227. doi:10.1001/archgenpsychiatry.2011.132
107. Machado-Vieira R, Baumann J, Wheeler-Castillo C, et al. The Timing of Antidepressant Effects: A Comparison of Diverse Pharmacological and Somatic Treatments. *Pharmaceuticals*. 2010;3(1):19-41. doi:10.3390/ph3010019
108. Baldessarini RJ, Tondo L, Ghiani C, Lepri B. Illness Risk Following Rapid Versus Gradual Discontinuation of Antidepressants. *American Journal of Psychiatry*. 2010;167(8):934-941. doi:10.1176/appi.ajp.2010.09060880
109. Faedda GL. Outcome After Rapid vs Gradual Discontinuation of Lithium Treatment in Bipolar Disorders. *Arch Gen Psychiatry*. 1993;50(6):448. doi:10.1001/archpsyc.1993.01820180046005

110. Viguera AC. Clinical Risk Following Abrupt and Gradual Withdrawal of Maintenance Neuroleptic Treatment. *Arch Gen Psychiatry*. 1997;54(1):49. doi:10.1001/archpsyc.1997.01830130055011
111. Fava GA, Offidani E. The mechanisms of tolerance in antidepressant action. *Prog Neuropsychopharmacol Biol Psychiatry*. 2011;35(7):1593-1602. doi:10.1016/j.pnpbp.2010.07.026
112. Fava GA. Do Antidepressant and Antianxiety Drugs Increase Chronicity in Affective Disorders? *Psychother Psychosom*. 1994;61(3-4):125-131. doi:10.1159/000288880
113. Young AM, Goudie AJ. Adaptive processes regulating tolerance to behavioral effects of drugs. In: Bloom FE, Kupfer DJ, eds. *Psychopharmacology: The Fourth Generation of Progress*. Raven Press; 1995:733-742.
114. Byrne SE, Rothschild AJ. Loss of Antidepressant Efficacy During Maintenance Therapy. *J Clin Psychiatry*. 1998;59(6):279-288. doi:10.4088/JCP.v59n0602
115. Thase ME, Rush JA. Treatment-resistant depression. In: *Psychopharmacology*. Raven; 1995.
116. El-Mallakh RS, Gao Y, Jeannie Roberts R. Tardive dysphoria: The role of long term antidepressant use in-inducing chronic depression. *Med Hypotheses*. 2011;76(6):769-773. doi:10.1016/j.mehy.2011.01.020
117. Miller G. Is pharma running out of brainy ideas? *Science*. 2010;329(5991):502-504. doi:10.1126/science.329.5991.502
118. Schenberg EE. Psychedelic-Assisted Psychotherapy: A Paradigm Shift in Psychiatric Research and Development. *Front Pharmacol*. 2018;9. doi:10.3389/fphar.2018.00733
119. Catalá-López F, Gènova-Maleras R, Vieta E, Tabarés-Seisdedos R. The increasing burden of mental and neurological disorders. *Eur Neuropsychopharmacol*. 2013;23(11):1337-1339. doi:10.1016/j.euroneuro.2013.04.001
120. Carhart-Harris RL, Goodwin GM. The Therapeutic Potential of Psychedelic Drugs: Past, Present, and Future. *Neuropsychopharmacology*. 2017;42(11):2105-2113. doi:10.1038/npp.2017.84
121. Berman RM, Cappiello A, Anand A, et al. Antidepressant effects of ketamine in depressed patients. *Biol Psychiatry*. 2000;47(4):351-354. doi:10.1016/S0006-3223(99)00230-9
122. Ionescu DF, Swee MB, Pavone KJ, et al. Rapid and Sustained Reductions in Current Suicidal Ideation Following Repeated Doses of Intravenous Ketamine. *J Clin Psychiatry*. 2016;77(06):e719-e725. doi:10.4088/JCP.15m10056
123. DiazGranados N, Ibrahim LA, Brutsche NE, et al. Rapid resolution of suicidal ideation after a single infusion of an N-methyl-D-aspartate antagonist in patients with treatment-resistant major depressive disorder. *J Clin Psychiatry*. 2010;71(12):1605-1611. doi:10.4088/JCP.09m05327blu
124. Zarate CA, Singh JB, Carlson PJ, et al. A Randomized Trial of an N-methyl-D-aspartate Antagonist in Treatment-Resistant Major Depression. *Arch Gen Psychiatry*. 2006;63(8):856. doi:10.1001/archpsyc.63.8.856
125. Zarate CA, Brutsche NE, Ibrahim L, et al. Replication of Ketamine's Antidepressant Efficacy in Bipolar Depression: A Randomized Controlled Add-On Trial. *Biol Psychiatry*. 2012;71(11):939-946. doi:10.1016/j.biopsych.2011.12.010
126. Murrough JW, Perez AM, Pillemer S, et al. Rapid and Longer-Term Antidepressant Effects of Repeated Ketamine Infusions in Treatment-Resistant Major Depression. *Biol Psychiatry*. 2013;74(4):250-256. doi:10.1016/j.biopsych.2012.06.022
127. Bartoli F, Riboldi I, Crocamo C, di Brita C, Clerici M, Carrà G. Ketamine as a rapid-acting agent for suicidal ideation: A meta-analysis. *Neurosci Biobehav Rev*. 2017;77:232-236. doi:10.1016/j.neubiorev.2017.03.010
128. Feder A, Parides MK, Murrough JW, et al. Efficacy of Intravenous Ketamine for Treatment of Chronic Posttraumatic Stress Disorder. *JAMA Psychiatry*. 2014;71(6):681. doi:10.1001/jamapsychiatry.2014.62
129. Krupitsky EM, Grinenko AY. Ketamine Psychedelic Therapy (KPT): A Review of the Results of Ten Years of Research. *J Psychoactive Drugs*. 1997;29(2):165-183. doi:10.1080/02791072.1997.10400185
130. Krupitsky E, Burakov A, Romanova T, Dunaevsky I, Strassman R, Grinenko A. Ketamine psychotherapy for heroin addiction: immediate effects and two-year follow-up. *J Subst Abuse Treat*. 2002;23(4). doi:10.1016/s0740-5472(02)00275-1
131. Krupitsky EM, Burakov AM, Dunaevsky I v, Romanova TN, Slavina TY, Grinenko AY. Single versus repeated sessions of ketamine-assisted psychotherapy for people with heroin dependence. *J Psychoactive Drugs*. 2007;39(1). doi:10.1080/02791072.2007.10399860
132. Dakwar E, Levin F, Foltin RW, Nunes E v, Hart CL. The effects of subanesthetic ketamine infusions on motivation to quit and cue-induced craving in cocaine-dependent research volunteers. *Biol Psychiatry*. 2014;76(1). doi:10.1016/j.biopsych.2013.08.009
133. Dakwar E, Hart CL, Levin FR, Nunes E v, Foltin RW. Cocaine self-administration disrupted by the N-methyl-D-aspartate receptor antagonist ketamine: a randomized, crossover trial. *Mol Psychiatry*. 2017;22(1). doi:10.1038/mp.2016.39
134. Jovaisa T, Laurinenas G, Vosylius S, Sipylaite J, Badaras R, Ivaskevicius J. Effects of ketamine on precipitated opiate withdrawal. *Medicina (Kaunas)*. 2006;42(8).

135. Wong A, Benedict NJ, Armahizer MJ, Kane-Gill SL. Evaluation of adjunctive ketamine to benzodiazepines for management of alcohol withdrawal syndrome. *Ann Pharmacother*. 2015;49(1). doi:10.1177/1060028014555859
136. Vargas M v., Meyer R, Avanes AA, Rus M, Olson DE. Psychedelics and Other Psychoplastogens for Treating Mental Illness. *Front Psychiatry*. 2021;12. doi:10.3389/fpsyt.2021.727117
137. Mithoefer MC JLRJ et al. MDMA-assisted psychotherapy for the treatment of posttraumatic stress disorder: A revised teaching manual draft. Published online 2011.
138. Mithoefer MC, Wagner MT, Mithoefer AT, et al. Durability of improvement in post-traumatic stress disorder symptoms and absence of harmful effects or drug dependency after 3,4-methylenedioxymethamphetamine-assisted psychotherapy: a prospective long-term follow-up study. *Journal of Psychopharmacology*. 2013;27(1):28-39. doi:10.1177/0269881112456611
139. Oehen P, Traber R, Widmer V, Schnyder U. A randomized, controlled pilot study of MDMA (±3,4-Methylenedioxymethamphetamine)-assisted psychotherapy for treatment of resistant, chronic Post-Traumatic Stress Disorder (PTSD). *Journal of Psychopharmacology*. 2013;27(1):40-52. doi:10.1177/0269881112464827
140. Osório F de L, Sanches RF, Macedo LR, et al. Antidepressant effects of a single dose of ayahuasca in patients with recurrent depression: a preliminary report. *Revista Brasileira de Psiquiatria*. 2015;37(1):13-20. doi:10.1590/1516-4446-2014-1496
141. Sanches RF, de Lima Osório F, dos Santos RG, et al. Antidepressant Effects of a Single Dose of Ayahuasca in Patients With Recurrent Depression. *J Clin Psychopharmacol*. 2016;36(1):77-81. doi:10.1097/JCP.0000000000000436
142. Carhart-Harris RL, Nutt DJ. Question-based Drug Development for psilocybin - Authors' reply. *Lancet Psychiatry*. 2016;3(9):807. doi:10.1016/S2215-0366(16)30217-6
143. Carhart-Harris RL, Bolstridge M, Day CMJ, et al. Psilocybin with psychological support for treatment-resistant depression: six-month follow-up. *Psychopharmacology (Berl)*. 2018;235(2). doi:10.1007/s00213-017-4771-x
144. Davis AK, Barrett FS, May DG, et al. Effects of Psilocybin-Assisted Therapy on Major Depressive Disorder: A Randomized Clinical Trial. *JAMA Psychiatry*. 2021;78(5). doi:10.1001/jamapsychiatry.2020.3285
145. Grob CS, Danforth AL, Chopra GS, et al. Pilot study of psilocybin treatment for anxiety in patients with advanced-stage cancer. *Arch Gen Psychiatry*. 2011;68(1):71-78. doi:10.1001/archgenpsychiatry.2010.116
146. Ross S, Bossis A, Guss J, et al. Rapid and sustained symptom reduction following psilocybin treatment for anxiety and depression in patients with life-threatening cancer: a randomized controlled trial. *J Psychopharmacol*. 2016;30(12). doi:10.1177/0269881116675512
147. Moreno FA, Wiegand CB, Taitano EK, Delgado PL. Safety, Tolerability, and Efficacy of Psilocybin in 9 Patients With Obsessive-Compulsive Disorder. *J Clin Psychiatry*. 2006;67(11):1735-1740. doi:10.4088/JCP.v67n1110
148. Carhart-Harris RL, Roseman L, Bolstridge M, et al. Psilocybin for treatment-resistant depression: fMRI-measured brain mechanisms. *Sci Rep*. 2017;7(1):13187. doi:10.1038/s41598-017-13282-7
149. Nielson EM, May DG, Forcehimes AA, Bogenschutz MP. The Psychedelic Debriefing in Alcohol Dependence Treatment: Illustrating Key Change Phenomena through Qualitative Content Analysis of Clinical Sessions. *Front Pharmacol*. 2018;9. doi:10.3389/fphar.2018.00132
150. Bogenschutz MP, Forcehimes AA, Pommy JA, Wilcox CE, Barbosa PCR, Strassman RJ. Psilocybin-assisted treatment for alcohol dependence: a proof-of-concept study. *J Psychopharmacol*. 2015;29(3). doi:10.1177/0269881114565144
151. Goodwin GM, Aaronson ST, Alvarez O, et al. Single-Dose Psilocybin for a Treatment-Resistant Episode of Major Depression. *New England Journal of Medicine*. 2022;387(18):1637-1648. doi:10.1056/NEJMoa2206443
152. Carhart-Harris RL, Bolstridge M, Rucker J, et al. Psilocybin with psychological support for treatment-resistant depression: an open-label feasibility study. *Lancet Psychiatry*. 2016;3(7):619-627. doi:10.1016/S2215-0366(16)30065-7
153. Bogenschutz MP, Ross S, Bhatt S, et al. Percentage of Heavy Drinking Days Following Psilocybin-Assisted Psychotherapy vs Placebo in the Treatment of Adult Patients With Alcohol Use Disorder. *JAMA Psychiatry*. Published online August 24, 2022. doi:10.1001/jamapsychiatry.2022.2096
154. Garcia-Romeu A, Griffiths RR, Johnson MW. Psilocybin-occasioned mystical experiences in the treatment of tobacco addiction. *Curr Drug Abuse Rev*. 2014;7(3). doi:10.2174/1874473708666150107121331
155. Johnson MW, Garcia-Romeu A, Cosimano MP, Griffiths RR. Pilot study of the 5-HT2AR agonist psilocybin in the treatment of tobacco addiction. *J Psychopharmacol*. 2014;28(11). doi:10.1177/0269881114548296

156. Johnson MW, Garcia-Romeu A, Griffiths RR. Long-term follow-up of psilocybin-facilitated smoking cessation. *Am J Drug Alcohol Abuse*. 2017;43(1). doi:10.3109/00952990.2016.1170135
157. Gouzoulis-Mayfrank E, Heekeren K, Neukirch A, et al. Psychological Effects of (S)-Ketamine and N,N-Dimethyltryptamine (DMT): A Double-Blind, Cross-Over Study in Healthy Volunteers. *Pharmacopsychiatry*. 2005;38(6):301-311. doi:10.1055/s-2005-916185
158. Vollenweider F. Positron Emission Tomography and Fluorodeoxyglucose Studies of Metabolic Hyperfrontality and Psychopathology in the Psilocybin Model of Psychosis. *Neuropsychopharmacology*. 1997;16(5):357-372. doi:10.1016/S0893-133X(96)00246-1
159. Vollenweider FX, Vollenweider-Scherpenhuyzen MF, Bäbler A, Vogel H, Hell D. Psilocybin induces schizophrenia-like psychosis in humans via a serotonin-2 agonist action. *Neuroreport*. 1998;9(17). doi:10.1097/00001756-199812010-00024
160. Vollenweider FX, Geyer MA. A systems model of altered consciousness: integrating natural and drug-induced psychoses. *Brain Res Bull*. 2001;56(5):495-507. doi:10.1016/S0361-9230(01)00646-3
161. Gouzoulis-Mayfrank E, Heekeren K, Neukirch A, et al. Inhibition of Return in the Human 5HT2A Agonist and NMDA Antagonist Model of Psychosis. *Neuropsychopharmacology*. 2006;31(2):431-441. doi:10.1038/sj.npp.1300882
162. Walker ER, McGee RE, Druss BG. Mortality in Mental Disorders and Global Disease Burden Implications. *JAMA Psychiatry*. 2015;72(4):334. doi:10.1001/jamapsychiatry.2014.2502
163. Harris E, Barraclough B. Suicide as an outcome for mental disorders: a meta-analysis. *Brit J Psychiat*. 1997;170:205-228.
164. Whiteford HA, Degenhardt L, Rehm J, et al. Global burden of disease attributable to mental and substance use disorders: findings from the Global Burden of Disease Study 2010. *The Lancet*. 2013;382(9904):1575-1586. doi:10.1016/S0140-6736(13)61611-6
165. Gustavsson A, Svensson M, Jacobi F, et al. Cost of disorders of the brain in Europe 2010. *European Neuropsychopharmacology*. 2011;21(10):718-779. doi:10.1016/j.euroneuro.2011.08.008
166. World Health Organization. *Depression and Other Common Mental Disorders: Global Health Estimates*. (World Health Organization, ed.).; 2017.
167. Otte C, Gold SM, Penninx BW, et al. Major depressive disorder. *Nat Rev Dis Primers*. 2016;2(1):16065. doi:10.1038/nrdp.2016.65
168. Rabeea SA, Merchant HA, Khan MU, Kow CS, Hasan SS. Surging trends in prescriptions and costs of antidepressants in England amid COVID-19. *DARU Journal of Pharmaceutical Sciences*. 2021;29(1):217-221. doi:10.1007/s40199-021-00390-z
169. Rehm J, Mathers C, Popova S, Thavorncharoensap M, Teerawattananon Y, Patra J. Global burden of disease and injury and economic cost attributable to alcohol use and alcohol-use disorders. *The Lancet*. 2009;373(9682):2223-2233. doi:10.1016/S0140-6736(09)60746-7
170. Kranzler HR, Soyka M. Diagnosis and Pharmacotherapy of Alcohol Use Disorder. *JAMA*. 2018;320(8):815. doi:10.1001/jama.2018.11406
171. Merikangas K, Akiskal H, Angst J, et al. Lifetime and 12-month prevalence of bipolar spectrum disorder in the national comorbidity survey replication. *Arch Gen Psychiatry*. 2007;64(5):543-552.
172. Carvalho AF, Firth J, Vieta E. Bipolar Disorder. *New England Journal of Medicine*. 2020;383(1):58-66. doi:10.1056/NEJMra1906193
173. Vigo D, Thornicroft G, Atun R. Estimating the true global burden of mental illness. *Lancet Psychiatry*. 2016;3(2):171-178. doi:10.1016/S2215-0366(15)00505-2
174. Baldessarini RJ, Pompili M TL. Suicide in bipolar disorder: Risks and management. *CNS Spectr*. 2006;11(6):465-471.
175. Hains AB, Arnsten AFT. Molecular mechanisms of stress-induced prefrontal cortical impairment: implications for mental illness. *Learn Mem*. 2008;15(8):551-564. doi:10.1101/lm.921708
176. Doss MK, Považan M, Rosenberg MD, et al. Psilocybin therapy increases cognitive and neural flexibility in patients with major depressive disorder. *Transl Psychiatry*. 2021;11(1):574. doi:10.1038/s41398-021-01706-y
177. Stange JP, Alloy LB, Fresco DM. Inflexibility as a Vulnerability to Depression: A Systematic Qualitative Review. *Clin Psychol (New York)*. 2017;24(3):245-276. doi:10.1111/cpsp.12201
178. Verdejo-Garcia A, Clark L, Verdejo-Román J, et al. Neural substrates of cognitive flexibility in cocaine and gambling addictions. *British Journal of Psychiatry*. 2015;207(2):158-164. doi:10.1192/bjp.bp.114.152223
179. Channon S. Executive dysfunction in depression: The Wisconsin Card Sorting Test. *J Affect Disord*. 1996;39(2):107-114. doi:10.1016/0165-0327(96)00027-4
180. le Berre AP, Fama R, Sullivan E v. Executive Functions, Memory, and Social Cognitive Deficits and Recovery in Chronic Alcoholism: A Critical Review to Inform Future Research. *Alcohol Clin Exp Res*. 2017;41(8):1432-1443. doi:10.1111/acer.13431
181. Goodkind M, Eickhoff SB, Oathes DJ, et al. Identification of a common neurobiological substrate for mental illness. *JAMA Psychiatry*. 2015;72(4). doi:10.1001/jamapsychiatry.2014.2206

182. Torres VI, Vallejo D, Inestrosa NC. Emerging Synaptic Molecules as Candidates in the Etiology of Neurological Disorders. *Neural Plast*. 2017;2017. doi:10.1155/2017/8081758
183. Christoffel DJ, Golden SA, Russo SJ. Structural and synaptic plasticity in stress-related disorders. *Rev Neurosci*. 2011;22(5). doi:10.1515/RNS.2011.044
184. Duman RS, Aghajanian GK. Synaptic Dysfunction in Depression: Potential Therapeutic Targets. *Science (1979)*. 2012;338(6103):68-72. doi:10.1126/science.1222939
185. Pittenger C, Duman RS. Stress, Depression, and Neuroplasticity: A Convergence of Mechanisms. *Neuropsychopharmacology*. 2008;33(1). doi:10.1038/sj.npp.1301574
186. Qiao H, Li MX, Xu C, Chen HB, An SC, Ma XM. Dendritic Spines in Depression: What We Learned from Animal Models. *Neural Plast*. 2016;2016. doi:10.1155/2016/8056370
187. Russo SJ, Mazei-Robison MS, Ables JL, Nestler EJ. Neurotrophic factors and structural plasticity in addiction. *Neuropharmacology*. 2009;56:73-82. doi:10.1016/j.neuropharm.2008.06.059
188. Meinhardt MW, Pfarr S, Fouquet G, et al. Psilocybin targets a common molecular mechanism for cognitive impairment and increased craving in alcoholism. *Sci Adv*. 2021;7(47). doi:10.1126/sciadv.abh2399
189. Gallo FT, Katche C, Morici JF, Medina JH, Weisstaub N v. Immediate Early Genes, Memory and Psychiatric Disorders: Focus on c-Fos, Egr1 and Arc. *Front Behav Neurosci*. 2018;12. doi:10.3389/fnbeh.2018.00079
190. Pérez-Cadahía B, Drobic B, Davie JR. Activation and function of immediate-early genes in the nervous system. *Biochemistry and Cell Biology*. 2011;89(1):61-73. doi:10.1139/O10-138
191. Gallitano AL. Editorial: The Role of Immediate Early Genes in Neuropsychiatric Illness. *Front Behav Neurosci*. 2020;14. doi:10.3389/fnbeh.2020.00016
192. Daws RE, Timmermann C, Giribaldi B, et al. Increased global integration in the brain after psilocybin therapy for depression. *Nat Med*. 2022;28(4):844-851. doi:10.1038/s41591-022-01744-z
193. Lee HM, Roth BL. Hallucinogen actions on human brain revealed. *Proceedings of the National Academy of Sciences*. 2012;109(6):1820-1821. doi:10.1073/pnas.1121358109
194. Jakab RL, Goldman-Rakic PS. 5-Hydroxytryptamine2A serotonin receptors in the primate cerebral cortex: possible site of action of hallucinogenic and antipsychotic drugs in pyramidal cell apical dendrites. *Proc Natl Acad Sci U S A*. 1998;95(2). doi:10.1073/pnas.95.2.735
195. Willins DL, Deutch AY, Roth BL. Serotonin 5-HT2A receptors are expressed on pyramidal cells and interneurons in the rat cortex. *Synapse*. 1997;27(1). doi:10.1002/(SICI)1098-2396(199709)27:1<79::AID-SYN8>3.0.CO;2-A
196. de Almeida J, Mengod G. Quantitative analysis of glutamatergic and GABAergic neurons expressing 5-HT2A receptors in human and monkey prefrontal cortex. *J Neurochem*. 2007;103(2):475-486. doi:10.1111/j.1471-4159.2007.04768.x
197. Weber E, Andrade R. Htr2a gene and 5-HT2A receptor expression in the cerebral cortex studied using genetically modified mice. *Front Neurosci*. Published online 2010. doi:10.3389/fnins.2010.00036
198. Smausz R, Neill J, Gigg J. Neural mechanisms underlying psilocybin's therapeutic potential – the need for preclinical in vivo electrophysiology. *Journal of Psychopharmacology*. 2022;36(7):781-793. doi:10.1177/02698811221092508
199. Lee HM, Roth BL. Hallucinogen actions on human brain revealed. *Proc Natl Acad Sci U S A*. 2012;109(6):1820-1821. doi:10.1073/pnas.1121358109
200. Wood J, Kim Y, Moghaddam B. Disruption of Prefrontal Cortex Large Scale Neuronal Activity by Different Classes of Psychotomimetic Drugs. *Journal of Neuroscience*. 2012;32(9):3022-3031. doi:10.1523/JNEUROSCI.6377-11.2012
201. Celada P, Puig MV, Díaz-Mataix L, Artigas F. The Hallucinogen DOI Reduces Low-Frequency Oscillations in Rat Prefrontal Cortex: Reversal by Antipsychotic Drugs. *Biol Psychiatry*. 2008;64(5):392-400. doi:10.1016/j.biopsych.2008.03.013
202. Puig M v., Watakabe A, Ushimaru M, Yamamori T, Kawaguchi Y. Serotonin Modulates Fast-Spiking Interneuron and Synchronous Activity in the Rat Prefrontal Cortex through 5-HT1A and 5-HT2A Receptors. *Journal of Neuroscience*. 2010;30(6):2211-2222. doi:10.1523/JNEUROSCI.3335-09.2010
203. Carhart-Harris RL, Erritzoe D, Williams T, et al. Neural correlates of the psychedelic state as determined by fMRI studies with psilocybin. *Proceedings of the National Academy of Sciences*. 2012;109(6):2138-2143. doi:10.1073/pnas.1119598109
204. Carhart-Harris RL, Leech R, Hellyer PJ, et al. The entropic brain: A theory of conscious states informed by neuroimaging research with psychedelic drugs. *Front Hum Neurosci*. 2014;8(1 FEB). doi:10.3389/fnhum.2014.00020
205. Kometer M, Pokorny T, Seifritz E, Volleinweider FX. Psilocybin-induced spiritual experiences and insightfulness are associated with synchronization of neuronal oscillations. *Psychopharmacology (Berl)*. 2015;232(19):3663-3676. doi:10.1007/s00213-015-4026-7
206. Ma Z, Zhang N. Brain-wide connectivity architecture: Developmental aspects. In: *Factors Affecting Neurodevelopment. Genetics, Neurology, Behavior, and Diet*. Elsevier; 2021:247-257.

207. Raichle ME, MacLeod AM, Snyder AZ, Powers WJ, Gusnard DA, Shulman GL. A default mode of brain function. *Proceedings of the National Academy of Sciences*. 2001;98(2):676-682. doi:10.1073/pnas.98.2.676
208. Muthukumaraswamy SD, Carhart-Harris RL, Moran RJ, et al. Broadband Cortical Desynchronization Underlies the Human Psychedelic State. *Journal of Neuroscience*. 2013;33(38):15171-15183. doi:10.1523/JNEUROSCI.2063-13.2013
209. Shiroma PR, Thuras P, Wels J, et al. Neurocognitive performance of repeated versus single intravenous subanesthetic ketamine in treatment resistant depression. *J Affect Disord*. 2020;277:470-477. doi:10.1016/j.jad.2020.08.058
210. Shao LX, Liao C, Gregg I, et al. Psilocybin induces rapid and persistent growth of dendritic spines in frontal cortex in vivo. *Neuron*. 2021;109(16). doi:10.1016/j.neuron.2021.06.008
211. Hu L, Liu C, Dang M, Luo B, Guo Y, Wang H. Activation of 5-HT 2A/2C receptors reduces the excitability of cultured cortical neurons. *Neurosci Lett*. 2016;632:124-129. doi:10.1016/j.neulet.2016.08.052
212. Lima da Cruz RV, Moulin TC, Petiz LL, Leão RN. A Single Dose of 5-MeO-DMT Stimulates Cell Proliferation, Neuronal Survivability, Morphological and Functional Changes in Adult Mice Ventral Dentate Gyrus. *Front Mol Neurosci*. 2018;11. doi:10.3389/fnmol.2018.00312
213. Dakic V, Nascimento JM, Sartore RC, et al. Short term changes in the proteome of human cerebral organoids induced by 5-methoxy-N,N-dimethyltryptamine. *bioRxiv*. Published online 2017. doi:10.1101/108159
214. Morales-García JA, de la Fuente Revenga M, Alonso-Gil S, et al. The alkaloids of Banisteriopsis caapi, the plant source of the Amazonian hallucinogen Ayahuasca, stimulate adult neurogenesis in vitro. *Sci Rep*. 2017;7(1). doi:10.1038/s41598-017-05407-9
215. Szabo A, Kovacs A, Riba J, Djurovic S, Rajnavolgyi E, Frecska E. The Endogenous Hallucinogen and Trace Amine N,N-Dimethyltryptamine (DMT) Displays Potent Protective Effects against Hypoxia via Sigma-1 Receptor Activation in Human Primary iPSC-Derived Cortical Neurons and Microglia-Like Immune Cells. *Front Neurosci*. 2016;10. doi:10.3389/fnins.2016.00423
216. Nichols CD, Sanders-Bush E. A single dose of lysergic acid diethylamide influences gene expression patterns within the mammalian brain. *Neuropsychopharmacology*. 2002;26(5). doi:10.1016/S0893-133X(01)00405-5
217. Nichols CD, Garcia EE, Sanders-Bush E. Dynamic changes in prefrontal cortex gene expression following lysergic acid diethylamide administration. *Molecular Brain Research*. 2003;111(1-2):182-188. doi:10.1016/S0169-328X(03)00029-9
218. González-Maeso J, Weisstaub N v, Zhou M, et al. Hallucinogens recruit specific cortical 5-HT(2A) receptor-mediated signaling pathways to affect behavior. *Neuron*. 2007;53(3). doi:10.1016/j.neuron.2007.01.008
219. Reissig CJ, Rabin RA, Winter JC, Dlugos CA. d-LSD-induced c-Fos expression occurs in a population of oligodendrocytes in rat prefrontal cortex. *Eur J Pharmacol*. 2008;583(1). doi:10.1016/j.ejphar.2007.12.031
220. Frankel PS, Cunningham KA. The hallucinogen d-lysergic acid diethylamide (d-LSD) induces the immediate-early gene c-Fos in rat forebrain. *Brain Res*. 2002;958(2). doi:10.1016/s0006-8993(02)03548-5
221. Moreno JL, Holloway T, Albizu L, Sealfon SC, González-Maeso J. Metabotropic glutamate mGlu2 receptor is necessary for the pharmacological and behavioral effects induced by hallucinogenic 5-HT2A receptor agonists. *Neurosci Lett*. 2011;493(3):76-79. doi:10.1016/j.neulet.2011.01.046
222. Fortunato JJ, Réus GZ, Kirsch TR, et al. Acute harmine administration induces antidepressive-like effects and increases BDNF levels in the rat hippocampus. *Prog Neuropsychopharmacol Biol Psychiatry*. 2009;33(8). doi:10.1016/j.pnpbp.2009.07.021
223. Jefsen OH, Elfving B, Wegener G, Müller HK. Transcriptional regulation in the rat prefrontal cortex and hippocampus after a single administration of psilocybin. *J Psychopharmacol*. 2021;35(4). doi:10.1177/0269881120959614
224. González-Maeso J, Yuen T, Ebersole BJ, et al. Transcriptome Fingerprints Distinguish Hallucinogenic and Nonhallucinogenic 5-Hydroxytryptamine 2A Receptor Agonist Effects in Mouse Somatosensory Cortex. *The Journal of Neuroscience*. 2003;23(26):8836-8843. doi:10.1523/JNEUROSCI.23-26-08836.2003
225. Nichols CD, Sanders-Bush E. Molecular genetic responses to lysergic acid diethylamide include transcriptional activation of MAP kinase phosphatase-1, C/EBP-beta and ILAD-1, a novel gene with homology to arrestins. *J Neurochem*. 2004;90(3):576-584. doi:10.1111/j.1471-4159.2004.02515.x
226. Millan M, Marin P, Bockaert J, Mannourylacour C. Signaling at G-protein-coupled serotonin receptors: recent advances and future research directions. *Trends Pharmacol Sci*. 2008;29(9):454-464. doi:10.1016/j.tips.2008.06.007

227. Raymond JR, Mukhin Y v., Gelasco A, et al. Multiplicity of mechanisms of serotonin receptor signal transduction. *Pharmacol Ther*. 2001;92(2-3):179-212. doi:10.1016/S0163-7258(01)00169-3
228. Barnes NM, Sharp T. A review of central 5-HT receptors and their function. *Neuropharmacology*. 1999;38(8):1083-1152. doi:10.1016/S0028-3908(99)00010-6
229. Hoyer D, Hannon JP, Martin GR. Molecular, pharmacological and functional diversity of 5-HT receptors. *Pharmacol Biochem Behav*. 2002;71(4):533-554. doi:10.1016/S0091-3057(01)00746-8
230. López-Giménez JF, González-Maeso J. Hallucinogens and Serotonin 5-HT2A Receptor-Mediated Signaling Pathways. In: ; 2017:45-73. doi:10.1007/7854_2017_478
231. López-Giménez JF, Vilaró MT, Palacios JM, Mengod G. Mapping of 5-HT2A receptors and their mRNA in monkey brain: [3H]MDL100,907 autoradiography and in situ hybridization studies. *J Comp Neurol*. 2001;429(4):571-589. doi:10.1002/1096-9861(20010122)429:4<571::AID-CNE5>3.0.CO;2-X
232. Raote I, Bhattacharya A, Panicker MM. *Serotonin 2A (5-HT2A) Receptor Function: Ligand-Dependent Mechanisms and Pathways*.; 2007.
233. Mengod G, Palacios JM, Cortés R. Cartography of 5-HT1A and 5-HT 2A Receptor Subtypes in Prefrontal Cortex and Its Projections. *ACS Chem Neurosci*. 2015;6(7):1089-1098. doi:10.1021/acschemneuro.5b00023
234. Amargos-Bosch M. Co-expression and In Vivo Interaction of Serotonin1A and Serotonin2A Receptors in Pyramidal Neurons of Prefrontal Cortex. *Cerebral Cortex*. 2004;14(3):281-299. doi:10.1093/cercor/bhg128
235. Rickli A, Moning OD, Hoener MC, Liechti ME. Receptor interaction profiles of novel psychoactive tryptamines compared with classic hallucinogens. *Eur Neuropsychopharmacol*. 2016;26(8). doi:10.1016/j.euroneuro.2016.05.001
236. Kometer M, Schmidt A, Jancke L, Vollenweider FX. Activation of Serotonin 2A Receptors Underlies the Psilocybin-Induced Effects on Oscillations, N170 Visual-Evoked Potentials, and Visual Hallucinations. *Journal of Neuroscience*. 2013;33(25):10544-10551. doi:10.1523/JNEUROSCI.3007-12.2013
237. Kraehenmann R, Pokorny D, Vollenweider L, et al. Dreamlike effects of LSD on waking imagery in humans depend on serotonin 2A receptor activation. *Psychopharmacology (Berl)*. 2017;234(13):2031-2046. doi:10.1007/s00213-017-4610-0
238. Preller KH, Herdener M, Pokorny T, et al. The Fabric of Meaning and Subjective Effects in LSD-Induced States Depend on Serotonin 2A Receptor Activation. *Curr Biol*. 2017;27(3). doi:10.1016/j.cub.2016.12.030
239. Marek GJ. Interactions of hallucinogens with the glutamatergic system: Permissive network effects mediated through cortical layer V pyramidal neurons. In: *Current Topics in Behavioral Neurosciences*. Vol 36. Springer Verlag; 2018:107-135. doi:10.1007/7854_2017_480
240. Hannon J, Hoyer D. Molecular biology of 5-HT receptors. *Behavioural Brain Research*. 2008;195(1):198-213. doi:10.1016/j.bbr.2008.03.020
241. Nichols DE, Nichols CD. Serotonin receptors. *Chem Rev*. 2008;108(5):1614-1641. doi:10.1021/cr078224o
242. Hoyer D, Clarke DE, Fozard JR, et al. International Union of Pharmacology classification of receptors for 5-hydroxytryptamine (Serotonin). *Pharmacol Rev*. 1994;46(2).
243. Nishizuka Y. Intracellular signaling by hydrolysis of phospholipids and activation of protein kinase C. *Science (1979)*. 1992;258(5082):207-14Manj.
244. Wu DQ, Lee CH, Rhee SG, Simon MI. Activation of phospholipase C by the alpha subunits of the Gq and G11 proteins in transfected Cos-7 cells. *Journal of Biological Chemistry*. 1992;267(3):1811-1817. doi:10.1016/S0021-9258(18)46018-8
245. Garcia EE, Smith RL, Sanders-Bush E. Role of Gq protein in behavioral effects of the hallucinogenic drug 1-(2,5-dimethoxy-4-iodophenyl)-2-aminopropane. *Neuropharmacology*. 2007;52(8):1671-1677. doi:10.1016/j.neuropharm.2007.03.013
246. Oufkir T, Arseneault M, Sanderson JT, Vaillancourt C. The 5-HT2A serotonin receptor enhances cell viability, affects cell cycle progression and activates MEK–ERK1/2 and JAK2–STAT3 signalling pathways in human choriocarcinoma cell lines. *Placenta*. 2010;31(5):439-447. doi:10.1016/j.placenta.2010.02.019
247. Berg KA, Maayani S, Goldfarb J, Scaramellini C, Leff P, Clarke WP. Effector pathway-dependent relative efficacy at serotonin type 2A and 2C receptors: evidence for agonist-directed trafficking of receptor stimulus. *Mol Pharmacol*. 1998;54(1).
248. Kurrasch-Orbaugh DM, Watts VJ, Barker EL, Nichols DE. Serotonin 5-hydroxytryptamine 2A receptor-coupled phospholipase C and phospholipase A2 signaling pathways have different receptor reserves. *J Pharmacol Exp Ther*. 2003;304(1). doi:10.1124/jpet.102.042184
249. Qu Y, Chang L, Klaff J, Balbo A, Rapoport SI. Imaging Brain Phospholipase A2 Activation in Awake Rats in Response to the 5-HT2A/2C Agonist (±)2,5-Dimethoxy-4-Iodophenyl-2-Aminopropane (DOI). *Neuropsychopharmacology*. 2003;28(2):244-252. doi:10.1038/sj.npp.1300022

250. Gresch PJ, Strickland LV, Sanders-Bush E. Lysergic acid diethylamide-induced Fos expression in rat brain: role of serotonin-2A receptors. *Neuroscience*. 2002;114(3):707-713. doi:10.1016/S0306-4522(02)00349-4
251. Xia Z, Gray JA, Compton-Toth BA, Roth BL. A Direct Interaction of PSD-95 with 5-HT2A Serotonin Receptors Regulates Receptor Trafficking and Signal Transduction. *Journal of Biological Chemistry*. 2003;278(24):21901-21908. doi:10.1074/jbc.M301905200
252. Xia Z, Hufeisen SJ, Gray JA, Roth BL. The PDZ-binding domain is essential for the dendritic targeting of 5-HT2A serotonin receptors in cortical pyramidal neurons in vitro. *Neuroscience*. 2003;122(4):907-920. doi:10.1016/S0306-4522(03)00589-X
253. Abbas AI, Yadav PN, Yao WD, et al. PSD-95 Is Essential for Hallucinogen and Atypical Antipsychotic Drug Actions at Serotonin Receptors. *Journal of Neuroscience*. 2009;29(22):7124-7136. doi:10.1523/JNEUROSCI.1090-09.2009
254. Lowe H, Toyang N, Steele B, et al. The Therapeutic Potential of Psilocybin. *Molecules*. 2021;26(10):2948. doi:10.3390/molecules26102948
255. Mason NL, Kuypers KPC, Müller F, et al. Me, myself, bye: regional alterations in glutamate and the experience of ego dissolution with psilocybin. *Neuropsychopharmacology*. 2020;45(12):2003-2011. doi:10.1038/s41386-020-0718-8
256. Wojtas A, Bysiek A, Wawrzczak-Bargiela A, et al. Effect of Psilocybin and Ketamine on Brain Neurotransmitters, Glutamate Receptors, DNA and Rat Behavior. *Int J Mol Sci*. 2022;23(12):6713. doi:10.3390/ijms23126713
257. Scruggs JL, Schmidt D, Deutch AY. The hallucinogen 1-[2,5-dimethoxy-4-iodophenyl]-2-aminopropane (DOI) increases cortical extracellular glutamate levels in rats. *Neurosci Lett*. 2003;346(3):137-140. doi:10.1016/S0304-3940(03)00547-0
258. Aghajanian G. Serotonin and Hallucinogens. *Neuropsychopharmacology*. 1999;21(2):16S-23S. doi:10.1016/S0893-133X(98)00135-3
259. Ehrlich I. Postsynaptic Density 95 controls AMPA Receptor Incorporation during Long-Term Potentiation and Experience-Driven Synaptic Plasticity. *Journal of Neuroscience*. 2004;24(4):916-927. doi:10.1523/JNEUROSCI.4733-03.2004
260. Opazo P, Sainlos M, Choquet D. Regulation of AMPA receptor surface diffusion by PSD-95 slots. *Curr Opin Neurobiol*. 2012;22(3):453-460. doi:10.1016/j.conb.2011.10.010
261. Urban JD, Clarke WP, von Zastrow M, et al. Functional selectivity and classical concepts of quantitative pharmacology. *J Pharmacol Exp Ther*. 2007;320(1). doi:10.1124/jpet.106.104463
262. Kenakin T. Agonist-receptor efficacy II: agonist trafficking of receptor signals. *Trends Pharmacol Sci*. 1995;16(7):232-238. doi:10.1016/S0165-6147(00)89032-X
263. Kenakin T. Agonist-specific receptor conformations. *Trends Pharmacol Sci*. 1997;18(11):416-417. doi:10.1016/S0165-6147(97)01127-9
264. Berg KA, Maayani S, Goldfarb J, Clarke WP. Pleiotropic behavior of 5-HT2A and 5-HT2C receptor agonists. *Ann N Y Acad Sci*. 1998;861. doi:10.1111/j.1749-6632.1998.tb10180.x
265. Bhattacharyya S, Raote I, Bhattacharya A, Miledi R, Panicker MM. Activation, internalization, and recycling of the serotonin 2A receptor by dopamine. *Proc Natl Acad Sci U S A*. 2006;103(41). doi:10.1073/pnas.0606578103
266. Marona-Lewicka D, Kurrasch-Orbaugh D, Selken J, Cumbay M, Lisnicchia J, Nichols D. Re-evaluation of lisuride pharmacology: 5-hydroxytryptamine 1A receptor-mediated behavioral effects overlap its other properties in rats. *Psychopharmacology (Berl)*. 2002;164(1):93-107. doi:10.1007/s00213-002-1141-z
267. Silbergeld EK, Hruska RE. Lisuride and LSD: Dopaminergic and serotonergic interactions in the serotonin syndrome? *Psychopharmacology (Berl)*. 1979;65(3):233-237. doi:10.1007/BF00492209
268. Mokler DJ, Commissaris RL, Warner MR, Rech RH. Blockade of the behavioral effects of lysergic acid diethylamide, 2,5-dimethoxy-4-methylamphetamine, quipazine and lisuride by 5-hydroxytryptamine antagonists. *J Pharmacol Exp Ther*. 1983;227(3):557-562.
269. Eison AS, Mullins UL. Regulation of central 5-HT2A receptors: a review of in vivo studies. *Behavioural Brain Research*. 1995;73(1-2):177-181. doi:10.1016/0166-4328(96)00092-7
270. Assié MB, Lomenech H, Ravailhe V, Faucillon V, Newman-Tancredi A. Rapid desensitization of somatodendritic 5-HT1A receptors by chronic administration of the high-efficacy 5-HT1A agonist, F13714: a microdialysis study in the rat. *Br J Pharmacol*. 2006;149(2):170-178. doi:10.1038/sj.bjp.0706859
271. van Oekelen D, Luyten WHML, Leysen JE. 5-HT2A and 5-HT2C receptors and their atypical regulation properties. *Life Sci*. 2003;72(22):2429-2449. doi:10.1016/s0024-3205(03)00141-3
272. Gray JA, Roth BL. Paradoxical trafficking and regulation of 5-HT(2A) receptors by agonists and antagonists. *Brain Res Bull*. 2001;56(5). doi:10.1016/s0361-9230(01)00623-2
273. Elphick GF, Querbes W, Jordan JA, et al. The human polyomavirus, JCV, uses serotonin receptors to infect cells. *Science*. 2004;306(5700):1380-1383. doi:10.1126/science.1103492

274. O'Connor KA, Roth BL. Finding new tricks for old drugs: an efficient route for public-sector drug discovery. *Nat Rev Drug Discov*. 2005;4(12):1005-1014. doi:10.1038/nrd1900
275. Yadav PN, Kroeze WK, Farrell MS, Roth BL. Antagonist functional selectivity: 5-HT2A serotonin receptor antagonists differentially regulate 5-HT2A receptor protein level in vivo. *J Pharmacol Exp Ther*. 2011;339(1):99-105. doi:10.1124/jpet.111.183780
276. Raval NR, Johansen A, Donovan LL, et al. A Single Dose of Psilocybin Increases Synaptic Density and Decreases 5-HT2A Receptor Density in the Pig Brain. *Int J Mol Sci*. 2021;22(2):835. doi:10.3390/ijms22020835
277. Bhattacharyya S, Puri S, Miledi R, Panicker MM. Internalization and recycling of 5-HT 2A receptors activated by serotonin and protein kinase C-mediated mechanisms. *PNAS*. 2002;99(2):14470-14475.
278. Ohkura M, Tanaka N, Kobayashi H, Wada A, Nakai J, Yamamoto R. Insulin induces internalization of the 5-HT2A receptor expressed in HEK293 cells. *Eur J Pharmacol*. 2005;518(1):18-21. doi:10.1016/j.ejphar.2005.06.011
279. Willens DL, Alsayegh L, Berry SA, et al. Serotonergic Antagonist Effects on Trafficking of Serotonin 5-HT2A Receptors in Vitro and in Vivo. *Ann N Y Acad Sci*. 1998;861(1 ADVANCES IN S). doi:10.1111/j.1749-6632.1998.tb10182.x
280. Willins DL, Berry SA, Alsayegh L, et al. Clozapine and other 5-hydroxytryptamine-2A receptor antagonists alter the subcellular distribution of 5-hydroxytryptamine-2A receptors in vitro and in vivo. *Neuroscience*. 1999;91(2). doi:10.1016/s0306-4522(98)00653-8
281. Berry SA, Shah MC, Khan N, Roth BL. Rapid agonist-induced internalization of the 5-hydroxytryptamine2A receptor occurs via the endosome pathway in vitro. *Mol Pharmacol*. 1996;50(2).
282. Dunn KW, McGraw TE, Maxfield FR. Iterative fractionation of recycling receptors from lysosomally destined ligands in an early sorting endosome. *J Cell Biol*. 1989;109(6 Pt 2). doi:10.1083/jcb.109.6.3303
283. Moutkine I, Quentin E, Guiard BP, Maroteaux L, Doly S. Heterodimers of serotonin receptor subtypes 2 are driven by 5-HT2C protomers. *Journal of Biological Chemistry*. 2017;292(15):6352-6368. doi:10.1074/jbc.M117.779041
284. Herrick-Davis K, Grinde E, Mazurkiewicz JE. Biochemical and biophysical characterization of serotonin 5-HT2C receptor homodimers on the plasma membrane of living cells. *Biochemistry*. 2004;43(44):13963-13971. doi:10.1021/bi048398p
285. González-Maeso J, Ang RL, Yuen T, et al. Identification of a serotonin/glutamate receptor complex implicated in psychosis. *Nature*. 2008;452(7183):93-97. doi:10.1038/nature06612
286. Moreno JL, Muguruza C, Umali A, et al. Identification of Three Residues Essential for 5-Hydroxytryptamine 2A-Metabotropic Glutamate 2 (5-HT2A·mGlu2) Receptor Heteromerization and Its Psychoactive Behavioral Function. *Journal of Biological Chemistry*. 2012;287(53):44301-44319. doi:10.1074/jbc.M112.413161
287. Hofer M, Pagliusi SR, Hohn A, Leibrock J, Barde YA. Regional distribution of brain-derived neurotrophic factor mRNA in the adult mouse brain. *EMBO J*. 1990;9(8):2459-2464.
288. Yan Q, Rosenfeld RD, Matheson CR, et al. Expression of brain-derived neurotrophic factor protein in the adult rat central nervous system. *Neuroscience*. 1997;78(2):431-448. doi:10.1016/S0306-4522(96)00613-6
289. Kowiański P, Lietzau G, Czuba E, Waśkow M, Steliga A, Moryś J. BDNF: A Key Factor with Multipotent Impact on Brain Signaling and Synaptic Plasticity. *Cell Mol Neurobiol*. 2018;38(3):579-593. doi:10.1007/s10571-017-0510-4
290. Hwang JJ, Park MH, Choi SY, Koh JY. Activation of the Trk Signaling Pathway by Extracellular Zinc. *Journal of Biological Chemistry*. 2005;280(12):11995-12001. doi:10.1074/jbc.M403172200
291. Pang PT, Teng HK, Zaitsev E, et al. Cleavage of proBDNF by tPA/plasmin is essential for long-term hippocampal plasticity. *Science*. 2004;306(5695):487-491. doi:10.1126/science.1100135
292. Mowla SJ, Farhadi HF, Pareek S, et al. Biosynthesis and Post-translational Processing of the Precursor to Brain-derived Neurotrophic Factor. *Journal of Biological Chemistry*. 2001;276(16):12660-12666. doi:10.1074/jbc.M008104200
293. Lu B, Pang PT, Woo NH. The yin and yang of neurotrophin action. *Nat Rev Neurosci*. 2005;6(8):603-614. doi:10.1038/nrn1726
294. Cohen-Cory S, Kidane AH, Shirkey NJ, Marshak S. Brain-derived neurotrophic factor and the development of structural neuronal connectivity. *Dev Neurobiol*. 2010;70(5):271-288. doi:10.1002/dneu.20774
295. Conner JM, Lauterborn JC, Yan Q, Gall CM, Varon S. Distribution of Brain-Derived Neurotrophic Factor (BDNF) Protein and mRNA in the Normal Adult Rat CNS: Evidence for Anterograde Axonal Transport. *The Journal of Neuroscience*. 1997;17(7):2295-2313. doi:10.1523/JNEUROSCI.17-07-02295.1997
296. Yang J, Siao CJ, Nagappan G, et al. Neuronal release of proBDNF. *Nat Neurosci*. 2009;12(2):113-115. doi:10.1038/nn.2244

297. Roux P. Neurotrophin signaling through the p75 neurotrophin receptor. *Prog Neurobiol*. 2002;67(3):203-233. doi:10.1016/S0301-0082(02)00016-3
298. Chao M v, Hempstead BL. p75 and Trk: a two-receptor system. *Trends Neurosci*. 1995;18(7):321-326.
299. Reichardt LF. Neurotrophin-regulated signalling pathways. *Philosophical Transactions of the Royal Society B: Biological Sciences*. 2006;361(1473):1545-1564. doi:10.1098/rstb.2006.1894
300. Autry AE, Monteggia LM. Brain-derived neurotrophic factor and neuropsychiatric disorders. *Pharmacol Rev*. 2012;64(2). doi:10.1124/pr.111.005108
301. Kaplan DR, Miller FD. Neurotrophin signal transduction in the nervous system. *Curr Opin Neurobiol*. 2000;10(3):381-391. doi:10.1016/S0959-4388(00)00092-1
302. Gonzalez A, Moya-Alvarado G, Gonzalez-Billaut C, Bronfman FC. Cellular and molecular mechanisms regulating neuronal growth by brain-derived neurotrophic factor. *Cytoskeleton*. 2016;73(10):612-628. doi:10.1002/cm.21312
303. Foltran RB, Diaz SL. BDNF isoforms: a round trip ticket between neurogenesis and serotonin? *J Neurochem*. 2016;138(2):204-221. doi:10.1111/jnc.13658
304. Yoshii A, Constantine-Paton M. Postsynaptic BDNF-TrkB signaling in synapse maturation, plasticity, and disease. *Dev Neurobiol*. Published online 2010:NA-NA. doi:10.1002/dneu.20765
305. Baydyuk M, Xu B. BDNF signaling and survival of striatal neurons. *Front Cell Neurosci*. 2014;8. doi:10.3389/fncel.2014.00254
306. Park H, Poo M ming. Neurotrophin regulation of neural circuit development and function. *Nat Rev Neurosci*. 2013;14(1):7-23. doi:10.1038/nrn3379
307. Jaworski J. Control of Dendritic Arborization by the Phosphoinositide-3'-Kinase-Akt-Mammalian Target of Rapamycin Pathway. *Journal of Neuroscience*. 2005;25(49):11300-11312. doi:10.1523/JNEUROSCI.2270-05.2005
308. Kumar V. Regulation of Dendritic Morphogenesis by Ras-PI3K-Akt-mTOR and Ras-MAPK Signaling Pathways. *Journal of Neuroscience*. 2005;25(49):11288-11299. doi:10.1523/JNEUROSCI.2284-05.2005
309. Lepack AE, Bang E, Lee B, Dwyer JM, Duman RS. Fast-acting antidepressants rapidly stimulate ERK signaling and BDNF release in primary neuronal cultures. *Neuropharmacology*. 2016;111:242-252. doi:10.1016/j.neuropharm.2016.09.011
310. Zhou W, Wang N, Yang C, Li XM, Zhou ZQ, Yang JJ. Ketamine-induced antidepressant effects are associated with AMPA receptors-mediated upregulation of mTOR and BDNF in rat hippocampus and prefrontal cortex. *European Psychiatry*. 2014;29(7):419-423. doi:10.1016/j.eurpsy.2013.10.005
311. Savalia NK, Shao LX, Kwan AC. A Dendrite-Focused Framework for Understanding the Actions of Ketamine and Psychedelics. *Trends Neurosci*. 2021;44(4):260-275. doi:10.1016/j.tins.2020.11.008
312. Duman RS, Aghajanian GK, Sanacora G, Krystal JH. Synaptic plasticity and depression: new insights from stress and rapid-acting antidepressants. *Nat Med*. 2016;22(3). doi:10.1038/nm.4050
313. Vollenweider FX, Kometer M. The neurobiology of psychedelic drugs: implications for the treatment of mood disorders. *Nat Rev Neurosci*. 2010;11(9):642-651. doi:10.1038/nrn2884
314. Li N, Lee B, Liu RJ, et al. mTOR-Dependent Synapse Formation Underlies the Rapid Antidepressant Effects of NMDA Antagonists. *Science (1979)*. 2010;329(5994):959-964. doi:10.1126/science.1190287
315. Kwon M, Fernandez JR, Zegarek GF, Lo SB, Firestein BL. BDNF-Promoted Increases in Proximal Dendrites Occur via CREB-Dependent Transcriptional Regulation of Cypin. *Journal of Neuroscience*. 2011;31(26):9735-9745. doi:10.1523/JNEUROSCI.6785-10.2011
316. Segal RA. Selectivity in neurotrophic signaling: Theme and Variations. *Annu Rev Neurosci*. 2003;26(1):299-330. doi:10.1146/annurev.neuro.26.041002.131421
317. Minichiello L. TrkB signalling pathways in LTP and learning. *Nat Rev Neurosci*. 2009;10(12):850-860. doi:10.1038/nrn2738
318. Finkbeiner S, Tavazoie SF, Maloratsky A, Jacobs KM, Harris KM, Greenberg ME. CREB: A Major Mediator of Neuronal Neurotrophin Responses. *Neuron*. 1997;19(5):1031-1047. doi:10.1016/S0896-6273(00)80395-5
319. Xing J, Kornhauser JM, Xia Z, Thiele EA, Greenberg ME. Nerve Growth Factor Activates Extracellular Signal-Regulated Kinase and p38 Mitogen-Activated Protein Kinase Pathways To Stimulate CREB Serine 133 Phosphorylation. *Mol Cell Biol*. 1998;18(4):1946-1955. doi:10.1128/MCB.18.4.1946
320. Shieh PB, Hu SC, Bobb K, Timmusk T, Ghosh A. Identification of a Signaling Pathway Involved in Calcium Regulation of BDNF Expression. *Neuron*. 1998;20(4):727-740. doi:10.1016/S0896-6273(00)81011-9
321. Tao X, Finkbeiner S, Arnold DB, Shaywitz AJ, Greenberg ME. Ca2+ Influx Regulates BDNF Transcription by a CREB Family Transcription Factor-Dependent Mechanism. *Neuron*. 1998;20(4):709-726. doi:10.1016/S0896-6273(00)81010-7
322. de Foubert G, O'Neill MJ, Zetterström TSC. Acute onset by 5-HT6-receptor activation on rat brain brain-derived neurotrophic factor and activity-regulated cytoskeletal-associated protein mRNA expression. *Neuroscience*. 2007;147(3):778-785. doi:10.1016/j.neuroscience.2007.04.045

323. Ivy AS, Rodriguez FG, Garcia C, Chen MJ, Russo-Neustadt AA. Noradrenergic and serotonergic blockade inhibits BDNF mRNA activation following exercise and antidepressant. *Pharmacol Biochem Behav*. 2003;75(1):81-88. doi:10.1016/S0091-3057(03)00044-3
324. Tamburella A, Micale V, Navarria A, Drago F. Antidepressant properties of the 5-HT4 receptor partial agonist, SL65.0155: Behavioral and neurochemical studies in rats. *Prog Neuropsychopharmacol Biol Psychiatry*. 2009;33(7):1205-1210. doi:10.1016/j.pnpbp.2009.07.001
325. Warner-Schmidt JL, Chen EY, Zhang X, et al. A role for p11 in the antidepressant action of brain-derived neurotrophic factor. *Biol Psychiatry*. 2010;68(6):528-535. doi:10.1016/j.biopsych.2010.04.029
326. Meller R, Babity JM, Grahame-Smith david G. 5-HT2A Receptor Activation Leads to Increased BDNF mRNA Expression in C6 Glioma Cells. *Neuromolecular Med*. 2002;1(3):197-206. doi:10.1385/NMM:1:3:197
327. Lin CC, Huang TL. Brain-derived neurotrophic factor and mental disorders. *Biomed J*. 2020;43(2):134-142. doi:10.1016/j.bj.2020.01.001
328. Cunha ABM, Frey BN, Andreazza AC, et al. Serum brain-derived neurotrophic factor is decreased in bipolar disorder during depressive and manic episodes. *Neurosci Lett*. 2006;398(3). doi:10.1016/j.neulet.2005.12.085
329. de Oliveira GS, Ceresér KM, Fernandes BS, et al. Decreased brain-derived neurotrophic factor in medicated and drug-free bipolar patients. *J Psychiatr Res*. 2009;43(14). doi:10.1016/j.jpsychires.2009.04.002
330. Machado-Vieira R, Dietrich MO, Leke R, et al. Decreased plasma brain derived neurotrophic factor levels in unmedicated bipolar patients during manic episode. *Biol Psychiatry*. 2007;61(2). doi:10.1016/j.biopsych.2006.03.070
331. Pandey GN, Ren X, Rizavi HS, Conley RR, Roberts RC, Dwivedi Y. Brain-derived neurotrophic factor and tyrosine kinase B receptor signalling in post-mortem brain of teenage suicide victims. *Int J Neuropsychopharmacol*. 2008;11(8). doi:10.1017/S1461145708009000
332. Castrén E, Rantamäki T. The role of BDNF and its receptors in depression and antidepressant drug action: Reactivation of developmental plasticity. *Dev Neurobiol*. 2010;70(5):289-297. doi:10.1002/dneu.20758
333. Dwivedi Y, Rizavi HS, Conley RR, Roberts RC, Tamminga CA, Pandey GN. Altered gene expression of brain-derived neurotrophic factor and receptor tyrosine kinase B in postmortem brain of suicide subjects. *Arch Gen Psychiatry*. 2003;60(8). doi:10.1001/archpsyc.60.8.804
334. Zanardini R, Fontana A, Pagano R, et al. Alterations of Brain-Derived Neurotrophic Factor Serum Levels in Patients with Alcohol Dependence. *Alcohol Clin Exp Res*. Published online April 2011:no-no. doi:10.1111/j.1530-0277.2011.01489.x
335. Guilloux JP, Douillard-Guilloux G, Kota R, et al. Molecular evidence for BDNF- and GABA-related dysfunctions in the amygdala of female subjects with major depression. *Mol Psychiatry*. 2012;17(11):1130-1142. doi:10.1038/mp.2011.113
336. Karege F, Perret G, Bondolfi G, Schwald M, Bertschy G, Aubry JM. Decreased serum brain-derived neurotrophic factor levels in major depressed patients. *Psychiatry Res*. 2002;109(2):143-148. doi:10.1016/S0165-1781(02)00005-7
337. Dell'Osso L, Carmassi C, del Debbio A, et al. Brain-derived neurotrophic factor plasma levels in patients suffering from post-traumatic stress disorder. *Prog Neuropsychopharmacol Biol Psychiatry*. 2009;33(5):899-902. doi:10.1016/j.pnpbp.2009.04.018
338. Sen S, Duman R, Sanacora G. Serum Brain-Derived Neurotrophic Factor, Depression, and Antidepressant Medications: Meta-Analyses and Implications. *Biol Psychiatry*. 2008;64(6):527-532. doi:10.1016/j.biopsych.2008.05.005
339. Ueyama T, Kawai Y, Nemoto K, Sekimoto M, Toné S, Senba E. Immobilization stress reduced the expression of neurotrophins and their receptors in the rat brain. *Neurosci Res*. 1997;28(2):103-110. doi:10.1016/S0168-0102(97)00030-8
340. Tramontina JF, Andreazza AC, Kauer-Sant'anna M, et al. Brain-derived neurotrophic factor serum levels before and after treatment for acute mania. *Neurosci Lett*. 2009;452(2):111-113. doi:10.1016/j.neulet.2009.01.028
341. Segawa M, Morinobu S, Matsumoto T, Fuchikami M, Yamawaki S. Electroconvulsive seizure, but not imipramine, rapidly up-regulates pro-BDNF and t-PA, leading to mature BDNF production, in the rat hippocampus. *Int J Neuropsychopharmacol*. 2013;16(2):339-350. doi:10.1017/S1461145712000053
342. Duman RS, Monteggia LM. A Neurotrophic Model for Stress-Related Mood Disorders. *Biol Psychiatry*. 2006;59(12):1116-1127. doi:10.1016/j.biopsych.2006.02.013
343. Castren E, Vikar V, Rantamaki T. Role of neurotrophic factors in depression. *Curr Opin Pharmacol*. 2007;7(1):18-21. doi:10.1016/j.coph.2006.08.009
344. Nibuya M, Morinobu S, Duman R. Regulation of BDNF and trkB mRNA in rat brain by chronic electroconvulsive seizure and antidepressant drug treatments. *The Journal of Neuroscience*. 1995;15(11):7539-7547. doi:10.1523/JNEUROSCI.15-11-07539.1995

345. Polyakova M, Stuke K, Schuemberg K, Mueller K, Schoenknecht P, Schroeter ML. BDNF as a biomarker for successful treatment of mood disorders: a systematic & quantitative meta-analysis. *J Affect Disord*. 2015;174:432-440. doi:10.1016/j.jad.2014.11.044
346. Liu F, Wu J, Gong Y, et al. Harmine produces antidepressant-like effects via restoration of astrocytic functions. *Prog Neuropsychopharmacol Biol Psychiatry*. 2017;79(Pt B). doi:10.1016/j.pnpbp.2017.06.012
347. Martin DA, Marona-Lewicka D, Nichols DE, Nichols CD. Chronic LSD alters gene expression profiles in the mPFC relevant to schizophrenia. *Neuropharmacology*. 2014;83:1-8. doi:10.1016/j.neuropharm.2014.03.013
348. Hutten NRPW, Mason NL, Dolder PC, et al. Low Doses of LSD Acutely Increase BDNF Blood Plasma Levels in Healthy Volunteers. *ACS Pharmacol Transl Sci*. 2021;4(2):461-466. doi:10.1021/acsptsci.0c00099
349. Vaidya VA, Marek GJ, Aghajanian GK, Duman RS. 5-HT2A receptor-mediated regulation of brain-derived neurotrophic factor mRNA in the hippocampus and the neocortex. *J Neurosci*. 1997;17(8).
350. Colaço CS, Alves SS, Nolli LM, et al. Toxicity of ayahuasca after 28 days daily exposure and effects on monoamines and brain-derived neurotrophic factor (BDNF) in brain of Wistar rats. *Metab Brain Dis*. 2020;35(5):739-751. doi:10.1007/s11011-020-00547-w
351. Nardai S, László M, Szabó A, et al. N,N-dimethyltryptamine reduces infarct size and improves functional recovery following transient focal brain ischemia in rats. *Exp Neurol*. 2020;327:113245. doi:10.1016/j.expneurol.2020.113245
352. Galvão-Coelho NL, de Menezes Galvão AC, de Almeida RN, et al. Changes in inflammatory biomarkers are related to the antidepressant effects of Ayahuasca. *Journal of Psychopharmacology*. 2020;34(10):1125-1133. doi:10.1177/0269881120936486
353. Almeida RN de, Galvão AC de M, da Silva FS, et al. Modulation of Serum Brain-Derived Neurotrophic Factor by a Single Dose of Ayahuasca: Observation From a Randomized Controlled Trial. *Front Psychol*. 2019;10. doi:10.3389/fpsyg.2019.01234
354. Autry AE, Adachi M, Nosyreva E, et al. NMDA receptor blockade at rest triggers rapid behavioural antidepressant responses. *Nature*. 2011;475(7354):91-95. doi:10.1038/nature10130
355. Creutz CE, Pazoles CJ, Pollard HB. Identification and purification of an adrenal medullary protein (synexin) that causes calcium-dependent aggregation of isolated chromaffin granules. *J Biol Chem*. 1978;253(8):2858-2866.
356. Gerke V, Moss SE. Annexins: From Structure to Function. *Physiol Rev*. 2002;82(2):331-371. doi:10.1152/physrev.00030.2001
357. Moss SE, Morgan RO. The annexins. *Genome Biol*. 2004;5(4):219. doi:10.1186/gb-2004-5-4-219
358. Luo M, Hajjar KA. Annexin A2 system in human biology: Cell surface and beyond. *Semin Thromb Hemost*. 2013;39(4):338-346. doi:10.1055/s-0033-1334143
359. Gerke V, Creutz CE, Moss SE. Annexins: linking Ca2+ signalling to membrane dynamics. *Nat Rev Mol Cell Biol*. 2005;6(6):449-461. doi:10.1038/nrm1661
360. Moore BW. A soluble protein characteristic of the nervous system. *Biochem Biophys Res Commun*. 1965;19(6):739-744. doi:10.1016/0006-291X(65)90320-7
361. Donato R, Cannon BR, Sorci G, et al. Functions of S100 proteins. *Curr Mol Med*. 2013;13(1):24-57.
362. Hermann A, Donato R, Weiger TM, Chazin WJ. S100 Calcium Binding Proteins and Ion Channels. *Front Pharmacol*. 2012;3. doi:10.3389/fphar.2012.00067
363. Rescher U, Gerke V. S100A10/p11: family, friends and functions. *Pflugers Arch*. 2007;455(4):575-582. doi:10.1007/s00424-007-0313-4
364. Liu Y, Myrvang HK, Dekker L v. Themed Section: Annexins VII Programme Annexin A2 complexes with S100 proteins: structure, function and pharmacological manipulation. Published online 2014. doi:10.1111/bph.2015.172.issue-7
365. Madureira PA, O'Connell PA, Surette AP, Miller VA, Waisman DM. The biochemistry and regulation of S100A10: A multifunctional plasminogen receptor involved in oncogenesis. *J Biomed Biotechnol*. 2012;2012. doi:10.1155/2012/353687
366. Hou Y, Yang L, Mou M, et al. Annexin A2 Regulates the Levels of Plasmin, S100A10 and Fascin in L5178Y Cells. *Cancer Invest*. 2008;26(8):809-815. doi:10.1080/07357900801898664
367. Puisieux A, JI J, Ozturk M. Annexin II up-regulates cellular levels of p11 protein by a post-translational mechanisms. *Biochemical Journal*. 1996;313(1):51-55. doi:10.1042/bj3130051
368. He KL, Deora AB, Xiong H, et al. Endothelial Cell Annexin A2 Regulates Polyubiquitination and Degradation of Its Binding Partner S100A10/p11. *Journal of Biological Chemistry*. 2008;283(28):19192-19200. doi:10.1074/jbc.M800100200
369. Bharadwaj A, Bydoun M, Holloway R, Waisman D. Annexin A2 heterotetramer: Structure and function. *Int J Mol Sci*. 2013;14(3):6259-6305. doi:10.3390/ijms14036259

370. Phipps KD, Surette AP, O'Connell PA, Waisman DM. Plasminogen Receptor S100A10 Is Essential for the Migration of Tumor-Promoting Macrophages into Tumor Sites. *Cancer Res*. 2011;71(21):6676-6683. doi:10.1158/0008-5472.CAN-11-1748
371. Davalos D, Akassoglou K. Fibrinogen as a key regulator of inflammation in disease. *Semin Immunopathol*. 2012;34(1):43-62. doi:10.1007/s00281-011-0290-8
372. Oquendo MA, Sullivan GM, Sudol K, et al. Toward a Biosignature for Suicide. *American Journal of Psychiatry*. 2014;171(12):1259-1277. doi:10.1176/appi.ajp.2014.14020194
373. Dowlati Y, Herrmann N, Swardfager W, et al. A Meta-Analysis of Cytokines in Major Depression. *Biol Psychiatry*. 2010;67(5):446-457. doi:10.1016/j.biopsych.2009.09.033
374. Miller AH, Maletic V, Raison CL. Inflammation and Its Discontents: The Role of Cytokines in the Pathophysiology of Major Depression. *Biol Psychiatry*. 2009;65(9):732-741. doi:10.1016/j.biopsych.2008.11.029
375. Beurel E, Toups M, Nemeroff CB. The Bidirectional Relationship of Depression and Inflammation: Double Trouble. *Neuron*. 2020;107(2):234-256. doi:10.1016/j.neuron.2020.06.002
376. Idell RD, Florova G, Komissarov AA, Shetty S, Girard RBS, Idell S. The fibrinolytic system: A new target for treatment of depression with psychedelics. *Med Hypotheses*. 2017;100:46-53. doi:10.1016/j.mehy.2017.01.013
377. Schachtrup C, Lu P, Jones LL, et al. Fibrinogen inhibits neurite outgrowth via β3 integrin-mediated phosphorylation of the EGF receptor. *Proceedings of the National Academy of Sciences*. 2007;104(28):11814-11819. doi:10.1073/pnas.0704045104
378. Adams RA, Bauer J, Flick MJ, et al. The fibrin-derived γ377-395 peptide inhibits microglia activation and suppresses relapsing paralysis in central nervous system autoimmune disease. *Journal of Experimental Medicine*. 2007;204(3):571-582. doi:10.1084/jem.20061931
379. Teesalu T, Kulla A, Simisker A, et al. Tissue plasminogen activator and neuroserpin are widely expressed in the human central nervous system. *Thromb Haemost*. 2004;92(08):358-368. doi:10.1160/TH02-12-0310
380. Qian Z, Gilbert ME, Colicos MA, Kandel ER, Kuhl D. Tissue-plasminogen activator is induced as an immediate–early gene during seizure, kindling and long-term potentiation. *Nature*. 1993;361(6411):453-457. doi:10.1038/361453a0
381. Huang YY, Bach ME, Lipp HP, et al. Mice lacking the gene encoding tissue-type plasminogen activator show a selective interference with late-phase long-term potentiation in both Schaffer collateral and mossy fiber pathways. *Proceedings of the National Academy of Sciences*. 1996;93(16):8699-8704. doi:10.1073/pnas.93.16.8699
382. Madani R. Enhanced hippocampal long-term potentiation and learning by increased neuronal expression of tissue-type plasminogen activator in transgenic mice. *EMBO J*. 1999;18(11):3007-3012. doi:10.1093/emboj/18.11.3007
383. Baranes D, Lederfein D, Huang YY, Chen M, Bailey CH, Kandel ER. Tissue Plasminogen Activator Contributes to the Late Phase of LTP and to Synaptic Growth in the Hippocampal Mossy Fiber Pathway. *Neuron*. 1998;21(4):813-825. doi:10.1016/S0896-6273(00)80597-8
384. Fernández-Monreal M, López-Atalaya JP, Benchenane K, et al. Is tissue-type plasminogen activator a neuromodulator? *Molecular and Cellular Neuroscience*. 2004;25(4):594-601. doi:10.1016/j.mcn.2003.11.002
385. Chen ZL, Strickland S. Neuronal Death in the Hippocampus Is Promoted by Plasmin-Catalyzed Degradation of Laminin. *Cell*. 1997;91(7):917-925. doi:10.1016/S0092-8674(00)80483-3
386. Hu K, Yang J, Tanaka S, Gonias SL, Mars WM, Liu Y. Tissue-type Plasminogen Activator Acts as a Cytokine That Triggers Intracellular Signal Transduction and Induces Matrix Metalloproteinase-9 Gene Expression. *Journal of Biological Chemistry*. 2006;281(4):2120-2127. doi:10.1074/jbc.M504988200
387. Wu YP, Siao CJ, Lu W, et al. The Tissue Plasminogen Activator (Tpa/Plasmin) Extracellular Proteolytic System Regulates Seizure-Induced Hippocampal Mossy Fiber Outgrowth through a Proteoglycan Substrate. *Journal of Cell Biology*. 2000;148(6):1295-1304. doi:10.1083/jcb.148.6.1295
388. Samson AL, Medcalf RL. Tissue-Type Plasminogen Activator: A Multifaceted Modulator of Neurotransmission and Synaptic Plasticity. *Neuron*. 2006;50(5):673-678. doi:10.1016/j.neuron.2006.04.013
389. Jiang H, Chen S, Li C, et al. The serum protein levels of the tPA–BDNF pathway are implicated in depression and antidepressant treatment. *Transl Psychiatry*. 2017;7(4):e1079-e1079. doi:10.1038/tp.2017.43
390. Sartori CR, Vieira AS, Ferrari EM, Langone F, Tongiorgi E, Parada CA. The antidepressive effect of the physical exercise correlates with increased levels of mature BDNF, and proBDNF proteolytic cleavage-related genes, p11 and tPA. *Neuroscience*. 2011;180:9-18. doi:10.1016/j.neuroscience.2011.02.055
391. Ding Q, Ying Z, Gómez-Pinilla F. Exercise influences hippocampal plasticity by modulating brain-derived neurotrophic factor processing. *Neuroscience*. 2011;192:773-780. doi:10.1016/j.neuroscience.2011.06.032

392. Tang M, Jiang P, Li H, et al. Antidepressant-like effect of n-3 PUFAs in CUMS rats: role of tPA/PAI-1 system. *Physiol Behav*. 2015;139:210-215. doi:10.1016/j.physbeh.2014.11.054
393. Ludka FK, Cunha MP, Dal-Cim T, et al. Atorvastatin Protects from Aβ1–40-Induced Cell Damage and Depressive-Like Behavior via ProBDNF Cleavage. *Mol Neurobiol*. 2017;54(8):6163-6173. doi:10.1007/s12035-016-0134-6
394. Bahi A, Dreyer JL. Hippocampus-specific deletion of tissue plasminogen activator "tPA" in adult mice impairs depression- and anxiety-like behaviors. *European Neuropsychopharmacology*. 2012;22(9):672-682. doi:10.1016/j.euroneuro.2012.01.008
395. Ventorp F, Gustafsson A, Träskman-Bendz L, Westrin Å, Ljunggren L. Increased Soluble Urokinase-Type Plasminogen Activator Receptor (suPAR) Levels in Plasma of Suicide Attempters. *PLoS One*. 2015;10(10):e0140052. doi:10.1371/journal.pone.0140052
396. Kwon M. S100A10, annexin A2, and annexin a2 heterotetramer as candidate plasminogen receptors. *Frontiers in Bioscience*. 2005;10(1-3):300. doi:10.2741/1529
397. Bissonette GB, Bae MH, Suresh T, Jaffe DE, Powell EM. Prefrontal cognitive deficits in mice with altered cerebral cortical GABAergic interneurons. *Behavioural brain research*. 2014;259:143-151. doi:10.1016/j.bbr.2013.10.051
398. Powell EM, Campbell DB, Stanwood GD, Davis C, Noebels JL, Levitt P. Genetic Disruption of Cortical Interneuron Development Causes Region- and GABA Cell Type-Specific Deficits, Epilepsy, and Behavioral Dysfunction. *The Journal of Neuroscience*. 2003;23(2):622-631. doi:10.1523/JNEUROSCI.23-02-00622.2003
399. Gur-Wahnon D, Mizrachi T, Maaravi-Pinto FY, et al. The plasminogen activator system: involvement in central nervous system inflammation and a potential site for therapeutic intervention. *J Neuroinflammation*. 2013;10(1):891. doi:10.1186/1742-2094-10-124
400. Oh YS, Gao P, Lee KW, et al. SMARCA3, a Chromatin-Remodeling Factor, Is Required for p11-Dependent Antidepressant Action. *Cell*. 2013;152(4):831-843. doi:10.1016/j.cell.2013.01.014
401. Benaud C, Gentil BJ, Assard N, et al. AHNAK interaction with the annexin 2/S100A10 complex regulates cell membrane cytoarchitecture. *Journal of Cell Biology*. 2004;164(1):133-144. doi:10.1083/jcb.200307098
402. Haase H. Ahnak, a new player in β-adrenergic regulation of the cardiac L-type Ca2+ channel. *Cardiovasc Res*. 2007;73(1):19-25. doi:10.1016/j.cardiores.2006.09.001
403. Liu Y, Blackwood DH, Caesar S, et al. Meta-analysis of genome-wide association data of bipolar disorder and major depressive disorder. *Mol Psychiatry*. 2011;16(1):2-4. doi:10.1038/mp.2009.107
404. Jin J, Bhatti DL, Lee KW, et al. Ahnak scaffolds p11/Anxa2 complex and L-type voltage-gated calcium channel and modulates depressive behavior. *Mol Psychiatry*. 2020;25(5):1035-1049. doi:10.1038/s41380-019-0371-y
405. Ding H, Benotmane AM, Suske G, Collen D, Belayew A. Functional Interactions between Sp1 or Sp3 and the Helicase-like Transcription Factor Mediate Basal Expression from the Human Plasminogen Activator Inhibitor-1 Gene. *Journal of Biological Chemistry*. 1999;274(28):19573-19580. doi:10.1074/jbc.274.28.19573
406. Kato H, Okazaki K, Urano T. Spt6. Two fundamentally distinct functions in the regulation of histone modification. *Epigenetics*. 2013;8(12):1249-1253. doi:10.4161/epi.26487
407. Cramer P. Organization and regulation of gene transcription. *Nature*. 2019;573(7772):45-54. doi:10.1038/s41586-019-1517-4
408. Svenningsson P, Kim Y, Warner-Schmidt J, Oh YS, Greengard P. P11 and its role in depression and therapeutic responses to antidepressants. *Nat Rev Neurosci*. 2013;14(10):673-680. doi:10.1038/nrn3564
409. Anisman H, Du L, Palkovits M, et al. Serotonin receptor subtype and p11 mRNA expression in stress-relevant brain regions of suicide and control subjects. *J Psychiatry Neurosci*. 2008;33(2):131-141.
410. Svenningsson P, Chergui K, Rachleff I, et al. Alterations in 5-HT1B receptor function by p11 in depression-like states. *Science*. 2006;311(5757):77-80. doi:10.1126/science.1117571
411. Warner-Schmidt JL, Flajolet M, Maller A, et al. Role of p11 in cellular and behavioral effects of 5-HT4 receptor stimulation. *J Neurosci*. 2009;29(6):1937-1946. doi:10.1523/JNEUROSCI.5343-08.2009
412. Egeland M, Warner-Schmidt J, Greengard P, Svenningsson P. Neurogenic Effects of Fluoxetine Are Attenuated in p11 (S100A10) Knockout Mice. *Biol Psychiatry*. 2010;67(11):1048-1056. doi:10.1016/j.biopsych.2010.01.024
413. Seo JS, Svenningsson P. Modulation of Ion Channels and Receptors by p11 (S100A10). *Trends Pharmacol Sci*. 2020;41(7):487-497. doi:10.1016/j.tips.2020.04.004
414. Zhou L, Xiong J, Lim Y, et al. Upregulation of blood proBDNF and its receptors in major depression. *J Affect Disord*. 2013;150(3):776-784. doi:10.1016/j.jad.2013.03.002
415. Wang M, Xie Y, Qin D. Proteolytic cleavage of proBDNF to mBDNF in neuropsychiatric and neurodegenerative diseases. *Brain Res Bull*. 2021;166:172-184. doi:10.1016/j.brainresbull.2020.11.005

416. Li J, Chen J, Ma N, et al. Effects of corticosterone on the expression of mature brain-derived neurotrophic factor (mBDNF) and proBDNF in the hippocampal dentate gyrus. *Behavioural Brain Research*. 2019;365:150-156. doi:10.1016/j.bbr.2019.03.010
417. Qiao H, An SC, Xu C, Ma XM. Role of proBDNF and BDNF in dendritic spine plasticity and depressive-like behaviors induced by an animal model of depression. *Brain Res*. 2017;1663:29-37. doi:10.1016/j.brainres.2017.02.020
418. Lin LY, Luo SY, Al-Hawwas M, Herselman MF, Zhou XF, Bobrovskaya L. The Long-Term Effects of Ethanol and Corticosterone on the Mood-Related Behaviours and the Balance Between Mature BDNF and proBDNF in Mice. *Journal of Molecular Neuroscience*. 2019;69(1):60-68. doi:10.1007/s12031-019-01328-6
419. Yang CR, Zhang XY, Liu Y, et al. Antidepressant Drugs Correct the Imbalance Between proBDNF/p75NTR/Sortilin and Mature BDNF/TrkB in the Brain of Mice with Chronic Stress. *Neurotox Res*. 2020;37(1):171-182. doi:10.1007/s12640-019-00101-2
420. Chen MX, Oh YS, Kim Y. S100A10 and its binding partners in depression and antidepressant actions. *Front Mol Neurosci*. 2022;15. doi:10.3389/fnmol.2022.953066
421. Toneatti R, Shin JM, Shah UH, et al. *Interclass GPCR Heteromerization Affects Localization and Trafficking*. Vol 13.; 2020. http://stke.sciencemag.org/
422. Kemp PJ, Rushton DJ, Yarova PL, et al. Improving and accelerating the differentiation and functional maturation of human stem cell-derived neurons: role of extracellular calcium and GABA. *J Physiol*. 2016;594(22):6583-6594. doi:10.1113/JP270655
423. Telezhkin V, Schnell C, Yarova P, et al. Forced cell cycle exit and modulation of GABAA, CREB, and GSK3β signaling promote functional maturation of induced pluripotent stem cell-derived neurons. *American Journal of Physiology-Cell Physiology*. 2016;310(7):C520-C541. doi:10.1152/ajpcell.00166.2015
424. R Core Team. R: A Language and Environment for Statistical Computing. https://www.r-project.org/. Published online 2020.
425. Love MI, Huber W, Anders S. Moderated estimation of fold change and dispersion for RNA-seq data with DESeq2. *Genome Biol*. 2014;15(12):550. doi:10.1186/s13059-014-0550-8
426. Kolde R. pheatmap: Pretty Heatmaps https://cran.r-project.org/package=pheatmap.
427. Garnier S. viridis: Default Color Maps from "matplotlib." https://cran.r- project.org/package=viridis. Published online 2018.
428. Yu G, Wang LG, Han Y, He QY. clusterProfiler: an R package for comparing biological themes among gene clusters. *OMICS*. 2012;16(5):284-287. doi:10.1089/omi.2011.0118
429. Carlson M. org.Hs.eg.db: Genome wide annotation for Human. Published online 2020.
430. Walter W, Sánchez-Cabo F, Ricote M. GOplot: an R package for visually combining expression data with functional analysis: Fig. 1. *Bioinformatics*. 2015;31(17):2912-2914. doi:10.1093/bioinformatics/btv300
431. Ly C, Shimizu AJ, Vargas M v, Duim WC, Wender PA, Olson DE. Bryostatin 1 Promotes Synaptogenesis and Reduces Dendritic Spine Density in Cortical Cultures through a PKC-Dependent Mechanism. *ACS Chem Neurosci*. 2020;11(11):1545-1554. doi:10.1021/acschemneuro.0c00175
432. Hevner RF, Shi L, Justice N, et al. Tbr1 Regulates Differentiation of the Preplate and Layer 6. *Neuron*. 2001;29(2):353-366. doi:10.1016/S0896-6273(01)00211-2
433. Canovas J, Berndt FA, Sepulveda H, et al. The Specification of Cortical Subcerebral Projection Neurons Depends on the Direct Repression of TBR1 by CTIP1/BCL11a. *Journal of Neuroscience*. 2015;35(19):7552-7564. doi:10.1523/JNEUROSCI.0169-15.2015
434. Huang CYM, Rasband MN. Axon initial segments: structure, function, and disease. *Ann N Y Acad Sci*. 2018;1420(1):46-61. doi:10.1111/nyas.13718
435. Kometer M, Schmidt A, Jancke L, Vollenweider FX. Activation of Serotonin 2A Receptors Underlies the Psilocybin-Induced Effects on Oscillations, N170 Visual-Evoked Potentials, and Visual Hallucinations. *Journal of Neuroscience*. 2013;33(25):10544-10551. doi:10.1523/JNEUROSCI.3007-12.2013
436. Preller KH, Herdener M, Pokorny T, et al. The Fabric of Meaning and Subjective Effects in LSD-Induced States Depend on Serotonin 2A Receptor Activation. *Current Biology*. 2017;27(3):451-457. doi:10.1016/j.cub.2016.12.030
437. Willins DL, Deutch AY, Roth BL. Serotonin 5-HT2A receptors are expressed on pyramidal cells and interneurons in the rat cortex. *Synapse*. 1997;27(1):79-82. doi:10.1002/(SICI)1098-2396(199709)27:1<79::AID-SYN8>3.0.CO;2-A
438. Jaggar M, Vaidya VA. 5-HT2A Receptors and BDNF Regulation: Implications for Psychopathology. In: *5-HT2A Receptors in the Central Nervous System*. Springer International Publishing; 2018:395-438. doi:10.1007/978-3-319-70474-6_17

439. Bhattacharyya S, Puri S, Miledi R, Panicker MM. Internalization and recycling of 5-HT2A receptors activated by serotonin and protein kinase C-mediated mechanisms. *Proceedings of the National Academy of Sciences*. 2002;99(22). doi:10.1073/pnas.212517999
440. Gray JA, Roth BL. Paradoxical trafficking and regulation of 5-HT(2A) receptors by agonists and antagonists. *Brain Res Bull*. 2001;56(5). doi:10.1016/s0361-9230(01)00623-2
441. Aigner L, Arber S, Kapfhammer JP, et al. Overexpression of the neural growth-associated protein GAP-43 induces nerve sprouting in the adult nervous system of transgenic mice. *Cell*. 1995;83(2):269-278. doi:10.1016/0092-8674(95)90168-X
442. Gianola S, Rossi F. GAP-43 overexpression in adult mouse Purkinje cells overrides myelin-derived inhibition of neurite growth. *European Journal of Neuroscience*. 2004;19(4):819-830. doi:10.1111/j.0953-816X.2004.03190.x
443. González-Maeso J, Yuen T, Ebersole BJ, et al. Transcriptome Fingerprints Distinguish Hallucinogenic and Nonhallucinogenic 5-Hydroxytryptamine 2A Receptor Agonist Effects in Mouse Somatosensory Cortex. *The Journal of Neuroscience*. 2003;23(26):8836-8843. doi:10.1523/JNEUROSCI.23-26-08836.2003
444. González-Maeso J, Yuen T, Ebersole BJ, et al. Transcriptome Fingerprints Distinguish Hallucinogenic and Nonhallucinogenic 5-Hydroxytryptamine 2A Receptor Agonist Effects in Mouse Somatosensory Cortex. *The Journal of Neuroscience*. 2003;23(26):8836-8843. doi:10.1523/JNEUROSCI.23-26-08836.2003
445. Duclot F, Kabbaj M. The Role of Early Growth Response 1 (EGR1) in Brain Plasticity and Neuropsychiatric Disorders. *Front Behav Neurosci*. 2017;11. doi:10.3389/fnbeh.2017.00035
446. Berry SA, Shah MC, Khan N, Roth BL. Rapid agonist-induced internalization of the 5-hydroxytryptamine2A receptor occurs via the endosome pathway in vitro. *Mol Pharmacol*. 1996;50(2):306-313.
447. Herbert JM, Augereau JM, Gleye J, Maffrand JP. Chelerythrine is a potent and specific inhibitor of protein kinase C. *Biochem Biophys Res Commun*. 1990;172(3):993-999. doi:10.1016/0006-291X(90)91544-3
448. Nishizuka Y. The role of protein kinase C in cell surface signal transduction and tumour promotion. *Nature*. 1984;308(5961):693-698. doi:10.1038/308693a0
449. Preta G, Cronin JG, Sheldon IM. Dynasore - Not just a dynamin inhibitor. *Cell Communication and Signaling*. 2015;13(1). doi:10.1186/s12964-015-0102-1
450. Fukuchi-Shimogori T, Grove EA. Neocortex Patterning by the Secreted Signaling Molecule FGF8. *Science (1979)*. 2001;294(5544):1071-1074. doi:10.1126/science.1064252
451. Cederquist GY, Tchieu J, Callahan SJ, et al. A Multiplex Human Pluripotent Stem Cell Platform Defines Molecular and Functional Subclasses of Autism-Related Genes. *Cell Stem Cell*. 2020;27(1):35-49.e6. doi:10.1016/j.stem.2020.06.004
452. Hergenreder E, Zorina Y, Zhao Z, et al. Combined small molecule treatment accelerates timing of maturation in human pluripotent stem cell-derived neurons. *bioRxiv*. Published online 2022.
453. Kim E, Leonardo E, Dranovsky A. iPSC-derived neurons as a tool for probing molecular pharmacology of antipsychotic action. *bioRxiv*. Published online 2018.
454. Gresch PJ, Smith RL, Barrett RJ, Sanders-Bush E. Behavioral Tolerance to Lysergic Acid Diethylamide is Associated with Reduced Serotonin-2A Receptor Signaling in Rat Cortex. *Neuropsychopharmacology*. 2005;30(9):1693-1702. doi:10.1038/sj.npp.1300711
455. Harvey JA, Quinn JL, Liu R, Aloyo VJ, Romano AG. Selective remodeling of rabbit frontal cortex: relationship between 5-HT 2A receptor density and associative learning. *Psychopharmacology (Berl)*. 2004;172(4):435-442. doi:10.1007/s00213-003-1687-4
456. Pandey GN, Dwivedi Y, Rizavi HS, et al. Higher Expression of Serotonin 5-HT (2A) Receptors in the Postmortem Brains of Teenage Suicide Victims. *American Journal of Psychiatry*. 2002;159(3):419-429. doi:10.1176/appi.ajp.159.3.419
457. Shelton RC, Sanders-Bush E, Manier DH, Lewis DA. Elevated 5-HT 2A receptors in postmortem prefrontal cortex in major depression is associated with reduced activity of protein kinase A. *Neuroscience*. 2009;158(4):1406-1415. doi:10.1016/j.neuroscience.2008.11.036
458. Mayor S, Presley JF, Maxfield FR. Sorting of membrane components from endosomes and subsequent recycling to the cell surface occurs by a bulk flow process. *Journal of Cell Biology*. 1993;121(6):1257-1269. doi:10.1083/jcb.121.6.1257
459. Gorvel JP, Chavrier P, Zerial M, Gruenberg J. rab5 controls early endosome fusion in vitro. *Cell*. 1991;64(5). doi:10.1016/0092-8674(91)90316-q
460. Jovic M, Sharma M, Rahajeng J, Caplan S. The early endosome: a busy sorting station for proteins at the crossroads. *Histol Histopathol*. 2010;25(1). doi:10.14670/HH-25.99
461. Mills IG, Jones AT, Clague MJ. Regulation of endosome fusion. *Mol Membr Biol*. 1999;16(1). doi:10.1080/096876899294788

462. Mills IG, Jones AT, Clague MJ. Involvement of the endosomal autoantigen EEA1 in homotypic fusion of early endosomes. *Curr Biol*. 1998;8(15). doi:10.1016/s0960-9822(07)00351-x
463. Simonsen A, Lippe R, Christoforidis S, et al. EEA1 links PI(3)K function to Rab5 regulation of endosome fusion. *Nature*. 1998;394(6692):494-498. doi:10.1038/28879
464. Christoforidis S, Miaczynska M, Ashman K, et al. Phosphatidylinositol-3-OH kinases are Rab5 effectors. *Nat Cell Biol*. 1999;1(4). doi:10.1038/12075
465. Murray JT, Panaretou C, Stenmark H, Miaczynska M, Backer JM. Role of Rab5 in the Recruitment of hVps34/p150 to the Early Endosome. *Traffic*. 2002;3(6):416-427. doi:10.1034/j.1600-0854.2002.30605.x
466. Bucci C, Parton RG, Mather IH, et al. The small GTPase rab5 functions as a regulatory factor in the early endocytic pathway. *Cell*. 1992;70(5). doi:10.1016/0092-8674(92)90306-w
467. Deneka M, van der Sluijs P. 'Rab'ing up endosomal membrane transport. *Nat Cell Biol*. 2002;4(2). doi:10.1038/ncb0202-e33
468. Grosshans BL, Ortiz D, Novick P. Rabs and their effectors: achieving specificity in membrane traffic. *Proc Natl Acad Sci U S A*. 2006;103(32). doi:10.1073/pnas.0601617103
469. van der Sluijs P, Hull M, Webster P, Mâle P, Goud B, Mellman I. The small GTP-binding protein rab4 controls an early sorting event on the endocytic pathway. *Cell*. 1992;70(5). doi:10.1016/0092-8674(92)90307-x
470. Daro E, van der Sluijs P, Galli T, Mellman I. Rab4 and cellubrevin define different early endosome populations on the pathway of transferrin receptor recycling. *Proc Natl Acad Sci U S A*. 1996;93(18). doi:10.1073/pnas.93.18.9559
471. Singh RK, Dai Y, Staudinger JL, Muma NA. Activation of the JAK-STAT pathway is necessary for desensitization of 5-HT2A receptor-stimulated phospholipase C signalling by olanzapine, clozapine and MDL 100907. *Int J Neuropsychopharmacol*. 2009;12(05):651. doi:10.1017/S1461145708009590
472. de la Fuente Revenga M, Zhu B, Guevara CA, et al. Prolonged epigenomic and synaptic plasticity alterations following single exposure to a psychedelic in mice. *Cell Rep*. 2021;37(3):109836. doi:10.1016/j.celrep.2021.109836
473. Muschamp JW, Regina MJ, Hull EM, Winter JC, Rabin RA. Lysergic acid diethylamide and [−]-2,5-dimethoxy-4-methylamphetamine increase extracellular glutamate in rat prefrontal cortex. *Brain Res*. 2004;1023(1):134-140. doi:10.1016/j.brainres.2004.07.044
474. Kim K, Che T, Panova O, et al. Structure of a Hallucinogen-Activated Gq-Coupled 5-HT2A Serotonin Receptor. *Cell*. 2020;182(6):1574-1588.e19. doi:10.1016/j.cell.2020.08.024
475. Aghajanian GK. Modeling "psychosis" in vitro by inducing disordered neuronal network activity in cortical brain slices. *Psychopharmacology (Berl)*. 2009;206(4):575-585. doi:10.1007/s00213-009-1484-9
476. Martin DA, Nichols CD. Psychedelics Recruit Multiple Cellular Types and Produce Complex Transcriptional Responses Within the Brain. *EBioMedicine*. 2016;11:262-277. doi:10.1016/j.ebiom.2016.08.049
477. Prolo LM. Circadian Rhythm Generation and Entrainment in Astrocytes. *Journal of Neuroscience*. 2005;25(2):404-408. doi:10.1523/JNEUROSCI.4133-04.2005
478. Boothman LJ, Allers KA, Rasmussen K, Sharp T. Evidence that central 5-HT2A and 5-HT2B/C receptors regulate 5-HT cell firing in the dorsal raphe nucleus of the anaesthetised rat. *Br J Pharmacol*. 2003;139(5):998-1004. doi:10.1038/sj.bjp.0705328
479. Garcia-Garcia AL, Newman-Tancredi A, Leonardo ED. P5-HT1A receptors in mood and anxiety: recent insights into autoreceptor versus heteroreceptor function. *Psychopharmacology (Berl)*. 2014;231(4):623-636. doi:10.1007/s00213-013-3389-x
480. Andrade R. Serotonergic regulation of neuronal excitability in the prefrontal cortex. *Neuropharmacology*. 2011;61(3):382-386. doi:10.1016/j.neuropharm.2011.01.015
481. Chater TE, Goda Y. The role of AMPA receptors in postsynaptic mechanisms of synaptic plasticity. *Front Cell Neurosci*. 2014;8. doi:10.3389/fncel.2014.00401
482. de Gregorio D, Popic J, Enns JP, et al. Lysergic acid diethylamide (LSD) promotes social behavior through mTORC1 in the excitatory neurotransmission. *Proceedings of the National Academy of Sciences*. 2021;118(5):e2020705118. doi:10.1073/pnas.2020705118
483. Goslin K, Schreyer DJ, Skene JHP, Banker G. Development of neuronal polarity: GAP-43 distinguishes axonal from dendritic growth cones. *Nature*. 1988;336(6200):672-674. doi:10.1038/336672a0
484. Skene JHP, Jacobson RD, Snipes GJ, McGuire CB, Norden JJ, Freeman JA. A Protein Induced During Nerve Growth (GAP-43) is a Major Component of Growth-Cone Membranes. *Science (1979)*. 1986;233(4765):783-786. doi:10.1126/science.3738509
485. Jacobson R, Virag I, Skene J. A protein associated with axon growth, GAP-43, is widely distributed and developmentally regulated in rat CNS. *The Journal of Neuroscience*. 1986;6(6):1843-1855. doi:10.1523/JNEUROSCI.06-06-01843.1986

486. Benowitz LI, Routtenberg A. A membrane phosphoprotein associated with neural development, axonal regeneration, phospholipid metabolism, and synaptic plasticity. *Trends Neurosci*. 1987;10(12):527-532. doi:10.1016/0166-2236(87)90135-4
487. Scruggs JL, Patel S, Bubser M, Deutch AY. DOI-Induced Activation of the Cortex: Dependence on 5-HT2A Heteroceptors on Thalamocortical Glutamatergic Neurons. *The Journal of Neuroscience*. 2000;20(23):8846-8852. doi:10.1523/JNEUROSCI.20-23-08846.2000
488. Fries GR, Saldana VA, Finnstein J, Rein T. Molecular pathways of major depressive disorder converge on the synapse. *Mol Psychiatry*. Published online October 6, 2022. doi:10.1038/s41380-022-01806-1
489. Mitoma M, Yoshimura R, Sugita A, et al. Stress at work alters serum brain-derived neurotrophic factor (BDNF) levels and plasma 3-methoxy-4-hydroxyphenylglycol (MHPG) levels in healthy volunteers: BDNF and MHPG as possible biological markers of mental stress? *Prog Neuropsychopharmacol Biol Psychiatry*. 2008;32(3):679-685. doi:10.1016/j.pnpbp.2007.11.011
490. Fernandes BS, Molendijk ML, Köhler CA, et al. Peripheral brain-derived neurotrophic factor (BDNF) as a biomarker in bipolar disorder: a meta-analysis of 52 studies. *BMC Med*. 2015;13(1):289. doi:10.1186/s12916-015-0529-7
491. Barbosa IG, Rocha NP, Miranda AS de, et al. Increased BDNF Levels in Long-term Bipolar Disorder Patients. *Revista Brasileira de Psiquiatria*. 2013;35(1):67-69. doi:10.1016/j.rbp.2012.05.011
492. Gard DE, Pleet MM, Bradley ER, et al. Evaluating the risk of psilocybin for the treatment of bipolar depression: A review of the research literature and published case studies. *J Affect Disord Rep*. 2021;6:100240. doi:10.1016/j.jadr.2021.100240
493. de Gregorio D, Comai S, Posa L, Gobbi G. d-Lysergic Acid Diethylamide (LSD) as a Model of Psychosis: Mechanism of Action and Pharmacology. *Int J Mol Sci*. 2016;17(11):1953. doi:10.3390/ijms17111953
494. Bosch OG, Halm S, Seifritz E. Psychedelics in the treatment of unipolar and bipolar depression. *Int J Bipolar Disord*. 2022;10(1):18. doi:10.1186/s40345-022-00265-5
495. Kraus C, Rabl U, Vanicek T, et al. Administration of ketamine for unipolar and bipolar depression. *Int J Psychiatry Clin Pract*. 2017;21(1):2-12. doi:10.1080/13651501.2016.1254802
496. Svenningsson P, Chergui K, Rachleff I, et al. Alterations in 5-HT1B Receptor Function by p11 in Depression-Like States. *Science (1979)*. 2006;311(5757):77-80. doi:10.1126/science.1117571
497. Oh YS, Gao P, Lee KW, et al. SMARCA3, a Chromatin-Remodeling Factor, Is Required for p11-Dependent Antidepressant Action. *Cell*. 2013;152(4):831-843. doi:10.1016/j.cell.2013.01.014
498. Melas PA, Rogdaki M, Lennartsson A, et al. Antidepressant treatment is associated with epigenetic alterations in the promoter of P11 in a genetic model of depression. *Int J Neuropsychopharmacol*. 2012;15(05):669-679. doi:10.1017/S1461145711000940
499. Neyazi A, Theilmann W, Brandt C, et al. P11 promoter methylation predicts the antidepressant effect of electroconvulsive therapy. *Transl Psychiatry*. 2018;8(1):25. doi:10.1038/s41398-017-0077-3
500. Chottekalapanda RU, Kalik S, Gresack J, et al. AP-1 controls the p11-dependent antidepressant response. *Mol Psychiatry*. 2020;25(7):1364-1381. doi:10.1038/s41380-020-0767-8
501. Schmidt EF, Warner-Schmidt JL, Otopalik BG, Pickett SB, Greengard P, Heintz N. Identification of the Cortical Neurons that Mediate Antidepressant Responses. *Cell*. 2012;149(5):1152-1163. doi:10.1016/j.cell.2012.03.038
502. Svenningsson P, Greengard P. p11 (S100A10) — an inducible adaptor protein that modulates neuronal functions. *Curr Opin Pharmacol*. 2007;7(1):27-32. doi:10.1016/j.coph.2006.10.001
503. Tiger M, Varnäs K, Okubo Y, Lundberg J. The 5-HT1B receptor - a potential target for antidepressant treatment. *Psychopharmacology (Berl)*. 2018;235(5):1317-1334. doi:10.1007/s00213-018-4872-1
504. Murphy SE, de Cates AN, Gillespie AL, et al. Translating the promise of 5HT4 receptor agonists for the treatment of depression. *Psychol Med*. 2021;51(7):1111-1120. doi:10.1017/S0033291720000604
505. Lee KW, Westin L, Kim J, et al. Alteration by p11 of mGluR5 localization regulates depression-like behaviors. *Mol Psychiatry*. 2015;20(12):1546-1556. doi:10.1038/mp.2015.132
506. Chaki S, Ago Y, Palucha-Paniewiera A, Matrisciano F, Pilc A. mGlu2/3 and mGlu5 receptors: Potential targets for novel antidepressants. *Neuropharmacology*. 2013;66:40-52. doi:10.1016/j.neuropharm.2012.05.022
507. Sun HL, Zhou ZQ, Zhang GF, et al. Role of hippocampal p11 in the sustained antidepressant effect of ketamine in the chronic unpredictable mild stress model. *Transl Psychiatry*. 2016;6(2):e741-e741. doi:10.1038/tp.2016.21
508. Veldman ER, Mamula D, Jiang H, et al. P11 (S100A10) as a potential predictor of ketamine response in patients with SSRI-resistant depression. *J Affect Disord*. 2021;290:240-244. doi:10.1016/j.jad.2021.04.055
509. Baranes D, Lederfein D, Huang YY, Chen M, Bailey CH, Kandel ER. Tissue Plasminogen Activator Contributes to the Late Phase of LTP and to Synaptic Growth in the Hippocampal Mossy Fiber Pathway. *Neuron*. 1998;21(4):813-825. doi:10.1016/S0896-6273(00)80597-8

510. Melchor J, Strickland S. Tissue plasminogen activator in central nervous system physiology and pathology. *Thromb Haemost*. 2005;93(04):655-660. doi:10.1160/TH04-12-0838
511. Lee TW, Tsang VWK, Birch NP. Physiological and pathological roles of tissue plasminogen activator and its inhibitor neuroserpin in the nervous system. *Front Cell Neurosci*. 2015;9. doi:10.3389/fncel.2015.00396
512. Wu F, Torre E, Cuellar-Giraldo D, et al. Tissue-Type Plasminogen Activator Triggers the Synaptic Vesicle Cycle in Cerebral Cortical Neurons. *Journal of Cerebral Blood Flow & Metabolism*. 2015;35(12):1966-1976. doi:10.1038/jcbfm.2015.155
513. Calabresi P, Napolitano M, Centonze D, et al. Tissue plasminogen activator controls multiple forms of synaptic plasticity and memory. *European Journal of Neuroscience*. 2000;12(3):1002-1012. doi:10.1046/j.1460-9568.2000.00991.x
514. Obiang P, Maubert E, Bardou I, et al. Enriched housing reverses age-associated impairment of cognitive functions and tPA-dependent maturation of BDNF. *Neurobiol Learn Mem*. 2011;96(2):121-129. doi:10.1016/j.nlm.2011.03.004
515. Lee TW, Tsang VWK, Birch NP. Physiological and pathological roles of tissue plasminogen activator and its inhibitor neuroserpin in the nervous system. *Front Cell Neurosci*. 2015;9. doi:10.3389/fncel.2015.00396
516. Jeanneret V, Wu F, Merino P, et al. Tissue-type Plasminogen Activator (tPA) Modulates the Postsynaptic Response of Cerebral Cortical Neurons to the Presynaptic Release of Glutamate. *Front Mol Neurosci*. 2016;9. doi:10.3389/fnmol.2016.00121
517. Yepes M. Urokinase-type plasminogen activator is a modulator of synaptic plasticity in the central nervous system: implications for neurorepair in the ischemic brain. *Neural Regen Res*. 2020;15(4):620. doi:10.4103/1673-5374.266904
518. Echeverry R, Wu J, Haile WB, Guzman J, Yepes M. Tissue-type plasminogen activator is a neuroprotectant in the mouse hippocampus. *J Clin Invest*. 2010;120(6):2194-2205. doi:10.1172/JCI41722
519. Jeanneret V, Ospina JP, Diaz A, et al. Tissue-type plasminogen activator protects the postsynaptic density in the ischemic brain. *Journal of Cerebral Blood Flow & Metabolism*. 2018;38(11):1896-1910. doi:10.1177/0271678X18764495
520. Diaz A, Merino P, Manrique LG, et al. A Cross Talk between Neuronal Urokinase-type Plasminogen Activator (uPA) and Astrocytic uPA Receptor (uPAR) Promotes Astrocytic Activation and Synaptic Recovery in the Ischemic Brain. *The Journal of Neuroscience*. 2017;37(43):10310-10322. doi:10.1523/JNEUROSCI.1630-17.2017
521. Merino P, Diaz A, Manrique LG, Cheng L, Yepes M. Urokinase-type plasminogen activator (uPA) promotes ezrin-mediated reorganization of the synaptic cytoskeleton in the ischemic brain. *Journal of Biological Chemistry*. 2018;293(24):9234-9247. doi:10.1074/jbc.RA118.002534
522. Diaz A, Merino P, Guo JD, et al. Urokinase-type plasminogen activator protects cerebral cortical neurons from soluble Ab-induced synaptic damage. *Journal of Neuroscience*. 2020;40(21):4251-4263. doi:10.1523/JNEUROSCI.2804-19.2020
523. Merino P, Diaz A, Jeanneret V, et al. Urokinase-type Plasminogen Activator (uPA) Binding to the uPA Receptor (uPAR) Promotes Axonal Regeneration in the Central Nervous System. *Journal of Biological Chemistry*. 2017;292(7):2741-2753. doi:10.1074/jbc.M116.761650
524. Wu F, Wu J, Nicholson AD, et al. Tissue-Type Plasminogen Activator Regulates the Neuronal Uptake of Glucose in the Ischemic Brain. *Journal of Neuroscience*. 2012;32(29):9848-9858. doi:10.1523/JNEUROSCI.1241-12.2012
525. Wu F, Nicholson AD, Haile WB, et al. Tissue-Type Plasminogen Activator Mediates Neuronal Detection and Adaptation to Metabolic Stress. *Journal of Cerebral Blood Flow & Metabolism*. 2013;33(11):1761-1769. doi:10.1038/jcbfm.2013.124
526. Wu F, Catano M, Echeverry R, et al. Urokinase-Type Plasminogen Activator Promotes Dendritic Spine Recovery and Improves Neurological Outcome Following Ischemic Stroke. *Journal of Neuroscience*. 2014;34(43):14219-14232. doi:10.1523/JNEUROSCI.5309-13.2014
527. Dolmetsch RE, Pajvani U, Fife K, Spotts JM, Greenberg ME. Signaling to the Nucleus by an L-type Calcium Channel-Calmodulin Complex Through the MAP Kinase Pathway. *Science (1979)*. 2001;294(5541):333-339. doi:10.1126/science.1063395
528. Umschweif G, Medrihan L, McCabe KA, Sagi Y, Greengard P. Activation of the p11/SMARCA3/Neurensin-2 pathway in parvalbumin interneurons mediates the response to chronic antidepressants. *Mol Psychiatry*. 2021;26(7):3350-3362. doi:10.1038/s41380-021-01059-4
529. Oquendo MA, Sullivan GM, Sudol K, et al. Toward a Biosignature for Suicide. *American Journal of Psychiatry*. 2014;171(12):1259-1277. doi:10.1176/appi.ajp.2014.14020194
530. Felger JC, Lotrich FE. Inflammatory cytokines in depression: Neurobiological mechanisms and therapeutic implications. *Neuroscience*. 2013;246:199-229. doi:10.1016/j.neuroscience.2013.04.060

531. Uchida-Kitajima S, Yamauchi T, Takashina Y, et al. 5-Hydroxytryptamine 2A receptor signaling cascade modulates adiponectin and plasminogen activator inhibitor 1 expression in adipose tissue. *FEBS Lett*. 2008;582(20):3037-3044. doi:10.1016/j.febslet.2008.07.044
532. Yu B, Becnel J, Zerfaoui M, Rohatgi R, Boulares AH, Nichols CD. Serotonin 5-Hydroxytryptamine 2A Receptor Activation Suppresses Tumor Necrosis Factor-α-Induced Inflammation with Extraordinary Potency. *Journal of Pharmacology and Experimental Therapeutics*. 2008;327(2):316-323. doi:10.1124/jpet.108.143461
533. Nau F, Yu B, Martin D, Nichols CD. Serotonin 5-HT2A Receptor Activation Blocks TNF-α Mediated Inflammation In Vivo. *PLoS One*. 2013;8(10):e75426. doi:10.1371/journal.pone.0075426
534. Park KM, Bowers WJ. Tumor necrosis factor-alpha mediated signaling in neuronal homeostasis and dysfunction. *Cell Signal*. 2010;22(7):977-983. doi:10.1016/j.cellsig.2010.01.010
535. Erta M, Quintana A, Hidalgo J. Interleukin-6, a Major Cytokine in the Central Nervous System. *Int J Biol Sci*. 2012;8(9):1254-1266. doi:10.7150/ijbs.4679
536. Petersen MA, Ryu JK, Akassoglou K. Fibrinogen in neurological diseases: mechanisms, imaging and therapeutics. *Nat Rev Neurosci*. 2018;19(5):283-301. doi:10.1038/nrn.2018.13
537. Jones R. Steps to lasting plasticity. *Nat Rev Neurosci*. 2004;5(12):898-898. doi:10.1038/nrn1562
538. Briens A, Bardou I, Lebas H, et al. Astrocytes regulate the balance between plasminogen activation and plasmin clearance via cell-surface actin. *Cell Discov*. 2017;3. doi:10.1038/celldisc.2017.1

Contributions

Dr. Anne Hoffrichter (Hector Institute for Translational Brain Research, Central Institute of Mental Health, Mannheim, Germany) performed the pre-processing and visualization (heat maps, GO terms, GO circle blots) of RNAseq data. I visualized TPM-scaled RNAseq data by using a custom-made R application, provided by Dr. Anne Hoffrichter.

Dr. Mahnaz Davoudi (Hector Institute for Translational Brain Research, Central Institute of Mental Health, Mannheim, Germany) performed the electrophysiological measurements in cooperation with PD Dr. Georg Köhr (Department of Neurophysiology, Mannheim Center for Translational Neuroscience, University of Heidelberg/Medical Faculty Mannheim, Germany) of the cortical neurons that I provided. Representative traces of electrophysiological properties were generated by Dr. Mahnaz Davoudi.

Acknowledgements

Die Arbeit im Labor hat mir immer sehr viel Spaß gemacht. Dafür möchte ich allen meinen Kollegen danken. Ich kann mich glücklich schätzen so viele interessante, hilfsbereite und motivierende Menschen kennen gelernt zu haben.

Vor allem Euch, Elena, Julia und Klara möchte ich von ganzem Herzen danken. Ihr habt mich von Anfang an begleitet, wart immer für mich da und habt mir in vielfältiger Weise geholfen. Vielen Dank auch an Isa und Ruven für die zahlreichen amüsanten Stunden in der Zellkultur. Und natürlich dir, Gina für deine herzliche und freundliche Art. Vielen Dank auch an Thorsten für das Korrekturlesen meiner Arbeit.

Herzlichen Dank gilt auch Herrn Prof. Rainer Spanagel als Fakultätsgutachter meiner Arbeit. Ich möchte zudem Dr. Radhika Puttagunta und Prof. Daniela Mauceri als Mitglieder meines Prüfungskomitees danken.

Schlussendlich möchte ich mich bei Prof. Philipp Koch bedanken. Ich finde es grandios, dass ich genau an dem arbeiten kann was ich liebe und von dem ich überzeugt bin. Auch möchte ich mich für Dein Vertrauen und Deine Neugier bedanken neue Wege zu gehen.

Für alle die für mich gekämpft haben.

Mom & Dad

Janna

Michi

Nelly und Daniel

Für Dich.

Stefan Reeb